Optical parametric processes to the extreme:

From new insights in first principles
to tunability over more than 4 octaves

Christian Homann

Dissertation
an der Fakultät für Physik
der Ludwig-Maximilians-Universität
München

vorgelegt von
Christian Homann
aus Rosenheim

München, im Dezember 2012

Erstgutachter: Prof. Dr. E. Riedle
Zweitgutachter: Prof. Dr. S. Karsch

Tag der mündlichen Prüfung: 27.2.2013

Kurzfassung

Optisch parametrische Verstärkung (OPA) ist ein nichtlinearer Prozess, der die Verstärkung einer elektromagnetischen Welle auf Kosten einer kürzerwelligen in einem geeigneten Medium erlaubt. Da dieser Prozess in Kombination mit spektraler Verbreiterung eines schmalbandigen Laserimpulses die Erzeugung von einerseits äußerst breitbandigen, und damit potenziell sehr kurzen Impulsen, und andererseits von weit spektral durchstimmbaren Impulsen erlaubt, erfreut er sich großer Beliebtheit in vielen Bereichen der Physik, wie z.B. der zeitaufgelösten Spektroskopie oder der Hochfeldphysik, die sich mit intensiver Licht-Materie-Wechselwirkung beschäftigt.
Im Rahmen der vorliegenden Arbeit wurde der durch optische parametrische Prozesse effizient erreichbare Parameterraum erheblich erweitert. Die Entwicklungen wurden dabei immer durch konkrete Anforderungen angestoßen, die bisher nicht oder nur äußerst aufwändig erfüllt werden konnten. Dies beinhaltet eine Ausweitung des Durchstimmbereichs im Tiefultraviolet- und Mittelinfraroten Spektralbereich, Weiterentwicklung der Konzepte für MHz Wiederholraten, die Erzeugung von Sub-2-Zyklen Impulsen im Infraroten mit stabiler Träger-Einhüllenden-Phase, und eine Verbreiterung der mit multi Millijoule Energien erreichbaren Spektren. Die entwickelten Systeme und Konzepte werden mittlerweile in so unterschiedlichen Bereichen wie der laserangeregten Photoemissions-Elektronenmikroskopie, zeitaufgelöster Photoelektronenspektroskopie, der Untersuchung von Polaronenpaaren in Polymeren mit kleiner Bandlücke für die Photovoltaik, und der laserinduzierten Elektronenemission von metallischen Nanospitzen verwendet.
Im Laufe dieser Entwicklungen wurden dabei neue fundamentale Erkenntnisse über den parametrischen Verstärkungsprozess gewonnen, insbesondere über die spontan entstehende parametrische Superfluoreszenz. Unter anderem konnte erstmalig die Anzahl der Photonen, die als Seedquelle für diesen Prozess fungieren, experimentell absolut bestimmt werden. Zusätzlich wurde gezeigt, dass die Anzahl dieser Seedphotonen unabhängig von der Pumpenergie, aber proportional zur Fläche des Pumpimpulses ist. Das gewonnene Wissen liefert nun neue Designrichtlinien um parametrische Verstärkerketten mit einem möglichst guten Verhältnis von verstärktem Signal zu erzeugter parametrischer Superfluoreszenz zu bauen.
Im Detail wurde ein nichtkollinearer OPA (NOPA) entwickelt, der einen mehr als oktav-breiten Abstimmbereich von 440 bis 990 nm mit nur einer Verstärkungsstufe bei einer Wiederholrate von 2 MHz erlaubt. Durch geschicktes Ausnutzen der verfügbaren Pumpenergie wurde es außerdem möglich gleichzeitig einen zweiten, unabhängig durchstimmbaren Verstärker in einem Wellenlängenbereich von 620 bis 990 nm zu betreiben, was dieses einzigartige System äußerst attraktiv für spektroskopische Anwendungen macht. Um den Nah- und Mittelinfraroten Wellenlängenbereich zu erschließen, wurde ein OPA entwickelt, der durchstimmbare Impulse von 1 bis 5 µm bei 100 kHz Wiederholrate und Fourier-Limits größtenteils unter 50 fs liefert. Die breite Anwendbarkeit dieses Konzepts wurde für zwei verschiedene Pumplaser, mit unterschiedlicher Zentralwellenlänge (800 nm und 1025 nm) und unterschiedlicher Impulslänge (50 fs und 300 fs) erfolgreich demonstriert. In der Region um 2 µm konnten sogar Sub-2-Zyklen-Impulse (~ 10 fs Dauer) mit stabiler Träger-Einhüllenden-Phase bei 100 kHz Wiederholrate erzeugt werden. Erste Experimente mit diesen Impulsen an Wolframspitzen liefern bereits vielversprechende Ergebnisse, die auf „neue Physik“ im Zusammenspiel von Multiphotonenionisation und Tunnelregime hinweisen.
Durch die Kombination von zwei Verstärkerstufen, die von unterschiedlichen Harmonischen des Pumplasers gepumpt werden, konnte das Ausgangsspektrum bei zeitlich gestreckter OPA deutlich verbreitert werden. Dadurch wurde der Grundstein für die Erzeugung von hochenergetischen sub-5-fs Impulsen im multi Millijoule Bereich gelegt. Dabei wurde ein Einfluss der optisch parametrischen Phase festgestellt, der besonders im spektralen Überlappbereich der beiden Stufen wichtig ist. Dass dieser gut handhabbar ist, und das zusammengesetzte Spektrum komprimierbar ist, wurde in einem zweiten Experiment nachgewiesen.
Durch chirpoptimierte Summenfrequenzmischung wurden durchstimmbare Impulse von 190 bis 220 nm mit Pulsdauern um 30 fs für die zeitaufgelöste Photoelektronenspektroskopie erzeugt. Da für die Impulsdauermessung bisher kein routinemäßiges und leicht handhabbares Verfahren zur Verfügung stand, wurde ein Autokorrelator basierend auf Zwei-Photonen-Absorption entwickelt. Dieser erlaubt nun die Impulsdauernmessung in einem Wellenlängenbereich von 150 nm bis zum Sichtbaren. Seine Anwendbarkeit wurde für sub-20 fs Impulse und bei geringen Impulsenergien von wenigen Nanojoule gezeigt.

Short summary

Optical parametric amplification (OPA) is a nonlinear process that allows amplification of an electromagnetic wave at the expense of a wave with shorter wavelength in a suitable medium. In combination with spectral broadening of a narrow bandwidth laser pulse, this allows the generation of extremely broadband, and therefore potentially very short pulses, as well as widely tunable pulses. Therefore it is very popular in many areas of physics, as e.g. time-resolved spectroscopy or high field physics, which studies intense light-matter interaction.
In this thesis, the efficiently accessible parameter range by optical parametric processes was substantially expanded. The new developments were thereby always initiated by specific requirements, that could not be fulfilled previously or only in very complex ways. This includes expanding the tuning range of ultrashort pulses in the deep ultraviolet and mid-infrared spectral region, adapting these concepts for MHz repetition rate, generating carrier-envelope phase stable sub-two-cycle pulses in the infrared with 100 kHz repetition rate and broadening the spectral range accessible with multi-mJ energies. The developed systems and concepts are now routinely used in such different fields as laser-excited photoemission electron microscopy, time-resolved photoelectron spectroscopy, investigations of polaron pairs in low-bandgap polymers for photovoltaics, and laser induced electron emission from nano-scale metal tips.
In the course of these investigations, new fundamental insights about the parametric amplification process were gained, especially about the spontaneously generated parametric superfluorescence. The number of photons acting as seed source for this process was determined experimentally for the first time in absolute numbers. Additionally it was shown that this number is independent of the pump pulse energy, but proportional to the area of the pump pulse. The newly gained insight now provides design guidelines for parametric amplifier chains with a highly optimized ratio between amplified signal and unwanted superfluorescence noise.
In more detail, a noncollinear OPA (NOPA) was developed with a more than octave-wide tuning range from 440 to 990 nm in a single amplification stage and with a repetition rate of up to 2 MHz. By careful and optimized use of the available pump energy it was furthermore possible to operate a second, independently tunable NOPA with a tuning range from 620 to 990 nm, which makes this unique system very useful for pump-probe spectroscopy. To access the near- and midinfrared region, an OPA was developed that delivers tunable pulses from 1 to 5 µm at 100 kHz repetition rate and with Fourier-limits below 50 fs over large parts of the tuning range. The broad applicability of the underlying concept was demonstrated for two different pump laser systems with differing central wavelength (800 nm and 1025 nm) and pulse duration (50 fs and 300 fs). In the region around 2 µm even carrier-envelope phase stable pulses with sub-two-cycle duration (~ 10 fs) could be generated at 100 kHz. First experiments with these pulses on tungsten tips already show promising results indicating new physics in the interplay between multi-photon ionization and the tunneling regime.
By combining two amplification stages pumped by different harmonics of the pump laser, the output spectrum in optical parametric chirped pulse amplification was significantly broadened. This opens up the route to sub-5-fs pulses with energies in the multi millijoule regime. In these experiments an influence of the optical parametric phase was found, that is especially important in the spectral overlap region of the two amplifiers. That this influence is controllable and can be compensated for was shown in an additional experiment at 100 kHz repetition rate and with microjoule energies.
By chirp-optimized sum-frequency mixing, tunable pulses from 190 to 220 nm with durations around 30 fs for time-resolved photoelectron spectroscopy were generated. As no routinely available and easy to handle method was established for the measurement of the pulse duration of UV pulses, an autocorrelator based on two-photon absorption was developed. It now allows measuring pulse durations down to below 20 fs and up to several hundreds fs in a spectral range from 150 nm up to the visible, and for energies down to a few nanojoules.

Publications

This thesis is based on the following publications. They are reprinted in part II, chapters 1 to 5 (publications 1 to 5), and in the appendices A1 to A5 (publications 6 to 10).

1 **Convenient pulse length measurement of sub-20-fs pulses down to the deep UV via two-photon absorption in bulk material**
C. Homann, N. Krebs, and E. Riedle
Appl. Phys. B **104**, 783 - 791 (2011).

2 **Generation of 30 fs-pulses tunable from 189 to 240 nm with an all-solid-state setup**
C. Homann, P. Lang, and E. Riedle
J. Opt. Soc. Am. B **29**, 2765 - 2769 (2012).

selected for “Spotlight on Optics” – highlighted articles from OSA journals by the Optical Society of America

3 **Seeding of picosecond and femtosecond optical parametric amplifiers by weak single mode continuous lasers**
C. Homann, M. Breuer, F. Setzpfandt, T. Pertsch, and E. Riedle
Opt. Express **21**, 730 - 739 (2013).

4 **Direct measurement of the effective input noise power of an optical parametric amplifier**
C. Homann and E. Riedle
submitted to Laser & Photonics Reviews (accepted)

5 **Analysis of the output fluctuations of a cw seeded optical parametric amplifier**
C. Homann and E. Riedle
in preparation

6 **Octave wide tunable UV-pumped NOPA: pulses down to 20 fs at 0.5 MHz repetition rate**
C. Homann, C. Schriever, P. Baum, and E. Riedle
Opt. Express **16**, 5746 - 5756 (2008).

7 **Approaching the full octave: Noncollinear optical parametric chirped pulse amplification with two-color pumping**
D. Herrmann, C. Homann, R. Tautz, M. Scharrer, P. St.J. Russell, F. Krausz, L. Veisz, and E. Riedle
Opt. Express **18**, 18752 - 18762 (2010).

8 Approaching the Full Octave: Noncollinear Optical Parametric Chirped Pulse Amplification with Two-Color Pumping
C. Homann, D. Herrmann, R. Tautz, L. Veisz, F. Krausz, and E. Riedle
Ultrafast Phenomena XVII, M. Chergui, D. Jonas, E. Riedle, R.W. Schoenlein, A. Taylor, eds. (Oxford University Press, Inc., New York 2011), 691 – 693.

9 Mid-IR femtosecond pulse generation on the microjoule level up to 5 µm at high repetition rates
M. Bradler, C. Homann, and E. Riedle
Opt. Lett. **36**, 4212 - 4214 (2011).

10 Carrier-envelope phase-stable sub-two-cycle pulses tunable around 1.8 µm at 100 kHz
C. Homann, M. Bradler, M. Förster, P. Hommelhoff, and E. Riedle
Opt. Lett. **37**, 1673 - 1675 (2012).

Aditionally the following book contributions originated (not reprinted):

11 Octave-wide tunable NOPA pulses at up to 2 MHz repetition rate
C. Homann, C. Schriever, P. Baum, and E. Riedle
Ultrafast Phenomena XVI, Springer Series in Chemical Physics 92, P. Corkum, S. De Silvestri, K.A. Nelson, E. Riedle, R.W. Schoenlein, eds. (Springer-Verlag, Berlin Heidelberg 2009), 801 – 803.

12 Widely Tunable Infrared Pulse Generation up to 5 µm with Novel Optical Parametric Amplifiers at 100 kHz Repetition Rate
M. Bradler, E. Riedle, and C. Homann
Ultrafast Phenomena XVII, M. Chergui, D. Jonas, E. Riedle, R.W. Schoenlein, A. Taylor, eds. (Oxford University Press, Inc., New York 2011), 733 – 735.

13 Noncollinear optical parametric amplification of cw light, continua and vacuum fluctuations
M. Breuer, C. Homann, and E. Riedle
Ultrafast Phenomena XVI, Springer Series in Chemical Physics 92, P. Corkum, S. De Silvestri, K.A. Nelson, E. Riedle, R.W. Schoenlein, eds. (Springer-Verlag, Berlin Heidelberg 2009), 771 – 773.

Contents

1. Introduction

Optical parametric amplification (OPA) is a powerful tool for the amplification and generation of ultrashort pulses in an extremely broad wavelength range. Together with spectral broadening techniques, as for example supercontinuum generation in bulk materials, it allows converting the given pulses of a pump laser with fixed wavelength and pulse duration to pulses matched precisely to the needs of an application. All this with great flexibility towards the pump source and the output pulses. Pump energies can be utilized from the range of nanojoules in synchronously pumped optical parametric oscillators (OPOs) [1,2] to microjoules in OPAs [3-5] and millijoules up to joules in optical parametric chirped pulsed amplifiers (OPCPAs) [6,7]. The used repetition rates range from a few hertz up to tens of megahertz, the pump wavelengths from the ultraviolet (UV) to the infrared (IR), and the pump pulse lengths from tens of femtoseconds [8] to nanoseconds [9]. Output pulses were demonstrated with pulse durations of only 2.4 fs with 1 nJ energy [10], 4 fs with 0.5 µJ [11], and 7.7 fs with 130 mJ [7] to almost transform limited 3 ns pulses with linewidths of only 315 MHz [12]. Tunable pulses directly out of an OPA were shown from 335 nm [13] to 5380 nm [A4].

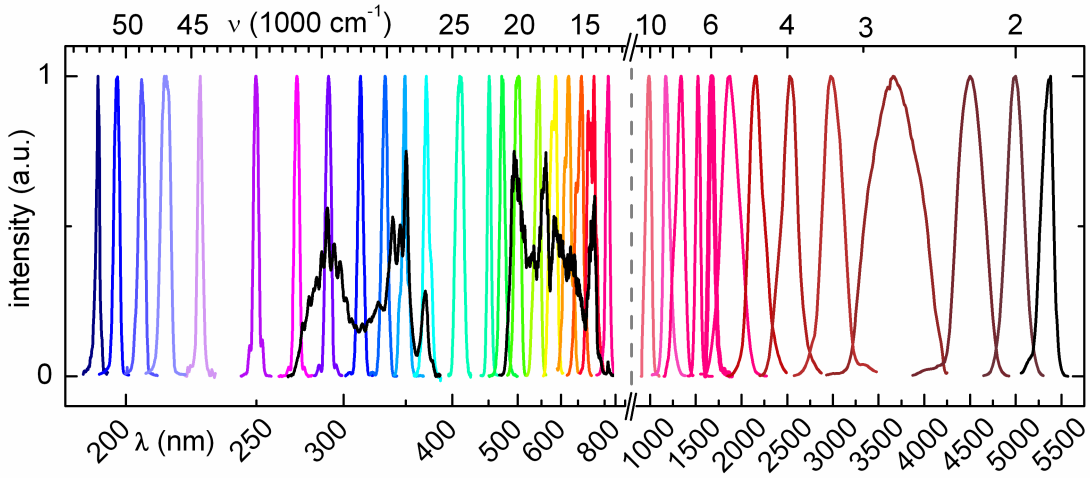

Fig. 1.1 Sample spectra from 192 nm to 5380 nm generated by optical parametric processes starting with a laser pulse from a Ti:sapphire amplifier. Widely tunable as well as very broad spectra can be obtained, tailored to the specific requirements. The Fourier-Limits of the two broadband spectra in the UV and the visible are 2.9 fs and 4.0 fs.

Due to this flexibility, the broad spectral amplification range and high single pass gain, OPA is applied in many areas of modern physics. The most prominent being time-resolved spectroscopy with all its variations, and high-field physics for the study of intense light-matter interactions. While spectroscopic applications typically require only moderate pulse durations in the range from about 10 to 100 femtoseconds and pulse energies in the range from nanojoules to few microjoules, they often profit from high wavelength tunability. In contrast, high-power applications often yearn for pulse durations as short as possible and highest possible energies, whereas wavelength tunability is of minor importance. All these aspects, wavelength tunability, adjustable spectral width, and energy scalability can be pro-

vided by optical parametric amplifiers. Figure 1.1 gives an idea what can be reached by OPA of a supercontinuum generated in a bulk material in combination with second harmonic generation (SHG) and sum-frequency mixing (SFM), starting from a Ti:sapphire laser pump pulse.

However, not all spectral regions and widths can be accessed with the same ease. *The* device that delivers ultrashort pulses over the whole wavelength range, with a knob for wavelength and spectral width control and with highest quantum efficiencies, does not yet exist, and likely will never be built. Instead flexible solutions are in demand and a variety of concepts have to be used for optimal performance. Additionally, more and more different pump lasers become available and attractive for OPA, as for instance Yb^{3+} based systems operating around 1030 nm. Also Tm^{3+} and Ho^{3+} doped pulsed lasers with central wavelengths around 2 µm might become available with sufficient energies in the coming years [14-17]. This offers new alternatives in OPA design, as for example the possibility of efficiently pumping with the third or even fourth harmonic of the pump laser, and influences the "easily" accessible wavelength regions. Naturally, this leads to an ever increasing diversity in OPA designs and concepts, which makes it more and more difficult to judge which is the best solution for a specific requirement.

In the first part of my thesis I therefore want to give guidelines on how to obtain the needed parameters for a certain application most efficiently. The main focus will be on the possible underlying concepts with their advantages and disadvantages that can be applied to any pump source. Exemplarily these are then illustrated for the two most interesting pump laser systems for spectroscopic applications. These are the still most often used Ti:sapphire regenerative amplifier, and the newly evolving Yb^{3+} based fiber or thin disk amplifiers, with their advantage of providing a high repetition rate and still suitable pulse energies for multiple nonlinear processes. The main focus in the following is on laser systems with pump pulses in the regime of up to a few hundred femtoseconds, although most concepts will also be applicable with ps and even ns pump pulses. An exception is the supercontinuum generation in bulk, which is typically used for providing the seed and which was not yet shown for pulses longer than about 1 ps [18].

The first part of the thesis is structured as follows. To get a first impression of how optical parametric amplifiers work and look like, the two most commonly used "standard" implementations of OPAs are presented in chapter 2, together with a realistic setup routinely used in our laboratories. A look at the measured output spectra in different spectral regions already raises first questions how their shape and bandwidth can be explained and influenced. To clarify these questions, chapter 3 shortly reviews the basic physics of optical parametric amplification and identifies which limitations exist for the accessible wavelength range. This leads to the question which pump wavelength is best used and how to get the required seed pulses.

In chapter 4 we will consider how we can achieve the required spectral width within the accessible range, and what limitations we face here. This is closely related to the choice of the geometry (collinear or non-collinear) and the pulse durations of the pump and the seed light. Also the choice of the nonlinear amplifier crystal is of importance.

In chapter 5 we will see, that this point is also related to the efficiency of the amplification process. On the one hand, a noncollinear geometry also enhances the output energy, on the other hand a collinear geometry can provide light in spectral regions that are otherwise not accessible or only with poor efficiency. An important role for the efficiency of OPA with pump pulses in the 100 fs regime plays the group velocity mismatch (GVM) between the three interacting pulses. To be able to handle the GVM correctly, the refraction and propagation properties in a birefringent crystal are shortly reviewed in chapter 5, and applied to OPA. This analysis reveals qualitatively and quantitatively new results and shows the influence of the crystal orientation on the GVM, which was not described before.

Chapter 6 discusses how several amplification or frequency-mixing stages can be combined efficiently to achieve parameters that are otherwise not accessible, and how this can be used to generate passively carrier-envelope phase (CEP) stabilized output pulses in a wide wavelength range. A short paragraph is also devoted to first experimental results with the developed CEP stable sub-two-cycle system on electron emission on a nano-scale tungsten tip.

Practical guidelines for choosing a suitable OPA design based on the required output parameter range and the available pump laser system are given in chapter 7. In chapter 8 the gained knowledge is summarized and the developed concepts are applied to a not yet existing, but very likely soon available sub-ps 2 µm pump laser system.

This thesis is cumulative, the main part are therefore the publications reprinted in part II and in the appendices A1 to A5. The first part is not intended to just summarize the achieved developments and gained knowledge of the publications, but to extract the underlying concepts and enable the readers to transfer them to their own demands. Where results from own publications contribute to the concepts of the first part, they are referenced with [A1] to [A5].

In chapter 1 of part II, a scheme based on chirped-optimized sum-frequency mixing is introduced and explained to generate tunable pulses in the range from 189 to 240 nm with Fourier-limits below 30 fs. These pulses are essential for experiments on time-resolved photoelectron spectroscopy on large molecules in our own laboratory. In these experiments, the molecules are electronically excited by a first laser pulse in the UV, and subsequently ionized by a second laser pulse. The shorter the wavelength of the second laser pulse, the more kinetic energy is gained by the emitted electrons. The tunability helps minimizing the generation of detrimental one-color signal contributions, and the short pulse length allows for a good time resolution.

As no routinely available and easy to handle method is established for the measurement of the pulse duration of UV pulses, an autocorrelator based on two-photon absorption was developed. This is shown in chapter 2 of part II. It allows measuring pulse durations down to below 20 fs and up to several hundreds of femtoseconds in a spectral range from 150 nm up to the visible. For 1 kHz repetition rate, pulse energies down to a few nanojoules are sufficient for the measurement. A detailed description is provided that explains which crystal is best suited for a certain wavelength range and which conditions must be met for a reliable measurement. Due to the online measurement capability it is now also an invaluable tool

used for optimizing and characterizing the UV pulses used in the spectroscopic experiments in our laboratories.

The use of a tunable cw laser as seed source in a NOPA allows generating extremely controlled nearly Fourier-limited pulses in a wide wavelength region. This is demonstrated in chapter 3 of part II for fs and ps pump pulses. This enabled for example the development of a NOPA that delivers nearly Fourier-limited output pulses with a duration of ~ 5 ps and μJ energies in a tuning range from 1260 to 1630 nm. The high peak power together with the small bandwidth (around 0.5 nm) and the tuning ability make this system very suitable for the investigation of nonlinear effects in lithium niobate waveguides and one-dimensional waveguide arrays. The system already led to fundamentally new insights in the coupling of different fundamental and second-harmonic modes and their propagation behavior in the waveguides [19-22].

When using a highly stable cw laser with mW output power together with fs pump pulses, only a few hundred photons act as seed for the amplification process. In chapter 4 of part II this is utilized as an internal standard to determine experimentally and very accurately the effective noise power responsible for the spontaneous optical parametric fluorescence. With this absolute measurement we can now predict the background level in OPCPA applications and the number of spontaneously down-converted photons in quantum optics experiments. It is also shown that the effective input noise power is independent from the pump energy, but proportional to the area of the pump pulse and presumably also to its duration. The newly gained insight thus provides design guidelines for parametric amplifier chains with a highly optimized ratio between amplified signal and unwanted superfluorescence noise.

In chapter 5 of part II finally, the fluctuations of the fs pumped and cw seeded system are analyzed on a shot to shot basis. It is shown that the expected Poissonian input fluctuations of the seed with its small photon numbers are transferred to the nJ output with its up to 10^{10} photons. This allows insights in the transition from the particle to the wave picture of quantum mechanics and indicates that an optical parametric amplifier can be regarded as an ideal amplifier with strictly the same amplification factor from shot to shot.

The publications reprinted in the appendices [A1] to [A5] cover OPAs developed for other groups, who had demands that could not be fulfilled previously or only in very complex ways. The developed systems are all still existing, in use and producing great results.

The system described in appendix [A1], which delivers two independently tunable outputs at MHz repetition rate is used for laser-excited photoemission electron microscopy (PEEM) and time- and angle-resolved two-photon photoemission spectroscopy (tr-2PPE) [23-25]. With it, momentum-resolved lifetimes of image-potential states on Ag(001) could be explored [23,24], and the persistence of surface domain structures for a bulk ferroelectric above T_C was demonstrated [25]. Essential for these experiments were the high repetition rate of the system as well as the capability to produce enough output energy to allow frequency doubling. For [23] and [24] additionally the two perfectly synchronized outputs as well as the fs-pulse duration were vital.

The new concept of pumping two subsequent NOPA stages with different harmonics of the pump laser, that was introduced in publications [A2] and [A3] is now being implemented

in an existing OPCPA system at the Max-Planck-Institut für Quantenoptik in Garching, Germany. A first step, the development of a suitable grism stretcher that allows handling the whole bandwidth supported by the new amplification scheme is already achieved [26]. The final system aims at generating 5-fs pulses with more than hundred millijoules at a repetition rate of 10 Hz, which will allow access to a new parameter regime in high-field physics.

The concept introduced in publication [A4] allows the efficient generation of tunable pulses in the range from 1 to 5 µm with Fourier-limits below 50 fs over large parts of the tuning range, even for high repetition rates and consequently low pump pulse energies. The developed system already allowed studying the influence of the carrier density on the electronic cooling channels of bilayer graphene [27], the effect of molecular doping on the recombination of electrons and holes in organic semiconductor heterojunctions [28], and the generation of polaron pairs in low-bandgap polymers for photovoltaics [29].

The generation of sub-two-cycle pulses with stable carrier-envelope phase and tunable in central wavelength from 1.6 to 2.0 µm at 100 kHz repetition rate is shown in appendix [A5]. This system, which provides unprecedented short pulses at this high repetition rate and long wavelength region, is used for the photoemission of electrons from nano-scale metal tips. First experimental results that already show a clear dependence of the electron spectra on the carrier-envelope phase are summarized in chapter 6 of part I.

2. The “standard” optical parametric amplifier

For a start I want to summarize what are probably still the two most and very successfully used OPA implementations worldwide. They are based on a Ti:sapphire pump laser system and use its fundamental or second harmonic as pump pulse. Their basic layouts are shown in Fig. 2.1.

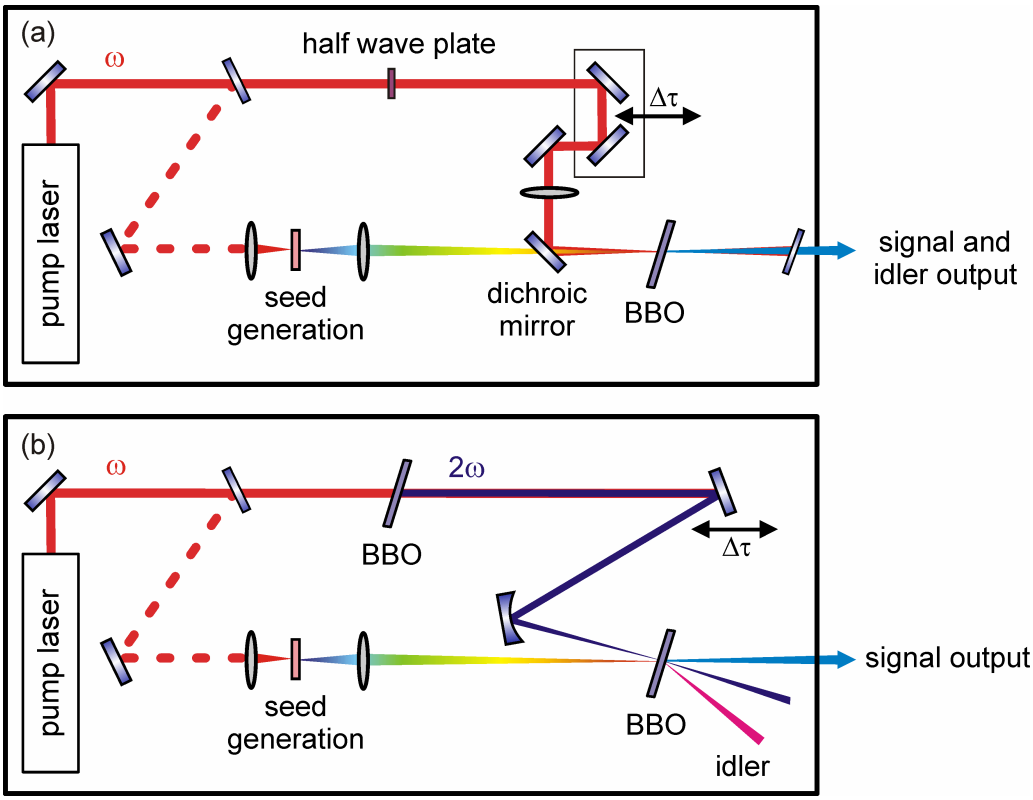

Fig. 2.1 Basic layout of an optical parametric amplifier pumped by the pump laser fundamental (a), and of a noncollinear OPA pumped by the second harmonic (b).

In both implementations, a part of the pump laser is used for the seed generation. In the vast majority of the systems this is done by supercontinuum generation (SCG) in sapphire or YAG [3,30] (details and other approaches will be discussed in Chapter 3). The seed is then overlapped spatially and temporally in the amplifier crystal (in this case BBO) with the pump pulse. In the implementation shown in Fig. 2.1(a) this is done collinearly with a dichroic mirror and the laser fundamental as pump pulse [3,4,31]. In Fig. 2.1(b) a noncollinear geometry for the amplification is chosen with the second harmonic of the pump laser as pump pulse [5,32,33].

The advantage of the first setup is that no frequency conversion for the pump pulse generation is necessary, and therefore the full pulse energy can be utilized. This allows very high overall conversion efficiencies from the pump laser energy to the signal and idler output. This is normally not achievable in a single amplification step as shown schematically in Fig. 2.1(a), but in several (typically 2 to 5) passes through either the same crystal or different crystals. The output of the preceding pass is thereby the seed for the next amplification step.

One disadvantage of this setup is, that amplification only in the NIR region above approximately 1000 nm is possible, and to reach the visible spectral region, additional frequency conversion of the OPA output is needed.

This is in turn the advantage of the second implementation shown in Fig. 2.1(b). Here direct amplification of the visible spectral region, starting from about 450 nm up to about 740 nm, and also in the NIR region starting from about 840 nm up to more than 1600 nm can be achieved. Additionally much broader spectra in the visible spectral region can be amplified.

A realistic implementation of this configuration with two amplification stages as used routinely in our laboratories is depicted in Fig. 2.2

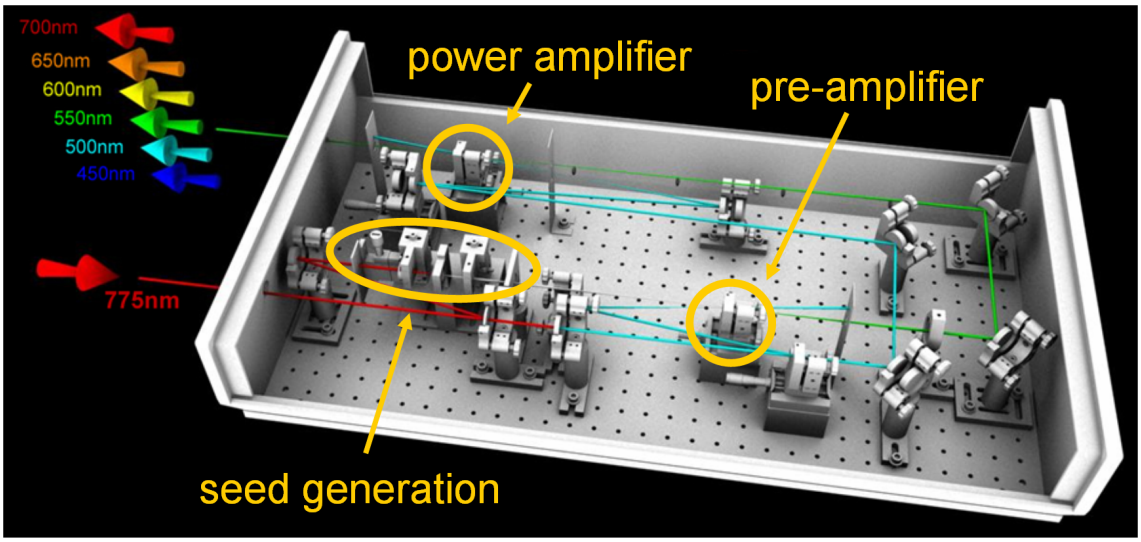

Fig. 2.2 Setup of a two-stage noncollinear optical parametric amplifier. The seed is generated by focusing approximately 400 nJ of the fundamental 775 nm pulses in a sapphire disc. The remaining part is frequency doubled and the second harmonic used for pumping two subsequent amplification stages (courtesy of C. Elsner).

When pumping with a pulse energy of about 250 µJ at 775 nm, this setup typically provides pulses with an energy of around 15 µJ in the blue/green spectral region and around 10 µJ in the red spectral region. Pulse durations of 20 fs are routinely achieved, and compression down to 5.6 fs with chirped mirrors has been demonstrated [34]. The setup is flexible and all parts are easily accessible, so that changes of the pump wavelength (ω / 2ω) or the geometry (collinear / noncollinear) can readily be implemented.

Fig. 2.3(a) shows typical output spectra from a collinear OPA pumped by 775 nm pulses, Fig. 2.3(b) output spectra from a noncollinear OPA (NOPA) pumped by the second harmonic. Both implementations are based on the setup shown in Fig. 2.2.

In the following I want to explain why the output spectra are the way they are and how they can be influenced. Why yields, for example, the 775 nm pumped OPA only spectra starting from about 1000 nm, and why are they so narrow at around 1000 nm, get broader for longer wavelengths and even rise again at the end of the detection range at about 1600 nm? Why can the 387 nm pumped NOPA deliver so broadband pulses in the visible and why are they much narrower in the NIR? Why is there a gap at around 800 nm?

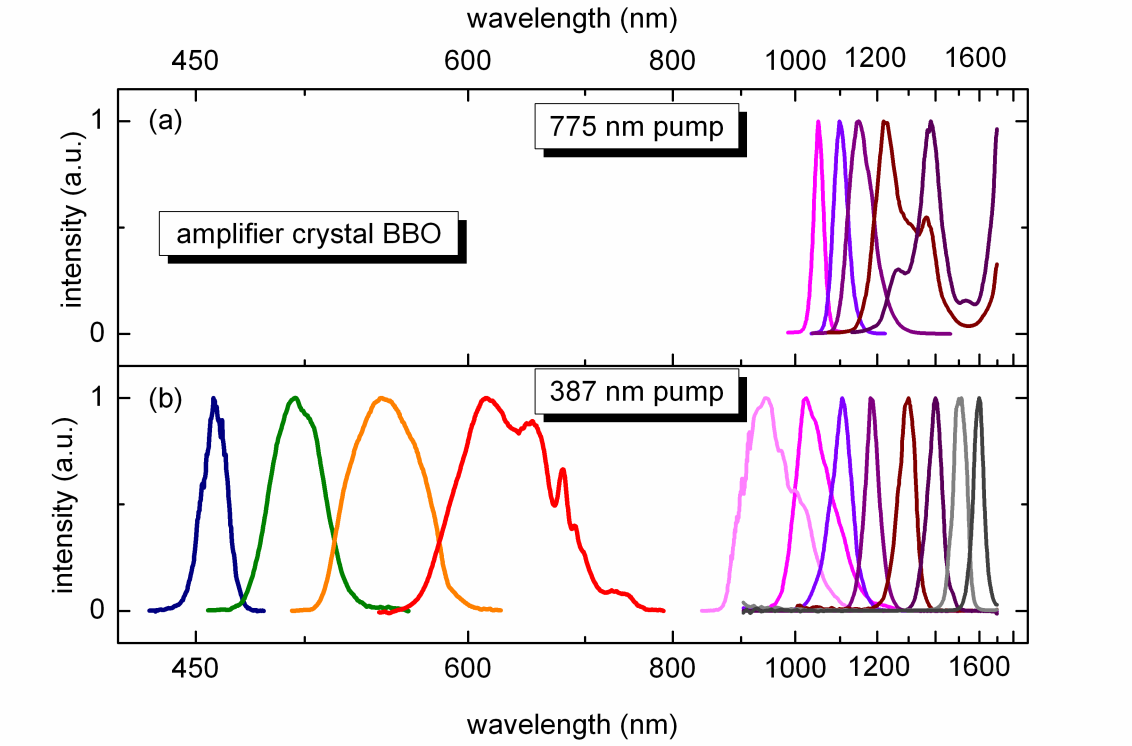

Fig. 2.3 Output spectra obtained from a collinear OPA pumped by 775 nm pulses (upper row), and from a noncollinear OPA pumped by the 2nd harmonic at 387 nm.

These questions, and also the question how the spectral output range be expanded shall be addressed in the following. To do so, first a review of the basic physics of the optical parametric amplification process shall be accomplished and the restrictions for the achievable wavelength range shall be identified.

3. Basic physics of optical parametric amplification and accessible wavelength range

Optical parametric amplification (OPA) is a three-wave-mixing process in a nonlinear medium, in which a high frequency, high energy pump pulse is depleted in favor of an existing lower frequency, lower energy seed pulse that gets amplified (at least parts of it) to the signal pulse. In this process, a third pulse is generated, called idler pulse, whose angular frequency is determined by energy conservation. For the instantaneous angular frequencies ω_P, ω_S, and ω_i of the pump, signal and idler energy conversion reads

$$\hbar\omega_p = \hbar\omega_s + \hbar\omega_i \tag{3.1}$$

This poses a first limitation on the accessible wavelength range with OPA: no pulse with higher frequency than the pump can be amplified. Therefore a suitably high frequency pump has to be provided if a certain wavelength region is to be amplified.

The generation of the signal and the idler pulses are equally essential to the OPA process, which means OPA only happens efficiently if both beams can propagate inside the nonlinear medium. This means the medium must be transparent also for the idler pulse, whose frequency gets lower the closer the signal frequency gets to the pump frequency. This poses a second constraint on the accessible wavelength range. For example, β-barium borate (β-BBO), the most commonly used crystal for OPA, strongly absorbs light with wavelengths above 3200 nm. For a pump beam centered around 512 nm (second harmonic of an Yb:KYW based laser system), this means that signal wavelengths below 610 nm cannot be amplified. This process can also cause crystal damage in high power amplifiers, if amplification is not fully suppressed and a significant amount of the idler is absorbed by the crystal.

Besides energy conservation, momentum conservation (often called phase matching) also has to be fulfilled, at least approximately, for an efficient interaction. This can be written as

$$\hbar k_p = \hbar k_s + \hbar k_i \tag{3.2}$$

with k_p, k_s, k_i being the respective wave vectors. With

$$k = \frac{n\omega}{c} \tag{3.3}$$

where n is the refractive index and c the speed of light, this translates to

$$n_p\omega_p = n_s\omega_s + n_i\omega_i \tag{3.4}$$

In this form, we can see that phase matching in normal dispersive media, where $n_p > n_s > n_i$, is only possible in a birefringent material. Additionally the material should have a high 2nd order susceptibility and high damage threshold. The most common materials that fulfill these requirements, and are therefore nowadays used in OPA besides BBO, are lithium niobate ($LiNbO_3$), lithium iodate ($LiIO_3$), (deuterated) potassium dihydrogen phosphate ((D)KDP), potassium titanyl phosphate (KTP), and bismuth triborate (BiBO). With the exception of KTP and BiBO, which are positive biaxial, all these materials are negative uniaxial, which means that their extraordinary refractive index n_e is smaller than the ordinary re-

fractive index n_o. Therefore the pump pulse has to be an extraordinary beam. If signal and idler both are identically polarized (ordinary in case of a negative uniaxial crystal), we speak of type I phase matching, when only one of the two is ordinary polarized and the other extraordinary, we speak of type II phase matching [35]. The refractive index n of an extraordinary beam with an angle θ between its polarization vector and the optical axis of the crystal is given by

$$n(\theta) = \sqrt{\left(\frac{\cos(\theta)}{n_o}\right)^2 + \left(\frac{\sin(\theta)}{n_e}\right)^2}^{-1} \tag{3.5}$$

In principle, phase matching restricts the accessible wavelength region further, as can be seen exemplarily for BBO and $LiNbO_3$ in Fig. 3.1.

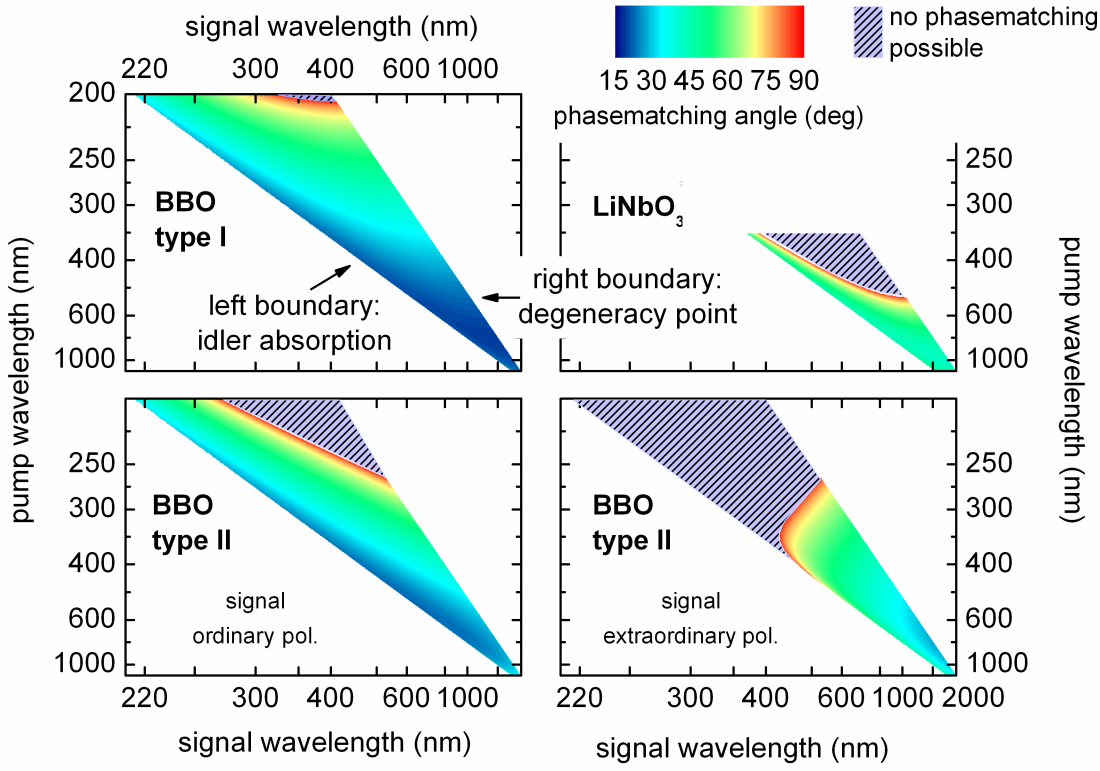

Fig. 3.1 Color-coded is the phase matching angle for phase matched OPA in dependence of the signal wavelength for different pump wavelengths. The short wavelength boundary for the signal is given by idler absorption, the long wavelength boundary by the degeneracy point. In the shaded areas the phase matching condition cannot be fulfilled.

In the shaded regions OPA is not restricted by energy conservation nor idler absorption, but only by phase matching. For these wavelength combinations, n_e for the pump wavelength is too high that equation (3.4) can be fulfilled.

For type I phase matching (upper panels) this happens only close to the absorption edge of the respective crystal, which means that two-photon absorption (TPA) is already strong for these pump wavelengths. Since in OPA the pump is typically very intense (typical intensities on the crystal for fs pulses are in the order of 100 GW/cm^2), these pump wavelengths are unfavorable anyway, so that the phase matching restriction is of minor practical rele-

vance for type I phase matching. It is, however, important in second-harmonic generation and sum-frequency mixing, where the high-frequency beam is less intense.

It is also important for type II phase matching, where the refractive index for the pump has to be even lower for a given wavelength combination than for type I phase matching (in a negative uniaxial crystal). This leads to a larger restricted region where phase matching cannot be fulfilled. This can be seen in the lower two panels of Fig. 3.1. For example for type II phase matching with an extraordinary polarized signal, and a pump wavelength of 400 nm, a signal at 460 nm cannot be amplified due to this constraint.

A fourth factor that influences the accessible wavelength range is the availability of seed photons. Although OPA also happens spontaneously without external seed (then called optical parametric generation (OPG) or parametric superfluorescence) [36], this amplified light has low coherence and cannot be compressed or focused properly. Additionally it fluctuates strongly in spectrum and energy from shot to shot (see Fig. 3.2, upper row). Only when averaging about 500 shots, a stable distribution emerges. Nevertheless this OPG/OPA scheme was used for many years [37] until much more stable seed sources, as for example supercontinuum generation in bulk materials, have been found (see Fig 3.2, lower row).

Nowadays, except for OPOs, where the many amplification steps inside the cavity stabilize spectrum and energy, the superfluorescence is therefore hardly used any more. In contrast, it poses typically an unwanted background that one tries to suppress as much as possible, especially in high power applications [38].

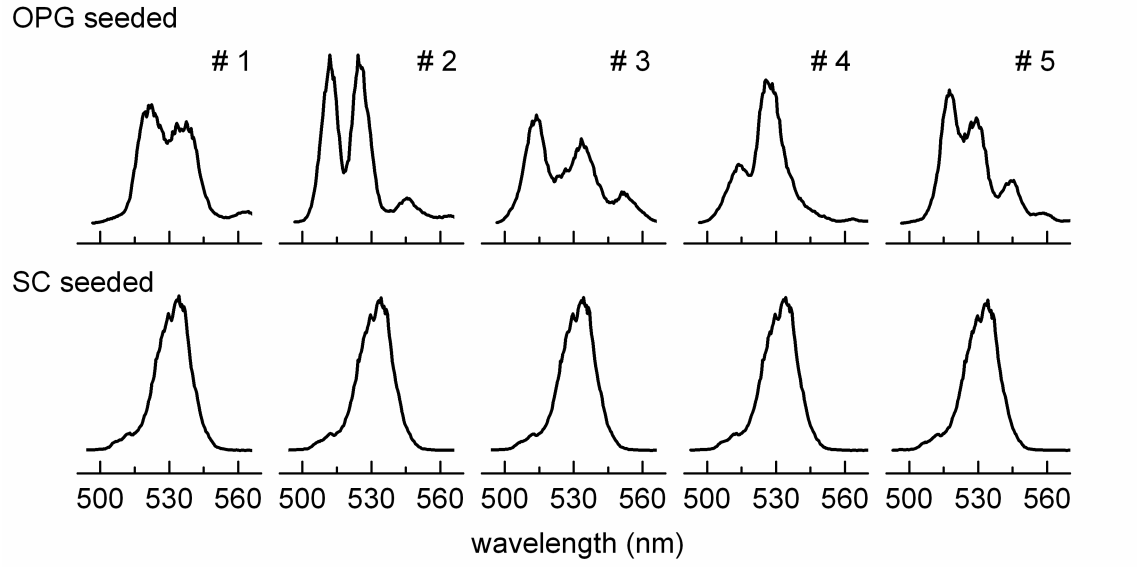

Fig. 3.2 Single shot output spectra of an OPA seeded by optical parametric generation (upper row), and seeded by a supercontinuum (SC) generated in sapphire (lower panel).

Today, supercontinuum generation in bulk materials, with the most commonly employed being sapphire and yttrium aluminum garnet (YAG) [30], is one of the most widely used methods for the seed generation in spectroscopy. When pumped with ultrashort pulses, extreme spectral broadening can be achieved in these materials. On the short wavelength side of the pump a nearly flat plateau arises, whose cutoff is nearly independent of the pump wavelength [30]. On the long wavelength side an exponential decrease is frequently ob-

served. In both regions the phase is continuous and mainly given by material dispersion, with a group delay jump on the order of the pump pulse duration between them [32]. Nevertheless both regions are phase-locked [30]. The energy stability of the supercontinuum is close to or even better than the stability of the pump pulse [30] and the spectral shape nearly identical from shot to shot. This makes it a very good seed source for OPA. However, the total energy converted to new frequencies is only about 1 % of the pump energy, which causes a strong change in intensity around the pump wavelength. This, together with the jump in group delay, makes it nearly impossible to amplify smooth spectra in the vicinity of the pump wavelength.

In summary, we have identified four restrictions for the accessible wavelength range in OPA, namely energy conservation, idler absorption, phase matching and the availability of seed photons. Figure 3.3 illustrates these restrictions for the case of noncollinear OPA (NOPA) in BBO pumped by the 2nd harmonic of an Yb:KYW based pump laser system at 512 nm, with a seed generated by 1025 nm pulses in a YAG crystal. Although seed photons are available already below 512 nm, energy conservation prohibits amplification in this region. Between 512 nm and ~ 610 nm no amplification is possible due to idler absorption. In the wavelength range from 610 nm to about 960 nm amplification works very well, before the vicinity to the pump wavelength causes problems up to about 1150 nm. Up to about 1500 nm amplification again works well, before the seed ceases.

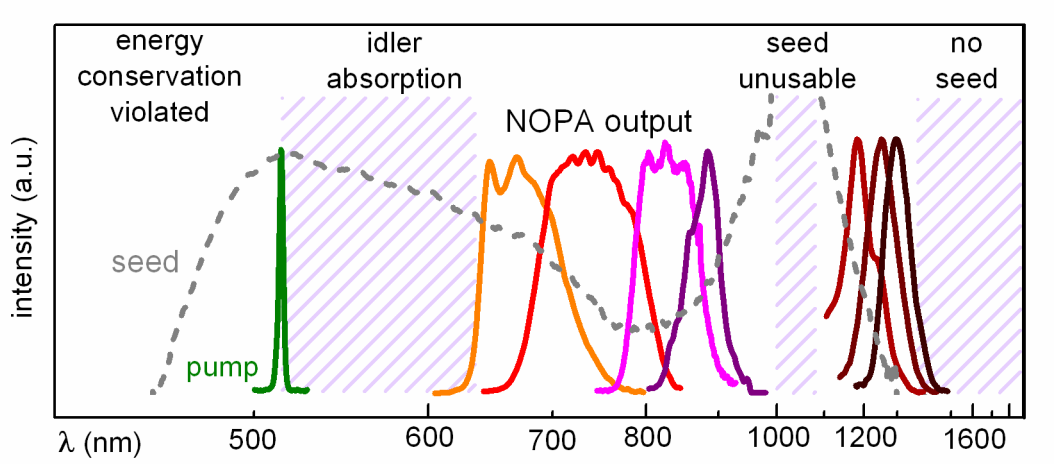

Fig. 3.3 Directly accessible wavelength range by noncollinear optical parametric amplification in a BBO crystal with a pump pulse centered at 512 nm and its limitations. In this case phase matching does not restrict the accessible range.

Extending the accessible tuning range

To extend the output wavelength range, new concepts have to be applied. The most straightforward possibility to amplify pulses with shorter wavelengths is to use pump pulses with shorter wavelengths. For an Yb^{3+} based pump laser system, this is very conveniently possible by using the third harmonic of the pump laser with a central wavelength around 345 nm. With such pump pulses a tuning range without any gap from 440 nm to 990 nm was demonstrated (see [A1]).

The use of pump pulses with even shorter wavelength becomes more and more difficult because of the increasing TPA in the amplifier crystal. The crystal with the best compromise of amplification bandwidth, nonlinearity and practicability for amplification in the wavelength region from 300 to 450 nm is BBO [39]. However, its TPA coefficient β rises strongly below 340 nm, which leads to strong absorption. This can be seen in Fig. 3.4 for a 2 mm thick BBO crystal and typical pump pulse intensities for efficient amplification in the femtosecond regime. Nevertheless several groups have studied femtosecond OPA with a pump pulse centered around 266 nm [13,39-40]. Yet all these approaches suffer from very low energy conversion efficiencies below 1 % [13,39,40], or peak gain factors of only 12 [41]. According to Fig. 3.4 amplification with a pump wavelength of 345 nm is only weakly affected by TPA, and it might still be reasonable with wavelengths down to 320 nm, whereas it will always be strongly hampered by TPA for wavelengths far below. For amplification of narrowband pulses with Fourier-limits well above 100 fs, crystals like lithium triborate (LBO) and (D)KDP become available, which have significantly lower TPA coefficients [42]. However, they also have lower nonlinearities, so that in the end amplification in the visible in BBO and subsequent frequency doubling with a thick BBO crystal seems more reasonable.

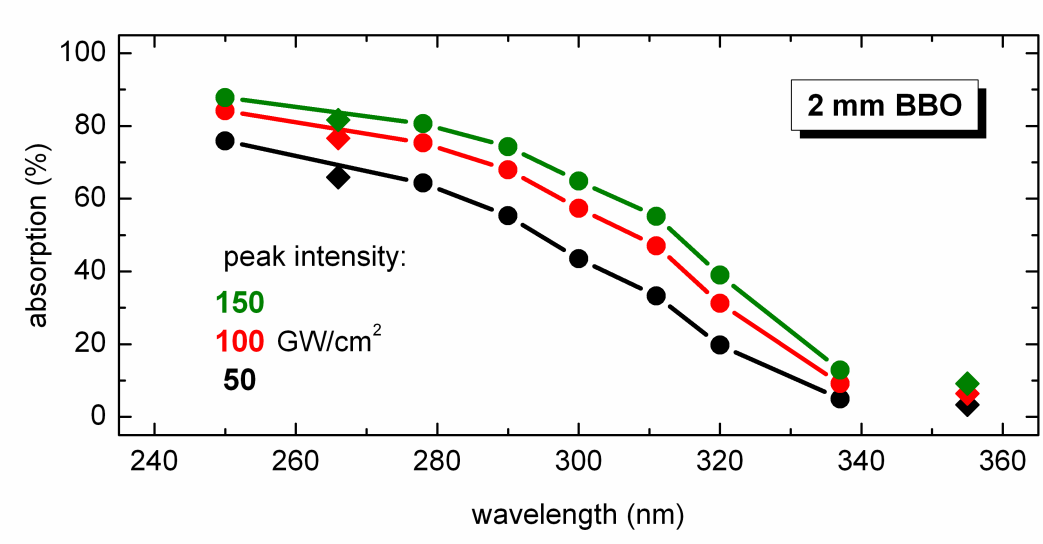

Fig. 3.4 Calculated absorption in a 2 mm thick BBO crystal due to two photon absorption for a pulse with Gaussian intensity distribution in space and time with a peak intensity of 50, 100, and 150 GW/cm^2, respectively. The values of the TPA coefficients are taken from chapter 2 of part II (bullets) and [42,43] (diamonds).

A possibility to extend the output range to longer wavelengths where no seed photons are available, is the use of the idler beam in a collinear geometry. This is shown in Fig. 3.5. The upper panel shows the spectra normalized to the pulse energy obtained in a noncollinear geometry directly seeded by the near-infrared part of the supercontinuum with a pump pulse centered at 512 nm. The lower panel shows the idler spectra and energies obtained with the same pump pulse conditions, but in a collinear geometry when the visible part of the supercontinuum is used as seed.

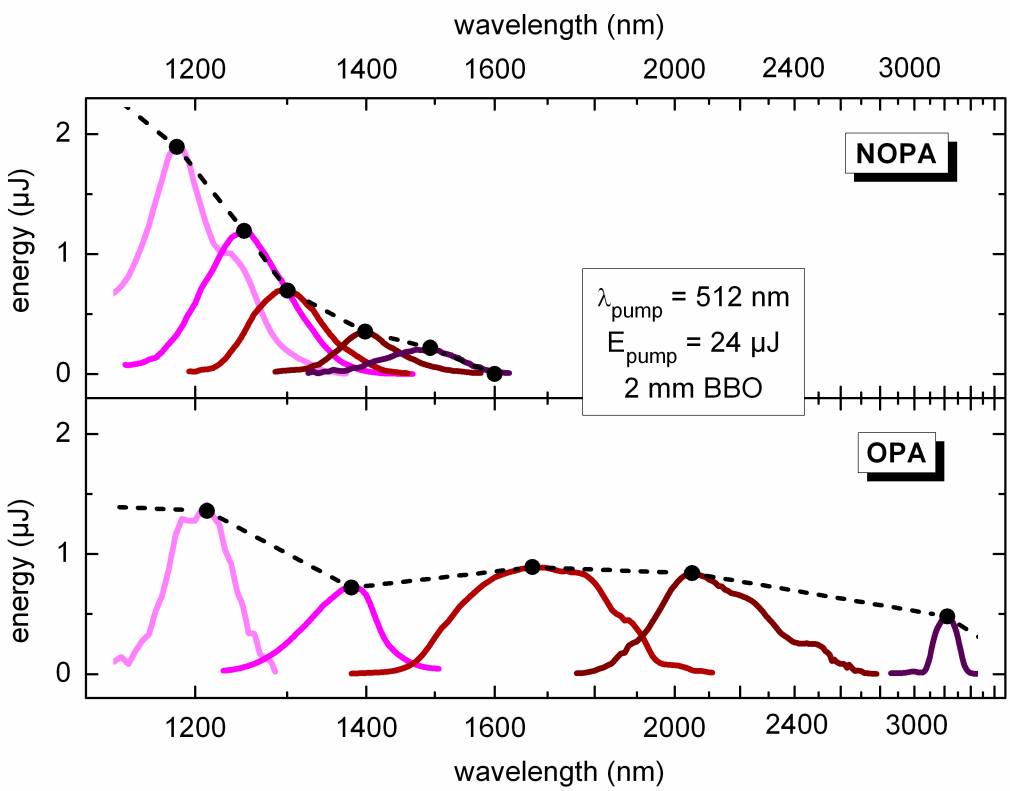

Fig. 3.5 Comparison of the output spectra and energies from a NOPA that directly amplifies the supercontinuum and a collinear OPA that amplifies the visible part of the supercontinuum and provides an idler output in the NIR. Both amplifiers were pumped by pulses centered at 512 nm with an energy of 24 µJ and a duration of 220 fs and used a 2 mm thick BBO crystal.

As can be seen, this method allows generating idler pulses from about 1200 nm to 3200 nm in BBO. To get further into the infrared crystals like $LiNbO_3$ or $LiIO_3$ have to be used, that have an absorption edge further in the infrared. However, they suffer from TPA of the pump pulse at 512 nm, and the fundamental at 1025 nm has to be used. This in turn allows no idler in the region below 3300 nm, because this requires seed light above 1500 nm. To get a full coverage of the infrared region from about 1100 nm up to 5500 nm, more complex concepts with cascaded amplification stages have to be used. These will be discussed in detail in chapter 6.

The last gap to be closed is the region around the wavelength that generates the seed continuum. If pumping with the third harmonic of this wavelength is feasible, as e.g., for 1025 nm, then again the idler can be used in a collinear geometry. If this is not feasible, as e.g., for 800 nm, again more effort with cascaded stages is required. One possibility is to generate a second supercontinuum with a different, preferably longer pump wavelength. For example a first OPA pumped by 400 nm light can amplify a signal wavelength of 1200 nm, which then generates a supercontinuum that will smoothly cover the 800 nm region [44].

4. Controlling the amplification bandwidth

We now know how to reach a wide wavelength region by OPA, however nothing has been said about the achievable spectral bandwidth. The amplification bandwidth is mainly determined by two parameters: the evolution of the wave vector mismatch with wavelength and the time-overlap between the pump and seed pulses.

The relation between the wave vector mismatch and the amplification bandwidth

The wave-vector mismatch Δk is defined as

$$\Delta\vec{k} = \vec{k}_p - \vec{k}_s - \vec{k}_i \tag{4.1}$$

To connect it to the parametric gain in OPA, the three coupled wave equations that describe the evolution of the amplitudes A_P, A_S, A_i of the envelopes of the electric fields of pump, signal and idler have to be solved. For plane waves propagating in the z direction they read

$$\frac{\partial A_p}{\partial z} = -i\frac{\omega_p d_{eff}}{n_p c_0} A_i A_s e^{i\Delta kz} \tag{4.2}$$

$$\frac{\partial A_s}{\partial z} = -i\frac{\omega_s d_{eff}}{n_s c_0} A_i^* A_p e^{-i\Delta kz} \tag{4.3}$$

$$\frac{\partial A_i}{\partial z} = -i\frac{\omega_i d_{eff}}{n_i c_0} A_s^* A_p e^{-i\Delta kz} \tag{4.4}$$

Here d_{eff} is the effective nonlinear optical coefficient that depends on the propagation direction of the beams in the crystal and their polarizations. The deduction of these equations from the Maxwell equations and their solution can be found, e.g., in [45,46]. For the assumption of negligible pump depletion ($A_P \cong$ const.), the parametric gain G for the signal after propagating the distance L through the nonlinear crystal can be written as

$$G = \frac{I_s(L)}{I_s(0)} = 1 + \frac{\Gamma^2}{g^2}\sinh^2(gL) \tag{4.5}$$

with the intensity of the signal I_S, and

$$g = \sqrt{\Gamma^2 - \left(\frac{\Delta k}{2}\right)^2} \tag{4.6}$$

with the nonlinear coefficient Γ, that is defined as

$$\Gamma^2 = \frac{8\pi^2 d_{eff}^2 I_p}{n_i n_s n_p \lambda_i \lambda_s \varepsilon_0 c} \tag{4.7}$$

Here I_p is the pump intensity and ε_0 the vacuum permittivity.

Γ and Δk both depend on the signal and idler wavelength, and therefore also the gain. The influence of the crystal length on the amplification bandwidth is not easily seen from these equations. In contrast to SHG, where the bandwidth is in good approximation inversely pro-

portional to the crystal length [46], the influence in OPA is typically weaker. In some cases longer crystals can even lead to spectrally broader output pulses as can be seen in Fig. 5.8.

According to (4.5) and (4.6) the highest gain is achieved when $\Delta k = 0$, and it falls to $1 + (\Gamma \cdot L)^2$ when Δk approaches 2Γ. Since Δk depends on the signal wavelength, the condition for efficient broadband amplification is that Δk only varies slowly with wavelength around the phase matching point where Δk is zero. This means that in a Taylor expansion of Δk with respect to λ_S

$$\Delta\vec{k}(\lambda_S) = \Delta\vec{k}(\lambda_{S0}) + \left.\frac{\partial\Delta\vec{k}}{\partial\lambda_S}\right|_{\lambda_{S0}} \cdot (\lambda_S - \lambda_{S0}) + \frac{1}{2}\left.\frac{\partial^2\Delta\vec{k}}{\partial\lambda_S^2}\right|_{\lambda_{S0}} \cdot (\lambda_S - \lambda_{S0})^2 + \ldots \quad (4.8)$$

with $\Delta\vec{k}(\lambda_{S0}) = 0$, the term $\frac{\partial\Delta\vec{k}}{\partial\lambda_S}$ must vanish for λ_{S0}.

This condition can also be written in terms of the angular frequency ω_S of the signal

$$\Delta\vec{k}(\omega_S) = \Delta\vec{k}(\omega_{S0}) + \left.\frac{\partial\Delta\vec{k}}{\partial\omega_S}\right|_{\omega_{S0}} \cdot (\omega_S - \omega_{S0}) + \frac{1}{2}\left.\frac{\partial^2\Delta\vec{k}}{\partial\omega_S^2}\right|_{\omega_{S0}} \cdot (\omega_S - \omega_{S0})^2 + \ldots \quad (4.9)$$

with the condition that the term $\frac{\partial\Delta\vec{k}}{\partial\omega_S}$ must vanish for ω_{S0}.

Written out that is $\frac{\partial\Delta\vec{k}}{\partial\omega_S} = \frac{\partial\vec{k}_p}{\partial\omega_S} - \frac{\partial\vec{k}_S}{\partial\omega_S} - \frac{\partial\vec{k}_i}{\partial\omega_S} = -\frac{\partial\vec{k}_S}{\partial\omega_S} + \frac{\partial\vec{k}_i}{\partial\omega_i}$

because k_P does not depend on the signal angular frequency, and the change in signal angular frequency is equal to minus the idler angular frequency due to energy conservation.

If we now assume a collinear geometry, and recall that the group velocity is defined as

$$v_g = \frac{\partial\omega}{\partial k} \quad (4.10)$$

we find that

$$\frac{\partial\Delta k}{\partial\omega_S} = \frac{1}{v_{g,i}} - \frac{1}{v_{g,s}} \quad (4.11)$$

That means, that **in a collinear geometry**, **a broad amplification bandwidth** for which $\frac{\partial\Delta k}{\partial\omega_S}$ vanishes **is equivalent to a matching of the group velocities of signal and idler**.

This is fulfilled at the degeneracy point, where the signal and idler wavelength are equal to twice the pump wavelength. Indeed very broadband amplification is possible around this point [47].

In some cases a second wavelength combination with matching group velocity exists, when signal and idler wavelengths are on opposite sides of the zero dispersion point of the amplifier material. Here also broadband amplification is possible. This is illustrated in Fig. 4.1, which shows the group velocity of BBO with its zero dispersion point at 1488 nm in dependence of frequency.

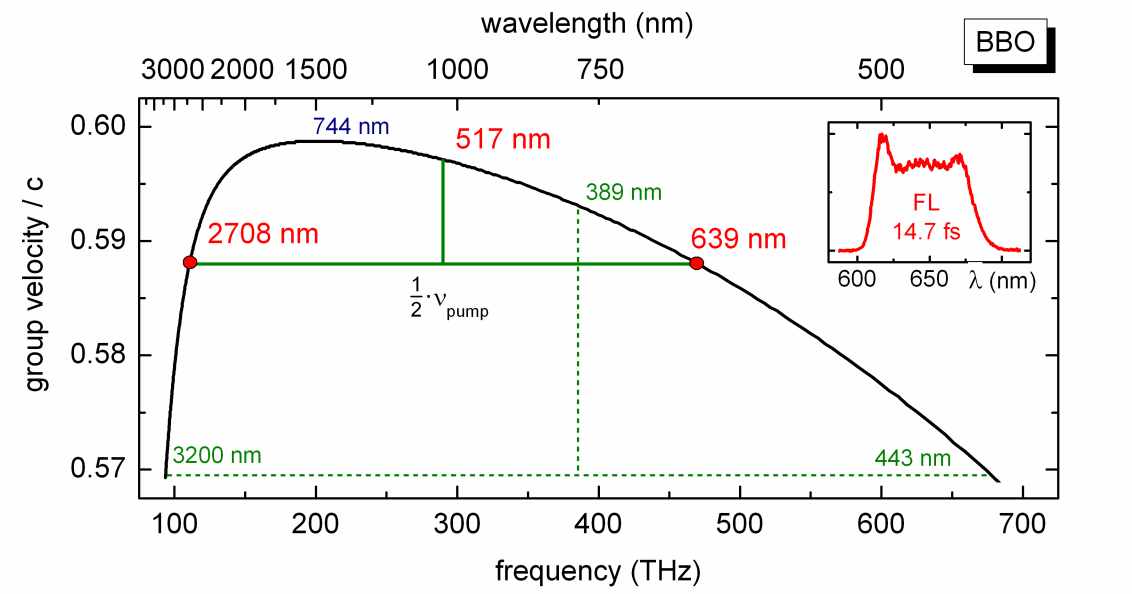

Fig. 4.1 Group velocity of BBO in dependence of frequency. For pump wavelengths between 389 nm and 744 nm, signal/idler pairs exist with identical group velocities (apart from degeneracy), allowing for broadband amplification in a collinear geometry. In the graph these signal/idler pairs are connected by horizontal lines, the vertical lines give the corresponding pump wavelengths. The inset shows an example of an amplified spectrum for a pump wavelength of 517 nm.

For pump wavelengths shorter than 744 nm, wavelength combinations of signal and idler can be found with the same group velocity. In BBO this is possible for pump wavelengths down to approximately 389 nm, with a matching signal/idler pair of 443 nm and 3200 nm. For even lower pump wavelengths, the appropriate idler would have to be above 3200 nm where BBO absorbs strongly. For a pump wavelength of 744 nm, the degeneracy and the zero dispersion point are identical, which is equivalent to a vanishing of the third term in equation (4.8), which should lead to an extremely broadband amplification around this point.

Fig. 4.2 illustrates these considerations for pump wavelengths of 807 nm and 1025 nm. The green dots show the experimentally obtained Fourier-Limits for amplification in a 1.5 mm thick $LiNbO_3$ crystal. The lines show the calculated Fourier-Limits for different amplifier crystals when taking into account only the second term of equation (4.8) and the experimental parameters for the pump intensity. For 807 nm pumping, group velocity matching apart from the degeneracy point is possible in $LiNbO_3$ and $LiIO_3$, since this pump wavelength is shorter than half of their zero dispersion wavelengths at 1902 nm and 2006 nm respectively. The corresponding idler wavelengths are 3.45 µm for $LiNbO_3$ and 4.01 µm for $LiIO_3$. Here broadband phase matching is possible, which is nicely confirmed experimentally with a measured Fourier-Limit of 27 fs at 3.4 µm. The limiting factor here and especially for the wavelengths below 2.5 µm was the bandwidth of the seed pulses, which in this case were no supercontinuum, but the output pulses of another OPA. For the longer wavelengths the GVM between signal and idler gets more and more severe, and only much longer Fourier-Limits are possible. Here the measured and calculated Fourier-Limits agree very well, which shows that the applied approximations provide reasonable results. Group velocity matching in BBO apart from the degeneracy point is not possible for this pump wavelength.

For a pump wavelength of 1025 nm for all three crystals group velocity matching is only possible at the degeneracy point any more. This results in higher Fourier-Limits already at 3.5 µm, where pumping at 807 nm still yielded short pulses. Experimental and calculated values agree again very well.

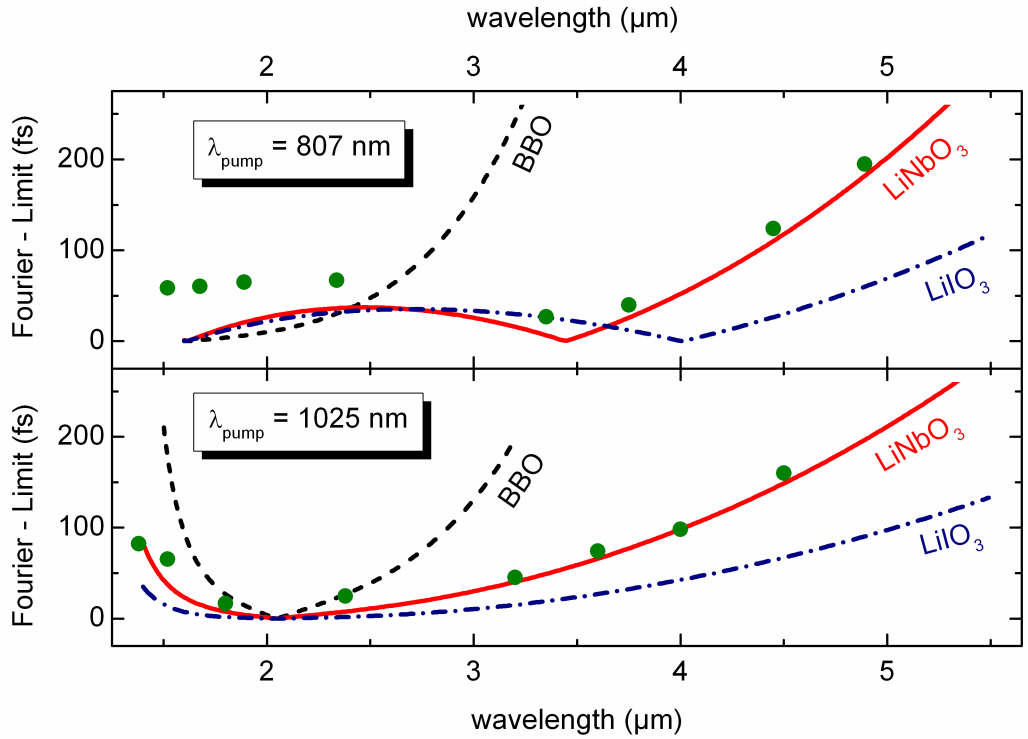

Fig. 4.2 Measured Fourier-Limits of pulses amplified in a $LiNbO_3$ crystal (1.5 mm thick) in collinear geometry pumped by (a) 807 nm and (b) 1025 nm (dots). The lines show the calculated Fourier limits for BBO, $LiNbO_3$, or $LiIO_3$ as amplifier crystal with the experimental parameters for crystal thickness and pump intensity and agree well with the measured values.

Enhancing the amplification bandwidth by a noncollinear geometry

As can be seen in Fig. 4.1 the group velocity in BBO has its most flat evolution in the near-infrared (NIR) spectral region, much more so than in the visible. Therefore originally the prevailing opinion was that working in the NIR as long as possible to keep the group velocity mismatch small is advantageous for the generation of broadband pulses [48]. If visible pulses were needed, these were generated by SHG or sum-frequency mixing only after amplification.

Later it was realized, that the vector equation $\frac{\partial \Delta \vec{k}}{\partial \lambda_s} = 0$ can be fulfilled for a much larger wavelength region if a noncollinear geometry is applied, with a noncollinearity angle α between the pump and signal wave vector. In this case, vanishing of this term is equivalent to a matching of the projections of the group velocities of signal and idler in signal propagation direction [44]. The generation of sub-20-fs pulses by this technique was first demonstrated for an OPO [49], and shortly thereafter for a single stage traveling wave amplifier by several groups [5,32,33]. Today, noncollinear OPA is the standard technique for the amplification of

ultrabroad bandwidth pulses. This is comprehensible when looking at Fig. 4.3, which shows the huge enhancement in amplification bandwidth that is possible by a noncollinear geometry.

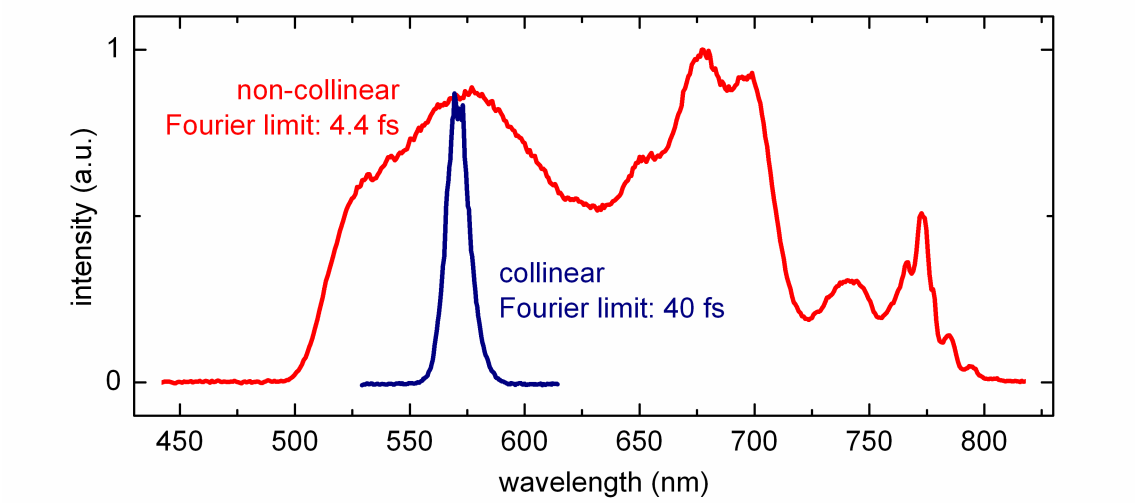

Fig. 4.3 Spectra achieved by collinear (blue) and noncollinear (red) OPA in BBO with a pump wavelength of 387 nm, demonstrating the huge enhancement in amplification bandwidth through a noncollinear geometry.

To be able to match the projections of the group velocities of signal and idler in signal propagation direction, the group velocity of the idler must be higher than that of the signal. In BBO that means that for wavelengths below 1488 nm the signal must be the higher frequency beam. For 345 nm pumping that means that for signal wavelengths up to 690 nm a noncollinear geometry is advantageous and broadband amplification can be achieved (see Fig. 4.4). Simulations show that for a noncollinearity angle of 4.3° and a phase matching angle of 36.6° simultaneous amplification from 435 nm to 690 nm is possible, allowing for a Fourier limit of about 3 fs. If broadband pulses at longer wavelengths are needed, pumping with for example 512 nm pulses is to prefer, allowing noncollinear phase matching up to 1025 nm.

The maximum of the group velocity in BBO at 1488 nm and the decreasing group velocity afterwards allows for a “reversed” phase matching scheme in the infrared. Here broadband noncollinear amplification can be performed for a lower frequency signal beam, and a spectrally dispersed higher frequency idler (see Fig. 4.4, pump wavelengths 800 nm and 1025 nm). With an 800 nm pump, a noncollinearity angle of 3.3° and a phase matching angle of 21.4° simultaneous amplification should be feasible from about 1555 nm up to 2840 nm with a Fourier-Limit of below 4 fs, according to simulations. This of course assumes that a seed pulse covering this wavelength region is available.

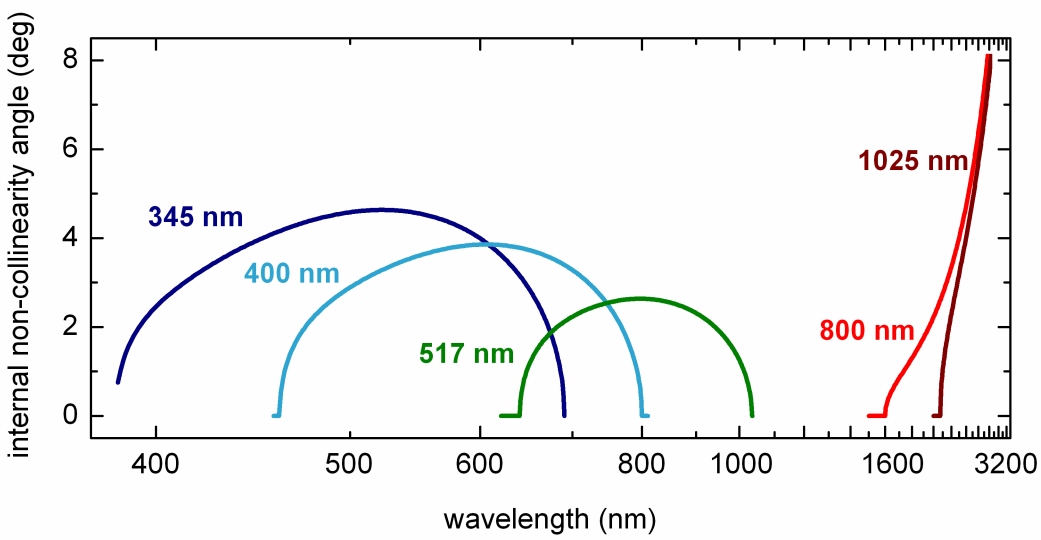

Fig. 4.4 Optimal internal noncollinearity angle for broadband phase matching in a BBO crystal around a given signal wavelength for different pump pulse wavelengths. The regions where the noncollinearity angle is different from 0 can be advantageously exploited by a non-collinear geometry. Outside, a collinear geometry is typically to prefer.

The disadvantage of a noncollinear geometry is, that now the idler is spectrally dispersed and therefore difficult to use. Although it can be recombined [50], this is quite inconvenient and was to date not used for applications. A conceivable application of the idler however could be the use as a probe whitelight in pump-probe spectroscopy. For example the idler corresponding to the broadband signal spectrum shown in Fig. 1.1 covers a wavelength region from 820 nm to 2050 nm. A region which is spectroscopically interesting, and only accessible with some effort otherwise. By relay imaging of the amplification spot in the BBO crystal to the spectroscopic sample this could be readily utilized.

Influence of the pump and seed pulse duration on the amplification bandwidth

Apart from the phase matching a prerequisite for broadband amplification is of course that the pump pulse overlaps in time with all frequency components of the seed that are to be amplified. For ps pump pulses commonly employed in OPCPA this typically poses no problems, although a proper matching of pump and seed pulse duration is important for an efficient amplification [A2]. For fs pump pulses more care is needed and it is also important to avoid material dispersion in the seed beam path. This can mean for example using only reflective optics. If a supercontinuum generated in bulk material is used as seed, some dispersion already in the generating crystal is inevitable, as is the dispersion experienced in the amplifier crystal. For pump pulses shorter than approximately 100 fs, a compression of the supercontinuum or, most often more practical, a chirping of the pump pulse might therefore be necessary to exploit the full amplification bandwidth.

On the other hand, narrowband pulses might sometimes be in demand for spectroscopic applications, e.g., to excite only a specific vibronic state. This can be in turn achieved by chirping the continuum seed, so that only a narrow spectral part of it overlaps in time with the pump pulse. When this is combined with a noncollinear geometry, very simple frequency

tuning by only changing the time delay between pump and seed can be achieved over a wide frequency range. The spectral width of the amplified pulses is in this case adjusted by the amount of chirp introduced in the seed, which can be done for example by inserting materials of different thickness or dispersion in the seed path (Fig. 4.5, upper panel). A limit on how narrowband the amplified pulses can get is however set by the pump pulse duration. This is because the amplified output pulses have a duration that is connected to the pump pulse duration, and therefore have to have a certain spectral width according to the Fourier constraint. The output pulse will gain this spectral width, even if the seed pulse is monochromatic (Fig. 4.5, lower panel). This leads to the seemingly surprising fact that in this case a chirping of the pump pulse will lead to a narrower amplified spectrum [51]. Apart from the pump pulse duration, the duration of the output pulses is determined by the gain factor and material dispersion.

Chirping of the seed also helps to amplify wavelengths close to the fundamental light used for generating the seed supercontinuum in bulk material. Amplification in the vicinity of this wavelength always tends to amplify the fundamental pulse, because it contains much more seed photons. Therefore it has to be separated in time from the light that is to be amplified. In this way wavelengths up to 750 nm and from 810 nm onwards can be amplified for a supercontinuum generating wavelength of 775 nm [52].

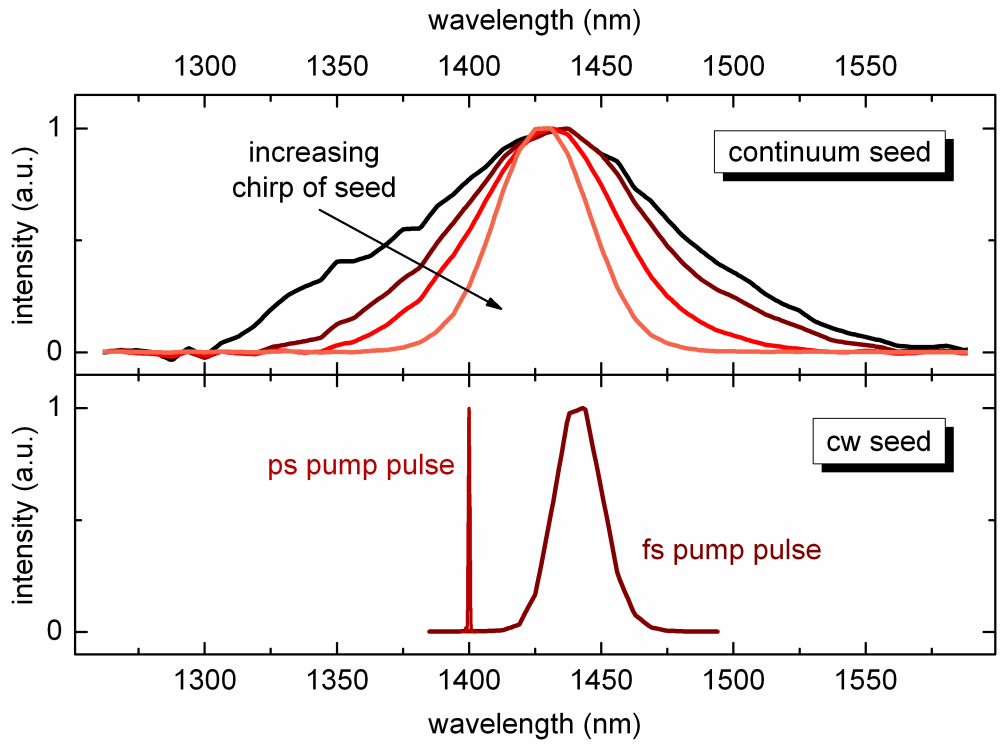

Fig. 4.5 The amplified output spectra get more and more narrow the more the seed continuum is chirped (upper panel), down to a minimum given by the pump pulse duration. To achieve even smaller spectral widths, a longer pump pulse has to be used, even for a quasi monochromatic cw seed (lower panel). The pump pulses employed here had a duration of 150 fs and 7 ps, respectively.

5. Efficiency in optical parametric amplification

The overall energy efficiency of a (N)OPA, defined as the ratio of the incoming pump pulse energy to the energy of the output pulse in the desired wavelength range is determined by a number of factors. First of all by the gain in the amplification process itself, given approximately by formula (4.5), but also by the available seed energy, the efficiency of any frequency conversion steps to generate the necessary pump pulses, and the correct distribution of the pump energy in the potentially several existing amplification stages.

Typical overall energy efficiencies are in the range of a few percent with a maximum typically around 10 % for a certain fraction of the tuning range, although efficiencies of up to 20 % have been observed in our group. The quantum efficiencies of the amplification process, defined as the number of the signal photons divided by the number of the incoming pump photons reach up to about 40 %. Even higher quantum efficiencies typically cause beam distortions, since then the pump intensities are so high that strong parasitic nonlinear processes occur in the amplifier crystal. This includes for example self-focusing of the pump, supercontinuum generation and back-conversion of signal and idler to the pump wavelength [53].

Although formula (4.5) is only valid for small quantum efficiencies because it neglects pump depletion, it still gives a good insight in the important dependencies of the gain. For the case of perfect phase-matching ($\Delta k = 0$) and the assumption $\Gamma L >> 1$, formula (4.5) can be further simplified to

$$G = \frac{1}{4}\exp(2\Gamma L) = \frac{1}{4}\exp\left(4\pi\sqrt{\frac{2d_{eff}^2 I_p}{n_i n_s n_p \lambda_i \lambda_s \varepsilon_0 c}}L\right) \tag{5.1}$$

This shows that the gain depends exponentially on the effective nonlinearity d_{eff}, the crystal length and the square root of the pump intensity. The effective nonlinearity is determined by the choice of the amplifier material and the phase-matching type, and hence no tunable parameter. In general one will choose the crystal with the highest effective nonlinearity that additionally fulfills the required phase-matching properties and has a high enough damage threshold. For amplification in the visible region this typically is BBO with a d_{eff} around 2 pm/V, for wavelengths above 2 to 3 µm $LiNbO_3$ ($d_{eff} \approx 4$ pm/V) and $LiIO_3$ ($d_{eff} \approx 1.6$ pm/V) are good choices (all d_{eff} values are for type I phase-matching). The pump intensity can rather easily be changed, e.g., by varying the spot size of the pump pulse on the amplifier crystal, and is therefore an important parameter to control the gain. Typical pump intensities used for amplification in BBO are in the range of 150 to 200 GW/cm². For intensities higher than 400 GW/cm², we observe beam break-up in a 2 mm thick BBO crystal, which renders the output pulse useless for most applications. This value is still below the damage threshold of BBO for femtosecond pulses, which is therefore not the limiting factor for the pump intensity that can be sensibly used. For other crystals this can be different. For example we measured the damage threshold of $LiIO_3$ for 800 nm pulses (150 fs duration) to 180 GW/cm², which is below the occurrence of too strong parasitic nonlinear processes. When raising the pump intensity one should therefore act with caution.

Influence of the crystal orientation in a noncollinear geometry

Apart from the pump intensity, the pump beam diameter is also subject to certain limitations, originating in the walk-off of the extraordinary pump beam and the noncollinearity between signal, pump and idler. If the beams get too small, they will completely separate spatially in the crystal and only a fraction of the crystal is effectively used. The walk-off of the extraordinary beam is also present in a collinear geometry, so that even here too small beam diameters lead to a separation of the beams. In a noncollinear geometry, a crystal geometry can be chosen that partially compensates the walk-off (called "walk-off compensating orientation", see Fig. 5.1) and allows a very small angle between pump and signal [49,54]. However this leads to a reduced spatial overlap between pump and idler, which is equally essential for a high parametric gain. The reversed crystal orientation (achieved experimentally by rotating the crystal by 180° and readjusting the phase-matching angle), called "tangential phase-matched orientation" [54,55], consequently leads typically to a higher output energy. However, here the beam profile of the output beam is often elongated, whereas the beam profile achieved in the walk-off compensated orientation is more round. Additionally a good spatial overlap of the seed beam and the amplified output, which is not ensured automatically, can only be achieved in this configuration. This is especially important, if two or more amplification stages are to be combined that amplify different spectral parts [A2], or that have only a low gain factor in the single digit range.

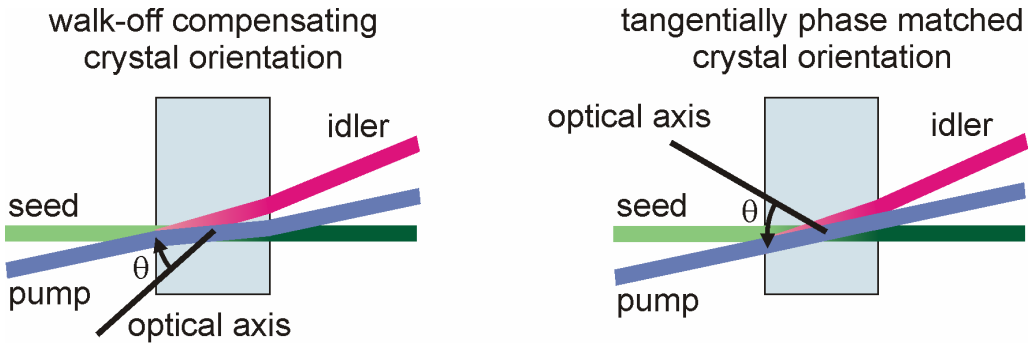

Fig. 5.1 The optical axis can be arranged in two ways with regard to the seed while maintaining the same phase matching angle θ with the pump. Since the walk-off always directs the pump away from the optical axis in BBO, the configuration in which the pump is located between seed and optical axis shifts the pump closer to the seed (left). In the configuration where the seed is located between the optical axis and the pump, the pump gets shifted closer to the idler (right).

The disadvantages of the walk-off compensated orientation are a reduced angular acceptance bandwidth towards the pump beam, which can be important for strongly focused pump pulses [54], and the occurrence of parasitic SHG of the signal beam at wavelengths where a noncollinear geometry is advantageous (see table 1 and [56]).

pump wavelength	**345 nm**	**400 nm**	**517 nm**
phase matching angle	$\theta = 36.6°$	$\theta = 31.2°$	$\theta = 24.5°$
noncollinearity angle	$\alpha = 4.3°$	$\alpha = 3.7°$	$\alpha = 2.5°$
SHG wavelength in WC orientation	**595 nm**	**678 nm**	**870 nm**
SHG wavelength in TPM orientation	**728 nm**	**852 nm**	**1130 nm**

Table 1: Wavelengths for which parasitic SHG of the signal beam occurs for the two possible crystal orientations for different pump wavelengths. In the walk-off compensated (WC) orientation this wavelength is in the range where a noncollinear geometry is advantageous for broadband amplification, in the tangentially phase matched (TPM) orientation, it is outside this range and a collinear geometry is to prefer.

Influence of the group velocity mismatch on the efficiency

Inside the amplifier crystal the involved beams not only separate in transverse direction, but also in propagation direction due to their differing group velocities. One can define an effective crystal length as the minimum of the lengths after which pump and signal, respectively pump and idler are separated due to their group velocity mismatch (GVM).

$$l_{eff} = \min(l_{ps}, l_{pi}) \tag{5.2}$$

with

$$l_{ps} = \frac{\tau}{GVM_{p,s}} \quad \text{and} \quad l_{pi} = \frac{\tau}{GVM_{p,i}} \tag{5.3}$$

where τ is the pulse duration and $GVM_{P,S}$ ($GVM_{P,i}$) the group velocity mismatch between pump and signal (idler), often defined for a collinear geometry as

$$GVM_{p,s} = \frac{1}{v_{g,s}} - \frac{1}{v_{g,p}} \quad \text{and} \quad GVM_{p,i} = \frac{1}{v_{g,i}} - \frac{1}{v_{g,p}} \tag{5.4}$$

compare also [37].

This effective length l_{eff} of course depends on the pulse length of the involved pulses. Short pulses separate faster than longer pulses, which is why a pump laser system with very short output pulses (shorter than ~ 100 fs) is not necessarily better for pumping an OPA than systems with longer output pulses. On the contrary, active chirping of the pump pulses can be required for efficient OPA if they are too short initially [57].

Calculating the group velocity of the extraordinary beam in a birefringent crystal is however not straightforward. Additionally the GVM between pump and signal/idler depends on the chosen crystal orientation (walk-off compensating or tangentially phase matched), a fact that is completely neglected in the literature by the simple definition of the GVM by formula (5.4). Therefore a short excursion about refraction and propagation in an uniaxial birefringent crystal shall be given in the following with special attention to the resulting implications for OPA and a more accurate definition of the GVM.

Refraction and propagation in uniaxial crystals

In birefringent crystals the refractive index depends on the polarization state and the propagation direction of the incident electromagnetic wave. This complicates the calculation of the refraction and propagation properties of the wave and implicates for example that wave vector $\vec{k}$ and group velocity $\vec{v}_g$ can point in different directions.

An uniaxial crystal possesses one optical axis, which I assume lies in the incident plane. Incident waves with their polarization perpendicular to the incident plane (and hence optical axis) are called ordinary waves, as in this case the refractive index does not depend on the propagation direction, and the waves behave as in an isotropic medium. For the ordinary wave with the corresponding ordinary refractive index n_o, Snell's law is valid and the wave vector, the group velocity and the Poynting vector all point in the same direction in the crystal.

For waves with their polarization in the incident plane, called extraordinary waves, this is not true any more. Snell's law can still be formulated for the direction of the wave vectors, but its evaluation is now much more complicated. With the angles as defined in Fig. 5.2 and assuming a refractive index of 1 on the outside of the crystal, it can be written as

$$\sin(\delta) = n_{eff}\left(\Psi(\delta')\right) \cdot \sin(\delta') \tag{5.5}$$

The problem is, that the effective refractive index of the refracted wave depends on the direction of propagation Ψ with respect to the optical axis, which is not known in advance.

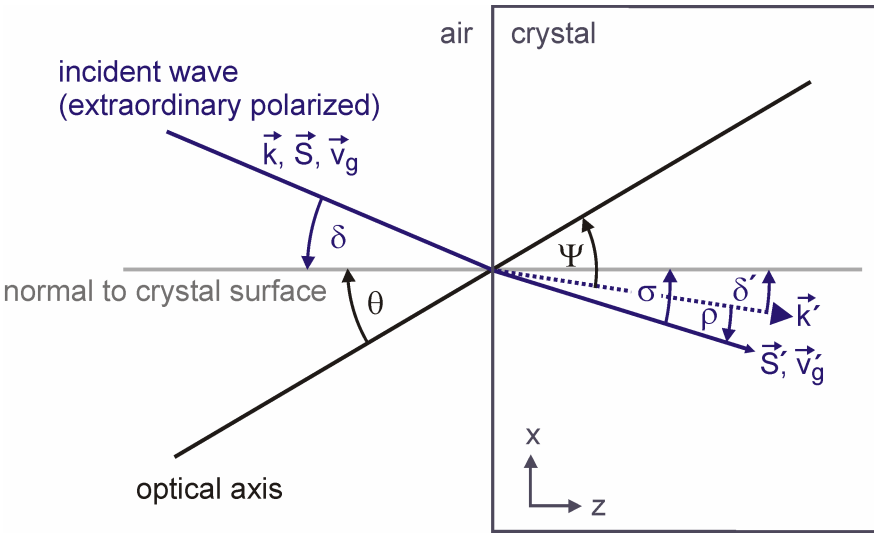

Fig. 5.2 Definition of angles for refraction of an extraordinary wave on a negative uniaxial crystal. Angles in clockwise direction are positive, the others negative.

The exact solution for arbitrary orientation of the optical axis with respect to the incident wave (not in the incident plane), can be found in [58]. It requires solving a quartic equation, which can be analytically done. For the assumption that the optical axis lies in the incident plane, which can always be achieved in OPA, the formulas from [58] can be reduced in complexity and are given in the following.

The incident wave shall have the wave vector $\vec{k}$ and the incident angle δ, the optical axis the angle θ to the normal of the crystal. Then

$$k = \left|\vec{k}\right| = \frac{2\pi}{\lambda} \qquad \text{and} \qquad K_t = k \cdot \sin(\delta) \tag{5.6}$$

with K_t being the transverse component of the wave vector. To simplify the equations, the following abbreviations are useful:

$$\Delta n^2 = n_e^2 - n_o^2 \tag{5.7}$$

$$q_e = \frac{n_o n_e \sqrt{\left(n_o^2 + \Delta n^2 \cdot \cos^2(\theta)\right) k^2 - K_t^2} - \Delta n^2 \cdot K_t \cdot \sin(\theta)\cos(\theta)}{n_0^2 + \Delta n^2 \cdot \cos^2(\theta)} \tag{5.8}$$

The wave vector $\vec{k}'$ inside the crystal can then be written as

$$\vec{k}' = \begin{pmatrix} K_t \\ 0 \\ q_e \end{pmatrix} \tag{5.9}$$

with the angle

$$\delta' = \operatorname{atan}\left(\frac{K_t}{q_e}\right) \tag{5.10}$$

The wave vector is important in OPA for calculating the wave vector mismatch $\Delta\vec{k}$.

As it turns out when doing the calculations, the approximation

$$n_{eff}\left(\Psi(\delta')\right) = n_{eff}(\theta) \tag{5.11}$$

that the refractive index in the medium does not depend on the propagation direction, but only on the fixed effective refractive index for a given crystal orientation, which can be easily calculated by

$$n_{eff}(\theta) = \sqrt{\left(\frac{\cos(\theta)}{n_o}\right)^2 + \left(\frac{\sin(\theta)}{n_e}\right)^2}^{-1} \tag{5.12}$$

gives already very accurate and fully sufficient values for all practical cases in OPA. This is shown in Fig. 5.3 for BBO as nonlinear crystal with an angle θ = 32.5°. Depicted in black is the exact angle δ' of the wave vector inside the crystal, depicted in red the angle calculated with the approximated refractive index. It can be seen that for realistic incidence angles below 20° the difference is smaller than 0.2°, which can be neglected. Even for unrealistically large incidence angles approaching 90° the difference stays below 1°.

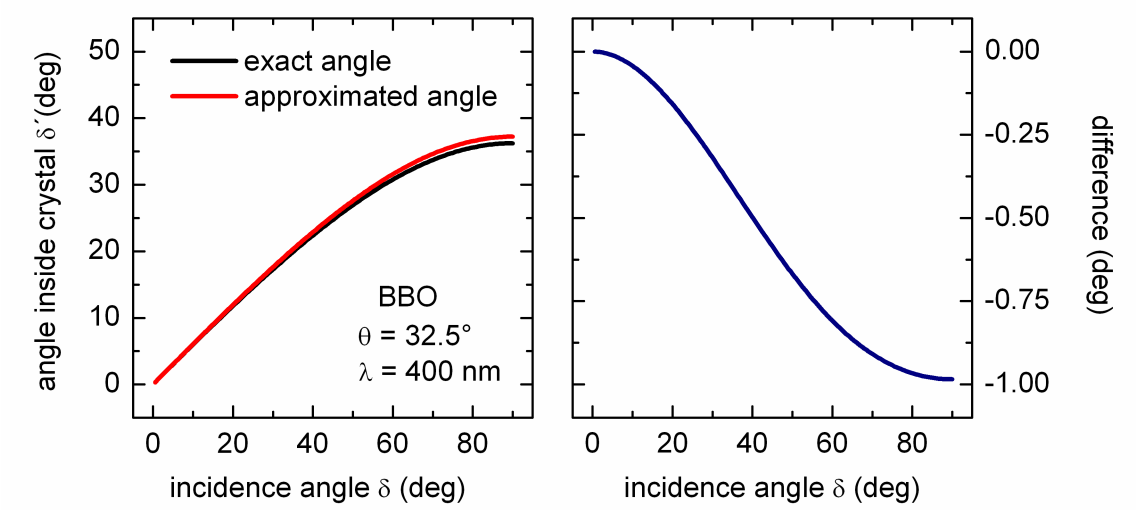

Fig. 5.3 Angle of the wave vector of an extraordinary refracted wave inside a BBO crystal calculated with the exact formula (black) and an approximate formula (red). The blue line on the right shows the difference between both values.

As a first result we can therefore conclude, that using **Snell's law with the effective refractive index** $n_{eff}(\theta)$ **yields fully adequate results**. $n_{eff}(\theta)$ is thereby also the refractive index that is given by the program SNLO [59] in the module "Ref. Ind." for the extraordinary beam.

A fact that cannot be neglected is, that the group velocity and the Poynting vector point in a different direction than the wave vector. The group velocity, and connected to it the group velocity mismatch (GVM) to signal and idler are important as they influence the efficiency of the OPA process.

For wave propagation in one dimension, the group velocity is defined as

$$v_g = \frac{\partial \omega}{\partial k} \tag{5.13}$$

which can be generalized to three dimensions by

$$\vec{v}_g = \nabla_{\vec{k}} \left(\omega(\vec{k}) \right) = \begin{pmatrix} \frac{\partial \omega}{\partial k_x} \\ \frac{\partial \omega}{\partial k_y} \\ \frac{\partial \omega}{\partial k_z} \end{pmatrix} \tag{5.14}$$

It can be shown, that the thus defined group velocity is equivalent to the velocity of the energy flow, defined as

$$\vec{v}_e = \frac{\vec{S}}{U} \tag{5.15}$$

with the Poynting vector $\vec{S}$ and the energy density U [60]. This means in particular, that **group velocity and Poynting vector point in the same direction**.

The angle between the wave vector and the group velocity is called spatial walk-off angle ρ. It is given by

$$\tan(\rho) = -\frac{1}{n_{eff}(\Psi)} \cdot \frac{\partial n_{eff}(\beta)}{\partial \beta}\bigg|_{\beta=\Psi} \tag{5.16}$$

As can be seen in the left panel of Fig 5.4, the walk-off angle for normal incidence depends on the angle of the optical axis and has a maximum of 4.4° at θ = 43° (for a wavelength of 400 nm in BBO). Typical values for θ in OPA are between about 20° and 40°, where the walk-off angle varies between 3.0° and 4.4°. For these small values of the walk-off angle the tangent in formula (5.16) can be approximated to good accuracy by the angle itself, which gives the formula most often seen in publications.

The right panel of Fig. 5.4 shows the dependence of the walk-off angle on the angle of incidence for an angle θ of 32.5°. At an incidence angle of 65.5° the walk-off angle gets 0, as in this case the refracted wave inside the crystals propagates along the optical axis.

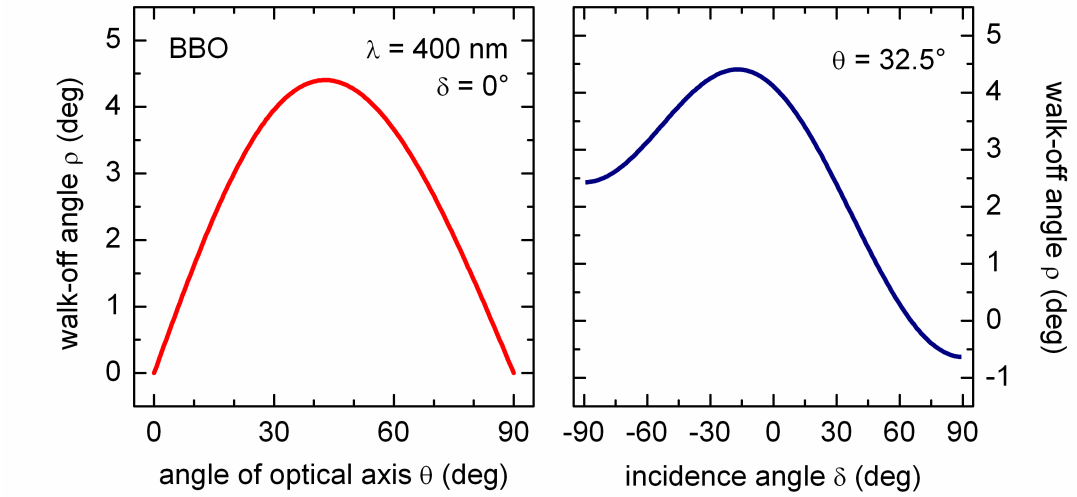

Fig. 5.4 Dependence of the walk-off angle ρ on the angle of the optical axis for normal incidence of a wave with λ = 400 nm (right panel). The right panel shows the dependence of the walk-off angle on the incidence angle for θ = 32.5°.

Realistic angles of incidence in OPA are between about -10° to 10°, where the walk-off angle varies only slightly between 4.4° and 3.7°. For realistic values of the angle of incidence and the angle θ, one can therefore state that **the walk-off always directs the beam away from the optical axis in a negative uniaxial crystal**. At large angles θ and large angles of incidence, where the angle between the optical axis and the refracted beam gets larger than 90°, this is not true anymore. However, these cases never occur in realistic OPA implementations.

The walk-off angle tells us the direction of the group velocity, but not its magnitude. For the general case it is quite tedious to determine, therefore it is given here only for the case of normal incidence:

$$v_g = \frac{c \cdot n_{eff}^2(\theta)}{n_{eff}(\theta) - \lambda \cdot \frac{\partial n_{eff}(\theta)}{\partial \lambda}} \cdot \sqrt{\frac{\cos^2(\theta)}{n_o^4} + \frac{\sin^2(\theta)}{n_e^4}} \tag{5.17}$$

For θ = 0 this simplifies to the well know formula

$$v_g = \frac{c}{n_o - \lambda \cdot \frac{\partial n_o}{\partial \lambda}} \tag{5.18}$$

for the group velocity of an ordinary propagating beam.

To determine the GVM between pump and signal (idler) in OPA we have to project the signal (idler) group velocity onto the direction of the group velocity of the pump. This shall be done in the following for a realistic example in walk-off compensating geometry and in tangential phase-matched geometry.

Calculating the GVM in walk-off compensated and tangential phase-matched geometry

For broadband amplification around 600 nm in BBO with a pump wavelength of 400 nm, a noncollinearity angle $\alpha = 3.7°$ and a phase matching angle $\theta = 31.2°$ are optimal (see for example the SNLO module "OPO angles"). The noncollinearity angle α is the angle between the wave vectors of pump and seed inside the crystal. The pump shall enter the crystal at normal incidence, which means that its wave vector gets not refracted. The incident angle of the seed can therefore be calculated via

$$\delta_{seed} = \mathrm{asin}\left(n_o(600\mathrm{nm}) \cdot \sin(3.7°) \right) = 6.2° \tag{5.19}$$

To be able to calculate the GVM, we need to calculate the walk-off angle ρ of the pump beam according to formula (5.16). For the given values this yields $\rho = 4.0°$.

As can be seen in Fig. 5.5 two distinct geometries are possible, in which the walk-off directs the pump beam closer to the signal beam (walk-off compensating geometry), or closer to the idler beam (tangential phase-matched geometry). For the first configuration the resulting angle φ between pump and signal group velocity is $\varphi_{WO} = -0.3°$, for the second configuration $\varphi_{TP} = 7.7°$.

The group velocity of the pump is the same in both configurations and can be calculated with formula (5.17). This yields $v_{g,pump} = 0.577 \cdot c$, with the speed of light c. The GVM between pump and signal is given by

$$\mathrm{GVM} = \frac{1}{v_{g,signal} \cdot \cos(\varphi)} - \frac{1}{v_{g,pump}} \tag{5.20}$$

The term $\cos(\varphi)$ is to project the signal group velocity onto the pump group velocity. For the two configurations this yields $GVM_{WO} = -88$ fs/mm and $GVM_{TP} = -37$ fs/mm. The minus sign indicates that the group velocity of the signal is larger than that of the pump.

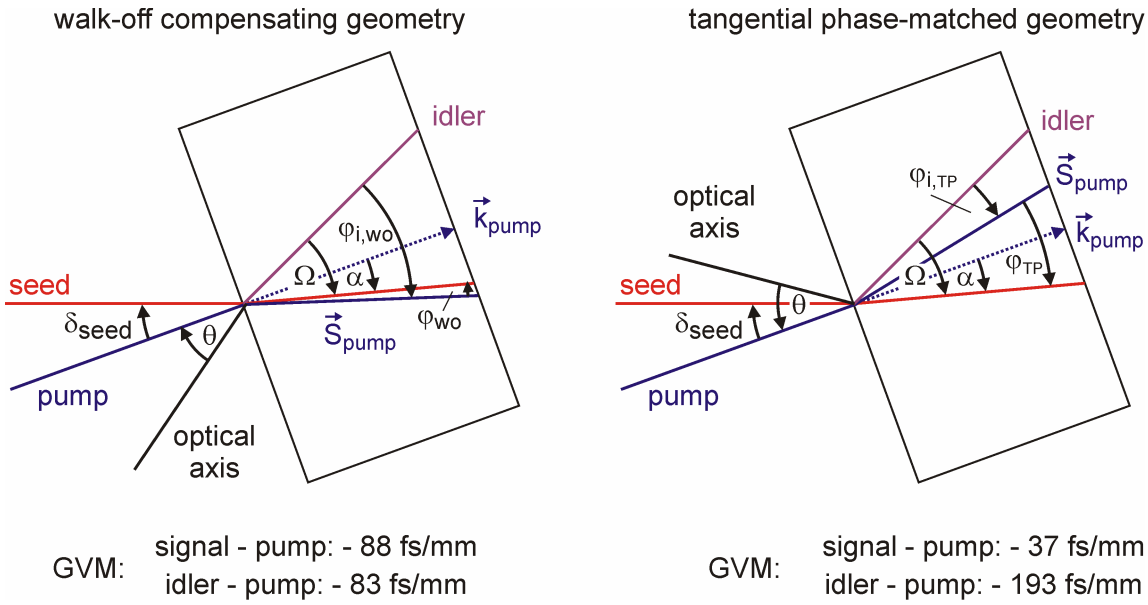

Fig. 5.5 Illustration of the two possible phase matching geometries in noncollinear optical parametric amplification with the involved angles. The GVM values correspond to the example in the text with a phase matching angle θ of 31.2° and a noncollinearity angle α of 3.7°.

To calculate the GVM between pump and idler, the direction of the idler has to be calculated first. For the optimum noncollinearity angle, the projection of the idler group velocity onto the signal group velocity equals the signal velocity. This means the angle Ω between signal and idler can be calculated via

$$\cos(\Omega) = \frac{v_{g,signal}}{v_{g,idler}} \tag{5.21}$$

compare [44].

For our example this gives $\Omega = 11.6°$ for the idler wavelength $\lambda_i = 1200$ nm. The angles between idler and pump for the two configurations are therefore $\varphi_{i,WO} = 11.9°$ and $\varphi_{i,TP} = 3.9°$ with the corresponding group velocity mismatches of $GVM_{i,WO} = -83$ fs/mm and $GVM_{i,TP} = -193$ fs/mm.

For the walk-off compensating geometry the GVM of signal and idler to the pump are with -88 fs/mm and -83 fs/mm very similar, for the tangential phase-matched geometry with -37 fs/mm and -193 fs/mm more distinct. This might tempt into assuming that the walk-off compensating geometry yields higher efficiency, as good overlap of the pump with signal and idler are equally essential. Experimentally however, often quite similar energies and in tendency higher output energies for the tangential phase-matched configuration are seen. This might be due to the fact that the spatial overlap of the pump with signal and idler is also important for the efficiency, which is more balanced for the tangential phase-matched geometry.

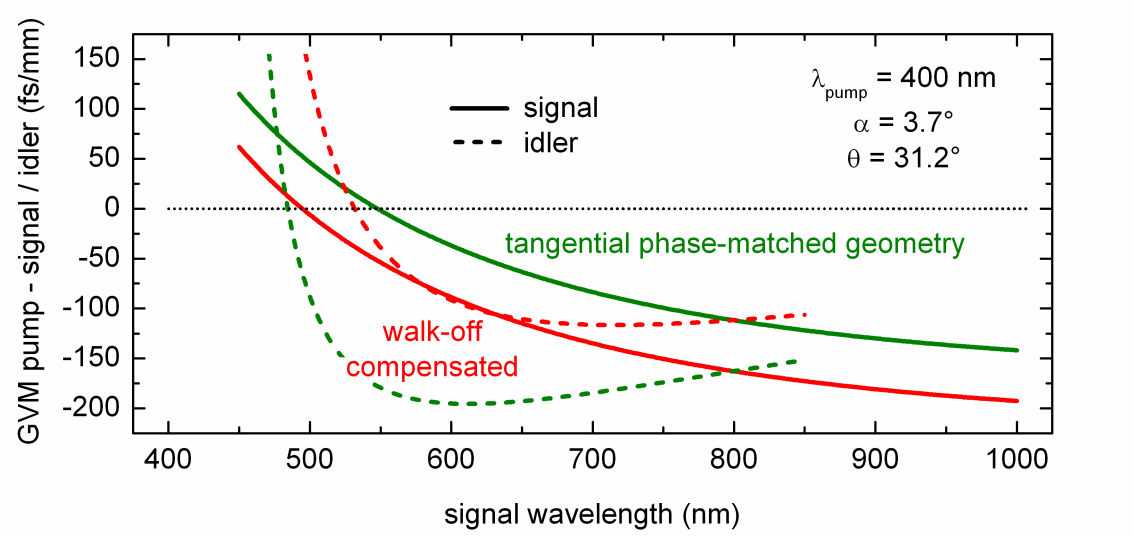

Fig. 5.6 Group velocity mismatch between pump and signal (idler) in dependence of the signal wavelength. The pump wavelength of 400 nm with a noncollinearity angle of 3.7° and a phase matching angle of 31.2°.

Fig. 5.6 shows the calculated GVM between pump and signal (pump and idler) for signal wavelengths from 450 nm to 1000 nm for the parameters of the above example. The angle of the idler was calculated by minimizing the magnitude of the wave vector mismatch $\Delta\vec{k}$ for each wavelength. One can see, that for the walk-off compensated geometry the GVM between pump and signal is 0 at about 495 nm, for the tangential phase-matched geometry at about 548 nm. For the corresponding GVMs between pump and idler this is almost reversed. In combination this leads to quite similar output energies for the two configurations.

For both configurations the GVM is smallest in the region around 500 nm to 550 nm. For pulse durations and/or crystal lengths where the GVM is important, one therefore expects that amplification works best in this region. This is indeed seen experimentally [57].

In Fig. 5.6 the GVM between pump and idler rises strongly for short wavelengths for both configurations. This might lead to the prediction that amplification should work poorly in this region. Indeed, the broadband spectrum shown in Fig. 4.3 falls off quite strongly below 500 nm. The experimental experience however shows, that amplification substantially below 500 nm is very efficiently possible. The important point here is the noncollinearity angle, which is with 3.7° too large for this wavelength region, as can already be seen in Fig. 4.4. The necessary (and experimentally typically adjusted) smaller noncollinearity angle then reduces the GVM and leads to the observed high amplification.

When we use formula (5.2) and the GVM values of Fig. 5.5 for 600 nm, we find an effective crystal length for 150 fs long pump pulses in the walk-off compensating geometry of 1.7 mm. A longer crystal will only increase the gain for this wavelength if the pump is additionally chirped. At constant energy this reduces the pump intensity, but since the gain coefficient only depends on the square root of the intensity, but linearly on the crystal length, an overall increase in output energy is predicted.

For a chirped supercontinuum seed longer than the pump pulse, the GVM leads to a sweeping of the pump pulse over the seed pulse, which results in the amplification of different spectral parts of the seed at different positions in the crystal. Since the GVM in the walk-

off compensating geometry and the tangential phase matched geometry differ, this can explain why different spectral widths of the output pulses for the two configurations are sometimes observed. In contrast to the efficiency, where the GVM between pump-signal and pump-idler are both essential, for the bandwidth only the GVM between pump and signal is important. If we take again the values for signal amplification at 600 nm with a 400 nm pump (Fig. 5.5), we can predict that in walk-off compensating geometry (GVM = - 88 fs/mm) a broader output spectrum should result, than in tangential phase marched geometry (GVM = - 37 fs/mm), especially for a long crystal.

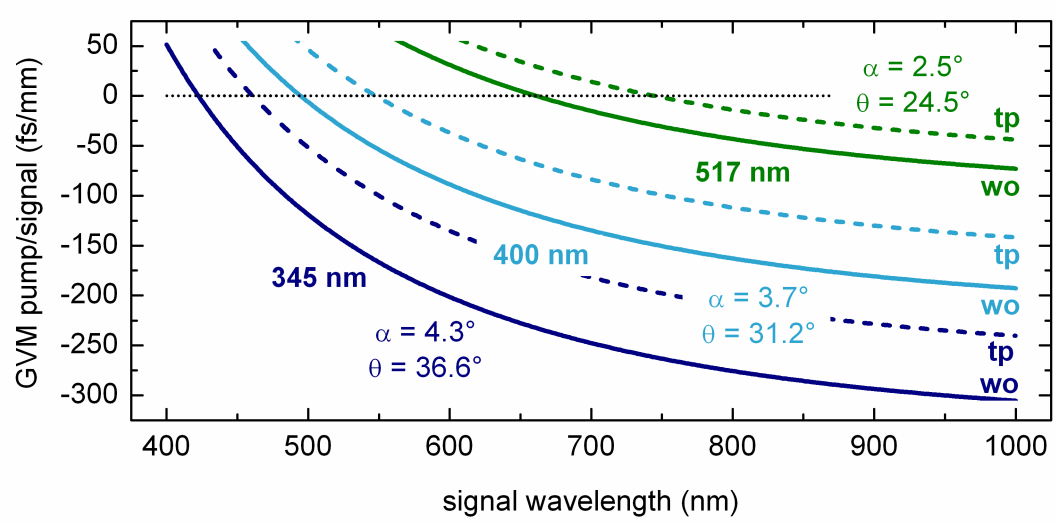

Fig. 5.7 Group velocity mismatch between an extraordinary polarized pump and an ordinary polarized signal beam in BBO for different pump wavelengths, calculated for a noncollinear geometry with the given noncollinearity angle α and phase matching angle θ. The solid lines are calculated for the walk-off compensating geometry (wo), the dashed lines for the tangential phase matched geometry (tp).

Fig. 5.7 gives an impression how the pump wavelength influences the GVM. It shows the GVM between pump and signal in a BBO crystal for three different pump wavelengths with the given noncollinearity and phase matching angles. As expected, the point where the GVM is zero is shifted to shorter (longer) signal wavelengths for shorter (longer) pump wavelengths.

Influence of the wavelength on the gain

Apart from pump intensity and effective crystal length, the wavelengths of signal and idler also influence the gain. Their product is inversely proportional to the gain coefficient, which is equivalent to Γ being proportional to the product of their angular frequencies. Its maximum is easily determined by differentiating the product by the signal frequency:

$$\frac{d}{d\omega_S}\left(\omega_S \cdot \omega_i\right) = \frac{d}{d\omega_S}\left(\omega_S \cdot (\omega_p - \omega_S)\right) = \omega_p - 2\omega_S \qquad (5.22)$$

and setting it to 0. This yields $\omega_S = \omega_p/2$, which means that the product is highest at the degeneracy point. If other influences, as e.g. the GVM, can be neglected, as for example for very short crystals or long pump pulses, this is where OPA yields the highest gain.

If a certain signal wavelength is to be amplified, the gain can be enhanced by using a shorter pump wavelength, because this will lead to a higher product of $\omega_s \cdot \omega_i$. In [A4] it is shown that a pump wavelength of 512 nm and using BBO is superior to pumping with 1025 nm and using $LiNbO_3$ for amplification in the NIR because of this reason. For even lower pump wavelengths, the GVM to the NIR wavelengths gets more and more important, leading to a reduction of the effective crystal length, which counteracts the enhancement of the gain.

In most OPA implementations, the GVM plays an important role and shifts the amplification maximum from the degeneracy point much closer to the pump wavelength [57]. Its strong influence is impressively seen, if the spectrum of the spontaneous superfluorescence is measured in dependence on the crystal thickness and the pump pulse duration (see Fig. 5.8). In the common models of superfluorescence generation, the amplification starts for every possible frequency mode from the vacuum level, which means one can assume an evenly distributed "seed" level so that the amplified output is not biased by a spectrally inhomogeneous seed pulse.

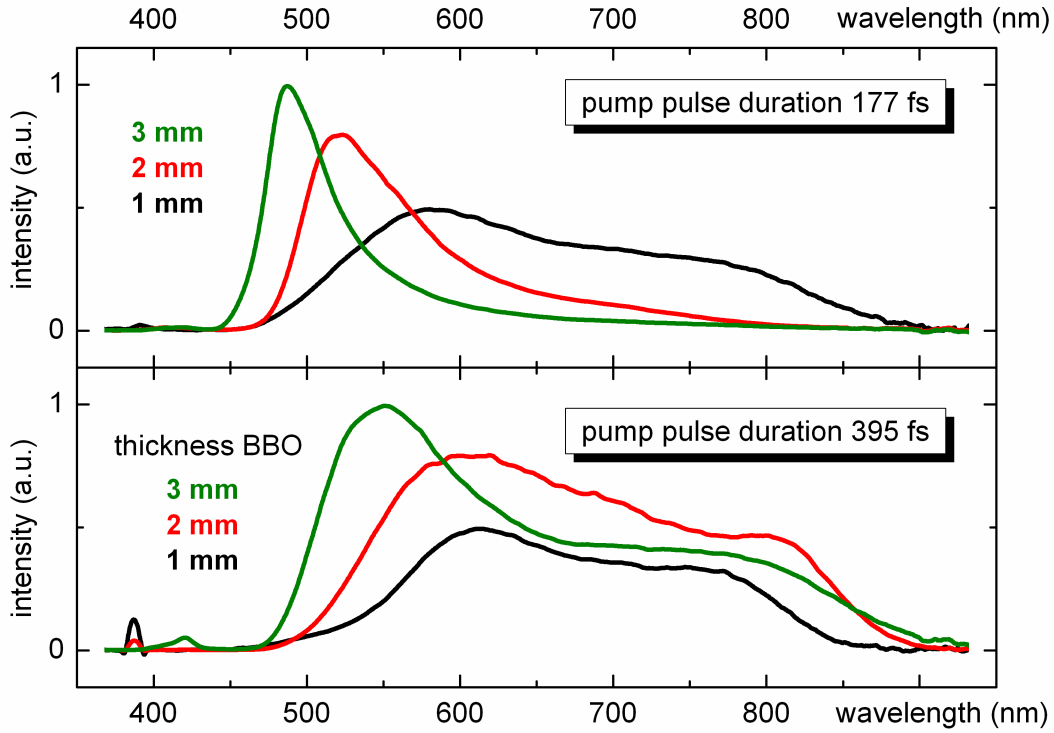

Fig. 5.8 Spectra of the superfluorescence generated in BBO with a pump pulse centered at 387 nm for different lengths of the crystal and measured pump pulse durations of 177 fs and 395 fs.

The spectra in Fig. 5.8 show the integrated intensity of the whole superfluorescence ring generated in BBO with the pump pulse blocked in front of the spectrometer. The generated NIR wavelengths were not collected by the used lens, as they had to large an angle to the pump propagation direction. The phase matching angle was adjusted for the broadest output spectrum. For the shorter pulse duration (FWHM 177 fs) and the longest amplification crystal (3 mm) employed, the most blue shifted spectrum with a maximum at 487 nm results.

The shorter a crystal is used, the more the spectrum shifts to longer wavelengths. If the pump pulse is chirped by the insertion of 90 mm fused silica to a pulse duration of 395 fs, the spectrum generated in the 3 mm thick crystal also shifts to longer wavelengths with a maximum at 551 nm. Again for shorter crystal lengths the spectrum shifts successively to longer wavelengths, however the shifts are not as pronounced as for the shorter pump pulses. This behavior can be nicely understood if one recalls that the GVM is most severe for the shortest pulse duration and the longest crystal, and consequently for this configuration the amplification works best where the GVM is small. For longer pulses or shorter crystals the influence of the GVM weakens and the amplification maximum shifts closer to the degeneracy point at 775 nm.

The spectra obtained with a pump pulse duration of 177 fs and the 1 mm thick crystal, and the one obtained with 395 fs and the 2 mm thick crystal, which is approximately twice the pulse duration and twice the crystal length, are very similar. The corresponding energies are 30 nJ and 110 nJ, which nicely confirms our prediction, that the longer crystal length overcompensates the reduced intensity. For the design of an OPA that means that if strong amplification far from the pump wavelength and close to the degeneracy point is required, chirping of the pump may be beneficial.

6. Combining several amplification stages

For many applications a combination of two or more amplification stages is useful or even necessary.

To reach high amplification factors and a stable output with low fluctuations, the combination of two stages, a pre-amplifier and a power amplifier, with the same pump wavelength is often employed (Fig. 6.7 a)). The advantage of using two stages instead of one is that between the stages the GVM and the spatial separation due to the noncollinearity and the walk-off between pump, signal and idler can be compensated [61]. This leads to longer effective crystal lengths and helps keeping the necessary pump intensities to a level where parasitic nonlinear processes are still weak. The pre-amplifier typically amplifies the weak seed to a few percent of the pump energy with a high gain in the range of a few hundred to 10^5. Its output then seeds the power amplifier which is operated in saturation, has only a moderate gain of 10 to a few hundred, and delivers output energies of up to ~30 % of the pump energy with significant pump depletion. A typical example is the amplification of a 30 nm broad spectral part of a supercontinuum, centered e.g., at 550 nm, generated in a sapphire crystal. Its energy content of about 1 nJ [30] gets amplified to about 300 nJ with a pump energy of about 15 µJ (centered at 400 nm) in the pre-amplifier. In the power amplifier, pumped by 60 µJ pump energy, this seed is further amplified to about 15 µJ with a gain factor of 50 and a quantum efficiency of 35 %. Very similar amplification factors and quantum efficiencies are also used in OPCPA, starting with a much stronger seed of for example 3 µJ and resulting in 170 mJ output energy after two amplification stages [7].

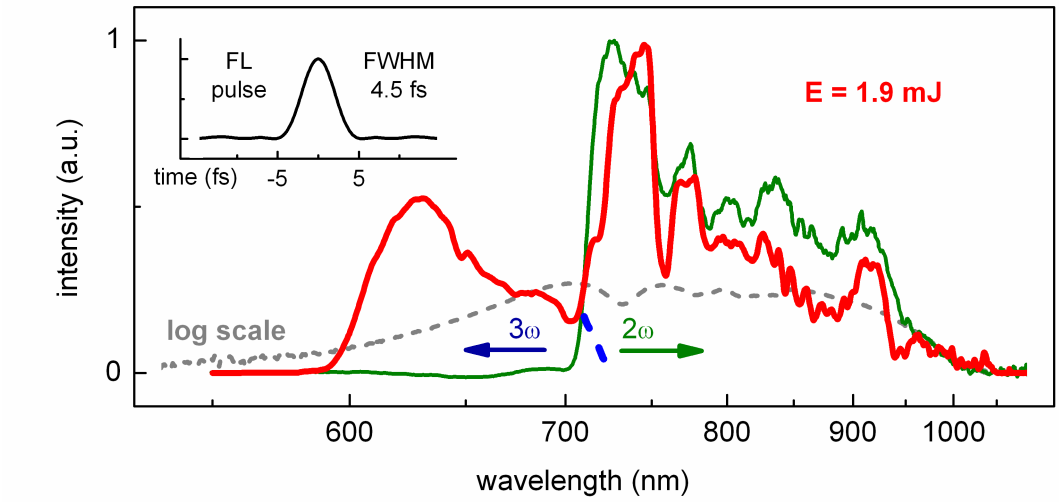

Fig. 6.1 Nearly octave-wide spectrum whose parts are amplified by different harmonics of a Nd:YAG pump laser (red curve) in two subsequent stages. The green curve is the part amplified by the 2nd harmonic alone, the grey dotted curve shows the supercontinuum seed. The Fourier-limit of the composed spectrum allows for a pulse duration of 4.5 fs (inset).

A second advantageous application of combining two stages is to broaden the output spectrum by amplifying different spectral parts of the supercontinuum in each stage. This was explored already in 1996 by cascading three stages pumped by pulses with the same central wavelength of 400 nm [62]. It allowed increasing the bandwidth from about 8 nm to

24 nm around 580 nm in a collinear geometry. Much larger spectral regions can be accessed, however, when different pump wavelengths are combined (see Fig. 6.7 b)). In [A2] it is shown that the combination of a stage pumped by the second harmonic of a Nd:YAG laser at 532 nm and a stage pumped by the third harmonic at 355 nm can deliver a spectrum ranging from 575 nm to 1050 nm with a Fourier limit of 4.5 fs, which is not possible by one of these pump wavelengths alone (Fig. 6.1). The compressibility of a spectrum composed by this method was also demonstrated in [A2].

To be able to amplify spectral regions in the NIR and MIR where no seed light is available, the combination of collinear stages and the use of the idler is a good possibility (see Fig. 6.7 c)). In the first stage, a high frequency pump (e.g. at 400 nm or 512 nm) amplifies the visible part of a supercontinuum seed and generates an idler in the NIR. When amplifying in a region from 530 nm to 750 nm with the 400 nm pump, an idler in the range from 860 nm to 1600 nm results, for the 512 nm pump a signal amplified in the range from 680 nm to 960 nm yields an idler from 1100 nm to 2050 nm (see Fig. 6.2).

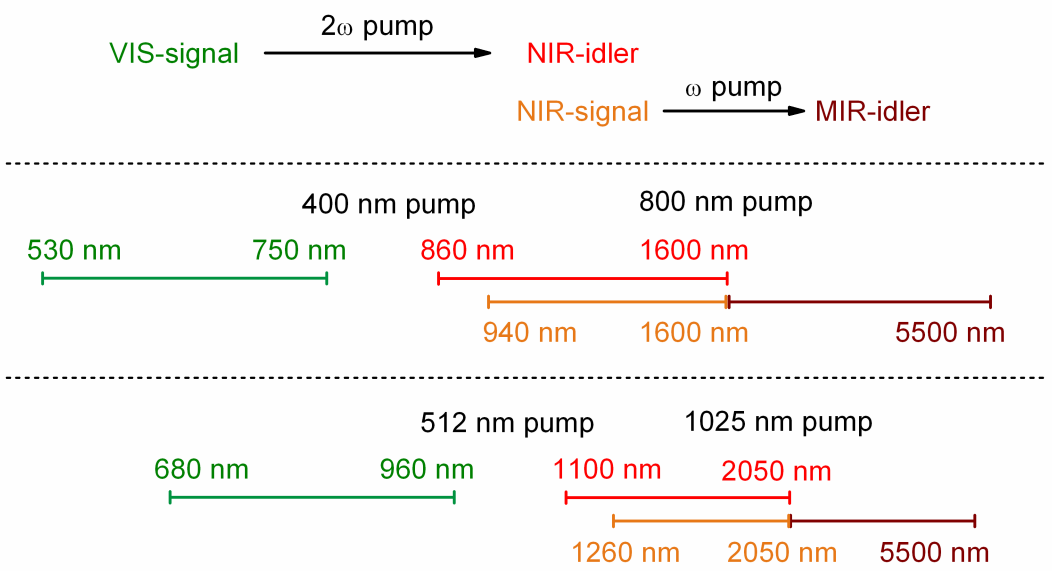

Fig. 6.2 Schematic of a two-stage concept for generating MIR wavelengths when starting with a seed in the visible spectrum (upper row). The middle (lower) row shows the respective wavelength regions for pump wavelengths of 400 nm and 800 nm (512 nm and 1025 nm).

When a second stage is added (IR amplifier) that is seeded by the idler of the first stage and pumped by a lower frequency beam (e.g. at 800 nm or 1025 nm), an idler up to more than 5.5 µm can be generated in $LiNbO_3$ or $LiIO_3$ [A4]. In this way, a full coverage of the region starting slightly above the pump wavelength up to the MIR is obtained. The phase-matching properties for both crystals are more favorable for an 800 nm pump than for 1025 nm at wavelengths above 3 µm (compare Fig. 4.2). Additionally the gain factor is higher for 800 nm pumping due to the lower product of signal and idler wavelengths (compare Chapter 5), so that this pump wavelength is to prefer for this wavelength region, if it is available.

Finally, two amplification stages with additional supercontinuum generation between them can be used for amplifying wavelengths around the fundamental light used for generat-

ing the original seed supercontinuum (see Fig. 6.7 d)). To do so, a first (N)OPA is used to amplify a wavelength longer than the original fundamental. This can be done noncollinearly by using the IR part of the first supercontinuum, or collinearly by amplifying the visible part and using the idler. This output is then used to generate a second, intermediate supercontinuum that now smoothly covers the wavelength region of the original fundamental. In a second (N)OPA this part can then be amplified without complications [44].

Of course a number of other combinations are also possible, as for example pumping the first stage with the fundamental light and amplifying the IR part of the supercontinuum seed. This has the advantage that the generated idler is passively carrier-envelope phase (CEP) stabilized [63]. This output can then be used for generating the intermediate supercontinuum, which is also CEP stable, as will be the thus amplified signal.

In general, always when a beam is the difference frequency between two pulses that have the same CEP variations from shot to shot, its CEP will be passively stabilized. This leads for example to a CEP stable idler output of the IR amplifier of Fig. 6.7 c).

Another possibility to utilize this, is to add a difference frequency mixing stage after a NOPA that is seeded by a supercontinuum generated by the laser fundamental, and mix the broadband signal output with the (narrowband) laser fundamental (see Fig. 6.3).

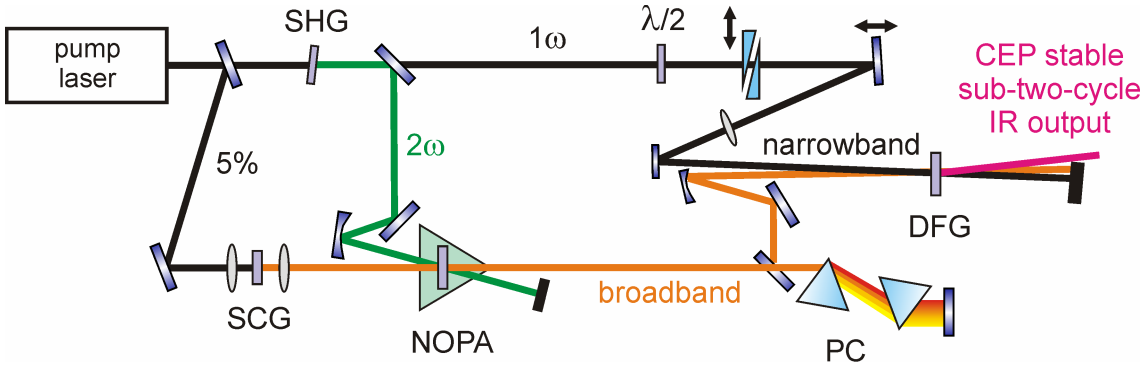

Fig. 6.3 Setup for the generation of passively CEP stabilized pulses in the infrared; SHG: second harmonic generation; λ/2: half wave plate; SCG: supercontinuum generation; PC: prism compressor; DFG: difference frequency generation.

For certain wavelength combinations, given in Table 2, where the group velocity of the signal matches the group velocity of the generated IR difference pulse, this allows to transfer a very broad bandwidth from the signal to the difference frequency. With this scheme sub-two-cycle pulses tunable around 1.8 µm with stable CEP have recently been demonstrated (see Fig. 6.4 and [A5]).

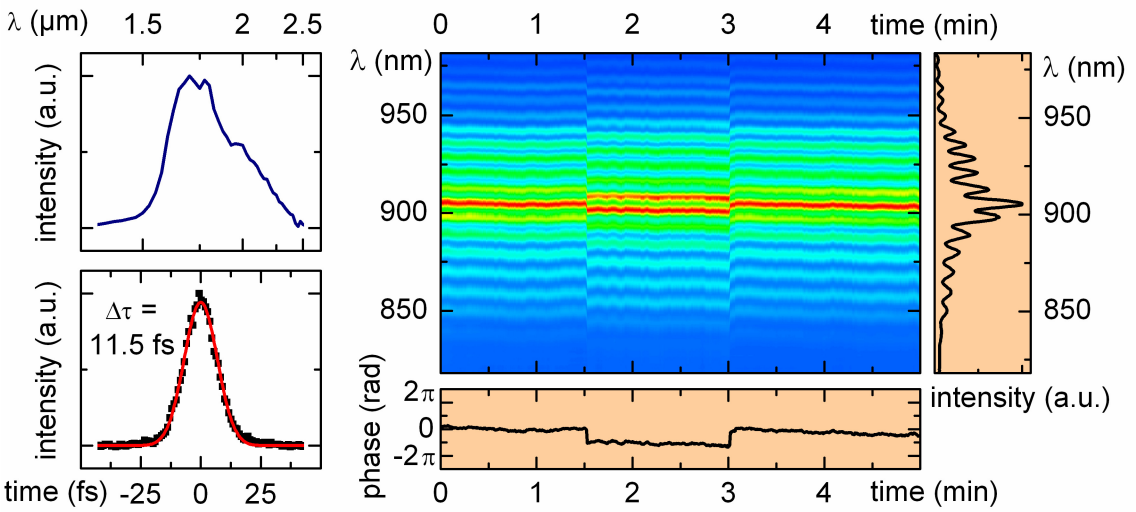

Fig. 6.4 Spectrum and autocorrelation of pulses generated by broadband difference-frequency mixing between the NOPA output around 650 nm and the 1025 nm pump beam of an Yb:KYW laser system (left). The color plot on the right shows an f-2f interference measurement that demonstrates the CEP stability and its control. After 1.5 min. the CEP is shifted by π by moving a wedge in the 1025 nm beam, which is reversed after 3 min. The lower and the right panel show the calculated phase and the interference spectrum. For details see [A5].

mixing wavelength	**800 nm**		**1025 nm**	
	VIS pulse	IR output	VIS pulse	IR output
BBO	606 nm	**2.5 µm**	696 nm	**2.2 µm**
$LiNbO_3$	677 nm	**4.4 µm**	796 nm	**3.6 µm**
$LiIO_3$	693 nm	**5.2 µm**	820 nm	**4.1 µm**

Table 2: Calculated wavelengths for which the group velocity of the visible signal pulse and the difference frequency in the IR are identical for type I difference-frequency generation (DFG) between the extraordinary polarized signal pulse and an ordinary polarized mixing wavelength of 800 nm and 1025 nm, respectively. In the vicinity of these wavelengths a broad bandwidth can be transferred from the visible pulse to the IR output.

Influence of the carrier-envelope phase on the generated output

With the system of [A5] (Fig. 6.3) a dependence of the energy of the generated difference frequency on the relative phase between the incoming pulses was observed. When the phase of the incoming 1025 nm pulses was shifted by π through the insertion of a glass wedge, the energy of the output difference frequency at 1.8 µm changed by 4 %. When the wedge was further inserted to introduce a further phase shift of π, the original energy was restored. This cycle could be repeated several times by moving the wedge in the same direction. In this way, other possible sources of the energy change, as for example better temporal or spatial overlap of the pulses, were excluded.

The explanation of this observation is not straightforward. The phase velocity mismatch of the incident 650 nm and 1025 nm beams is 13 fs/mm, which accounts for 11 fs over the crystal length of 800 µm. Similarly the GVM is 23 fs/mm, which accounts for 19 fs over the crystal length. Both values are larger than the optical periods of the beams, which amount to 2.2 fs for 650 nm and 3.4 fs for the 1025 nm beam. One could therefore suspect that any phase effects average out during propagation through the crystal.

However, since for DFG only the electric fields of the involved beams are important and interact and not the magnetic fields, it might be possible that when at the beginning of the crystal the electric fields of both incident pulses are approximately in phase more DFG is generated than when they are out of phase. Later in the crystal this light then acts as seed as in an OPA and gets amplified. In this way already a slight variation in the amount of primarily generated light might cause a measurable change in the end.

In an OPA with a seed derived from the fundamental and the second harmonic as pump from a not CEP-stabilized laser, the two pulses have differing CEP fluctuations from shot to shot, and therefore a different relative phase from shot to shot. If the above explanation is correct, one would therefore expect that the fluctuations of the relative phase cause intensity fluctuations in the OPA output. To test this hypothesis a pump laser with optional CEP stabilization that can be switched on and off would be optimal.

Other parameters that could influence this effect are the involved pulse lengths. In the above experiment, the 650 nm pulse was with ~ 15 fs rather short. The next experimental step therefore could be to lengthen this pulse and test if a CEP dependence is still observed.

An open question in this respect is also if a CEP dependence can be seen in SHG. For example one could suspect that a few-cycle cosine pulse with its higher maximal electric field generates more 2nd harmonic light than a sine pulse with its lower electric field. To ensure that this effect does not cancel during propagation the phase and group velocity of the fundamental pulse must not be too different, because otherwise a cosine pulse is transferred to a sine pulse during propagation and vice versa. For 1800 nm, the velocity mismatch is 96.7 fs/mm, the optical period 6 fs. If we allow a maximal slip between carrier and envelope of a fourth of the optical period, the maximal crystal thickness calculates to 15 µm. BBO crystals with this thickness are commercially available cemented on a glass support. An experimental verification should therefore be feasible.

Experimental results on electron emission from a nano-scale tungsten tip

The system described above was recently successfully used for the investigation of electron emission from a nano-scale tungsten tip. This field has attracted great attention in recent years [64-66], last but not least because here strong effects (and not only minuscule ones) sensitive on the CEP have been observed for the first time in metals [67]. All experiments to date that measured such CEP effects used pulses centered around 800 nm due to the lack of suitably short and CEP stabilized pulses at longer wavelengths with the required high repetition rate. However, theory predicts that at longer wavelengths interesting new effects can be observed, not only a scaling of the electron energy. This can be seen in Fig. 6.5 a), where first calculations are presented for 20 fs laser pulses centered around 1800 nm.

The calculated electron spectrum in 6.5 a) shows a peaked structure with a varying separation distance. This is in strong contrast to the calculated and measured spectrum for 800 nm irradiation, where above-threshold ionization leads to peaks separated exactly by the photon energy. Theory additionally predicts, that the position and number of the peaks depend on the CEP. The reason for this behavior is still unclear. A possible explanation are interferences between different electron trajectories emitted in the same single cycle of the laser pulse and which lead to the same electron energy. This might point to sub-cycle (or "attosecond") dynamics on metals.

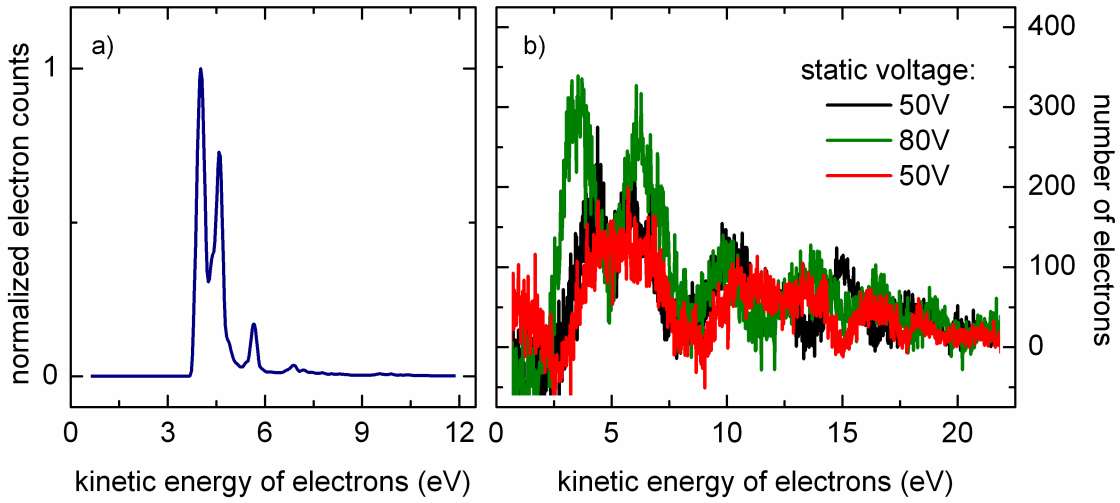

Fig. 6.5 a) Calculated electron spectrum for a carrier-envelope phase (CEP) of π/2 (courtesy of G. Wachter, C. Lemell, and J. Burgdörfer, TU Wien). b) Measured electron spectra for two different static voltages applied to a tungsten nano-tip, which is irradiated with few-cycle laser pulses at 1800 nm.

Fig. 6.5 b) shows first experimental results, where 18.5 fs pulses at 1800 nm generated with the developed system were focused onto a tungsten tip. With the peak electric field of the laser at the tip of 12 GV/m, a Keldysh parameter γ of 0.63 results. This parameter is a measure which process is more likely - multi-photon ionization for $\gamma >> 1$ or tunneling for $\gamma << 1$ [68]. In these measurements we therefore expect strong contributions of tunneling effects, more than in previous studies with 800 nm radiation, where γ was about 2 [67]. We measured the kinetic energies of the emitted electrons for two different static voltages applied on the tip. The used voltages of 50 and 80 V correspond to electric fields of 0.5 GV/m and 0.8 GV/m. They have a significant effect on the resulting electron spectra (see Fig. 6.5 b)).

For both voltages the spectrum has a peaked structure, however for a static voltage of 80 V the onset of the emitted electrons starts earlier at 2.5 eV and therefore more electrons with low energy are generated. The peak structure is more pronounced and the peaks are separated by about 2.7 eV each. For 50 V the electron onset occurs later, the first peak is much broader (the rise below 3 eV is presumably a measurement artifact) and the peak structure as a whole is not as pronounced as for 80 V.

This data has still to be understood. It compares qualitatively with theory as here also no peaked structure with a separation distance equal to the photon energy is seen. Additionally a strong influence of the static voltage on the electron spectra is also predicted by theory. However, the actual shape of the spectra is not yet reproduced by theory.

Latest improvements of the setup consisted in an additional active CEP stabilization that can compensate for slow drifts of the CEP. In this way long-term measurements with controlled CEP are now feasible. Fig. 6.6 shows most recent results obtained with this stabilization for two different settings of the CEP. Between the measurements the CEP was shifted by π. One can see that the maxima and minima in the electron yield approximately swap places for the two settings. This clearly shows a strong influence of the CEP on the produced electron spectra. The newly developed system therefore now allows for the first time CEP dependent measurements with nJ pulse energies at a central wavelength of about 2 µm and with 100 kHz repetition rate.

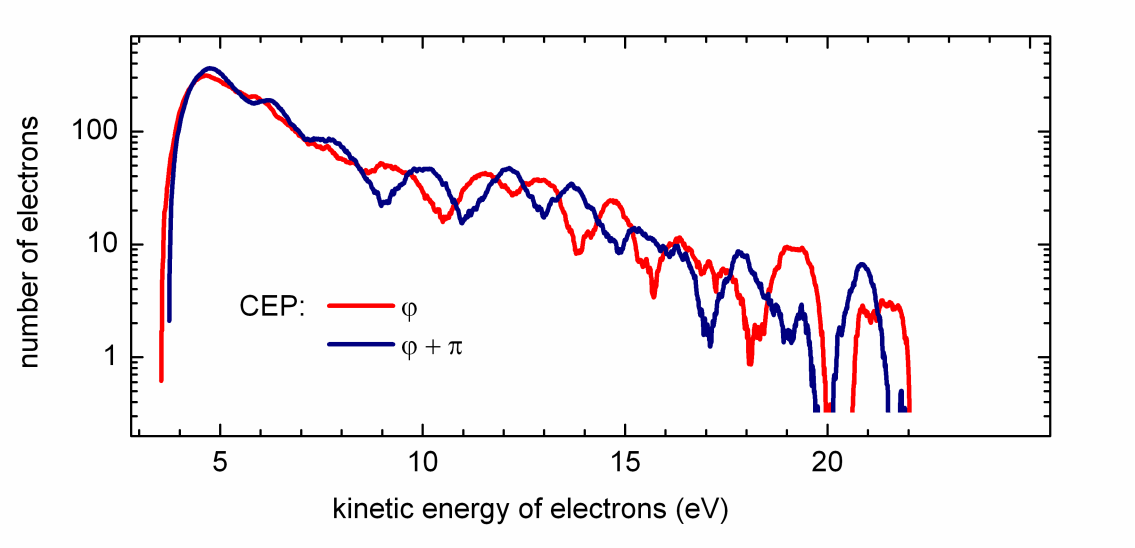

Fig. 6.6 Measured electron spectra for two different settings of the carrier-envelope phase.

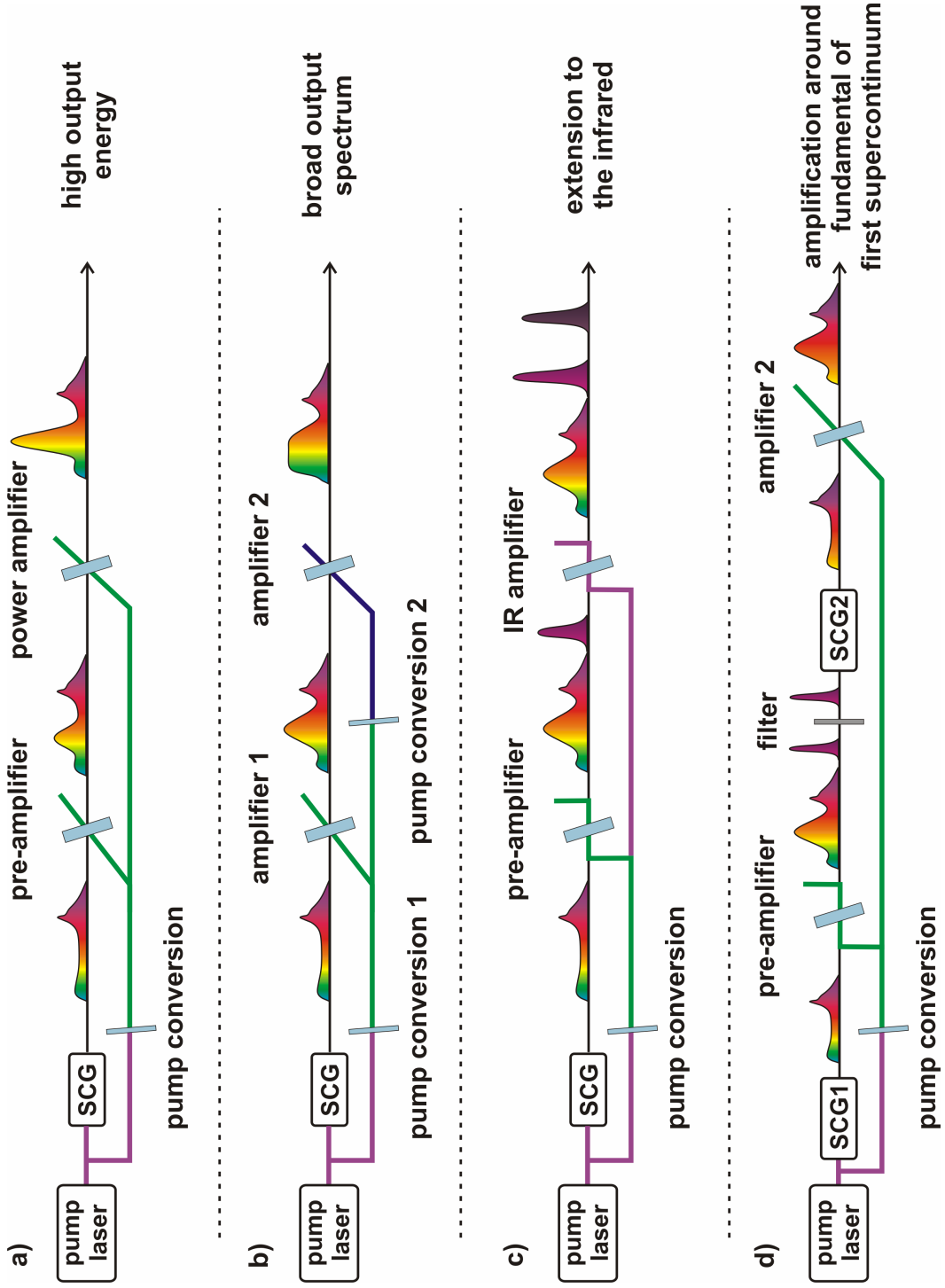

Fig. 6.7 Selected configurations of two cascaded amplification stages for various purposes (SCG: supercontinuum generation). For details see text.

7. Guidelines for choosing a suitable (N)OPA design

In the previous chapters the physical basics of OPA were explained and a variety of concepts presented on how to influence the process to provide the desired output. Here more practical details shall be given on how to proceed best when a new (N)OPA system is to be set up.

- Define the needed spectral tuning range, spectral width, and energy of the output pulses

The first important step is an honest and clear definition of the parameters which are the most likely needed in the experiments to come. To plan for all eventualities and trying to build *the* device which can provide "everything" typically leads to a reduced performance of the system in the most needed parameter range. For example a tuning range from 450 nm to 740 nm is easily accessible with a NOPA pumped by the second harmonic of a Ti:sapphire pump laser and seeded by a supercontinuum generated in sapphire. If the tuning range is to be extended to 840 nm, much more effort is required, because to generate a suitable supercontinuum seed, an additional OPA has to be incorporated (Fig. 6.7 d)). This effort is fully justified if this part of the tuning range is required for a certain experiment. However, it increases the complexity of the system, adds possible sources for failures, needs more time to be adjusted and tends to result in lower output stability. So if in the end only the tuning range from 450 nm to 740 nm is used, the more simple system will be the better choice.

- Decide on the suitable pump laser and pump wavelength

The optimum condition for setting up a (N)OPA system is if the pump laser system can be freely chosen to optimally support the (N)OPA. In this case Fig. 7.1 helps to decide which pump wavelength, and accordingly which pump laser is best suited to deliver certain output pulses. Here it is assumed that a supercontinuum generated by the respective fundamental laser frequency in bulk material (sapphire and YAG) is used as seed.

- big orange boxes mark the "fundamental" tuning ranges that can be most efficiently reached by broadband amplification in a noncollinear geometry
- small orange boxes mark the tuning ranges which can be accessed advantageously by a collinear geometry, including the use of the idler
- the light red sections mark the wavelength regions where an additional supercontinuum is needed as seed source, and therefore an additional amplifier stage (see Fig. 6.7 d)).
- the dark red sections mark the wavelength regions that can be reached by an amplification stage pumped by the laser fundamental frequency and use of its idler. For an efficient amplification and to exploit the full tuning range, a pre-amplifier stage pumped by the 2nd harmonic is typically necessary (see Chapter 6)
- the blue boxes mark the wavelength regions that can be accessed by additional frequency conversion of the (N)OPA output. The ranges marked by the big boxes can be reached by SHG of the fundamental tuning range (with broad bandwidth), the small boxes by SHG of the more narrowband collinear tuning range. The light blue regions can only be accessed by SHG of wavelengths that need an additional supercontinuum. To access the violet (dark blue) regions, an additional sum-frequency mixing stage

with the frequency-doubled (N)OPA output and the laser fundamental (2nd harmonic) frequency are needed. With thin crystals a bandwidth for pulses with a Fourier limit of about 20 fs can thus be reached even in the DUV (see chapter 1 of part II).

Fig. 7.1 shows that with a Ti:sapphire pump laser as well as an Yb^{3+} based laser system an output range from 190 nm up to almost 5 µm can be covered. This is good news when a pump laser already exists and has to be used. However, they diverse in their "fundamental" tuning ranges that can be most efficiently reached by noncollinear amplification. It also shows that wavelength combinations exist that are difficult to reach simultaneously with the same pump source, as for example pulses with broad bandwidth at 400 nm and 500 nm. While 400 nm output pulses are quite conveniently generated by SHG of the output pulses of a 517 nm pumped NOPA, they are difficult to reach in a 400 nm pumped system. In contrast, 500 nm output pulses are easily accessible with a NOPA pumped by 400 nm light, and difficult when pumping at 517 nm is used.

As was laid out in chapter 6, for a full coverage of the NIR/MIR spectral region, a two stage design is required with both pump laser systems and the idler has to be used in a collinear geometry. The pump wavelength of an Yb^{3+} based system is advantageous for generating pulses in a region from about 1150 nm to about 3 µm by collinearly amplifying the visible part of the supercontinuum und using the idler. Fourier limits below 30 fs can thus be reached, which is almost twice as short as is typically obtained for a 400 nm pump. As discussed in chapter 6, the Ti:sapphire pump wavelength however is advantageous for the region above 3 µm both in respect to the achievable bandwidth and output energy.

Apart from the (N)OPA wavelength characteristics, the choice of the pump laser system is often determined by the needed repetition rate and pulse energy for the experiments. In general, Ti:sapphire based systems are advantageously used at repetition rates of a few kHz, where they deliver output energies of a few mJ. With these systems several (N)OPA systems can be pumped simultaneously that will deliver output energies of tens to hundreds of µJ [5,69]. Ti:sapphire pump lasers up to 250 kHz are also available, however with reduced pulse energies of a few µJ. These have been successfully used for pumping (N)OPA systems [3,57,70], which deliver output energies up to a few hundred nJ and require careful alignment and optimized use of the available pump energy. In recent years, Ti:sapphire based pump lasers with cryogenic cooling became available that can deliver pulse energies up to 130 µJ at 100 kHz and still 27 µJ at 200 kHz [71]. With a similar system a NOPA output energy of 3 µJ at 100 kHz was demonstrated [72].

Also emerging in recent years and becoming more and more popular are Yb^{3+} based pump laser systems, which can provide high average output power without complex cooling concepts. These deliver output energies of several tens of µJ at 100 kHz and still about 10 µJ at 2 MHz repetition rate. With these energies pumping of at least two (N)OPA stages with µJ energy output at 100 kHz repetition rate is possible, and even at 2 MHz simultaneous operation of two stages, one pumped by the second harmonic, the other pumped by the third harmonic was demonstrated [A1].

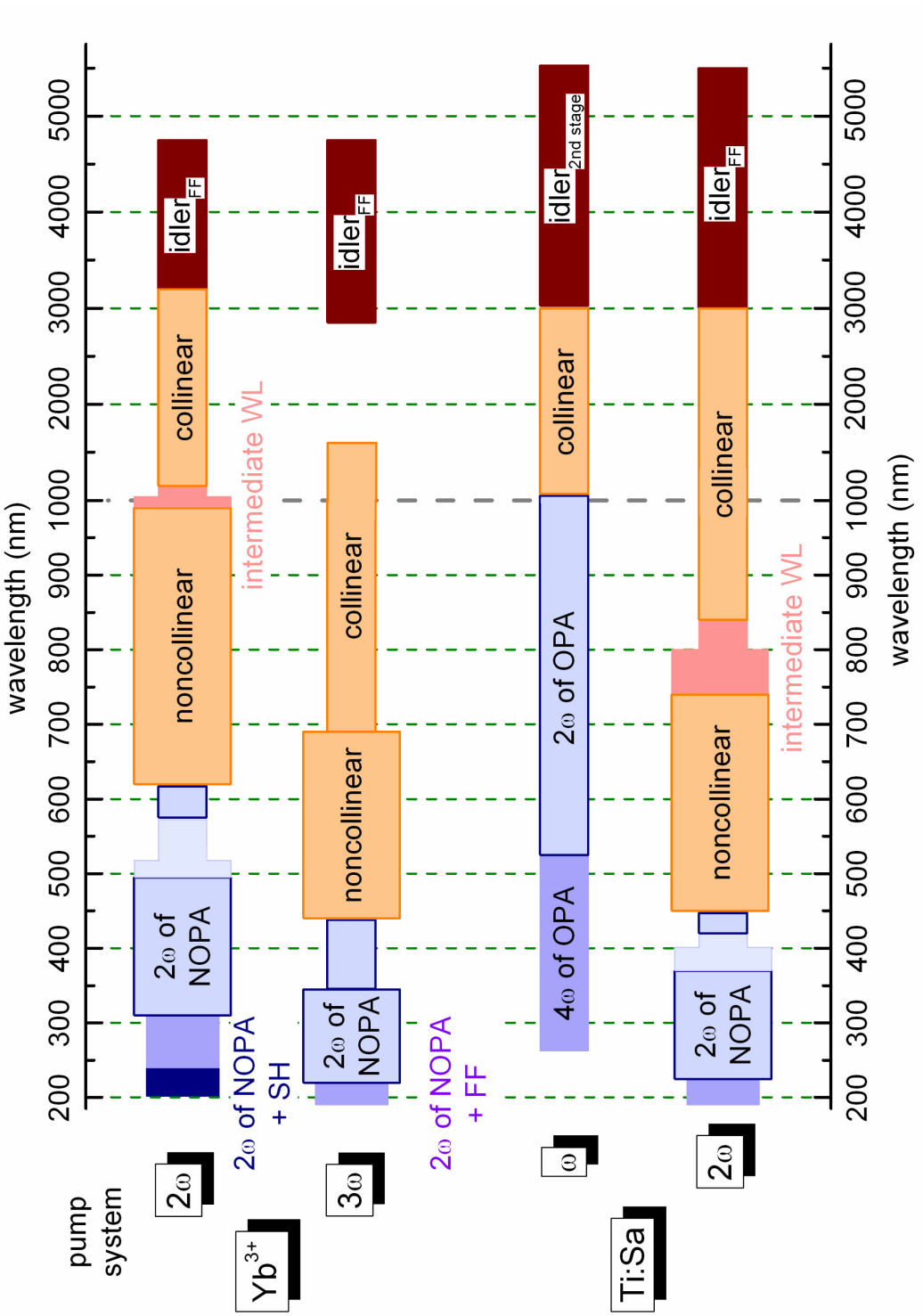

Fig. 7.1 Illustration which output wavelengths can be obtained with a certain technique for different pump laser systems and corresponding pump wavelengths. For details see text.

If the available pump energy is a limiting factor, special care has to be taken to efficiently use all available light. In the case of the two amplifiers with the different pump wavelengths (compare [A1]), and accordingly different optimal amplification regions, this can mean using the same seed supercontinuum and splitting it spectrally with a dichroic mirror, so that each amplifier receives the matching seed.

Another possibility for efficient pump usage is to use the remaining light after the pump frequency conversion. In the case of a third harmonic pumped (N)OPA, the second harmonic is generated in an intermediate step, and only part of it is converted to the third harmonic. The unconverted part can therefore easily be used for pumping an additional amplifier stage. Similarly the laser fundamental remaining after frequency doubling can be reused, for example in schemes as depicted in Fig. 6.7 c). The only prerequisite is that the spatial and temporal beam profile of the remaining light is not too much disturbed, as will happen at very high conversion efficiencies. As a rule of thumb we found that a conversion efficiency of about 30 % ensures that the unconverted light can still be used without any problems.

- Determine the number of amplification stages

The next step is to decide on the number of amplification stages. As just explained, this may already be determined by the needed spectral tuning range, e.g., if full tunability in the NIR/MIR region or the wavelengths around the fundamental frequency of the pump is required. For spectroscopic applications in the “fundamental” tuning range one stage is most often sufficient. If frequency doubled output in the µJ range is needed, a pre- and power amplifier design is typically required. This of course is only feasible if the pump laser provides enough pump energy.

- Choosing the correct amplifier crystal(s)

A first selection of the material of the amplifier crystal is given by the wavelength range that is to be amplified. For amplification in the visible spectral region, BBO is by far the most common and a sensible choice. For the NIR, BBO can still be a good choice, especially if for some reason a high frequency pump (2^{nd} harmonic of the pump laser) is used. Also KTP and BiBO are sometimes used [73], whereof especially BiBO provides an extremely broad amplification bandwidth [74,75]. More common are $LiNbO_3$ and $LiIO_3$, which are particularly good choices when wavelengths above 3 µm are needed. $LiNbO_3$ yields higher output energies for a fixed pump energy, as it has a higher nonlinearity and a higher damage threshold, and can thus be pumped harder. $LiIO_3$ instead has the more favorable phase-matching properties and allows more broadband amplification. A good help to review the phase-matching properties and to determine the needed cut angles of nonlinear crystals is the program SNLO from A.V. Smith [59].

For pump lasers with pulse durations up to a few hundred fs crystal thicknesses of 1 to about 3 mm are reasonable choices. Thinner crystals allow only small conversion efficiencies, thicker crystals can not be used effectively because of the GVM between the interacting pulses. For ps long pump pulses longer crystals with a thickness above 5 mm are used.

- Tuning of the ratio of pump and seed duration

The next important step is to adjust the duration of the pump and seed pulses for the needed output. This is explained in detail already in chapter 4. In summary, for as broadband amplification as possible, the pump has to be longer than the seed, which in low power implementations typically means to avoid dispersion in the seed path and potentially chirping the pump pulse. In high power OPCPA applications, both pulses are stretched to keep the intensities on the amplifier crystals reasonable.

For more narrowband output the seed is chirped to a duration longer than the pump pulse. Often focusing the supercontinuum seed with a lens (e.g. an achromatic lens) introduces already enough dispersion, otherwise suitable glass material can be inserted.

Limiting the bandwidth of the NOPA output can for example also make sense, if the NOPA output is to be frequency doubled and high conversion efficiency is needed. Then too broadband pulses can be cumbersome, as SHG of the full bandwidth necessitates very thin crystals which limits the conversion efficiency. By tailoring the spectral width of the NOPA output to match the acceptance bandwidth of the used frequency doubling crystal, the optimal conversion efficiency can be exploited (see chapter 1 of part II).

- Establishing suitable focusing conditions

The spot size of the pump beam on the amplifier crystal has to be chosen such that high enough intensities for sufficient gain are reached. This is discussed in chapter 5. A reasonable value to start with for most amplifier crystals is 150 GW/cm².

For pump wavelengths of 345 nm and 400 nm a good indication that the intensity is in a reasonable range to achieve good amplification is the visibility of the superfluorescence ring. At a laser repetition rate of 1 kHz the superfluorescence ring for a pre-amplifier stage should be barely visible, for a power amplifier stage it should be clearly visible. For a pump wavelength of 517 nm the superfluorescence ring is typically not visible by eye, because its peak wavelength is too far in the NIR.

If the pump beam is not nearly collimated but focused, moving the amplifier crystal along the propagation direction of the pump is a good possibility to adjust the intensity. Working after the focus of the pump beam is advantageous, because the diverging beam works against self-focusing, which allows higher intensities before parasitic nonlinear processes occur.

The seed should then also be focused before the amplifier crystal to ensure similar curvatures of the wave fronts for both beams. Therefore it is also helpful when the divergences are approximately matched. The beam sizes of pump and seed should also be matched approximately. To achieve the highest gain, a possibility to adjust the beam size of the seed beam, e.g. by moving a lens in its beam path is helpful.

A choice that has to be made is whether pump and seed are focused by lenses or mirrors. For most systems focusing of the pump pulses with a lens is unproblematic, as the amount of chirp it introduces is not relevant. In a noncollinear geometry mirrors can be advantageous for practical reasons, because then it is easier to change the noncollinearity angle and small spot sizes on mirrors can be avoided. In the seed path lenses are often more convenient and avoid astigmatism, however they introduce dispersion, which can limit the amplification bandwidth.

Especially when the parametric superfluorescence background is of importance, as for example in high power OPCPA applications, a focusing (to diameters in the region of about ~ 250 μm) in the first amplification stage is advantageous. This is due to the fact that the effective number of seed photons for the parametric fluorescence is proportional to the interaction area. A smaller interaction area will therefore produce less parametric superfluorescence. This is discussed in detail in chapter 4 of part II.

8. Summary and outlook

In this work the basics of optical parametric amplification were reviewed with a focus on previously neglected or overlooked aspects. First four restrictions for the accessible wavelength range were identified, namely energy conservation, idler absorption, phase matching and the availability of seed photons, whereof phase matching only plays a significant role in the seldom used type II phase matching scheme. To extend the tuning range, we discussed using a pump pulse with shorter wavelength and found that for BBO this is feasible in the femtosecond regime down to about 320 nm, before two-photon absorption causes serious problems. To be able to reach wavelengths in the (near-)infrared where no seed photons are available, the use of the idler in a collinear geometry is a good possibility. To minimize the problem of the idler absorption and to reach further into the IR, crystals with higher IR transparency than BBO, as for example $LiNbO_3$ and $LiIO_3$ can be used.

The phase matching bandwidth that can be reached in OPA is determined to first order by the group velocity mismatch of signal and idler. The smaller the mismatch, the broader is the amplification bandwidth. In a collinear geometry broadband amplification is therefore possible around the degeneracy point, but also for selected wavelength pairs, where signal and idler are on opposite sides of the zero dispersion point of the amplifier crystal. In BBO such wavelength pairs exist for pump wavelengths between 389 nm and 744 nm. This allows for example for broadband amplification around 640 nm and 2700 nm for a pump wavelength of 517 nm.

In a noncollinear geometry the matching of the projections of the group velocities of signal and idler is possible for a much larger wavelength range. This allows the amplification of extremely broadband spectra supporting pulses with durations of only a few femtoseconds. Additionally the efficiency is typically larger for a noncollinear geometry, as the projections of the group velocities of all three interacting beams are more similar than for a collinear geometry. The only potential disadvantage is the spatial chirp of the idler, which makes the idler difficult to use. When the idler is needed, a collinear geometry can thus be advantageous, otherwise a noncollinear geometry is to prefer.

Apart from the phase matching bandwidth, the actual amplification bandwidth is determined by the pulse lengths of pump and seed. Simplified, if the pump is longer than the seed the amplification bandwidth is given by the phase matching bandwidth. If the seed is chirped and longer than the pump pulse, the amplification bandwidth is determined by the spectral bandwidth of the seed that overlaps in time with the pump pulse.

In this case the GVM between pump and seed broadens the amplification bandwidth as the pump sweeps over the seed during propagation in the crystal. This is one of the reasons why it is important to properly calculate the GVM in a birefringent crystal. This is not straightforward, as the extraordinary wave (in type I phase matching the pump pulse) has a complex refraction and propagation behavior. How this is done correctly is demonstrated in detail in chapter 5. The analysis also shows that the GVM between pump and signal/idler depends on the chosen noncollinear geometry (walk-off compensating or tangential phase matched), a fact that was not yet described in the literature.

Apart from the bandwidth, the GVM also influences the efficiency in OPA. As shown in chapter 5 one expects the highest gain at the degeneracy point and lower gain the more signal and idler wavelength are apart. The GVM leads to a blueshift of the signal wavelength with highest gain, which can be seen impressively in Fig. 5.8. The influence is the stronger the shorter the pump pulse and the longer the used crystal is. As a consequence it follows for example, that for most efficient amplification far from the pump wavelength and close to the degeneracy point, chirping of the pump pulse is beneficial.

In chapter 6 different two-stage concepts are presented. With a pre- and power amplifier design high amplification factors of more than 10^7 can easily be reached. The combination of different pump wavelengths in subsequent stages with differing optimal phase matching regions allows extremely large amplification bandwidths when a sufficiently broadband seed is available. To get full tunability in the MIR region, a second harmonic pumped pre-amplifier and a fundamental pumped NIR amplifier are required. The typical gap in the tuning range around the laser fundamental, where the supercontinuum seed is strongly structured, can be closed when a pre-amplifier is employed whose NIR output is used to generate a second supercontinuum seed.

To illustrate the presented concepts once more, let us assume a pulsed laser operating at 2 µm with a pulse duration of a few hundred femtoseconds and an energy of several tens of microjoules is available. How would we proceed to build a (N)OPA starting with this laser?

The first thing to do is testing if a suitable seed can be produced with this system. Since supercontinuum generation was already demonstrated with pump wavelengths up to 3.1 µm [76] and up to about 1 ps [18], this is expected to cause no problems. Most likely the seed spectrum will then cover the wavelength region from at least about 500 nm to 3 µm with a structured region around 2 µm.

The next step is choosing a suitable pump wavelength. The most obvious are the fundamental wavelength itself, its 2nd harmonic at 1 µm and the 4th harmonic at 500 nm, which can be generated by simple SHG. But also the 3rd harmonic at 667 nm and the 6th harmonic at 333 nm that can be generated by additional sum-frequency mixing can make sense.

With 333 nm a tuning range in BBO covering two octaves from ~ 500 nm up to almost 2 µm is feasible, only limited by the seed continuum. In the range up to 666 nm broadband amplification in a noncollinear geometry is advantageous, for longer wavelengths a collinear geometry is to prefer. However, for wavelengths above about 700 nm the GVM between pump and signal/idler gets more and more important and will limit the output energy. For these wavelengths pumping with 500 nm will therefore be beneficial, additionally a noncollinear geometry can be employed advantageously up to 1000 nm. Following the same line of reasoning, for wavelengths above 1000 nm pumping with 666 nm is beneficial and can deliver broadband pulses up to about 1330 nm. Here the necessary noncollinearity angles get already very small (~1°), as we approach the zero dispersion point in BBO. Therefore a broad amplification bandwidth also in a collinear geometry is predicted with broadband pulses all the way up to ~ 2 µm. For all these pump wavelengths BBO and potentially BiBO are the most interesting amplifier materials, whereas $LiNbO_3$ and $LiIO_3$ will suffer from two-photon absorption.

This is no longer true for 1 µm pumping and these crystals become interesting. Since a seed is available almost up to 2 µm, pumping already the first stage with 1 µm can deliver signal output pulses up to ~ 1.8 µm and idler pulses from ~ 2.3 µm up to ~ 5.5 µm. In between the seed will be strongly structured and unusable for OPA. To additionally cover this wavelength region, the idler output in a collinear geometry with 666 nm can be used, which should yield broadband pulses. To generate a second supercontinuum pumped by a first pre-OPA, which has to be done to close the gap around 800 nm for a Ti:sapphire pumped system, is therefore not necessary for a 2 µm pump laser.

Practical design guidelines that are also applicable for the just presented 2 µm pump system are given in Chapter 7. If these are respected, there is no magic in building a (N)OPA. I therefore can only encourage every experimentalist to lay hands on their systems. In my experience, an open system with a modular construction that can be adapted to the current experimental needs is far superior to a black box that tries to deliver everything at once. This will most likely only lead to a reduced performance and increased complexity for a great part of the achievable parameter range. Therefore: just play!

References

[1] D.C. Edelstein, E.S. Wachman, and C.L. Tang, “Broadly tunable high repetition rate femtosecond optical parametric oscillator”, Appl. Phys. Lett. **54**, 1728 (1989).

[2] Q. Fu, G. Mak, and H.M. van Driel, “High-power, 62-fs infrared optical parametric oscillator synchronously pumped by a 76-MHz Ti:sapphire laser”, Opt. Lett. **17**, 1006 (1992).

[3] M.K. Reed, M.K. Steiner-Shepard, and D.K. Negus, “Widely tunable femtosecond optical parametric amplifier at 250 kHz with a Ti:sapphire regenerative amplifier”, Opt. Lett. **19**, 1855 (1994).

[4] F. Seifert, V. Petrov, and F. Noack, “Sub-100-fs optical parametric generator pumped by a high-repetition-rate Ti:sapphire regenerative amplifier system”, Opt. Lett. **19**, 837 (1994).

[5] T. Wilhelm, J. Piel, and E. Riedle, “Sub-20-fs pulses tunable across the visible from a blue-pumped single-pass noncollinear parametric converter”, Opt. Lett. **22**, 1494 (1997).

[6] S. Witte, R.Th. Zinkstok, A.L. Wolf, W. Hogervorst, W. Ubachs and K.S.E. Eikema, “A source of 2 terawatt, 2.7 cycle laser pulses based on noncollinear optical parametric chirped pulse amplification”, Opt. Express **14**, 8168 - 8177 (2006).

[7] D. Herrmann, L. Veisz, R. Tautz, F. Tavella, K. Schmid, V. Pervak, and F. Krausz, “Generation of sub-three-cycle, 16 TW light pulses by using noncollinear optical parametric chirped-pulse amplification”, Opt. Lett. **34**, 2459 (2009).

[8] M. Nisoli, S. Stagira, S. De Silvestri, O. Svelto, G. Valiulis and A. Varanavicius, “Parametric generation of high-energy 14.5-fs light pulses at 1.5 μm”, Opt. Lett. **23**, 630 (1998).

[9] B.C. Johnson, V.J. Newell, J.B. Clark, and E.S. McPhee, “Narrow-bandwidth low-divergence optical parametric oscillator for nonlinear frequency-conversion applications”, J. Opt. Soc. Am. B **12**, 2122 (1995).

[10] K. Okamura, and T. Kobayashi, “Octave-spanning carrier-envelope phase stabilized visible pulse with sub-3-fs pulse duration”, Opt. Lett. **36**, 226 (2011).

[11] A. Baltuska, T. Fuji, and T. Kobayashi, “Visible pulse compression to 4 fs by optical parametric amplification and programmable dispersion control”, Opt. Lett. **27**, 306 (2002).

[12] M.J. Johnson, J.G. Haub, and B.J. Orr, “Continuously tunable narrow-band operation of an injection-seeded ring-cavity optical parametric oscillator: spectroscopic applications”, Opt. Lett. **20**, 1277 (1995).

[13] P. Tzankov, T. Fiebig, and I. Buchvarov, “Tunable femtosecond pulses in the near-ultraviolet from ultrabroadband parametric amplification”, Appl. Phys. Lett. **82**, 517 (2003).

[14] F. Haxsen, D. Wandt, U. Morgner, J. Neumann, and D. Kracht, “Pulse energy of 151 nJ from ultrafast thulium-doped chirped-pulse fiber amplifier”, Opt. Lett. **35**, 2991 (2010).

[15] Y. Tang, L. Xu, Y. Yang, and J. Xu, “High-power gain-switched Tm^{3+}-doped fiber laser”, Opt. Express **18**, 22964 (2010).

[16] L.-M. Yang, P. Wan, V. Protopopov, and J. Liu, “2 μm femtosecond fiber laser at low repetition rate and high pulse energy”, Opt. Express **20**, 5683 (2012).

[17] N. Leindecker, A. Marandi, R.L. Byer, K.L. Vodopyanov, J.Jiang, I. Hartl, M. Fermann, and P.G. Schunemann, “Octave-spanning ultrafast OPO with 2.6-6.1 μm instantaneous bandwidth pumped by femtosecond Tm-fiber laser”, Opt. Express **20**, 7046 (2012).

[18] M. Bradler, E. Wittmann, and E. Riedle, “Filamentation and continuum generation in solids with pump sources from the UV to the infrared over the entire femtosecond regime”, in preparation for Opt. Express

[19] F. Setzpfandt, A. A. Sukhorukov, D. N. Neshev, R. Schiek, Y. S. Kivshar, and T. Pertsch, “Phase transitions of nonlinear waves in quadratic waveguide arrays,” Phys Rev. Lett. **105**, 233905-1 - 233905-4 (2010).

[20] F. Setzpfandt, D. N. Neshev, R. Schiek, F. Lederer, A. Tünnermann, and T. Pertsch, "Competing nonlinearities in quadratic nonlinear waveguide arrays," Opt. Lett. **34**, 3589 (2009).

[21] F. Setzpfandt, A. A. Sukhorukov, and T. Pertsch, "Discrete quadratic solitons with competing second-harmonic components", Phys. Rev. A **84**, 053843 (2011).

[22] F. Setzpfandt, D.N. Neshev, A.A. Sukhorukov, R. Schiek, R. Ricken, Y. Min, Y.S. Kivshar, W. Sohler, F. Lederer, A. Tünnermann, and T. Pertsch, "Nonlinear dynamics with higher-order modes in lithium niobate waveguide arrays", App. Phys. B **104**, 487 (2011).

[23] A. Höfer, K. Duncker, M. Kiel, S. Förster, and W. Widdra, "Laser-excited PEEM using a fully tunable fs-laser system", IBM J. Res. Dev. **55**, 4:1 (2011).

[24] K. Duncker, M. Kiel, and W. Widdra, "Momentum-resolved lifetimes of image-potential states on Ag(001)", Surf. Sci. **606**, L87 (2012).

[25] A. Höfer, M. Fechner, K. Duncker, M. Hölzer, I. Mertig, and W. Widdra, "Persistence of Surface Domain Structures for a Bulk Ferroelectric above T_C", Phys. Rev. Lett. **108**, 087602 (2012).

[26] T.H. Dou, R. Tautz, X. Gu, G. Marcus, T. Feurer, F. Krausz, and L. Veisz, "Dispersion control with reflection grisms of an ultra-broadband spectrum approaching a full octave", Opt. Express **18**, 27900 (2010).

[27] T. Limmer, A.J. Houtepen, A. Niggebaum, R. Tautz, and E. Da Como, "Influence of carrier density on the electronic cooling channels of bilayer graphene", Appl. Phys. Lett. **99**, 103104 (2011).

[28] F. Deschler, E. Da Como, T. Limmer, R. Tautz, T. Godde, M. Bayer, E. von Hauff, S. Yilmaz, S. Allard, U. Scherf, and J. Feldmann, "Reduced Charge Transfer Exciton Recombination in Organic Semiconductor Heterojunctions by Molecular Doping", Phys. Rev. Lett. **107**, 127402 (2011).

[29] R. Tautz, E. Da Como, T. Limmer, J. Feldmann, H.-J. Egelhaaf, E. von Hauff, V. Lemaur, D. Beljonne, S. Yilmaz, I. Dumsch, S. Allard, and U. Scherf, "", Nat. Commun. 3:970, doi: 10.1038/ncomms1967 (2012).

[30] M. Bradler, P. Baum, and E. Riedle, "Femtosecond continuum generation in bulk laser host materials with sub-μJ pump pulses", Appl. Phys. B **97**, 561 (2009).

[31] M. Nisoli, S. De Silvestri, V. Magni, O. Svelto, R. Danielius, A. Piskarskas, G. Valiulis, and A. Varanavicius, "Highly efficient parametric conversion of femtosecond Ti:sapphire laser pulses at 1 kHz", Opt. Lett. **19**, 1973 (1994).

[32] G. Cerullo, M. Nisoli, and S. De Silvestri, "Generation of 11 fs pulses tunable across the visible by optical parametric amplification", Appl. Phys. Lett. **71**, 3616 (1997).

[33] A. Shirakawa and T. Kobayashi, "Noncollinearly phase-matched femtosecond optical parametric amplification with a 2000 cm^{-1} bandwidth", Appl. Phys. Lett. **72**, 147 (1998).

[34] P. Baum, M. Breuer, E. Riedle, and G. Steinmeyer, "Brewster-angled chirped mirrors for broadband pulse compression without dispersion oscillations", Opt. Lett. **31**, 2220 (2006).

[35] J.E. Midwinter and J. Warner, "The effects of phase matching method and of uniaxial crystal symmetry on the polar distribution of second-order non-linear optical polarization", Brit. J. Appl. Phys. **16**, 1135 (1965).

[36] V. Krylov, A. Kalintsev, A. Rebane, D. Erni, and U.P. Wild, "Noncollinear parametric generation in $LiIO_3$ and β-barium borate by frequency-doubled femtosecond Ti:sapphire laser pulses", Opt. Lett. **20**, 151 (1995).

[37] R. Danielius, A. Piskarskas, A. Stabinis, G.P. Banfi, P.Di Trapani, and R. Righini, "Traveling-wave parametric generation of widely tunable, highly coherent femtosecond light pulses", J. Opt. Soc. Am. B **10**, 2222 (1993).

[38] F. Tavella, A. Marcinkevičius, and F. Krausz, "Investigation of the superfluorescence and signal amplification in an ultrabroadband multiterawatt optical parametric chirped pulse amplifier system", New J. Phys. **8**, 219 (2006).

[39] G. Kurdi, K. Osvay, M. Csatári, I.N. Ross, and J. Klebniczki, "Optical Parametric Amplification of Femtosecond Ultraviolet Laser Pulses", IEEE J. Sel. Top. Quantum Electron. **10**, 1259 (2004).

[40] P. Wnuk, Y. Stepanenko, and C. Radzewicz, “High gain broadband amplification of ultraviolet pulses in optical parametric chirped pulse amplifier”, Opt. Express **18**, 7911 (2010).

[41] T. Tanigawa, K. Yamane, N. Karasawa, and M. Yamashita, “Optical Parametric Amplifier Pumped at 266 nm toward Ultrashort Near-Ultraviolet Gigawatt Pulses”, Jap. J. Appl. Phys. **50**, 072701 (2011).

[42] A. Dubietis, G. Tamošauskas, A. Varanavičius, and G. Valiulis, “Two-photon absorbing properties of ultraviolet phase-matchable crystals at 264 and 211 nm”, Appl. Opt. **39**, 2437 (2000).

[43] R. DeSalvo, A.A. Said, D.J. Hagan, E.W. Van Stryland, and M. Sheik-Bahae, “Infrared to Ultraviolet Measurements of Two-Photon Absorption and n_2 in Wide Bandgap Solids”, IEEE J. Quantum Electron. **32**, 1324 (1996).

[44] E. Riedle, M. Beutter, S. Lochbrunner, J. Piel, S. Schenkl, S. Spörlein, W. Zinth, “Generation of 10 to 50 fs pulses tunable through all of the visible and the NIR”, Appl. Phys. B **71**, 457 (2000).

[45] Y.R. Shen, “The Principles of Nonlinear Optics” (Wiley, New York, 1984).

[46] R.W. Boyd, “Nonlinear Optics, Second Edition” (Academic Press, San Diego, 2003).

[47] A.M. Siddiqui, G. Cirmi, D. Brida, F.X. Kärtner, and G. Cerullo, “Generation of <7 fs pulses at 800 nm from a blue-pumped optical parametric amplifier at degeneracy”, Opt: Lett. **34**, 3592 (2009).

[48] M. Sueptitz, R.A. Kaindl, S. Lutgen, M. Woerner, E. Riedle, “1 kHz solid state laser system for the generation of 50 fs pulses tunable in the visible”, Opt. Commun. **131**, 195 (1996).

[49] G.M. Gale, M. Cavallari, T.J. Driscoll, and F. Hache, “Sub-20-fs tunable pulses in the visible from an 82-MHz optical parametric oscillator”, Opt. Lett. **20**, 1562 (1995).

[50] A. Shirakawa, I. Sakane, and T. Kobayashi, “Pulse-front-matched optical parametric amplification for sub-10-fs pulse generation tunable in the visible and near infrared”, Opt. Lett. **23**, 1292 (1998).

[51] M. Breuer, “NOPAs bei variabler Pumpwellenlänge und -dauer: innovative Quellen für die Untersuchung der chemischen Primärdynamik”, Diplomarbeit, Ludwig-Maximilians-Universität München, 2006.

[52] P. Sterflinger, “Spektrale Einengung abstimmbarer Femtosekundenimpulse mit dispersiven Materialien”, Bachelorarbeit, Ludwig-Maximilians-Universität München, 2009.

[53] G. Arisholm, R. Paschotta and T. Südmeyer, “Limits to the power scalability of high-gain optical parametric amplifiers”, J. Opt. Soc. Am. B **21**, 578 (2004).

[54] J. Wang, M.H. Dunn, and C.F. Rae, “Polychromatic optical parametric generation by simultaneous phase matching over a large spectral bandwidth”, Opt. Lett. **22**, 763 (1997).

[55] J. Warner, “Phase-Matching for Optical Up-Conversion with Maximum Angular Aperture - Theory and Practice”, Opto-Electron. 1, 25 (1969).

[56] J. Bromage, J. Rothhardt, S. Hädrich, C. Dorrer, C. Jocher, S. Demmler, J. Limpert, A. Tünnermann, and J.D. Zuegel, “Analysis and suppression of parasitic processes in noncollinear optical parametric amplifiers”, Opt. Express 19, 16797 (2011).

[57] J. Piel, E. Riedle, L. Gundlach, R. Ernstorfer, and R. Eichberger, “Sub-20 fs visible pulses with 750 nJ energy from a 100 kHz noncollinear optical parametric amplifier”, Opt. Lett. **31**, 1289 (2006).

[58] J. Lekner, “Reflection and refraction by uniaxial crystals”, J. Phys.: Condens. Matter **3**, 6121 (1991).

[59] SNLO nonlinear optics code, available from A.V. Smith, AS-Photonics, Albuquerque, NM

[60] A. Yariv and P. Yeh, “Optical waves in crystals” (Wiley, Hoboken, 2003).

[61] G. Cerullo and S. De Silvestri, “Ultrafast optical parametric amplifiers”, Rev. Sci. Instr. **74**, 1 (2003).

[62] T. S. Sosnowski, P. B. Stephens, and T. B. Norris, “Production of 30-fs pulses tunable throughout the visible spectral region by a new technique in optical parametric amplification,” Opt. Lett. **21**, 140 (1996).

[63] A. Baltuska, T. Fuji, and T. Kobayashi, "Controlling the Carrier-Envelope Phase of Ultrashort Light Pulses with Optical Parametric Amplifiers", Phys.Rev. Lett. **88**, 133901 (2002).

[64] R. Bormann, M. Gulde, A. Weismann, S.V. Yalunin, and C. Ropers, "Tip-Enhanced Strong-Field Photoemission", Phys. Rev. Lett. **105**, 147601 (2010).

[65] M. Schenk, M. Krüger, and P. Hommelhoff, "Strong-Field Above-Threshold Photoemission from Sharp Metal Tips", Phys. Rev. Lett. **105**, 257601 (2010).

[66] G. Herink, D.R. Solli, M. Gulde, and C. Ropers, "Field-driven photoemission from nanostructures quenches the quiver motion", Nature **483**, 190 (2012).

[67] M. Krüger, M. Schenk, and P. Hommelhoff, "Attosecond control of electrons emitted from a nanoscale metal tip", Nature **475**, 78 (2011).

[68] L.V. Keldysh, "Ionization in the field of a strong electromagnetic wave", Sov. Phys. JETP **20**, 1307 (1965).

[69] P. Tzankov, J. Zheng, M. Mero, D. Polli, C. Manzoni, and G. Cerullo, "300 μJ noncollinear optical parametric amplifier in the visible at 1 kHz repetition rate", Opt. Lett. **31**, 3629 (2006).

[70] M.K. Reed, M.S. Armas, M.K. Steiner-Shepard, and D.K. Negus, "30-fs pulses tunable across the visible with a 100-kHz Ti:sapphire regenerative amplifier", Opt. Lett. **20**, 605 (1995).

[71] datasheet "Wyvern^{TM} 500 Series", KMLabs, accessed May 31, 2012. http://www.kmlabs.com/downloads/Wyvern500Datasheet2011.11.01.pdf

[72] H. Shen, S. Adachi, T. Horio, and T. Suzuki, "Two-color deep-ultraviolet 40-fs pulses based on parametric amplification at 100 kHz", Opt. Express 19, 22637 (2011).

[73] O. Isaienko and E. Borguet, "Generation of ultra-broadband pulses in the near-IR by non-collinear optical parametric amplification in potassium titanyl phosphate", Opt. Express **16**, 3949 (2008).

[74] A. Gaydardzhiev, I. Nikolov, I. Buchvarov, V. Petrov, and F. Noack, "Ultrabroadband operation of a femtosecond optical parametric generator based on BiB_3O_6 in the near-IR", Opt. Express **16**, 2363 (2008).

[75] M. Ghotbi, M. Beutler, V. Petrov, A. Gaydardzhiev, and F. Noack, “High-energy, sub-30 fs near-IR pulses from a broadband optical parametric amplifier based on collinear interaction in BiB_3O_6”, Opt. Lett. **34**, 689 (2009).

[76] F. Silva, D.R. Austin, A. Thai, M. Baudisch, M. Hemmer, D. Faccio, A. Couairon, and J. Biegert, “Multi-octave supercontinuum generation from mid-infrared filamentation in a bulk crystal”, Nat. Commun. 3:807 doi: 10.1038/ncomms1816 (2012).

Generation of 30 fs-pulses tunable from 189 to 240 nm with an all-solid-state setup

published in

J. Opt. Soc. Am. B **29**, 2765 - 2769 (2012)

Christian Homann, Peter Lang, and Eberhard Riedle

selected for "Spotlight on Optics" – highlighted articles from OSA journals
by the Optical Society of America

Abstract:

Fully tunable deep UV pulses of 30 fs duration are generated in an all-solid-state scheme from 200 fs long pump pulses of a Ti:sapphire amplifier. The tunability comes from a non-collinear optical parametric amplifier with tailored spectral width. The output pulses are frequency doubled in a 50 µm BBO crystal and subsequently mixed in a 32 µm BBO crystal with part of the Ti:sapphire output. The compression is solely performed in the visible. This makes the setup extremely simple and efficient. Less than 400 µJ pump energy suffice to obtain sub-µJ deep UV pulses. The strategy for the bandwidth and chirp management is explained in detail.

1. Introduction

Ultrashort pulses tunable in the deep ultraviolet (DUV) down to the transmission limit of air (slightly below 190 nm) are important for spectroscopic applications. The needed pulse energies are in the range of hundreds of nJ, e.g., for the probe pulse in time resolved photo electron spectroscopy [1]. The direct excitation of bound higher electronic states in small molecules also can readily be performed with such a modest pulse energy and even the generation of solvated electrons from neat solvents has been demonstrated in this range [2]. In all mentioned applications, extremely fast processes are investigated, typically on the time scale of skeletal motions, i.e. with periods in the range of 20 to 50 fs. The investigations therefore need pulses with a duration significantly below 50 fs.

Early work was focused on the generation of the harmonics of the broadly available Ti:sapphire amplifier in consecutive nonlinear optical crystals [3,4]. No particular effort for the management of the chirp due to the dispersive materials was undertaken. The amount of traversed material was minimized by suitable geometries and the use of very thin crystals. In this way pulses in the 100 – 200 fs regime could be generated from suitably short 800 nm pulses. Tunability was added by a 800 nm pumped optical parametric amplifier (OPA) [5]. The OPA also is able to add spectral width to the final pulse and therefore allows in principal the generation of a DUV pulse shorter than the original pump pulse.

Later, frequency conversion in gases was demonstrated in various schemes. These include in particular four-wave-mixing of different harmonics of the Ti:sapphire pump laser [6,7] or with the output of an OPA [8-10]. For the enhancement of the efficiency even hollow fiber guiding had to be used [9]. In all attempts, rather high pump pulse energies were needed. Besides multi-mJ short pulse length Ti:sapphire amplifiers [6,7] a 300 µJ noncollinear OPA (NOPA) pumped by 10 mJ pulses at 800 nm was central to the conversion [10].

None of the schemes renders the needed combination of pump and output parameters of a prototype spectroscopic experiment: ~ 1 mJ pump energy of ~ 100 fs duration and fully tunable 30 fs output pulses with well above 100 nJ in the range from 189 to 240 nm, all with high reliability and low pulse fluctuations. In this contribution we will demonstrate that these goals can readily be achieved with an all-solid-state system pumped by less than 400 µJ at the Ti:sapphire fundamental. No compressor in the UV is needed despite the operation under ambient air. Instead we use a single two-prism arrangement in the visible output of the NOPA that provides the fundamental tunability. The proper chirp management in both the second harmonic generation (SHG) and the sum frequency generation (SFG) stage with part of the laser fundamental is sufficient to ensure the shortest DUV pulse length. By tailoring the spectral bandwidth to the acceptance bandwidth of the crystals, we achieve a good conversion efficiency despite the low pump energy and the extremely small crystal thicknesses.

2. Concept for the frequency conversion and the chirp management

The principal idea of our generation scheme is shown in Figure 1. A commercial Ti:sapphire amplifier system (CPA 2010; Clark-MXR) with an output wavelength of 779 nm and a pulse duration of 200 fs pumps a NOPA that provides the necessary spectral band-

width for the complete conversion chain [11,12]. Only 280 µJ of the available 750 µJ at 1.9 kHz repetition rate are used. This allows the operation of a second NOPA and even leaves some residual power for additional demands in the spectroscopic experiment. The horizontally polarized NOPA output is over-compressed in a double-passed pair of fused silica Brewster prisms. Subsequently it is frequency doubled in a thin BBO crystal and the resulting tunable mid-UV pulses are mixed in a further BBO crystal.

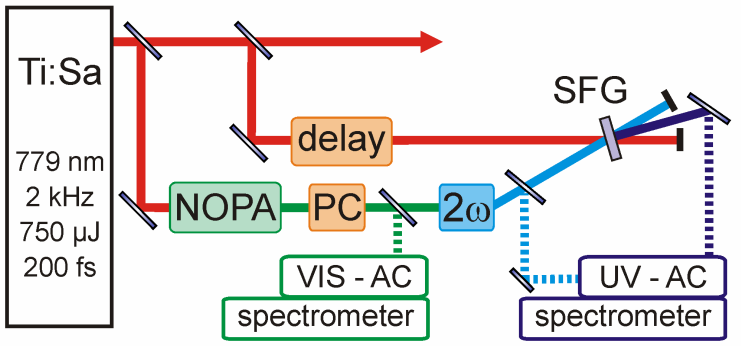

Fig.1: Schematic of the multistage frequency conversion to generate tunable 30 fs-pulses in the deep UV (from 190 to 240 nm)

For the design of our setup we start in the DUV. From the desired tuning range of 189 – 240 nm we can determine the intermediate UV tuning range to 250 – 347 nm. The corresponding fundamental range of 500 – 694 nm is readily reachable with the NOPA. We can also verify by the use of the program SNLO [13] that the necessary phase matching can be achieved in BBO. The required angles for type I phase matching range from 50.4° to 74.8°. Other commercially available crystals either do not allow such a wide tuning range or have a significantly lower effective nonlinearity.

The thinnest BBO crystals that we found to be commercially available without a glass support are nominally 30 µm. The one used in our experiments was manufactured and mounted by Castech Inc. and distributed by DÖHRER Elektrooptik GmbH. Ultrathin crystals cemented onto a support can most likely not withstand the extreme intensities in the UV and are thought to be only useful for pulse characterization. Careful handling avoiding mechanical shock or any attempts to clean the crystal is needed to ensure years of usage. For the 30 µm crystal we had to ensure by our own measurements that the crystal is indeed so thin. This can be done by observing the interference fringes in a high resolution spectral photometer.

For the measured crystal thickness of 32 µm we determine the acceptance bandwidth (FWHM; 29 THz for 198 nm generation) and set the bandwidth of the intermediate UV slightly larger. Since the bandwidth of the 779 nm light is just 3 THz, the generated bandwidth of the SFG stage will be equal to the acceptance bandwidth if sufficient UV width is available. For perfect compression, DUV pulse lengths below 20 fs are possible for the whole range from 189 to 240 nm.

Next we find that a BBO crystal in the range of 50 µm can produce this bandwidth in the SHG step. We show the calculated UV bandwidth obtainable in a 50 µm crystal in Table I. This estimate assumes that the visible pulse supplies enough bandwidth. Numerically we

find that a visible pulse with 50 % more bandwidth than the SHG acceptance bandwidth only leads to a 10 % decrease in the generated UV bandwidth. As this leads to some loss of conversion efficiency, we opted to match the visible bandwidth to the UV bandwidth (values shown in Table I). Any spectral components outside the acceptance bandwidth will only be poorly converted and at large spectral distances even possess a phase shifted by π. This makes the resulting pulse practically impossible to compress. To tailor the NOPA output, one can insert a glass block of suitable group delay dispersion after the seed light generator in the NOPA. For a variation of the DUV wavelength a slight variation of the material length or glass should be considered.

As a final step we perform a backward determination of the pulse chirp. We know that we want an optimally compressed pulse in the DUV. Propagation through air from the SFG crystal will already add chirp as does the SFG crystal. This is explicitly accounted for. The SHG step simply halves the linear chirp of the visible pulse [14], i.e.

$$\frac{d^2}{d\omega^2}\Phi(\omega) = \Phi''_{vis} = 2 \cdot \Phi''_{UV} \tag{1}$$

with the spectral phase $\Phi(\omega)$. Similarly, the SFG step adds the linear chirp of the visible and the 779 nm pulse [15]. Combining the spectral width and the chirp at each stage allows predicting the pulse length that can be checked experimentally.

To set the proper linear chirp of the NOPA output, we increase the prism separation in the compressor sufficiently to obtain strongly down chirped pulses. Usage of the prisms as close as possible to the apex is essential to avoid unnecessary higher order chirp contributions. Supplementary calculations and previous experience [14] show that in the present situation the influence of the higher order chirp does not yet influence our pulse parameters strongly. This is a consequence of the still modest demand for 30 fs pulses in the DUV. Accordingly, the spectral widths are quite small compared to what is typically achieved from a fully bandwidth optimized NOPA [16].

TABLE I: Design parameters and actually measured values for the generation of the DUV pulses.

		design		experiment	
	wavelength [nm]	bandwidth [nm]	pulse length [fs]	bandwidth [nm]	pulse length [fs]
NOPA	694	101 nm (63 THz)	420 fs	-	-
	530	28 nm (30 THZ)	408 fs	29 nm	324 fs
	500	22 nm (26 THz)	538 fs	-	-
UV	347	25.4 nm (63 THz)	142 fs	-	-
	265	7.1 nm (30 THz)	149 fs	6.6 nm	119 fs
	250	5.4 nm (26 THz)	215 fs	-	-
DUV	240	9.8 nm (51 THz)	8.6 fs	-	-
	198	3.7 nm (29 THz)	15.5 fs	1.3 nm	31 fs
	189	2.8 nm (24 THz)	18.5 fs	-	-

3. Experimental realization and characterization

The visible pulses out of the NOPA and the compressor are focused with a f = 250 mm spherical mirror with silver coating (see Figure 2b). The focal length is not particularly important, but the beam size has to be kept small enough to stay within the acceptance angle of the 50 μm BBO crystal of about 38 mrad. The intensity at the focus is way too high for proper SHG despite the long pulse length at this point. We find that the SHG crystal is best placed about 1 cm behind the focus, just at the point where a further approach to the focus does not increase the efficiency anymore. In this way a clean and round beam profile can be obtained. When the compression is optimized for the shortest DUV length, the position of the SHG crystal might have to be varied slightly.

The emerging UV beam of about 1 μJ pulses is recollimated and focused with just one f = 250 mm dielectric mirror. Again the numerical aperture is the decisive value to watch. In addition, as small as possible off-axis angles are used to avoid excessive astigmatism. The SFG crystal is placed slightly behind the UV focus and the supplementary 779 nm beam

(pulse energy 80 µJ) is overlapped within the crystal. The red beam is focused with a fused silica lens, since its bandwidth is quite small. Throughout our setup no dichroics are needed, as the small angle between the UV and the red allows geometric separation of the DUV pulse. The resulting weak spectral chirp is found to be much smaller than the natural divergence [17] and should therefore not influence the use of the DUV pulses.

To optimize the compression of the DUV, the effective prism separation of the folded visible compressor is varied as shown in Figure 2a). This demands an exactly equal change in the path length of the red sum beam. To ensure this linkage, we place a delay line for the 779 nm beam onto the manual delay line inserted between the prisms.

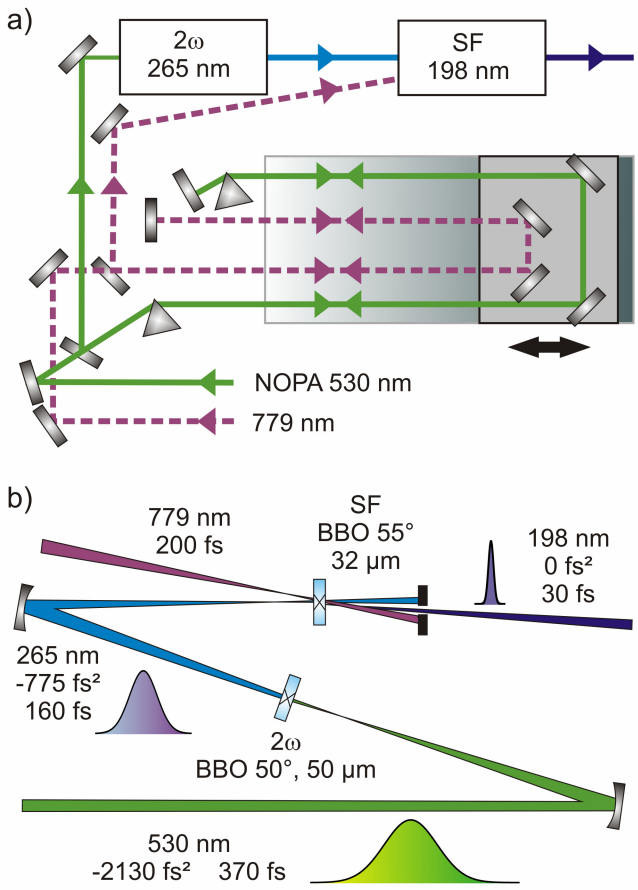

Fig. 2: a) Experimental setup for the simultaneous variation of the NOPA compression and the delay of the 779 nm Ti:sapphire fundamental. b) Schematic of the nonlinear mixing scheme. The relevant pulse parameters (center wavelength, linear chirp Φ'', and pulse length) are indicated.

With the setup we were readily able to generate pulses from 193 nm to 219 nm. Shorter wavelengths were not attempted, as proper steering mirrors and appropriately cut crystals were not available. Longer wavelengths than 220 nm were not of interest in our own laboratory, as they can be readily obtained by direct doubling of the NOPA. We are, however, sure that a good spectral overlap of the two schemes can be achieved. The width of the spectra (see Figure 3a) allows for approximately 20 fs-pulses throughout the tuning range (Figure 3b). The pulse energy (see Figure 3c) was not fully optimized as the beam transport in the visible and UV was generously designed due to other experimental demands. This resulted in a rather modest SHG conversion from 15 - 20 µJ NOPA output (10 - 13 µJ after the com-

pressor) to the typical 1 µJ intermediate UV. Still, pulse energies well above 100 nJ were measured throughout the DUV tuning range corresponding to energy conversion efficiencies from the intermediate UV to the DUV of well above 10 %. At particularly carefully optimized wavelengths we achieved much higher pulse energies up to 630 nJ. We believe that mechanics with higher adjustment sensitivity will readily lead to similarly high output throughout the tuning range. The pulse energies correspond to milliwatts of average power in the DUV. Visually we do not notice any significant fluctuations and the DUV is stable over many hours. The beam shape is close to Gaussian. No degradation of either the optics or the crystals has been observed.

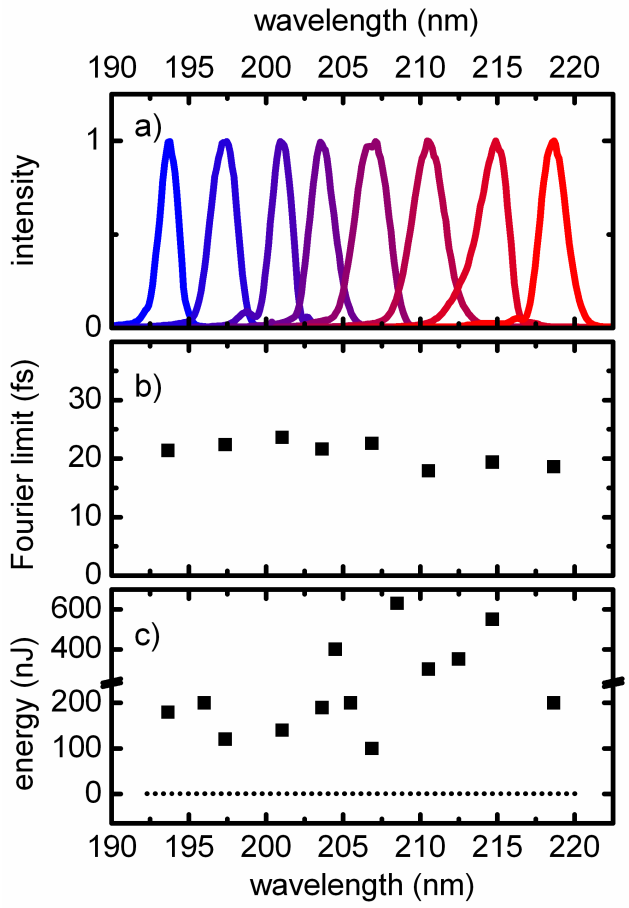

Fig. 3: a) Spectra of fully tunable DUV pulses. b) Fourier limit of the pulses derived from the spectral width. c) Measured energies.

To fully characterize the generation scheme and to validate the theoretical considerations, we measured the spectral width and pulse lengths with fiber coupled spectrometers and autocorrelators of our own design [18, 19]. The relevant values are summarized in Table 1. They compare very well with the predictions and thus confirm our concept. Strictly speaking, the acceptance bandwidths are calculated for the collinear case. However, they are only altered by less than 1 % if the small angle used in the experiment is considered explicitly. Remarkably, any possible higher order chirp does not prohibit the extremely simple and straight forward multi-stage conversion scheme.

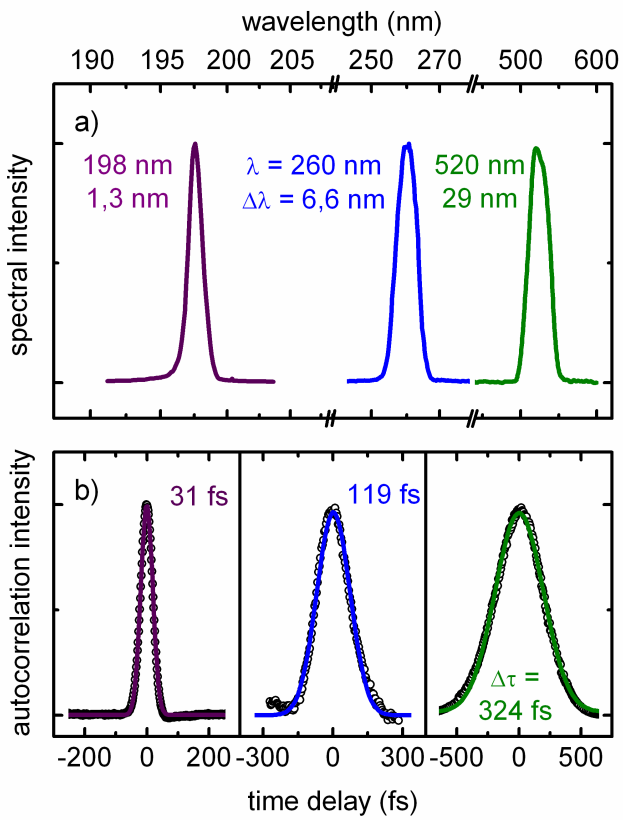

Fig. 4: Spectral and temporal characterization of the DUV and intermediate pulses.

Representative spectra and autocorrelation traces are shown in Figure 4. Note that the visible pulse is 324 fs long and the intermediate UV pulse 119 fs. They were measured with a 100 µm thick BBO crystal for the visible SHG autocorrelation and a 50 µm thick BBO crystal for the two-photon absorption UV autocorrelation. From the design we know that at these points the pulses are down chirped and propagation through normally dispersive material compresses them without any additional loss in energy. In this way we perform all the critical compression efforts in the visible region where the highest optical quality is available. The 198 nm pulse was characterized by two-photon absorption in a 50 µm thick sapphire disk, which overestimates the pulse length by less than 1 fs. To determine the pulse length from the autocorrelation curve we fit a Gaussian to it. This fits nicely and in addition shows that there are no detectable shoulders or satellites to the DUV pulse. This confirms our assumption that higher order contributions to the chirp do not lead to a pulse substructure. The deconvoluted pulse length is 31 fs and about 35 % above the Fourier limit of 22.9 fs calculated from the measured spectrum. Our scheme for generating compressed DUV pulses with just a compressor in the visible does indeed work quite well.

The FWHM spectral width of the 198 nm pulse is smaller then the predicted one. We believe this to be due to the fact that the red mixing pulse is roughly of the same length as the mid-UV pulse. We have shown previously that this leads to a decreased conversion efficiency in the spectral wings of the chirped pulse [20] which we do indeed see. To overcome this limitation which will be even stronger for still shorter wavelengths, the red pulse could also be chirped [15,20]. As sufficient red pulse energy is available, this will not lead to a decrease of efficiency.

4. Summary and Conclusions

We have presented a straight forward and simple to implement scheme for the generation of fully tunable DUV pulses. We generate energetic visible pulses with controlled bandwidth and down chirp from a NOPA followed by a long prism compressor. These pulses are then frequency doubled in a 50 μm thick BBO crystal and subsequently mixed with supplementary 779 nm light in a 32 μm BBO crystal. All processes are fully phase matched. No additional compression is needed in the UV or DUV and even a thin entrance window into a vacuum chamber can be precompensated [14]. Pulse energies in the sub-μJ regime have already been demonstrated and could readily be increased into the μJ regime.

The output energies are presently limited by our NOPA design that limits the pump energy to below 300 μJ. With a high power NOPA [21] we would immediately expect more than an order of magnitude higher output energy, getting us into the solid μJ regime. The present energy efficiency is roughly 1 ‰, as compared to values of about 10^{-9} for recently reported tunable high harmonic generation in krypton [22] and 0.1 ‰ for nonresonant four-wave mixing in argon [7]. This shows that the conversion in crystals is an excellent method if pulses above 189 nm - the accepted transmission edge of BBO - and in the 30 fs-regime are needed. This has also been corroborated recently at 250 kHz repetition rate where about 10 μW average power at 198 nm [23] and well above 100 nJ at 226 nm and 100 kHz [24] were reported, however without the possibility of wavelength tuning. Even shorter DUV pulses might become feasible with newly emerging crystals like $KBe_2BO_3F_2$ (KBBF) [25] - provided they become generally available.

The presented setup allows for the conversion of the 779 nm pulses of our Ti:sapphire amplifier system to the DUV. In addition, we achieve a pulse shortening from 200 fs to 30 fs, more than a factor 6. The necessary spectral bandwidth is provided by the NOPA. A NOPA and the continuum seed source can even be pumped by still longer pulses, e.g., from Yb^{3+} based laser systems [17]. The conversion scheme can be easily transferred to the center wavelength of around 1030 nm. The NIR pump wavelength even results in a 20 % larger mixing bandwidth in the SFG step. This will allow the generation of 30-fs DUV pulses with a repetition rate of 100 kHz.

The tunable DUV pulses in the 30 fs regime are believed to be of immediate use for many spectroscopic experiments. In time resolved photo electron spectroscopy they can render more electron kinetic energy as compared to the typical mid-UV pulses and the tunability can help to minimize the generation of detrimental one-color signal contributions. DUV pulses are also of great interest for the investigation of small polyatomic molecules to bridge the gap between the many ongoing investigations on H_2 and the wide field of work on organic molecules. All this comes at very low complexity and high stability of the setup due to the fully solid state design.

Acknowledgement

The authors thank Maximilian Bradler and Nils Krebs for valuable assistance. The work was supported by the DFG-Cluster of Excellence: Munich-Centre for Advanced Photonics. The International Max Planck Research School on Advanced Photon Science (C. H.) is gratefully acknowledged.

References

[1] A. Stolow and J.G. Underwood, "Time-Resolved Photoelectron Spectroscopy of Non-adiabatic Dynamics in Polyatomic Molecules", Adv. Chem. Phys. **139**, 497 (2008).

[2] C.G. Elles, A.E. Jailaubekov, R.A. Crowella, S.E. Bradforth, "Excitation-energy dependence of the mechanism for two-photon ionization of liquid H_2O and D_2O from 8.3 to 12.4 eV", J. Chem. Phys. **125**, 044515 (2006).

[3] A. Nebel and R. Beigang, "External frequency conversion of cw mode-locked Ti:Al_2O_3 laser radiation", Opt. Lett. **16**, 1729 (1991).

[4] J. Ringling, O. Kittelmann, F. Noack, G. Korn, and J. Squier, "Tunable femtosecond pulses in the near vacuum ultraviolet generated by frequency conversion of amplified Ti:sapphire laser pulses", Opt. Lett. **18**, 2035 (1993).

[5] F. Seifert, J. Ringling, F. Noack, V. Petrov, and O. Kittelmann, "Generation of tunable femtosecond pulses to as low as 172.7 nm by sum-frequency mixing in lithium triborate", Opt. Lett. **19**, 1538 (1994).

[6] T. Fuji, T. Horio, and T. Suzuki, "Generation of 12 fs deep-ultraviolet pulses by four-wave mixing through filamentation in neon gas", Opt. Lett. **32**, 2481 (2007).

[7] M. Beutler, M. Ghotbi, and F. Noack, "Generation of intense sub-20-fs vacuum ultraviolet pulses compressed by material dispersion", Opt. Lett. **36**, 3726 (2011).

[8] C. G. Durfee III, A. Rundquist, S. Backus, Z. Chang, C. Herne, H. C. Kapteyn, and M. M. Murnane, "Guided-wave phase-matching of ultrashort-pulse light", J. Nonlinear Opt. Phys. Mater. **8**, 211 (1999).

[9] A.E. Jailaubekov and S.E. Bradforth, "Tunable 30-femtosecond pulses across the deep ultraviolet", Appl. Phys. Lett. **87**, 021107 (2005).

[10] M. Mero and J. Zheng, "Femtosecond optical parametric converter in the 168–182-nm range", Appl. Phys. B **106**, 37 (2012).

[11] T. Wilhelm, J. Piel, and E. Riedle, "Sub-20-fs pulses tunable across the visible from a blue-pumped single-pass noncollinear parametric converter", Opt. Lett. **22**, 1494 (1997).

[12] E. Riedle, M. Beutter, S. Lochbrunner, J. Piel, S. Schenkl, S. Spörlein, W. Zinth, "Generation of 10 to 50 fs pulses tunable through all of the visible and the NIR", Appl. Phys. B **71**, 457 (2000).

[13] SNLO nonlinear optics code, available from A.V. Smith, AS-Photonics, Albuquerque, NM.

[14] P. Baum, S. Lochbrunner, and E. Riedle, "Generation of tunable 7-fs ultraviolet pulses: achromatic phase matching and chirp management", Appl. Phys. B **79**, 1027 (2004).

[15] C. Schriever, S. Lochbrunner, M. Optiz, and E. Riedle, "19 fs shaped ultraviolet pulses", Opt. Lett. **31**, 543 (2006).

[16] P. Baum, M. Breuer, and E. Riedle, "Brewster-angled chirped mirrors for broadband pulse compression without dispersion oscillations", Opt. Lett. **31**, 2220 (2006).

[17] C. Homann, M. Bradler, M. Förster, P. Hommelhoff, and E. Riedle, "Carrier-envelope phase stable sub-two-cycle pulses tunable around 1.8 μm at 100 kHz", Opt. Lett. **37**, 1673 (2012).

[18] I.Z. Kozma P. Baum, U. Schmidhammer, S. Lochbrunner, and E. Riedle, "Compact autocorrelator for the online measurement of tunable 10 femtosecond pulses", Rev. Sci. Instr. **75**, 2323 (2004).

[19] C. Homann, N. Krebs, and E. Riedle, "Convenient pulse length measurement of sub-20-fs pulses down to the deep UV via two-photon absorption in bulk material", Appl. Phys. B **104**, 783 (2011).

[20] I.Z. Kozma, P. Baum, S. Lochbrunner, and E. Riedle, "Widely tunable sub-30 fs ultraviolet pulses by chirped sum frequency mixing", Opt. Express **11**, 3110 (2003).

[21] P. Tzankov, J. Zheng, M. Mero, D. Polli, C. Manzoni, and G. Cerullo, "300 μJ noncollinear optical parametric amplifier in the visible at 1 kHz repetition rate", Opt. Lett. **31**, 3629 (2006).

[22] B. Mahieu, S. Coraggia, C. Callegari, M. Coreno, G. De Ninno, M. Devetta, F. Frassetto, D. Garzella, M. Negro, C. Spezzani, C. Vozzi, S. Stagira, and L. Poletto, "Full tunability of laser femtosecond high-order harmonics in the ultraviolet spectral range", Appl. Phys. B, online first, DOI: 10.1007/s00340-012-4944-6.

[23] J. Faure, J. Mauchain, E. Papalazarou, W. Yan, J. Pinon, M. Marsi, and L. Perfetti, "Full characterization and optimization of a femtosecond ultraviolet laser source for time and angle-resolved photoemission on solid surfaces", Rev. Sci. Instr. **83**, 043109 (2012).

[24] H. Shen, S. Adachi, T. Horio, and T. Suzuki, "Two-color deep-ultraviolet 40-fs pulses based on parametric amplification at 100 kHz", Opt. Express **19**, 22637 (2011).

[25] C. Zhou, T. Kanai, X. Wang, Y. Zhu, C. Chen, and S. Watanabe, "Generation of ultrashort 25-μJ pulses at 200 nm by dual broadband frequency doubling with a thin $KBe_2BO_3F_2$ crystal", Opt. Express **20**, 13684 (2012).

Convenient pulse length measurement of sub-20-fs pulses down to the deep UV via two-photon absorption in bulk material

published in

Appl. Phys. B **104**, 783 - 791 (2011)

Christian Homann, Nils Krebs, and Eberhard Riedle

Abstract

The beam attenuation by two-photon absorption in thin crystals and glass plates is utilized for directly measuring the intensity autocorrelation of UV femtosecond pulses without the need for an auxiliary pulse. We give a full description of the newly developed setup for operation from the blue down to the deep UV. The conditions that must be met to achieve reliable measurements are investigated. The choice of the two-photon absorbing material governs the attainable wavelength range, the material thickness determines the shortest pulse that can be reliably characterized, and high intensities influence the derived pulse duration due to saturation effects. The performance of the UV autocorrelator is demonstrated for pulses with durations below 20 fs, with energies of 3 nJ and with central wavelengths from the visible down to 195 nm. 2 Hz update rates are achieved at the 1 kHz repetition rate of the laser. The wavelength dependence of the two-photon absorption coefficient of BBO is determined by z-scan measurements and we find that it decreases much faster at longer wavelengths than is expected from the linear absorption spectrum.

1. Introduction

Ultrashort pulses in the UV are essential prerequisites for the investigation of the primary processes in physics, chemistry and biology. Particularly small molecules do not absorb in the visible, and two- or multi-photon excitation can lead to unwanted complexity in the interpretation. Tunable UV pulses with sufficient energy of a few μJs can be readily generated by second harmonic generation (SHG) or sum frequency generation (SFG) of tunable visible pulses generated in noncollinear parametric amplifiers (NOPAs) in thin nonlinear crystals [1, 2]. With some care even pulse lengths below 20 fs can be reached in the UV [3, 4].

The characterization of the UV pulses turns out to be more demanding than the generation. The method of phase matched second harmonic autocorrelation in nonlinear crystals - intensity or fringe resolved - that is widely used in the visible and near infrared, cannot be used in the UV due to the lack of suitable crystals. Even if new crystals were found, the resulting second harmonic would be in the vacuum UV and therefore hard to handle.

A viable alternative is SFG or difference frequency generation (DFG). This does, however, require an additional auxiliary pulse of comparable shortness and known duration. From a practical stand point, any mixing scheme is cumbersome as the time zero has to be regained after any alteration of the optical system.

When a full characterization of the pulse and its spectral and temporal phase is needed, this effort is justified and spectral phase interferometry for direct electric-field reconstruction (SPIDER) [5, 6] and X-FROG (cross-correlation frequency-resolved optical gating) [7] are well established. Recently, a shaper-assisted cross-correlation setup was introduced that is free of external references, additional pulses and a spectrometer, which employs a two-dimensional shaper that works in the UV and uses a solar blind multiplier as nonlinear detector [8].

However, for spectroscopic work and day to day application a much simpler setup is needed to optimally compress the UV pulses and monitor the length for the subsequent interpretation of the data. A number of techniques have been tested to directly characterize UV pulses. Multiple FROG techniques like transient-grating (TG), self-diffraction (SD) and polarization gating (PG) FROG have successfully been transferred to the UV spectral region [9, 10]. If the diffracted beam is not analyzed in a spectrometer, the TG- and SD-FROG signal renders a third order autocorrelation and the desired information on the pulse length. We notice, that these methods are not often invoked in spectroscopic publications and we can only speculate that too high a pulse energy is required or the beam shape influences the measured value of the pulse length.

Since $\chi^{(2)}$ processes are not attractive for the UV, several techniques exploiting two- or multi-photon absorption as nonlinear process have been investigated for the UV spectral domain. They can be arranged in two categories: measuring the generated charge or induced fluorescence, or measuring the depletion - both in dependence of the temporal overlap of two replicas of the UV pulse. The first approach has been realized with CsI as photocathode in a photomultiplier tube, but with the problem of suppressing the one-photon absorption background in the photomultiplier tube material [11]. In fused silica, microstructured electrodes on top of the substrate are required, that are complex to manufacture, together with a high

bias voltage that leads to a high dark current [12]. Recently, diamond pin diodes have been developed, that allow pulse length measurements down to a wavelength of 225 nm, but again with a complex fabrication procedure and limited durability [13].

For gas phase and particular molecular beam experiments opportunities like the two-photon induced fluorescence of xenon excimers for measuring sub-picosecond pulse durations at 248 nm [14] or the ionization of rare gases [15] arise. These methods are, however, not easily incorporated into typical laser setups.

Two-photon absorption (TPA) of even modest energy femtosecond pulses is present in liquids and bulk materials if the photon energy is larger than half the absorption edge. To utilize this for autocorrelation measurements, a strong pump and a weak probe beam, both derived from the pulse to be characterized, are spatially overlapped in the medium. Both beams are individually depleted by TPA, however at temporal overlap an additional contribution due to TPA with one photon from each beam arises. This two-beam contribution creates the autocorrelation signal.

In solution an autocorrelation trace of 180 fs pulses in a 1 mm water cell at 282 nm [16], and even 30 fs pulses in a 50 μm thin water film have been reported [17]. Already in 1991, Dadap et al. [18] successfully demonstrated the applicability of TPA in diamond for pulse length measurements. They showed autocorrelation traces of 180 fs pulses at 310 nm and claimed that their method is applicable in a wavelength range from 220 nm to 550 nm.

Despite these promising reports TPA depletion has not been widely used. Traditionally, the back ground free signal of SHG seems to have been important for the fluctuating sources of early days and insensitive detection. Now, laser systems and parametric converters as well as SHG schemes are available with pulse fluctuation below 1 % and high enough repetition rate to allow for rapid data taking. Transient spectroscopy has matured greatly and readily allows to detect broadband transmission changes below 10^{-4} [19, 20] and even 10^{-6} for single detection wavelengths [21].

In this work we report on our investigation about the suitability of different materials for TPA depletion, the experimental conditions needed to perform reliable measurements and the methods used for evaluation of the raw data. The resulting UV autocorrelator is found to be a highly stable and simple device capable of characterizing pulses from the blue down into the VUV, with durations shorter than 20 fs and for nJ pulse energies. Practical guidelines for the implementation are given at the end.

2. Experimental setup and design considerations

The layout of the UV autocorrelator is shown in Fig. 1a). It is similar to standard autocorrelators for the visible or NIR. However, no nonlinear crystal for frequency mixing of two pulse replicas is used. Instead the attenuation at temporal overlap of the weaker of the two beams is monitored.

To generate the pump and probe pulses the input beam is split by a thin fused silica cover slip (thickness 160 μm, Esco Products Inc.), which introduces only a negligible amount of dispersion for typical experimental conditions. The front side reflection of the cover slip is used as probe pulse. It is temporally and also spatially separated from the back side reflecti-

on at the measurement point. However, the back side reflection doubles the total signal from the photodiode while the signal due to the two-photon interaction is not influenced by the second reflection due to the lack of temporal overlap. One might therefore consider a wedged substrate. We prefer to allow for this effect in the data evaluation.

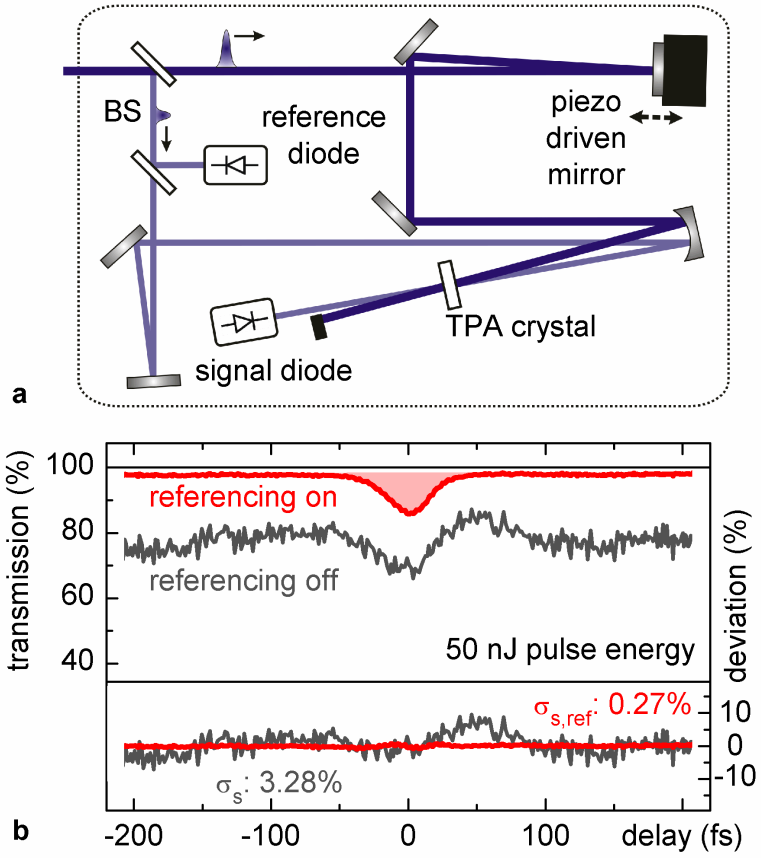

Fig. 1: a) Layout of the autocorrelator setup. BS: beam splitter (fused silica, 160 µm). b) Typical measured signal (single scan of 0.5 s duration, each individual laser shot detected and shown) of a pulse with an energy of 50 nJ and a central wavelength of 277 nm, with (red curve) and without (grey curve) using a second diode for pulse energy referencing. The lower panel shows the significant reduction of noise by referencing (Gaussian fit subtracted from the measured data).

Since the depletion in the probe beam due to TPA of one pump and one probe photon is proportional to the pump pulse intensity, a strong pump pulse is desirable. When using s-polarized light, the reflection at 45° off the fused silica cover slip yields a favorable energy ratio of ~ 15 : 1 for pump and probe out of the total available pulse. An identical cover slip in the path of the reflected probe pulses compensates for the dispersion in the path of the pump pulses. The reflection off this plate is used for referencing (see Fig. 1a). With p-polarized light, the energy ratio between pump and probe increases to ~ 100 : 1, which might lead to hardly detectable probe and reference pulses. In this case the use of appropriately coated beam splitters or an angle far from Brewster's angle might be preferential.

The delay between the pump and probe pulses is controlled by a piezo-based delay line, yielding a maximum delay of approximately 500 fs, which was calibrated interferometrically

with a HeNe laser [22]. The piezo position is scanned via a sawtooth shaped voltage with a frequency of 2 Hz, generated by a home-built circuit. An additional manual delay line is helpful for initially adjusting the temporal overlap. Both pulses are then focused by the same spherical mirror (radius of curvature 500 mm) into the two-photon absorbing medium.

The depleted probe beam as well as the reference beam are detected on large area (5 x 5 mm²) photodiodes (S1227-66BQ; Hamamatsu Photonics K.K.) integrated in a home-built amplifier circuit [21]. The large area ensures that the whole beam profiles are measured without the need for additional focusing optics even for slight self focusing or beam distortion. The spectrally integrated detection avoids problems with a possible frequency redistribution due to cross phase modulation. The photodiodes and the piezo driver voltage are read out simultaneously by a multi-channel digitizer board (NI 6132; National Instruments) for each laser shot and displayed without smoothing or next neighbor averaging.Tunable UV pulses for the test of the autocorrelator were generated by frequency-doubling the output of a single stage NOPA pumped by a 1 kHz Ti:Sa amplifier system (CPA 2001; Clark MXR). The pulses were pre-compressed in the visible by a pair of fused silica Brewster prisms [3] and frequency-doubled in BBO crystals with thicknesses between 30 µm and 100 µm depending on the spectral width of the particular visible pulses. For wavelengths below 225 nm, the primary UV pulses were mixed with the fundamental Ti:Sa pulses in a second BBO crystal. To adjust the UV pulse energy, a $\lambda/2$ retarder is inserted in front of the doubling crystal. Before entering the autocorrelator setup the pulses are reflected off three dielectric mirrors to strongly suppress the visible background.

3. Results and discussion

Figure 1b) shows a typical single scan from 400 consecutive laser shots, recorded with our setup for input pulses with an energy of 50 nJ at a central wavelength of 277 nm measured in a BBO crystal (134 µm thick) as the two-photon absorbing medium. BBO was chosen for its availability in thin samples and the high TPA coefficient. The depleted probe beam, detected on the signal diode, is subject to pulse energy fluctuations, that can be similar in magnitude to the autocorrelation depletion signal (grey curve). By dividing the signal through the pulse energy reference, we compensate for these fluctuations to first order. This enhances the signal to noise ratio by more than an order of magnitude (red curve) from a standard deviation of $\sigma_s = 3.28$ % to $\sigma_{s,ref} = 0.27$ %, as can be seen after subtracting a Gaussian function from the measured data (lower panel in Fig. 1b). As a consequence, already a maximum transmission change of less than 1 % is sufficient in single scan mode for a usable autocorrelation. An even better noise level can be obtained by modest signal averaging over repeated scans and the detectivity is accordingly increased to the 1 ‰ range, well below the pump laser noise. We find it important that the full beam profiles are detected on each diode and that the diodes are both operated in their linear response regime.

A slight asymmetry in the autocorrelation trace is observed as depletion offset of about 1 % when the pump precedes the probe. This is due to long-living free-carrier-absorption and the different intensities in the pump and the probe beam [23]. This offset is negligible for the practical application of the autocorrelator.

At high energies, we additionally see a self-diffracted beam in the direction $2\vec{k}_{pump} - \vec{k}_{probe}$. In our case, when working at energies below 100 nJ, the diffracted energy is so low, that it does not disturb the depletion autocorrelation measurement. A possibility to avoid the diffracted beam is to rotate the polarization of either pump or probe beam so that their polarizations are orthogonal. However, this also reduces the two-beam TPA cross section and hence the depletion signal.

To retrieve a precise value for the pulse length from the measured autocorrelation trace, we perform a deconvolution based on the following theoretical considerations:
Since the one-photon absorption can be neglected, the coupled differential equations describing the decrease of the pump intensity I_{pump} and the probe intensity I_{probe} due to TPA after propagating the distance x read

$$\frac{dI_{pump}}{dx} = -\beta I_{pump}^2 - \beta I_{pump} I_{probe} \tag{1}$$

$$\frac{dI_{probe}}{dx} = -\beta I_{probe}^2 - \beta I_{pump} I_{probe} \tag{2}$$

with the TPA coefficient β. The attenuation of the pump/probe pulse is due to a delay time independent term from the TPA of the pulse itself and the delay time dependent interaction of both pulses. For input pulses with the spatial and temporal profile described by $I^0(r,t)$, e.g., Gaussian input pulses with pulse length τ (FWHM) and beam waist w_0: $I^0(r,t) = I_o \exp\left(-4\ln 2\, t^2/\tau^2 - 2r^2/w_0^2\right)$, the solution for I_{probe} is given by

$$I_{probe}(x,r,t,\Delta t) = \frac{I^0_{probe}(r,t)}{1 + \beta x \left(I^0_{pump}(r, t-\Delta t) + I^0_{probe}(r,t) \right)} \tag{3}$$

with the pump-probe delay Δt. In the autocorrelation measurement the time delay Δt is scanned while the probe pulse is integrated in space, time and frequency by the photodiode. For Gaussian pulses this leads to an autocorrelation trace with a width depending on the pulse length τ and the intensity of the input pulses. For low intensities, the trace can be deconvoluted with a factor of $\sqrt{2}$, according to the procedure in SHG autocorrelation [24]. A derivation of the asymptotic equality of the TPA depletion curve and the autocorrelation function is given in reference [25]. For higher intensities a broadening of the autocorrelation trace is predicted as well as seen in the experiment.

Figure 2a) shows the increase of the measured autocorrelation width by 19 % when the input pulse energy is increased to a maximum of 200 nJ corresponding to a pump pulse peak intensity of 470 GW/cm² and a maximum probe depletion of 68 %. To compare the measurements with theory, we calculated the autocorrelation traces by numerically integrating equation (3) for different pump-probe delays Δt, and using the experimentally determined values for β = 0.85 cm/GW (see section 4), crystal thickness 173 µm (BBO) and surface reflection losses of 1.05 %. The retrieved autocorrelation widths (red line in Fig. 2a) show excellent agreement with the measured ones (circles in Fig. 2a) for a pulse length τ of 22 fs.

As a rule of thumb we found that the measured autocorrelation width can be deconvoluted with a factor of $\sqrt{2}$ when the transmission change is smaller than 15 %, and an overestimate

of 5 % is accepted. We define the transmission change as the probe depletion at zero time delay normalized by the total signal from the probe pulse far from temporal overlap. The stated values for the transmission change are corrected to only the front side reflection.

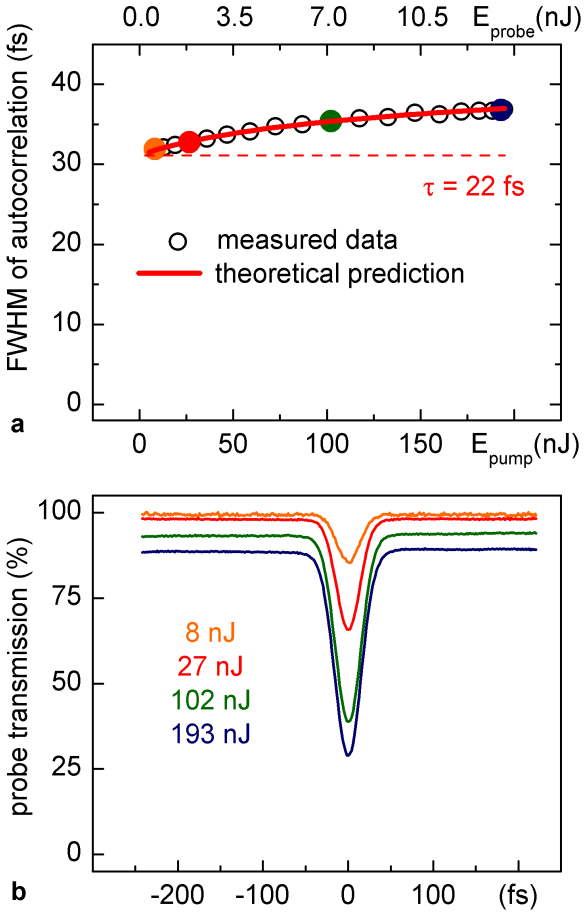

Fig. 2: a) Measured and calculated width of the depletion autocorrelation signal with increasing pulse energy. For probe transmission changes smaller than 15 % the pulses can be deconvoluted with good accuracy by a factor of $\sqrt{2}$ for Gaussian pulses. b) shows selected traces at different pump energies; the baseline offset is due to the TPA of the probe beam itself.

In phase matched SHG autocorrelation the finite phase matching band width can limit the precision of the measurement. This is particularly important for chirped pulses as the extreme spectral components are suppressed and too short a value is determined [26]. In the TPA depletion such a limitation is not present. The only consequence of the material dispersion that can lead to distorted pulse length measurements is the pulse lengthening introduced by the TPA medium.

A first order approximation of the pulse duration after propagating through a medium of length L for an initially Fourier-limited Gaussian pulse with pulse duration τ_0 and central wavelength λ_c is given by

$$\tau = \tau_0 \sqrt{1 + \left(\frac{4 \ln 2 \, L \lambda_c^3}{2\pi c^2 \tau_0^2} \frac{d^2 n(\lambda)}{d\lambda^2}\bigg|_{\lambda_c} \right)^2} \qquad (4)$$

(compare e.g. [27]), with c being the speed of light in vacuum. To help estimating the expected pulse lengthening with this formula, calculated values for the second derivate of the refractive index with respect to the wavelength are shown for selected materials in Fig. 3a). Figure 3b) indicates down to which minimal pulse duration the respective materials with a thickness of 200 µm can be used when accepting a maximal pulse lengthening of 20 %. For example, when working at a central wavelength of 300 nm and using a 200 µm thick BBO crystal as TPA medium, pulses with a Fourier-limit of 18 fs (or larger) are lengthened by (less than) 3.6 fs. If even shorter pulses are to be measured, a material with less dispersion (e.g., sapphire or fused silica) has to be used, or a thinner crystal is needed, however at the expense of a decreasing transmission change.

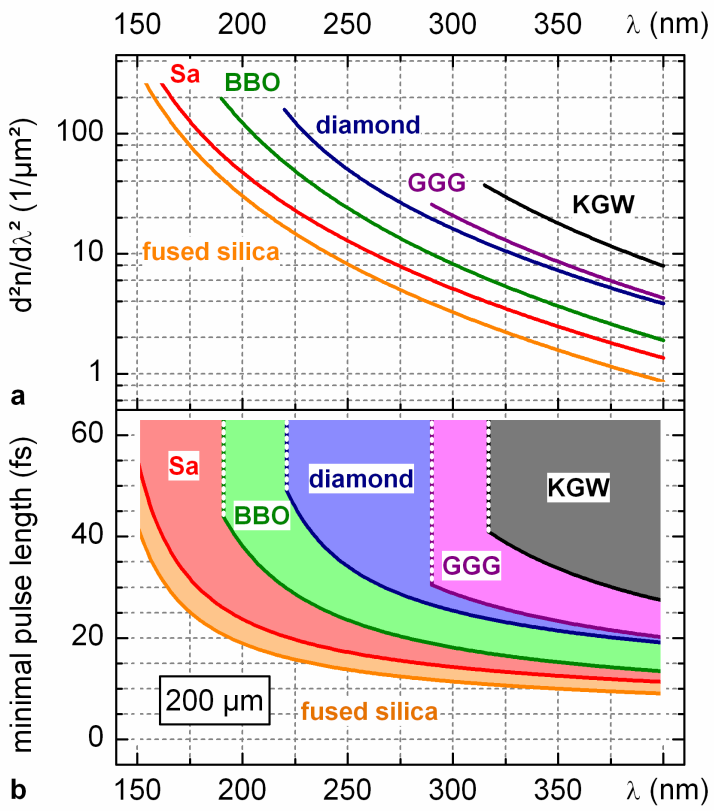

Fig. 3: a) Calculated 2nd derivates of the refractive index with respect to wavelength for different materials to estimate the pulse lengthening due to dispersion with equation (4). b) The lines indicate the calculated Fourier-limit of pulses which are elongated by 20 % due to dispersion in materials with a thickness of 200 µm. The filled areas mark the conditions where the pulse lengthening is below 20 %.

Apart from their differing dispersion the various materials vary strongly in the strength and wavelength dependence of their β values, which makes them well suited for selected intensity regimes and wavelength regions. As a general rule β increases with decreasing wavelength. Each material can only be used above the one-photon absorption edge - signalized in Fig. 3 with the dashed vertical lines. We summarize the relative merit of the various TPA materials tested in our investigations in Fig. 4. The raw measured signals were scaled according to the varying pulse length, energy and focal spot size.

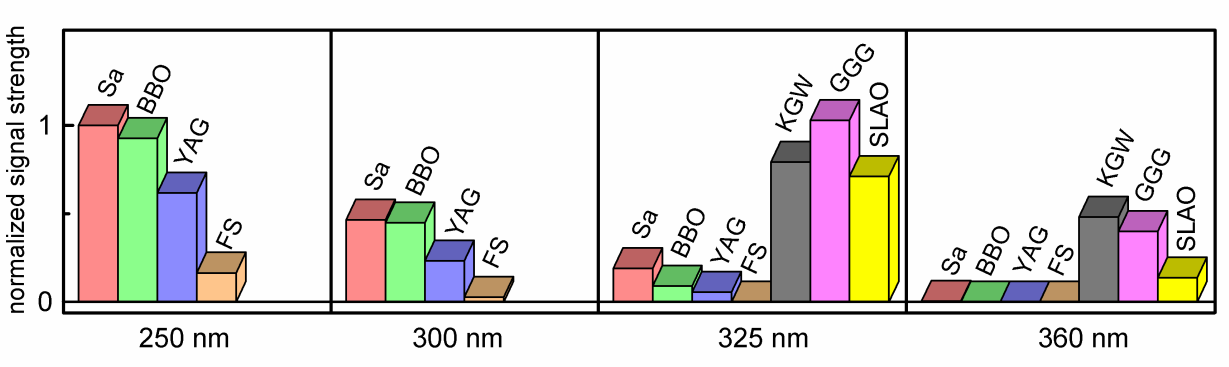

Fig. 4: Normalized two-photon absorption strength of various materials in dependence on the pulse wavelength. Sa = standard grade sapphire, BBO = barium borate, YAG = yttrium aluminium garnet, FS = UV grade fused silica, KGW = potassium gadolinium tungstate, GGG = gadolinium gallium garnet, SLAO = strontium lanthanum aluminate.

BBO is highly suited for measurements in the wide wavelength region from 195 nm up to 330 nm, and has the advantage that it is often available in a variety of thicknesses in laser laboratories. Please note, that the crystal cut is of no relevance as the TPA depletion autocorrelator does not rely on phase matching but on the high β that only depends weakly on the orientation. We checked this fact by comparing the TPA depletion of the more common β-BBO with similar size α-BBO crystals and found no significant difference.

In the course of our measurements we found, that sapphire shows a very similar transmission change compared to BBO in the investigated wavelength region, but with considerably smaller dispersion. However sufficiently thin samples might not be at hand easily. Fused silica shows even less dispersion, however only very small transmission changes are observed due to its low β value [28]. We found YAG samples that show a good TPA strength at 250 and 300 nm, but there are doubts about the UV transmission of YAG. The dispersion of YAG is even somewhat lower in the deep UV than that of BBO.

For pulses with central wavelengths above 330 nm materials with a smaller band gap are needed as the TPA strength of the materials discussed so far starts to vanish (see Fig. 4). We found that diamond is well suited for measurements up to about 360 nm and potassium gadolinium tungstate (KGW) extends the accessible wavelength region even further into the visible. KGW shows a very large transmission change due to its unusually high β [29]. It is therefore advantageous for primarily finding the autocorrelation signal, but has the drawback of being strongly dispersive (see Fig. 3) even in the near UV spectral domain [30].

Due to the dispersion problems encountered with KGW we investigated even less well known crystals with respect to their applicability for TPA autocorrelation measurements. Salt crystals like NaCl, KCl and KBr look very promising according to an early report of the β value [31], but at the longer wavelength region of interest, we did not find similiarly large values, and the damage threshold was only moderate. MgO showed a TPA signal twice as large as BBO at 310 nm with a very similar dispersion, but no signal at 360 nm. For $MgAl_2O_4$ no signal was found at 310 and 360 nm. BK7 and CaF_2 showed no significant signals at any tested wavelength.

Very useful materials in the near UV are gadolinium gallium garnet (GGG) and strontium lanthanum aluminate (SLAO). The dispersion of GGG [32] is much lower than that of KGW

(see Fig. 3) and close to the one of diamond. GGG of good crystal quality is easier to obtain than for diamond that is typically supplied as polycrystalline material. We particularly suggest thin samples of GGG for measurements in the spectroscopically important range around 350 nm.

With the proper choice of the TPA material, an adequate thickness and a moderate pulse intensity and by using the referencing technique, autocorrelation measurements can be performed for a large variety of experimental conditions.

To demonstrate the capability to measure pulses below 20 fs, we generated pulses with a central wavelength of 297 nm and a Fourier-limit of 12 fs, which were compressed down to 18 fs by optimizing the prism compressor in the visible (Fig. 5a). The trace is almost of Gaussian shape, as expected from the nearly Gaussian like spectrum, with slight wings due to residual higher order chirp. Due to the high sensitivity achieved through the pulse energy referencing (see beginning of section 3), pulses with energies of only 3.2 nJ (sum of pump and probe) at kHz repetition rate and a duration of 24 fs at a central wavelength of 277 nm were successfully measured in a 135 µm thick BBO crystal (Fig. 5b). Even pulses with central wavelengths as short as 195 nm can be characterized without difficulty (Fig. 5c). We expect that UV grade sapphire with its optical band gap of 8.8 eV [33] allows for TPA autocorrelation measurements down to about 150 nm.

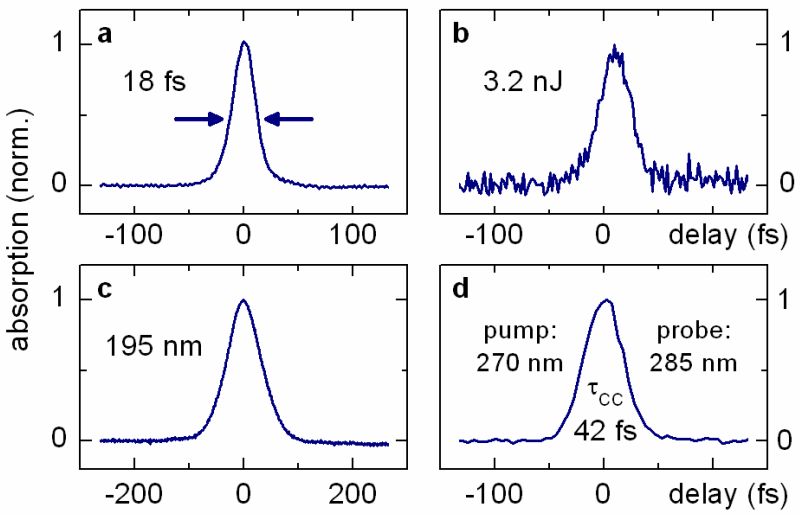

Fig. 5: Measured auto- and cross-correlation traces showing the applicability of our concept to a) pulse durations below 20 fs (λ_c = 300 nm), b) pulse energies down to 3.2 nJ (λ_c = 277 nm), c) central wavelengths down to 195 nm, d) cross-correlation of pulses in the UV spectral region, where neither sum- nor difference frequency mixing are possible.

Our scheme also allows measuring the cross-correlation of UV pulses with closely spaced central frequencies by two-color TPA where neither SFG nor DFG are feasible. As an example Fig. 5d) shows a cross-correlation of pulses with 270 nm and 285 nm in BBO with a width of 42 fs. To our knowledge no crystal is currently available that allows phase-matching to the sum or difference frequency of nominally 139 nm and 5130 nm. In addition the TPA autocorrelator avoids any erroneous measurements of chirped pulses as can easily be made with phase matched schemes [26].

Our concept also readily applies to measure pulses with durations in the range of hundreds of femtoseconds, where spectrometer based pulse characterization methods, e.g., SPIDER and FROG, are troublesome due to the narrow spectra involved and the accompanying need of high resolution spectrometers. The only limiting factor in our case is the travel range of the piezo. A measurement of the frequency-doubled output of our Ti:Sa amplifier system in a 500 µm thick KGW crystal yields a pulse duration of 148 fs (Fig. 6). Calculations show that the pulse lengthening introduced by the KGW crystal amounts to only 1 fs in this case. For comparison we measured the cross-correlation with a 20 fs NOPA pulse at 540 nm by SFG. The derived pulse lengths agree within experimental accuracy and confirm the validity of the TPA depletion measurements.

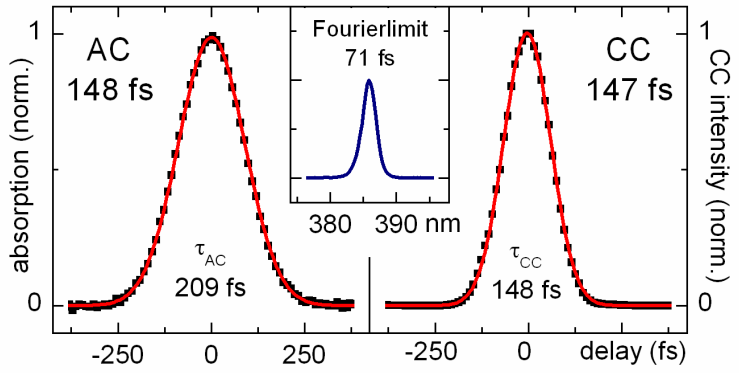

Fig. 6: Comparison of the autocorrelation (width τ_{AC}) of a frequency-doubled Ti:Sa laser (λ_c = 386 nm) measured in a KGW crystal with a thickness of 500 µm to the cross-correlation (width τ_{CC}) with a 20 fs NOPA pulse.

4. Wavelength dependence of one- and two-photon absorption in BBO

The band gap of β-BBO has been reported as 6.4 eV [34], corresponding to a one photon absorption band edge at 193 nm. This suggests that autocorrelation measurements based on TPA should be feasible up to 386 nm. However, the observed depletion at wavelengths significantly below this value was found to be extremely small. To the best of our knowledge, for this wavelength region there is no coherent set of values for the TPA coefficient β of BBO reported in the literature. We therefore conducted z-scan measurements at different wavelengths to determine β_{BBO} between 250 nm and 340 nm.

Fig. 7a) depicts the schematic setup for measuring open-aperture z-scans. A detailed description of this technique can be found in [35]. The transmission through a BBO crystal (thickness 173 µm) was measured in dependence on its position along the focused beam (radius of curvature of focusing mirror 500 mm). For an accurate determination of the respective intensities incident on the crystal, the beam size was recorded with a beam profiler at every position. Additionally we measured for every wavelength the pulse duration, pulse energy and crystal reflectivity. Again, referencing was used to enhance the signal to noise ratio.

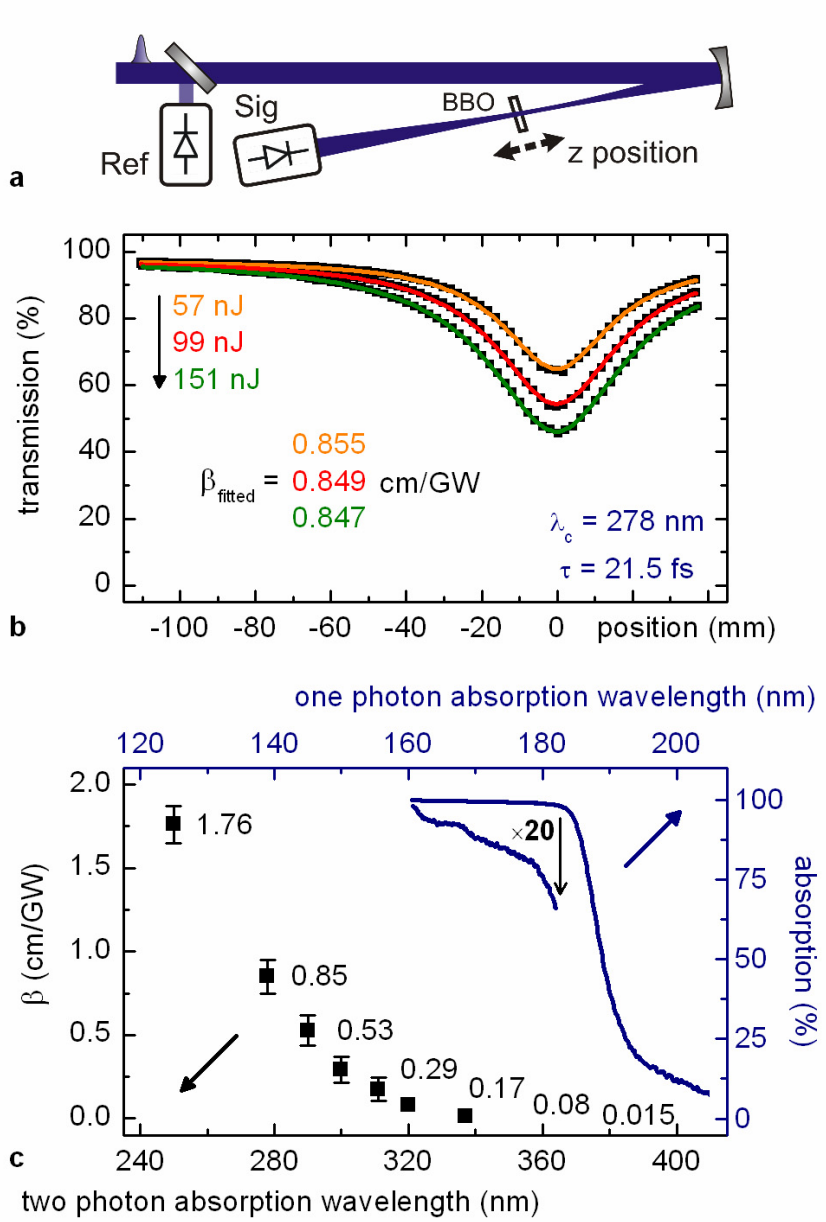

Fig. 7: a) Layout of the setup for open aperture z-scan measurements. b) Experimental data with different pulse energies but otherwise unchanged parameters (black squares) and the fits to the measured data with the TPA coefficient β being the only fit parameter (colored lines). c) Obtained β coefficients for different central wavelengths (black squares) and measured one-photon absorption (blue line) of a 173 µm thick BBO crystal.

Exemplarily we show measurements at a central wavelength of 278 nm for three different pulse energies in Fig. 7b) together with their associated fits. The observed z dependence is modeled by equation (3) with $I_{pump} = 0$ and integrating over the beam profile and t. For the different energies, and accordingly intensity regimes, we obtain an absolute value of the fitting parameter β of 0.85 cm/GW. Fig. 7c) summarizes our results for different wavelengths. For the investigated β-BBO crystal the TPA coefficient decreases from 1.76 cm/GW at 250 nm to 0.015 cm/GW at 337 nm (black squares). This is in good agreement with earlier measurements at two wavelengths [36]. At longer wavelengths the decrease in transmission was too weak to be detected. We note that for selected wavelengths we also conducted z-

scan measurements of other BBO crystals. We found that the β-values can vary up to 20 % from sample to sample, somewhat more than the variation of the $\chi^{(2)}$ value reported [37].

For comparison we also measured the one-photon absorption of the crystal in a VUV spectrophotometer (blue line). Remarkably there exists a wavelength region from about 170 nm to 185 nm where the crystal is nearly opaque due to one-photon absorption but the corresponding TPA is hardly measurable. It has been postulated that the direct band gap of BBO is significantly higher than the effective linear absorption cutoff at about 190 nm and possible reasons for the increasing absorption at wavelengths below 193 nm were discussed [36]. In view of our TPA coefficient measurements one could reassign the direct band gap of BBO to 160 nm or 7.76 eV. Alternatively symmetry considerations might render a differing absorption cutoff for one- and two-photon absorption. The first interpretation is not unlikely, as we see some finite transmission for the 173 μm BBO between 160 nm and 185 nm in accordance with ref. [34].

5. Guideline for a reliable measurement

In summary, to achieve a quick and accurate pulse length measurement with TPA induced depletion, we suggest the following procedure:

- Choose the correct two-photon absorbing material according to the central wavelength of the pulse to be measured. We suggest sapphire for the wavelength range 150 nm to 270 nm, BBO for the range 200 nm to 330 nm, and GGG for wavelengths longer than 320 nm (for details see Fig. 4).
- Position the material in the focus of pump and probe beam, which can be easily achieved by minimizing the transmission of a single beam (preferably the pump beam) by moving the material along the beam propagation direction.
- Select the front reflection from the first beam splitter as probe beam.
- After overlapping pump and probe spatially at the focal point, e.g., by using a pinhole or a beam profiler, the temporal overlap is found by looking for a change in probe transmission when changing the delay between the beams. For this the probe detector should be well centered and have a sensitive area that is larger than the beam.
- For finding the autocorrelation signal for the first time, reasonably high energies and thick crystals (up to ~1 mm) are advantageous.
- To get an accurate measurement of the pulse length and to avoid pulse lengthening the transmission change and the dispersion introduced by the crystal must be controlled.
- The transmission change induced on the probe by the pump pulse, which is determined by the pulse intensities, the TPA coefficient and the thickness of the crystal, should be smaller than 15 %.

- The suitable thickness of the measurement crystal depends on the spectral width (Fourier limit) of the pulse and the chosen material due to chirp (for details see Fig. 3).
- For these conditions the pulse length can be calculated within an error of 5 % from the measured autocorrelation width by deconvolution with a factor of $\sqrt{2}$ for a Gaussian pulse.
- A strong improvement of the signal to noise ratio is gained by referencing the autocorrelation signal to the beam energy fluctuations.

6. Outlook and perspectives

In conclusion, we have demonstrated that probe beam depletion caused by two-photon absorption from the simultaneous interaction with a stronger pump pulse is a well suited method to determine the pulse length of UV femtosecond pulses. Measurements seem possible down to 150 nm and have explicitly been demonstrated for 3 nJ pulses at 1 kHz repetition rate - regimes that are at least difficult to access with other methods. In particular, the length of the second, third, fourth and fifth harmonic of the broadly used Ti:Sa systems can be readily measured. Any available thin plate with a band gap energy of $E_{gap}/2 < h\nu_{laser} < E_{gap}$ and a sufficiently high TPA coefficient can be employed.

In contrast to sum and difference frequency mixing, which are restricted by the need for phase-matching, TPA is not hampered by this constraint. In addition, the detector is simply positioned in the probe beam and no weak deflected or converted beam has to be found. We demonstrate measurements of pulses with a duration from sub-20 fs to hundreds of femtoseconds. In principle the only limit for long pulse durations is the travel range of the used piezo, while the shortest pulse durations are only limited by the small material dispersion.

Our setup is simple and robust, and it renders pulse lengths at 2 Hz update rate for the 1 kHz laser system used. This corresponds to 400 data points per curve. For higher repetition rates of the laser, proportionally faster updates seem feasible with suitable electronics and scanning mechanics. The autocorrelator can easily be incorporated into existing experimental setups where the pulse length is an important parameter, e.g. in pump-probe setups [19]. As a matter of fact, the sensitive detection schemes developed for pump-probe schemes are the basis of the autocorrelator setup. Because there is no need for an additional auxiliary pulse, as for example in cross-correlation measurements, our setup does not require finding time zero after an adjustment of the compressor. It therefore readily permits the online minimization of the pulse duration. The measured correlation width is a monotonous function of the true pulse length even for too high an intensity and therefore the pulse length minimization is a highly stable procedure. For too thick a TPA plate still the minimal pulse length obtainable by variation of the linear chirp, e.g., by variation of the insertion in a prism compressor, is found. This minimal length is reached halfway through the TPA plate and from the known dispersion the necessary compression correction for the shortest pulse at the front end can be determined.

The characterization of the wavelength-dependent two-photon absorption coefficient in BBO reveals a discrepancy between the one- and two-photon absorption edges. This discrepancy is quite advantageous for pumping of a BBO-based OPA in the UV. Is seems feasible down to a wavelength of approximately 330 nm. This agrees well with previous work, which showed that pumping at 266 nm yields only very low output energies, mainly due to TPA of the pump [38]. Pumping at 343 nm - the third harmonic of the increasingly available femtosecond systems based on Yb^+ - provided high conversion efficiencies [39] and tunability throughout the visible [40].

Acknowledgements

The authors thank Peter Lang and Alexandra Waritschlager for valuable experimental assistance, Johannes Piel for an early demonstration of the feasibility and Andreas Ulrich for the VUV measurement. The work was supported by the DFG-Cluster of Excellence: Munich-Centre for Advanced Photonics and the SFB 749. The International Max Planck Research School on Advanced Photon Science (C. H.) is gratefully acknowledged.

References

[1] M. Beutler, M. Ghotbi, F. Noack, D. Brida, C. Manzoni, and G. Cerullo, "Generation of high-energy sub-20 fs pulses tunable in the 250–310 nm region by frequency doubling of a high-power noncollinear optical parametric amplifier", Opt. Lett. **34**, 710 (2009).

[2] I.Z. Kozma, P. Baum, S. Lochbrunner, and E. Riedle, "Widely tunable sub-30 fs ultraviolet pulses by chirped sum frequency mixing", Opt. Express **11**, 3110 (2003).

[3] P. Baum, S. Lochbrunner, and E. Riedle, "Generation of tunable 7-fs ultraviolet pulses: achromatic phase matching and chirp management", Appl. Phys. B **79**, 1027 (2004).

[4] N. Krebs, R.A. Probst, and E. Riedle, "Sub-20 fs pulses shaped directly in the UV by an acousto-optic programmable dispersive filter", Opt. Express **18**, 6164 (2010).

[5] C. Iaconis, and I. A. Walmsley, "Spectral phase interferometry for direct electric-field reconstruction of ultrashort optical pulses", Opt. Lett. **23**, 792 (1998).

[6] P. Baum, S. Lochbrunner, and E. Riedle, "Zero-additional-phase SPIDER: full characterization of visible and sub-20-fs ultraviolet pulses", Opt. Lett. **29**, 210 (2004).

[7] S. Linden, J. Kuhl, and H. Giessen, "Amplitude and phase characterization of weak blue ultrashort pulses by downconversion", Opt. Lett. **24**, 569 (1999).

[8] J. Möhring, T. Buckup, and M. Motzkus, "Shaper-assisted full-phase characterization of UV pulses without a spectrometer", Opt. Lett. **35**, 3916 (2010).

[9] S. Backus, J. Peatross, Z. Zeek, A. Rundquist, G. Taft, M.M. Murnane, and H.C. Kapteyn, "16-fs, 1-μJ ultraviolet pulses generated by third-harmonic conversion in air", Opt. Lett. **21**, 665 (1996).

[10] D.J. Kane, A.J. Taylor, R. Trebino, and K.W. DeLong, "Single-shot measurement of the intensity and phase of a femtosecond UV laser pulse with frequency-resolved optical gating", Opt. Lett. **19**, 1061 (1994).

[11] Y. Takagi, "Simple autocorrelator for ultraviolet pulse-width measurements based on the nonlinear photoelectric effect", Appl. Opt. **33**, 6328 (1994).

[12] A.M. Streltsov, J.K. Ranka, and A.L. Gaeta, "Femtosecond ultraviolet autocorrelation measurements based on two-photon conductivity in fused silica", Opt. Lett. **23**, 798 (1998).

[13] N.F. Kleimeier, T. Haarlammert, H. Witte, U. Schühle, J.-F. Hochedez, A. BenMoussa, and H. Zacharias, "Autocorrelation and phase retrieval in the UV using two-photon absorption in diamond pin photodiodes", Opt. Express **18**, 6945 (2010).

[14] M.H.R. Hutchinson, I.A. McIntyre, G.N. Gibson, and C.K. Rhodes, "Measurement of 248-nm, subpicosecond pulse durations by two-photon fluorescence of xenon excimers", Opt. Lett. **12**, 102 (1987).

[15] S.A. Trushin, W. Fuss, K. Kosma, and W.E. Schmid, "Widely tunable ultraviolet sub-30-fs pulses from supercontinuum for transient spectroscopy", Appl. Phys. B **85**, 1 (2006).

[16] A. Reuther, A. Laubereau, D.N. Nikogosyan, "A simple method for the in situ analysis of femtosecond UV pulses in the pump-probe spectroscopy of solutions", Opt. Commun. **141**, 180 (1997).

[17] A.E. Jailaubekov and S.E. Bradforth, "Tunable 30-femtosecond pulses across the deep ultraviolet", Appl. Phys. Lett. **87**, 021107 (2005).

[18] J.I. Dadap, G.B. Focht, D.H. Reitze, and M.C. Downer, "Two-photon absorption in diamond and its application to ultraviolet femtosecond pulse-width measurement", Opt. Lett. **16**, 499 (1991).

[19] U. Megerle, I. Pugliesi, C. Schriever, C.F. Sailer, and E. Riedle, "Sub-50 fs broadband absorption spectroscopy with tunable excitation: putting the analysis of ultrafast molecular dynamics on solid ground", Appl. Phys. B **96**, 215 (2009).

[20] A.L. Dobryakov, S.A. Kovalenko, A.Weigel, J.L. Pérez-Lustres, J. Lange, A. Müller, and N.P. Ernsting, "Femtosecond pump/supercontinuum-probe spectroscopy: Optimized setup and signal analysis for single-shot spectral referencing", Rev. Sci. Instrum. **81**, 113106 (2010).

[21] C. Schriever, S. Lochbrunner, E. Riedle, and D.J. Nesbitt, "Ultrasensitive ultraviolet-visible 20 fs absorption spectroscopy of low vapor pressure molecules in the gas phase", Rev. Sci. Instrum. **79**, 013107 (2008).

[22] I.Z. Kozma, P. Baum, U. Schmidhammer, S. Lochbrunner, and E. Riedle "Compact autocorrelator for the online measurement of tunable 10 femtosecond pulses", Rev. Sci. Instrum. **75**, 2323 (2004).

[23] Y. Tomita, M. Shibata, and J. Bergquist, "Effects of free-carrier absorption on time-resolved pump-probe two-photon absorption in semi-insulating semiconductors", J. Appl. Phys. **72**, 1075 (1992).

[24] K. Sala, G. Kenney-Wallace, G. Hall, "CW autocorrelation measurements of picosecond laser pulses", IEEE J. Quantum Electron. **16**, 990 (1980).

[25] Y. Tomita, M. Shibata, and J. Bergquist, "Pulsewidth dependence of time-resolved two-photon absorption with picosecond pump-probe excitation", J. Appl. Phys. **72**, 2102 (1992).

[26] S. Lochbrunner, P. Huppmann, E. Riedle, "Crosscorrelation measurements of ultrashort visible pulses: comparison between nonlinear crystals and SiC photodiodes", Opt. Commun. **184**, 321 (2000).

[27] J.-C. Diels, W. Rudolph, "*Ultrashort laser pulse phenomena*" (Academic Press, San Diego, CA, 1996).

[28] A. Dragomir, J.G. McInerney, D.N. Nikogosyan, and P.G. Kazansky, "Two-photon absorption properties of commercial fused silica and germanosilicate glass at 264 nm", Appl. Phys. Lett. **80**, 1114 (2002).

[29] A.I. Vodchits, V.P. Kozich, V.A. Orlovich, P.A. Apanasevich, "Z-Scan studies of KYW, KYbW, KGW, and $Ba(NO_3)_2$ crystals", Opt. Commun. **263**, 304 (2006).

[30] M.C. Pujol, M. Rico, C. Zaldo, R. Solé, V.Nikolov, X. Solans, M. Aguiló, F. Díaz, "Crystalline structure and optical spectroscopy of Er^{3+}-doped $KGd(WO_4)_2$ single crystals", Appl. Phys. B **68**, 187 (1999).

[31] R. Pizzoferrato, M. Casalboni, R. Francini, U.M. Grassano, F. Antonangeli, M. Piacentini, N. Zema, and F. Bassani, "Two-Photon Absorption Using Synchrotron Radiation: a Novel Technique", Europhys. Lett. **2**, 571 (1986).

[32] D.L. Wood, and K. Nassau, "Optical properties of gadolinium gallium garnet", Appl. Opt. **29**, 3704 (1990).

[33] R.H. French, "Electronic Band Structure of Al_2O_3, with Comparison to AlON and AlN", J. Am. Ceram. Soc. **73**, 477 (1990).

[34] R.H. French, J.W. Ling, F.S. Ohuchi, and C.T. Chen, "Electronic structure of β-BaB_2O_4 and LiB_3O_5 nonlinear optical crystals", Phys. Rev. B **44**, 8496 (1991).

[35] M. Sheik-Bahae, A.A. Said, T.-H.Wei, D.J. Hagan, and E.W. van Stryland, "Sensitive Measurement of Optical Nonlinearities Using a Single Beam", IEEE J. Quantum Electron. **26**, 760 (1990).

[36] R. DeSalvo, A.A. Said, D.J. Hagan, E.W. van Stryland, and M. Sheik-Bahae, "Infrared to Ultraviolet Measurements of Two-Photon Absorption and n_2 in Wide Bandgap Solids", IEEE J. Quantum Electron. **32**, 1324 (1996).

[37] D.J. Armstrong, W.J. Alford, T.D. Raymond, and A.V. Smith, "Absolute measurement of the effective nonlinearities of KTP and BBO crystals by optical parametric amplification", Appl. Opt. **35**, 2032 (1996).

[38] P. Tzankov, T. Fiebig, and I. Buchvarov, "Tunable femtosecond pulses in the near-ultraviolet from ultrabroadband parametric amplification", Appl. Phys. Lett. **82**, 517 (2003).

[39] D. Herrmann, C. Homann, R. Tautz, M. Scharrer, P. St.J. Russell, F. Krausz, L. Veisz, and E. Riedle, "Approaching the full octave: Noncollinear optical parametric chirped pulse amplification with two-color pumping", Opt. Express **18**, 18752 (2010).

[40] C. Homann, C. Schriever, P. Baum, and E. Riedle, "Octave wide tunable UV-pumped NOPA: pulses down to 20 fs at 0.5 MHz repetition rate," Opt. Express **16**, 5746 (2008).

Seeding of picosecond and femtosecond optical parametric amplifiers by weak single mode continuous lasers

published in

Opt. Express **13**, 730 - 739 (2013)

Christian Homann, Markus Breuer, Frank Setzpfandt, Thomas Pertsch, and Eberhard Riedle

Abstract:

Optical parametric amplifiers are typically seeded with either parametric superfluorescence or broadband continuum pulses. We show both with picosecond and femtosecond pump pulses, that single longitudinal mode cw lasers with mW power can be well used to generate nearly Fourier-transform-limited output pulses. The 532 nm pumped picosecond system is seeded in the near infrared and fully tunable from 1260 to 1630 nm. The femtosecond system operates stable with just hundreds of seed photons. The output spectral width matches closely to the width of individual spectral features found in single shot spectra of parametric superfluorescence. Both systems provide interesting radiation sources for nonlinear optics experiments that need highly controlled and clean excitation.

1. Introduction

Optical parametric amplifiers (OPAs) offer the unique possibility to amplify optical signals from the UV to the mid infrared. This is possible without the necessity for resonances in the amplifying medium like it is encountered in laser amplifiers. It was only through the use of laser dyes that similar tunability was achieved [1]. But this comes at the cost of dye solutions that have to be replenished quite frequently. OPAs on the other hand are fully solid state devices and need practically no replacement of consumables. Even though OPA was demonstrated already very early, the process became technically most important with the advent of pico- and femtosecond lasers. This is due to the fact that the amplification scales exponentially with the square root of the pump intensity and for long pulses a high energy is needed. At the same time the damage threshold fluence scales as $\tau^{0.5}$ [2], which leads to a damage intensity proportional to $\tau^{-0.5}$.

For pulsed dye lasers it is well recognized that even the use of elaborate resonator designs does not lead to Fourier-transform-limited (FL) pulses. However, injection seeding or even locking with single longitudinal mode cw lasers readily leads to FL pulses [3-6]. The concept of cw seeding was subsequently transferred to nanosecond optical parametric oscillators and amplifiers and is used in a wide range of wavelengths [7-10]. The typical seeding power of a few mW renders roughly 10^7 photons during the ns amplification window and therefore leads to stable operation.

If the pump pulse duration is decreased to a few picoseconds, the number of seed photons goes down to 10^4. Still the feasibility of cw seeded OPA could be demonstrated and compared to the more often used case of optical parametric generation (OPG) [11]. The seeding indeed led to nearly FL pulses and a lowered OPA threshold. Recently even first reports of cw seeded femtosecond OPAs became available, however at the expense of 500 mW seeding [12] and only slight tunability in the near infrared (NIR) [13].

In this work we demonstrate that mW levels suffice to cleanly seed a fs OPA in the visible and a widely tunable ps OPA in the NIR. Both systems operate in the μJ range and with kHz repetition rate and are aimed at experiments that need highly controlled and clean optical excitation. The fs setup explores the limits of cw seeding, the ps OPA renders an unprecedented source of close to FL pulses with about 5 ps duration. This translates to less than 1 nm or about 3 cm^{-1} bandwidth. Such a bandwidth is below the homogeneous broadening in the condensed phase and therefore allows the optimal resolution of any excitation dependent dynamics. FL tunable pulses in the ps regime are otherwise hard to generate with an OPA, as the continuum seeding used in many modern fs OPAs is not available due to the lack of a compressible ps continuum. On the other hand, OPG as a source needs a rather high degree of spectral filtering with the associated loss in effective seed power. Even the most advanced synchronously pumped optical parametric oscillators (OPOs) in the fs or ps domain can at best render output pulses in the 10 nJ regime. Still higher pulse energies come at the expense of largely increased complexity and limited beam quality as well as tunability [14]. For many nonlinear applications pulse energies beyond these levels are needed.

2. Two-stage picosecond OPA

The setup used for the OPA with cw seed light is quite similar to the generic setup of continuum seeded OPAs [15, 16]. The laser output at 1064 nm is frequency doubled to obtain visible pump light. In our recent work we have discussed the advantages of visible or UV pumping in OPAs [17]. The increased group velocity mismatch is of no concern for the modestly short pulses generated.

The setup for the ps OPA is shown in Fig. 1. A commercial Nd:YVO_4 regenerative amplifier system (picoREGEN IC-10000; High Q Laser) delivers 10.6 ps pulses of 360 µJ energy at 1064 nm with 5 kHz repetition rate. These are frequency doubled in a 1.5 mm BBO crystal cut at 23.5° to 7 ps green pulses. To ensure a high second harmonic generation (SHG) of 130 µJ, we focus the fundamental light with an f = 250 mm AR coated lens, place the BBO crystal sufficiently behind the focus to avoid saturation, and finally recollimate the SHG light with another identical lens. We checked that the SHG divergence does not change as the BBO crystal is moved along the axis. In this way the SHG output can be smoothly varied without affecting the OPA alignment. As seed system an external cavity diode laser (TSL-210F; santec Corporation) tunable without mode hops from 1260 to 1630 nm is used. The pump light is split into two beams that each pump one of two OPA stages. The pump beams are focused with R = -500 mm dielectrically coated mirrors into the amplifier crystals. The focusing mirrors are both placed below the seed and the pre-amplified beam path to introduce a noncollinearity in the plane containing the BBO crystal axis. The output of the fiber delivering the NIR seed light is collimated and simultaneously weakly focused by an aspherical lens (f = 11.0 mm, N.A. 0.25; Thorlabs). This leads to a very clean focus and an excellent spatial overlap with the pump beam. The polarization of the cw seed light is set externally to horizontal polarization with a fiber polarization controller.

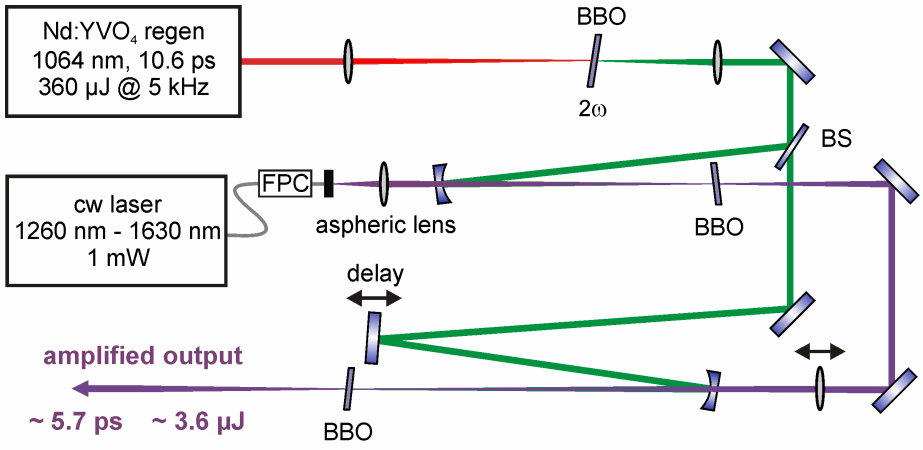

Fig. 1: Schematic of the two-stage noncollinear optical parametric amplifier pumped by a ps laser. BS: beam splitter; FPC: fiber polarization controller.

In the first amplifier stage 44 µJ pump energy are used and focused to a diameter of below 100 µm. This corresponds to an intensity of about 10 GW/cm^2 at the amplifier crystal, which is again placed behind the focus. As amplifier crystal we use an 8 mm thick BBO crystal cut at 26.5° for type I phase matching. In a preliminary experiment we tried shorter

crystals as we were concerned about the limited beam overlap in long crystals. We only found weak amplification and rapid crystal damage. This is due to the fact that the same overall amplification has to be generated in a shorter crystal through a higher intensity. Already in early work on ps OPAs it has been measured that the damage threshold of BBO for ps pulses is in the order of 10 GW/cm^2 for 250 ps pulses [18]. The above given scaling law thus predicts a damage threshold of 60 GW/cm^2 for our 7 ps pulses. Only through the use of the long crystal can we stay below the damage threshold and still get the desired single-stage amplification of 3 x 10^4 needed to amplify the mW seed to the µJ level. At the used pump intensity no damage was observed in many months of operation.

The second amplifier uses the same pump geometry at 84 µJ energy and an identical BBO crystal. We varied the noncollinearity angle in both amplifiers to find the maximum single pass amplification. The seeding in the idler branch does not allow the increase in amplification bandwidth found for a noncollinear OPA (NOPA) operated in the signal regime [16, 19]. However, the experiments showed that the best amplification is still found for an external angle of about 4.0° in both amplifiers and the crystals placed in walk-off compensating geometry. We believe that this geometry leads to the best compromise between signal-pump and idler-pump spatial walk-off and therefore the highest gain over the crystal length.

In between the two amplifiers we use an f = 250 mm fused silica lens to image all pre-amplified light into the pumped volume of the second amplifier. The spatial overlap between seed and first pump, and between pre-amplified beam and second pump is quite critical as the whole setup is just marginally operated in saturation with respect to the seed.

Due to the cw seed, the temporal overlap in the first stage is automatically ensured and the alignment consists simply of spatially overlapping seed and pump within the BBO crystal. After the initial alignment of the tilt angle of the amplifier crystal, the daily operation is quite easy despite the NIR operation. Even in the second amplifier the comparatively long pump pulse makes finding the temporal overlap quite simple. It can best be found with a high speed photodiode and an oscilloscope. Only for the final optimization monitoring of the increased output with a NIR detector or a sensitive powermeter is preferable. Quite helpful is the observation of the off-axis signal output. Its wavelength tunes from 920 to 790 nm. If the longest seed wavelengths are used, the signal can already be seen with the bare eye on a white card. This greatly facilitates the initial alignment. Once the temporal and spatial overlap is found, the seed can be tuned to the desired wavelength. Only a slight change of the internal phase matching angle by 0.6° is needed over the full tuning range.

With the described system we obtain up to 4 µJ output. The average power is up to 20 mW and thereby much higher than the 1 mW seed level used. Still, if a photodiode is used to determine the amplification factor, one has to consider its temporal response function of 1 ns in our case, which decreases the contrast from the full 3 x 10^4 amplification to about 150. We find roughly the same amplification in both OPA stages. The contribution of parametric superfluorescence is determined to be below 5 %.

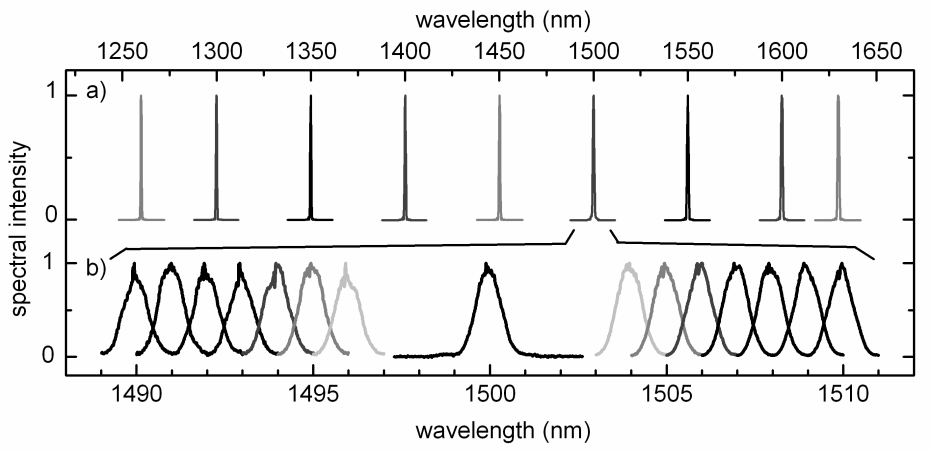

Fig. 2: Sample spectra of the ps-pumped NOPA output showing (a) the large tuning range from 1260 nm to 1630 nm, (b) the fine tuning capability exemplarily from 1490 nm to 1510 nm (the spikes are due to an imperfect subtraction of the cw background).

Typical output spectra are shown in Fig. 2 as measured with a spectrum analyzer (86142B OSA; Agilent Technologies, Inc.). In Fig. 2(a) it is shown how the output can be tuned over the full range from 1260 to 1630 nm without any gaps or discontinuities beyond the 0.1 nm tuning steps of the seed. This is done mainly by computer controlled tuning of the seed and only a minor adjustment of the phase matching angles. Only the polarization of the cw seed laser has to be readjusted, because the seed laser changes its polarization when the wavelength is scanned. For a limited tuning range of about 20 nm, e.g., 1490 to 1510 nm as shown in Fig. 2(b), no mechanical adjustment at all is needed. The new ps source therefore affords the possibility to do precise frequency spectroscopy with simultaneous high peak power for nonlinear excitation and gating in the ps range.

Measurements at high resolution show a smooth spectral distribution of the OPA output with a typical width of 0.63 nm at 1300 nm (see Fig. 3(a)). This can be compared to the measured pulse length (Pulsecheck, APE GmbH) of 5.3 ps (Fig. 3(b)). The resulting time-bandwidth-product is 0.59 and close to Fourier-limited. At the same time the spatial mode of the output is close to Gaussian (see Fig. 3(c)) and the energy fluctuations are only about 1 % rms.

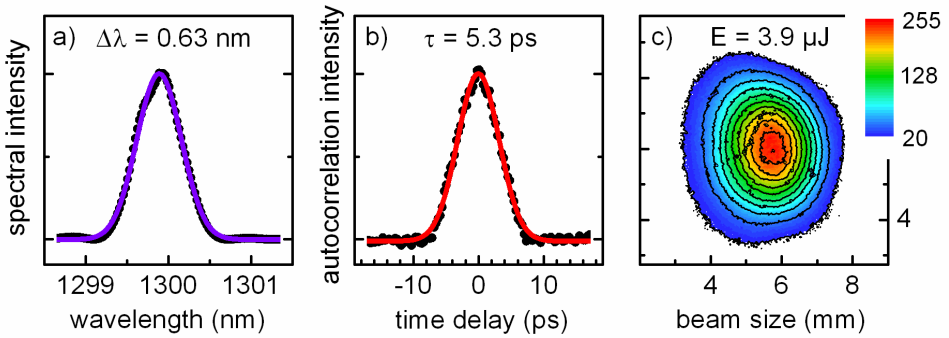

Fig. 3: Spectrum (a), autocorrelation trace (b), and far field beam profile (c) of the ps-pumped NOPA output at 1300 nm. The violet and red line in (a) and (b) are Gaussian fits to the data.

3. Application of the picosecond OPA

The unique properties of the cw seeded ps OPA are advantageously used in experiments investigating nonlinear effects in lithium niobate waveguides and one-dimensional waveguide arrays (WGAs). In these systems, interactions like SHG, nonlinear phase shifts and soliton propagation take place. These are controlled by the input power, the utilized waveguide modes of fundamental wave (FW) and SH and the phase mismatch between the modes. A suitable laser source to explore these nonlinear effects has to fulfill a number of requirements. First, the available peak power must be high enough to trigger the nonlinear processes, usually in the range of 1-20 kW. Second, the laser needs to be easily tunable to allow for measurements of different effects associated with different SH modes or phase mismatches. Since the phase mismatch changes with the wavelength, the bandwidth of the laser spectrum is required to be rather small, ideally around 0.5 nm. Finally, the laser should provide a clean beam for efficient coupling to the waveguides. These requirements are best met by a pulsed source with a nearly Fourier-limited pulse length of around 5 ps. The peak power then translates to at least 100 nJ, a pulse energy still out of range for synchronously pumped OPOs. The requirements are, however, well met by the OPA described above, which was actually designed for the described experimental investigations.

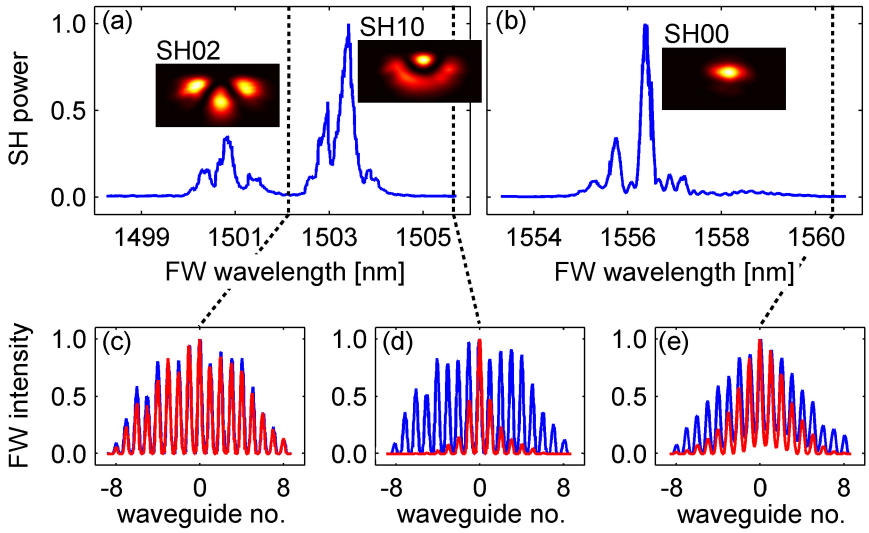

Fig. 4: a,b) Normalized SH output power in dependence on the FW input wavelength. The insets show measured mode profiles of the excited SH modes at the wavelengths of maximum conversion efficiency. (c,d,e) Normalized FW output intensity profiles of a WGA for linear propagation (blue line) and nonlinear propagation (red line) at the wavelengths marked by the dotted lines in (a,b). We find nonlinear competition and soliton formation (c) with higher order (d) and the first order SH component (e).

Figures 4(a) and (b) show the SH output power of a single waveguide in dependence on the input wavelength when only the seed beam of the OPA is coupled to the first order mode of the waveguide. We find several maxima of the SH power, corresponding to the phase matching wavelengths to different SH modes shown in the insets. At the wavelengths denoted by the dotted lines we show the qualitatively different propagation regimes in a WGA

consisting of 101 waveguides. A wide elliptic beam is coupled to the WGA and excites several waveguides. At low peak power the beam simply diffracts (see blue lines in Figs. 4 (c)-(e)). Between the phase matching wavelengths to different modes, the phase shifts induced by the two SH interactions on the FW compete [20] and nonlinear effects are inhibited [21] (see red line in Fig. 4(c) at peak power of 1.5 kW) and the profile matches that at low power. For wavelengths above the two SH resonances, the two phase shifts act cumulative and quadratic spatial solitons with two SH components exist, seen as narrow FW output (red line in Fig. 4(d)) [22]. Spatial solitons with only one SH component [23] are shown in Fig. 4(e).

All the experiments described above were performed with the ps OPA presented in this paper. Only minor adjustments of the BBO crystals in the OPA were necessary to switch between the wavelength ranges indicated in Figs. 4(a) and (b), whereas wavelength tuning within the wavelength ranges in either Fig. 4(a) or Fig. 4(b) could be conducted without adjustments by simply changing the wavelength of the seed diode laser. Thus, the presented OPA concept proves to be an invaluable instrument for conducting experiments in quadratically nonlinear systems.

4. Single-stage femtosecond OPA

In the ps OPA described so far, about 2 x 10^4 photons from the seed laser are amplified. They are found to be sufficient to render output pulses with fluctuations just given by the pump laser fluctuations. If the pump pulse length is decreased to the typical duration of amplified Ti:sapphire lasers of about 100 fs, the number of photons delivered in a 1 mW cw seed beam during the amplification window is just a few hundred. It is therefore not a priori clear whether such a low seed level is sufficient. In addition, it has to be seen whether the cw seed can compete with the parametric superfluorescence always present in OPAs [24].

The setup for amplification of mW level cw seed light with fs pump pulses is shown in Fig. 5. As pump laser we use a commercial Ti:sapphire amplifier system (CPA2001; Clark MXR), which delivers 190 fs pulses around 775 nm with a repetition rate of 1 kHz. Pulses with an energy of 220 µJ are frequency doubled in a 0.7 mm thick BBO crystal, cut at 30° for type I phase matching to generate the pump pulses for the NOPA. A motorized half-wave plate in front of the BBO crystal is used to continuously adjust the energy of the frequency-doubled pulses. Their pulse duration is measured with an autocorrelator based on two-photon absorption [25] in a 100 µm thick gadolinium gallium garnet crystal to 150 fs.

As seed we use a single longitudinal mode cw laser (Torus; LaserQuantum) which delivers up to 100 mW power at 532 nm. A combination of a motorized half-wave plate and a polarizing beam splitter cube is used to adjust the energy sent to the NOPA. The seed laser has a sideband suppression of about 60 dB. This is quite important for the measurements, as already a -20 dB second longitudinal mode (1 % power level) will lead to a 20 % mode beating and variation of the instantaneous photon number delivered to the amplifier.

The pump pulses are focused with a spherical mirror (R = - 1000 mm) towards the amplifier BBO crystal (2 mm, type I, cut at 32.5°) , the cw seed light with an achromatic lens (f = 500 mm), whereby both beams have their focus in front of the crystal [16]. At the position of the crystal the pump beam has a diameter of 300 µm (FWHM), the optimal seed dia-

meter for largest output was found to be 150 µm.

To achieve optimal amplification of the seed, the correct phase matching angle of the crystal, the correct noncollinearity angle and good spatial overlap between pump and seed have to be ensured. As an initial alignment help we additionally generated a supercontinuum by tightly focusing a small fraction of the Ti:sapphire fundamental pulses into a sapphire crystal, as is commonly done in NOPA applications [15, 19]. We overlapped the cw light and the continuum seed with a metallic beam splitter, and first looked for amplification of the continuum seed with blocked cw light.

Since the number of photons in the window of the 150 fs pump pulses is much higher for the continuum seed than for the cw laser (~10^9 compared to 4 x 10^4 for 100 mW seeding power), amplification is found here more easily even for non-optimal settings of the critical parameters. An additional advantage is that amplification is seen much more easily by eye, as the amplified output changes its color drastically from the white looking continuum. When some amplification is found, the NOPA can be optimized for best performance around the cw seed wavelength of 532 nm. Once this is achieved, the whitelight seed is blocked and the cw seed opened. If both seed beams were well overlapped spatially, amplification of the cw seed is readily found.

The amplified output is monitored with an AC coupled photodiode [26]. Although insensitive to cw light of small powers, the diode circuitry is saturated by the cw seed light for powers of more than about 30 mW. Since here we are only interested in the amplification behavior for small seed levels, this was of no great concern.

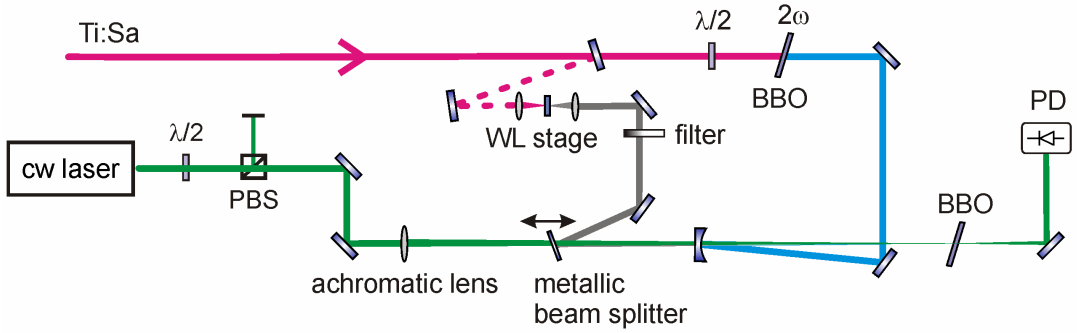

Fig. 5: Schematic of the NOPA with femtosecond pump pulses and cw seed. Optionally a whitelight (WL) supercontinuum was used as seed. λ/2: half-wave plate; PBS: polarizing beam splitter; PD: photodiode.

We achieve amplification factors of up to 10^8 for a pump energy of 35 µJ with seed powers in the range from 0.1 mW to 0.5 mW, where the output energy scales linearly with the seed power. For a typical seed power of 1 mW and an amplification of 10^7, the output pulse energy is in the range of 1 nJ. When we block the seed beam, the remaining output caused by parametric superfluorescence is in the range of 200 pJ, i.e. 20 % of the seeded output. We find that the parametric superfluorescence is extremely broadband and therefore an even better discrimination can be obtained with a bandpass filter. Due to the low number of seed photons we find a fluctuation of the output energy of a few percent.

The temporal autocorrelation of the seeded output is measured for pump energies in the range from 24 µJ to 27 µJ and for seed powers between 0.3 mW and 8 mW. In these ranges

the measured output pulse is Gaussian with a duration of almost constant 71 fs (see Fig. 6(a)).

To measure the output spectrum, the NOPA has to be slightly misaligned in noncollinearity and phase matching angle, so that the cw seed and the amplified output propagate in slightly different directions. If both beams are perfectly overlapped, our spectrometer, which integrates over a minimum of 1 ms, mainly measures the cw seed. Only when seed and amplified beam are spatially separated can we measure a clean amplified spectrum (see Fig. 6(b)). The measured spectral width of 6.4 nm corresponds to a FL of 65 fs, which means that we obtain nearly Fourier-limited pulses with a time bandwidth product of 0.48 even without a compressor.

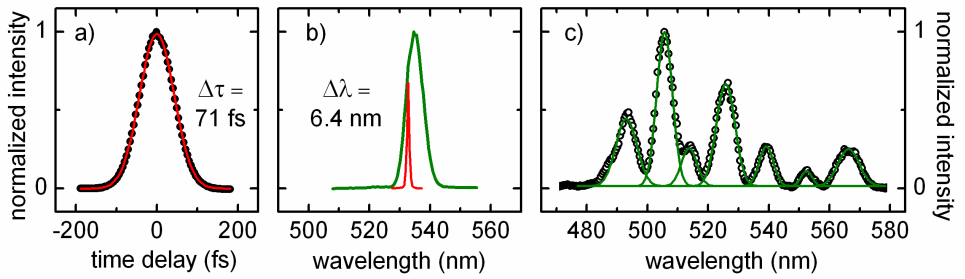

Fig. 6: Autocorrelation (a) and spectrum (b) of the fs-pumped cw seeded NOPA. The red line in (a) shows a Gaussian fit to the data. The red line in (b) indicates the spectral position of the cw seed and the resolution of the spectrometer. (c) Single shot output spectrum of an OPG seeded NOPA. The green lines show Gaussian fits to the individual peaks.

Figure 6(c) shows a typical spectrum of a single pulse when seeding the same amplifier with the parametric superfluorescence generated by focusing a part of the frequency doubled pump pulses into an additional identical BBO crystal for optical parametric generation (OPG). The measured spectra vary strongly in spectral distribution from shot to shot. However, they all show peaked structures that have nearly Gaussian shape and a spectral width of 6.5 ± 1.4 nm. This is very similar to the spectral width of the amplified output of 6.4 nm when using the cw seed. We therefore suggest that the peaks originate from single "monochromatic" seed photons present in the front part of the OPG crystal that get amplified. The different heights could correspond to different first interaction points of these seed photons with the pump pulse in the OPG crystal. Therefore for some of the spontaneous seed photons only part of the OPG crystal is available for pre-amplification. This concept is investigated in detail in a series of measurements described in a forthcoming publication. As a result we are able to measure the number of relevant modes in the vacuum fluctuations of the optical electromagnetic field.

Another noteworthy observation is that the center of the amplified spectrum is redshifted with respect to the cw seed by about 2 nm (see Fig. 6(b)). A similar observation was already reported in [11], where the amplified output of an OPA pumped by 3.5 ps pulses at 767 nm and seeded by a cw laser at 1310 nm was redshifted by about 1 nm. Although various parameters were varied, this observation could not be explained satisfactorily. In our own experiments with the ps pump pulses we did not see such a large offset, but only a maximum shift of about 0.1 nm. We performed a number of tests to clarify the origin of the shift in the fs

setup. We think that wavelength pulling caused by the operation off the amplification maximum and group velocity mismatch and spatial walk-off effects contribute jointly to the situation. A full explanation is beyond the scope of the current work.

5. Summary and discussion

Seeding of ultrafast optical parametric amplifiers is shown to be possible by mW levels of a cw source. By utilizing a commercial Nd:YVO_4 regenerative amplifier at 5 kHz repetition rate a unique source of 5 ps and 4 μJ pulses becomes available. It is fully tunable from 1260 to 1630 nm, presently limited by the commercial seed source. The pulses are both close to a Fourier-limited time-bandwidth product and nearly Gaussian in the far field. The successful use for an extended study of multi-waveguide second harmonic coupling is demonstrated.

Compared to the classical approach for ps OPA systems, i.e. the seeding by OPG, there are a number of silent advantages in the new system. The separation of the desired NIR output from the green pump and the red signal is readily achieved spatially. This is due to the fact that the highest small signal gain and output power is found for a noncollinear geometry. Since no lossy spectral filtering is needed for the nearly Fourier-limited operation, the low seed level is still sufficient to obtain a good contrast of the output to the amplified parametric superfluorescence.

The system is believed to be of great interest for CARS [27], wavelength critical machining [28] and laser ablation mass spectroscopy utilizing narrow spectral resonances [29]. With further amplification stages also a highly versatile source for molecular gas phase dynamics will result. The present spectral resolution of 3 cm^{-1} can be further tailored by varying the length of the of pump pulses.

With an amplified femtosecond Ti:sapphire laser as pump system, we amplified as few as 400 photons in a noncollinear blue pumped OPA. As a result nearly Fourier-limited output pulses at 532 nm with a duration of 71 fs result. Other seed wavelengths should work as well and therefore cw seeding is found to provide extremely controlled ultrafast pulses in the visible. Compared to previous work the presented system operates with much less cw power [12] and at much shorter pulse lengths [13]. The amplification factor of ~ 10^7- 10^8 in the single stage renders output pulse energy of about 1 nJ. Further amplification in a second NOPA stage already allowed us to generate well above 1 μJ of output (setup and data not shown).

The fs amplified cw seed system is a unique source for many quantum optical experiments. We have already analyzed the absolute strength of OPG and use the cw seed laser as an internal reference. Most interesting is the influence of seed statistics on the output fluctuations. For these measurements even seed levels below 100 photons are utilized that have an inherent Poissonian fluctuation already well above the technical noise of the pump laser. In this way we will be able to determine how the transition from the photon picture appropriate for weak cw sources evolves into the classical wave picture that is typically used in the description of OPAs.

Both the fs and the ps OPA seeded by a single frequency continuous laser are sources of pulses with highest control of pulse parameters available at present in the μJ regime. Such pulse energies are needed for many nonlinear excitation schemes. The concept of cw seeding

in combination with the appropriate pump laser gives the experimentalist new possibilities for dedicated investigations.

Acknowledgements

We thank Katrin Peeper for valuable experimental help, and High Q Laser for technical assistance. This work was supported by the Deutsche Forschungsgemeinschaft (DFG) through the Cluster of Excellence: Munich-Centre for Advanced Photonics and through the SPP 1391 “ultrafast nanooptics” and by the Thuringian Ministry of Education, Science and Culture (project “space-time”). C.H. gratefully acknowledges the International Max Planck Research School on Advanced Photon Science.

References

[1] F. P. Schäfer (Ed.), Dye Lasers, 3rd enlarged and revised edition, Vol. 1 of Topics in Applied Physics (Springer-Verlag, 1990).

[2] B. C. Stuart, M. D. Feit, A. M. Rubenchik, B. W. Shore, and M. D. Perry, "Laser-induced damage in dielectrics with nanosecond to subpicosecond pulses," Phys. Rev. Lett. **74**, 2248-2251 (1995).

[3] M. M. Salour, "Powerful dye laser oscillator-amplifier system for high resolution and coherent pulse spectroscopy," Opt. Commun. **22**, 202-206 (1977).

[4] E. Riedle, R. Moder, and H. J. Neusser, "Pulsed Doppler-free two-photon spectroscopy of polyatomic molecules," Opt. Commun. **43**, 388-394 (1982).

[5] E. E. Eyler, A. Yiannopoulou, S. Gangopadhyay, and N. Melikechi, "Chirp-free nano-second laser amplifier for precision spectroscopy," Opt. Lett. **22,** 49-51 (1997).

[6] R. Seiler, T. Paul, M. Andrist, and F. Merkt, "Generation of programmable near-Fourier-transform-limited pulses of narrow-band laser radiation from the near infrared to the vacuum ultraviolet," Rev. Sci. Instr. **76**, 103103-1 - 103103-10 (2005).

[7] M. J. T. Milton, T. D. Gardiner, G. Chourdakis, and P. T. Woods, "Injection seeding of an infrared optical parametric oscillator with a tunable diode laser," Opt. Lett. **19**, 281-283 (1994).

[8] O. Votava, J. R. Fair, D. F. Plusquellic, E. Riedle, and D. J. Nesbitt, "High resolution vibrational overtone studies of HOD and H_2O with single mode, injection seeded ring optical parametric oscillators," J. Chem. Phys. **107**, 8854-8865 (1997).

[9] S. Wu, V. A. Kapinus, and G. A. Blake, "A nanosecond optical parametric generator/amplifier seeded by an external cavity diode laser," Opt. Commun. **159**, 74-79 (1999).

[10] W. D. Kulatilaka, T. N. Anderson, T. L. Bougher, and R. P. Lucht, "Development of injection-seeded, pulsed optical parametric generator/oscillator systems for high-resolution spectroscopy," Appl. Phys. B **80**, 669-680 (2005).

[11] P. E. Britton, N. G. R. Broderick, D. J. Richardson, P. G. R. Smith, G.W. Ross, and D. C. Hanna, "Wavelength-tunable high-power picosecond pulses from a fiber-pumped diode-seeded high-gain parametric amplifier," Opt. Lett. **23**, 1588-1590 (1998).

[12] H. Luo, L. Qian, P. Yuan, and H. Zhu, "Hybrid seeded femtosecond optical parametric amplifier," Opt. Express **13**, 9747-9752 (2005).

[13] S. Hädrich, T. Gottschall, J. Rothhardt, J. Limpert, and A. Tünnermann, "CW seeded optical parametric amplifier providing wavelength and pulse duration tunable nearly transform limited pulses," Opt. Express **18**, 3158-3167 (2010).

[14] D. T. Reid, J. Sun, T. P. Lamour, and T. I. Ferreiro, "Advances in ultrafast optical parametric oscillators," Laser Phys. Lett. **8**, 8-15 (2011).

[15] G. Cerullo, and S. De Silvestri, "Ultrafast optical parametric amplifiers," Rev. Sci. Instr. **74**, 1-18 (2003).

[16] E. Riedle, M. Beutter, S. Lochbrunner, J. Piel, S. Schenkl, S. Spörlein, and W. Zinth, "Generation of 10 to 50 fs pulses tunable through all of the visible and the NIR," Appl. Phys. B **71**, 457-465 (2000).

[17] M. Bradler, C. Homann, and E. Riedle, "Mid-IR femtosecond pulse generation on the microjoule level up to 5 μm at high repetition rates," Opt. Lett. **36**, 4212-4214 (2011).

[18] V. G. Dmitriev, G. G. Gurzadyan, and D. N. Nikogosyan, Handbook of Nonlinear Optical Crystals, 2nd edition (Springer-Verlag, 1997), p.102.

[19] T. Wilhelm, J. Piel, and E. Riedle, "Sub-20-fs pulses tunable across the visible from a blue-pumped single-pass noncollinear parametric converter," Opt. Lett. **22**, 1494-1496 (1997).

[20] F. Setzpfandt, A. A. Sukhorukov, D. N. Neshev, R. Schiek, Y. S. Kivshar, and T. Pertsch, "Phase transitions of nonlinear waves in quadratic waveguide arrays," Phys Rev. Lett. **105**, 233905-1 - 233905-4 (2010).

[21] F. Setzpfandt, D. N. Neshev, R. Schiek, F. Lederer, A. Tünnermann, and T. Pertsch, "Competing nonlinearities in quadratic nonlinear waveguide arrays," Opt. Lett. **34**, 3589-3591 (2009).

[22] F. Setzpfandt, D. N. Neshev, A. A. Sukhorukov, R. Schiek, R. Ricken, Y. Min, Y. S. Kivshar, W. Sohler, F. Lederer, A. Tünnermann, and T. Pertsch, "Nonlinear dynamics with higher-order modes in lithium niobate waveguide arrays," App. Phys. B **104**, 487-493 (2011).

[23] R. Iwanow, R. Schiek, G. I. Stegeman, T. Pertsch, F. Lederer, Y. Min, and W. Sohler, "Observation of discrete quadratic solitons," Phys. Rev. Lett. **93**, 113902-1 - 113902-4 (2004).

[24] V. Krylov, A. Kalintsev, A. Rebane, D. Erni, and U. P. Wild, "Noncollinear parametric generation in $LiIO_3$ and β-barium borate by frequency-doubled femtosecond Ti:sapphire laser pulses," Opt. Lett. **20**, 151-153 (1995).

[25] C. Homann, N. Krebs, and E. Riedle, "Convenient pulse length measurement of sub-20-fs pulses down to the deep UV via two-photon absorption in bulk material," Appl. Phys. B **104**, 783-791 (2011).

[26] C. Schriever, S. Lochbrunner, E. Riedle, and D. J. Nesbitt, "Ultrasensitive ultraviolet-visible 20 fs absorption spectroscopy of low vapor pressure molecules in the gas phase," Rev. Sci. Instr. **79**, 013107-1 - 013107-9 (2008).

[27] A. Volkmer, "Vibrational imaging and microspectroscopies based on coherent anti-Stokes Raman scattering microscopy," J. Phys. D: Appl. Phys. **38**, R59-R81 (2005).

[28] A. Wolynski, T. Herrmann, P. Mucha, H. Haloui, and J. L'huillier, "Laser ablation of CFRP using picosecond laser pulses at different wavelengths from UV to IR," Phys. Procedia **12**, 292-301 (2011).

[29] K. Watanabe, K. Hattori, J. Kawarabayashi, and T. Iguchi, "Improvement of resonant laser ablation mass spectrometry using high-repetition-rate and short-pulse tunable laser system," Spectrochim. Acta Part B **58**, 1163-1169 (2003).

Direct measurement of the effective input noise power of an optical parametric amplifier

submitted to

Laser&Photonics Reviews (accepted)

Christian Homann and Eberhard Riedle

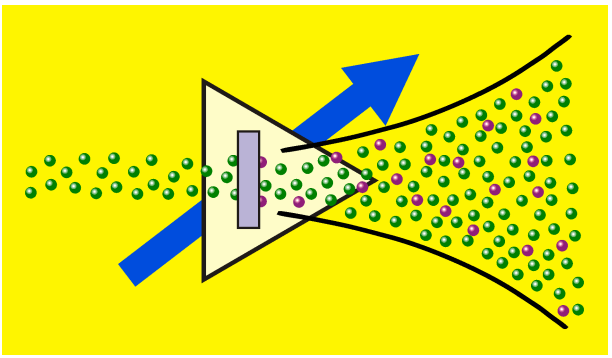

Abstract:

The spontaneous fluorescence background in optical parametric amplifiers is generally attributed to the zero-point fluctuations of the electromagnetic field. These are amplified in parallel to the seed light and lead to an uncompressible superfluorescence background that deteriorates the contrast in optical parametric chirped pulse amplifiers (OPCPA). The absolute level of the underlying parametric fluorescence has not been reported so far. Comparing the fluorescence to low level cw seed light and quantitatively monitoring the output of a noncollinear optical parametric amplifier for both sources, the level is now determined. In a situation of 50 nm visible output bandwidth and low Gaussian spatial modes about 58 photons are found in the signal direction within the femtosecond time window of the amplifier. The superfluorescence level is observed to be proportional to the pump area for constant signal amplification. The implications for the background in high power OPCPA are discussed.

1. Introduction

Optical parametric amplifiers (OPA) and oscillators (OPO) have initially been investigated in the 60ies of the last century soon after the invention of the laser [1,2]. It was however only after nonlinear crystals like β-barium-borate (BBO) were found that they matured to reliable technical devices that replace dye lasers as tunable coherent light sources. For continuous wave (cw) and nanosecond operation little thought is given to the starting mechanisms of such OPOs. In analogy to the easily accepted spontaneous fluorescence emission of excited dye molecules, spontaneous optical parametric fluorescence (OPF) is invoked. The main condition for effective frequency conversion is the net gain, i.e. more gain by the parametric process than the cavity round trip losses. As a consequence OPOs are found to start spontaneously like lasers without active Q switching. If a narrowband seed laser is supplied, not only the output spectrum is improved but also the effective threshold lowered. Seed powers of mW or even μW level are sufficient for a reduction of the buildup time and an increase in the output energy [3-5].

For the operation of an OPA the intensity of the pump wave determines the amplification factor. As the damage threshold intensity I_d scales with the pulse length τ as $I_d \propto \tau^{-0.5}$ in the range from 20 ps to nanoseconds and even more favorable for picosecond (ps) and femtosecond (fs) pulses [6], much higher amplification can be obtained with ps or even fs pulses [7]. To start an ultrafast OPA, initially the parametric fluorescence generated in a first nonlinear crystal was used [8]. Combined with the simultaneous amplification in this first crystal the resulting output is termed optical parametric superfluorescence (PSF) or optical parametric generation (OPG) [9,10].

The most used commercial ultrafast OPA system actually derives its name TOPAS from "traveling wave optical parametric amplifier of superfluorescence". Early reports indicate that the device had fluctuations well beyond the pump laser with individual shots missing totally. This sheds some light on the question how many spontaneous photons are actually used for the seeding. From the fluctuations one might guess that there are only quite few. What is also intriguing is the question why a unit seeded by uncorrelated spontaneous photons is extremely well compressible, as it renders pulses close to the Fourier limit.

Newer OPAs are seeded by highly coherent continuum light generated in a crystal with a small replica of the pump pulse [11,12], and display high pulse to pulse stability and compressibility into the few fs regime [13,14]. For large scale optical parametric chirped pulse amplifiers (OPCPA) often the output of the master Ti:sapphire oscillator is used as seed. Even though the seed energy amounts to about 1 nJ or 4 x 10^9 photons, many reports describe severe contributions from the PSF background [15]. After multi-stage amplification the background is found to not be compressible and limits the achievable pulse contrast. What transpires is that there must be quite many spontaneous photons in the OPCPA situation of long pump pulses and often large beam diameters.

An experimental approach to overcome this limit is to preamplify the nJ seed pulse in a Ti:sapphire multipass amplifier, spectrally broaden the output and add phase control [16]. To understand the origin and magnitude of the spontaneous background contribution, extended

modeling was used [17-19]. All of these papers aim at strategies how to minimize the detrimental effects of the PSF by the design of the OPCPA. None of them delivers a reproducible absolute estimate of the relevant number of spontaneous seed photons. Rather scaling to experimentally observed levels is frequently used. This is in startling contrast to the early theoretical work of Glauber [20] and others that already described the superfluorescence fully quantum mechanically as the manifestation of the vacuum fluctuations.

To overcome this longstanding shortcoming, we designed an experimental strategy to directly and absolutely measure the level of the effective input noise power to an OPA. In section 2 we describe this strategy and the experimental setup used. The results section 3 is concerned with the validation of our description of the PSF and reports the actual measurements. In section 4 we then compare the results to existing models and show good agreement with the experimentally derived number of parametric fluorescence photons. We conclude with answers to the questions raised above and give guidelines for an optimized OPCPA design.

2. Strategy of the experiment and setup

We base our investigation of the parametric superfluorescence background of an optical parametric amplifier on the concept of the effective input noise power. Like the noise equivalent power (NEP) in the description of photodetectors, we define the effective input noise power as the power that would have to be applied to the OPA at the signal wavelength to produce the same amount of output as the parametric fluorescence. We differentiate between this input power and the subsequent parametric amplification in the same crystal. As a result we have a comprehensive description of the OPG process. The measurements quantitatively compare the OPG output to the output obtained with an extremely well known seed power derived from a highly stable cw laser. For the interpretation of the effective input noise power we have to keep in mind that the signal and the idler input noise contribute equally to the experimentally observed OPG.

The experimental setup is depicted in Fig. 1. As OPA we use a noncollinearly phase matched amplifier (NOPA) for a number of reasons. First, the NOPA provides a very high gain of around 10^7 that facilitates the single shot measurement of pulse energies and spectra originating from single photons. Secondly it allows for an ultrabroad amplification bandwidth from 500 to 700 nm that permits collecting noise photons out of a large range. Thirdly the noncollinear geometry affords the easy overlapping of seed and pump beams and the high contrast separation of the weak output pulses from the strong pump pulses. Fourthly it allows separating the signal and idler output of the OPA without dichroic optics. Our design of the NOPA has been described in detail in [21,22]. As pump we use 220 μJ pulses at 775 nm from a commercial Ti:sapphire amplifier system (CPA2001; Clark MXR) with a repetition rate of 1 kHz. The frequency doubled pulses have an energy of up to 60 μJ with a measured duration of 151 fs [23]. The exact value of the pump energy can be controlled by a motorized half-wave plate in front of the frequency doubling crystal. As amplifier crystal we use a 2 mm thick BBO type I crystal cut at 32.5° in tangential phase matched geometry. The pump is focused from below into the BBO crystal and as a result the idler beam is propagating upwards.

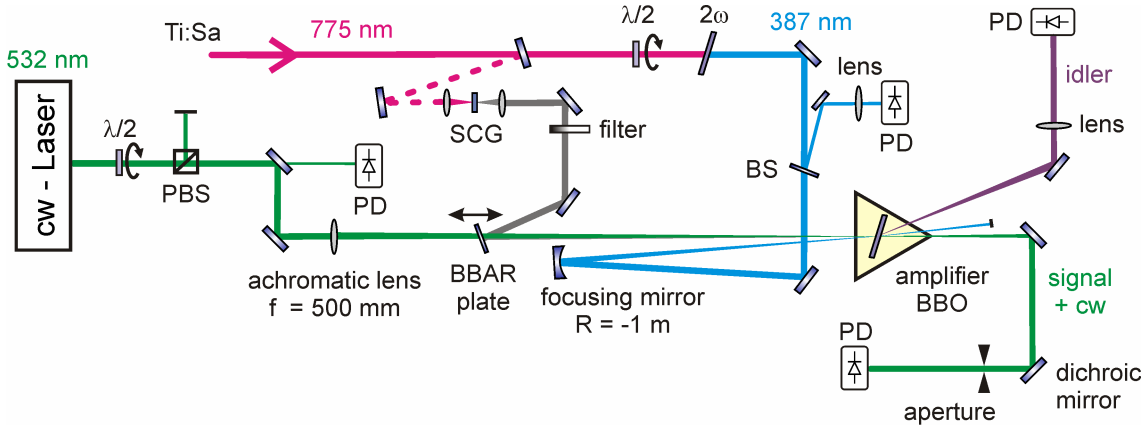

Fig. 1 Setup for blue pumped noncollinear optical parametric amplification of a cw seed source. Alternatively a fs continuum can be used as seed. SCG: supercontinuum generation; λ/2: motorized half-wave plate; PBS: polarizing beam splitter; BS: beam splitter; BBAR plate: fused silica plate with one side broadband AR coated; PD: photodiode

We were recently able to show that a weak cw laser at 532 nm is sufficient to seed a NOPA [24]. In this first report we did not concentrate on the single shot behavior and any possible fluctuations in the momentary seed power were averaged out. Such fluctuations can readily appear with a spurious second longitudinal mode in the cw laser output. The mode beating between the main mode with intensity I_1 and the side band mode with intensity I_2 can be written as:

$$I(t) = I_1 \sin^2(\omega_1 t) + I_2 \sin^2(\omega_2 t) - \sqrt{I_1 I_2}\cos((\omega_1 + \omega_2)t) + \sqrt{I_1 I_2}\cos((\omega_1 - \omega_2)t) \quad (1)$$

For $\langle I_2\rangle/\langle I_1\rangle$ of just 10^{-3} the peak-to-peak variation in photon flux amounts to 12.6 %, well above the technical noise in our experiment. We therefore chose a single longitudinal mode cw laser (Torus; LaserQuantum Ltd) with a side band suppression of certainly better than 10^{-5}, estimated to 10^{-6} (-60 dB). Even this extremely low level still corresponds to 0.4 % peak-to-peak fluctuation. As we have no means to phase stabilize the cavity modes of the cw laser to the Ti:sapphire amplifier repetition rate and phase, the possible number of cw seed photons will fluctuate statistically within these bounds. However, the level of 0.4 % is not any longer of concern, as the mW seed power corresponds to only about 400 photons in the 150 fs time window of the NOPA pump pulse. The Poissonian statistics of this number already amount to a 5 % rms variation and will be dominant. The rms is calculated as the ratio between the standard deviation and the root mean square average. The amount of seed power used is limited by the diode pump current to 8 mW and fine tuned by a combination of a motorized half-wave plate and a polarizer.

The pump pulses and the NOPA signal output are monitored shot-to-shot with a large-area photodiode (S1227-66BQ; Hamamatsu Photonics K.K.) integrated in a homebuilt amplifier circuit [25]. For the idler pulses a photodetector based on an InGaAs diode with an active area of 1 mm^2 (PDI-400-1-P; Becker&Hickl GmbH) is used. A suitable set of neutral density filters was placed before all photodiodes to optimally use the 14 bit digitizing range of our multi-channel digitizer board (NI PCI-6132; National Instruments) which reads out all photodiodes simultaneously. To suppress stray light each photodiode was placed in a suitable housing, additionally color filters were used for the pump and the idler diode to sup-

press stray light at other wavelengths. For a proper spatial stability of the seed and pump at the position of the amplifier crystal a housing of the complete setup to reduce air turbulences is essential. Without housing a position jitter of about ± 3 µm is observed at the crystal position. This reduces to ± 1 µm with the housing. All relevant beam diameters and the beam positions are measured with a CMOS beam profiler (USBeamPro, model 2323; Photon Inc.).

A second seeding branch provided by a femtosecond continuum generated in a 3 mm sapphire crystal is used for two reasons. First, it allows the precise alignment of the noncollinear angle in the NOPA, which ensures the extremely broadband amplification. In this way we can be sure that noise input over a wide range is amplified and detected at the output. Secondly, the fs continuum seed simulates the operational condition of an OPCPA much closer than the cw seed and therefore allows an even closer analogy to these sources of highest power pulses. The cw seed is overlapped to high precision with the continuum seed by utilizing a fused silica plate with one side broadband antireflection coated.

3. Results

Amplification of the single mode cw laser leads to a pulse in the range of 1 nJ energy. This allows the measurement of the spectrum for each shot and the autocorrelation with 2 Hz update rate (see Fig. 2 a) and b)). From these observations we can safely assume that the spectrum is identical for each shot and the pulse length does not depend on the amount of averaging.

The autocorrelation trace is very close to Gaussian and we therefore use a $\sqrt{2}$ deconvolution to get a value of 71 fs for the pulse length. The spectral width is 6.4 nm, the increase from the MHz linewidth of the cw laser is due to the short pulse duration imprinted by the 151 fs pump pulse and additional temporal gain narrowing due to the nearly perfect match of all three group velocities [26]. The resulting time-bandwidth-product is 0.48. This is within 10 % of the transform limit of 0.441 and shows that a nearly unchirped pulse is generated. From the pulse length and the cw seed power we can estimate the effective number of photons acting as seed for the pulsed amplification. It is in the range of just 100 photons for 0.5 mW cw power. From the pulse energy of each individual output shot we then determine the small signal amplification of the NOPA to $3 \cdot 10^6$ for ~ 25 µJ pump energy and $1 \cdot 10^8$ for ~35 µJ pump energy.

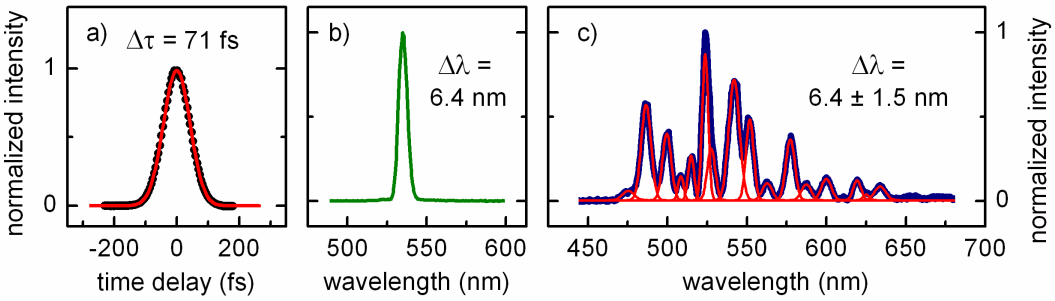

Fig. 2 (a) Autocorrelation of the amplified output. The spectrum of the cw seeded amplified output (b) has the same spectral width as the features of an OPG seeded amplifier (c).

When the cw seed is blocked, the output energy decreases and is not sufficient to measure

the single-shot spectrum directly. We therefore add a second NOPA stage and post-amplify the weak pulses. We find a typical spectrum as shown in Fig. 2 c). On every shot an extremely broad and highly structured spectrum is found. The particular spectral structures change statistically. Averaging over 500 shots smoothes the spectrum completely and renders a reproducible output. To analyze the single-shot spectrum we apply a multi-peak Gaussian fit. The result is shown as red lines superimposed onto the blue experimental trace. In this particular spectrum 16 peaks were fitted, the number varies slightly from shot to shot. The width of the peaks is 6.4 ± 1.5 nm. Within the fluctuation this is identical to the width obtained with the single frequency cw seed laser. We can therefore adopt a picture for the interpretation of our observations, that individual photons at statistically distributed frequencies constitute the OPF seeding of the NOPA.

Simultaneously with the signal output in the visible we also find idler output in the near infrared, centered at 1441 nm when the NOPA is seeded by the 532 nm cw laser. The idler wavelength seems incorrect at first sight, as the signal and idler photon energy does not exactly add up to the photon energy at the pump pulse spectral maximum. On close inspection we find that the maximum depletion of the pump pulse is at 389 nm, slightly off the central wavelength of 387 nm. The spectral width of the idler is 21.4 nm, corresponding to a Fourier limit of 143 fs. Due to the noncollinear geometry of the NOPA, the idler wavelengths are widely dispersed over a range of about 15 degrees. We collect just the angle that is spanned by the idler of the amplified cw seed by utilizing a circular aperture. The measured spectral width of the PSF into this range is 23.4 nm and confirms that we basically monitor the fundamental Gaussian mode.

The idler output is measured spatially integrated over the selected range on the InGaAs detector for every shot. The amplified output in signal direction is monitored by a Si photodiode placed after a dichroic mirror (highly reflecting around 532 nm) and another circular aperture (2.0 mm in diameter, placed 230 mm after the amplifier crystal) that again filters the fundamental Gaussian mode within experimental precision. The two photodetector voltages are compared for 5000 consecutive shots in Fig. 3 a) and for 60 shots out of this range in Fig. 3 b). The measurement was taken for a rather strong seed of 3 mW. This seed level corresponds to 600 photons and an expected fluctuation of 4 % due to the Poissonian statistics.

We observe a much higher level of fluctuation for both the signal and the idler output. This is due to the 0.5 % fluctuation in the pump energy and the exponential dependence of the amplification on the pump. Clearly the signal and idler fluctuations correlate very well. This immediately proves that the signal and idler output originate from the same amplification process as expected for an OPA.

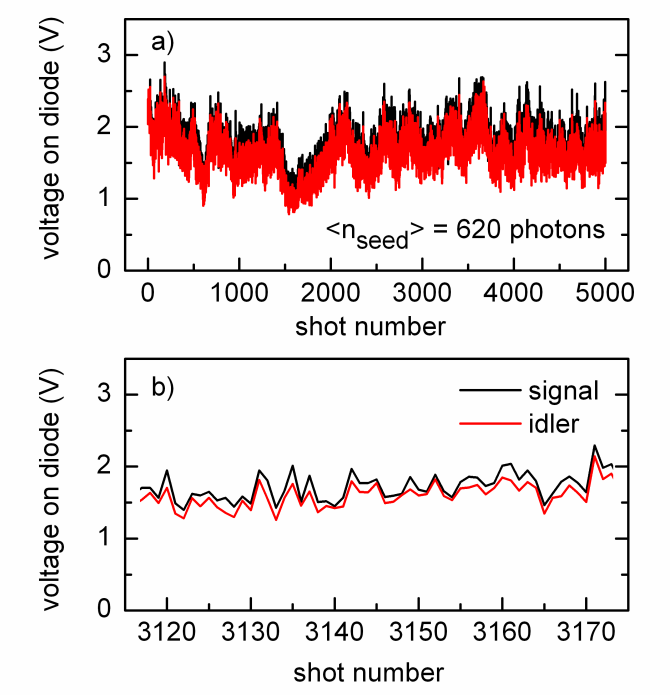

Fig. 3 Correlation between the output in signal direction and a selected range of idler directions. Data are shown for 5000 consecutive shots (a) and a selection of 60 (b).

Analysis of the nonsaturated amplification

For a detailed analysis we look at the standard description of optical parametric amplification [27]. Without any explicit idler input the signal amplitude A_S after the length L of the nonlinear crystal is given by the amplitude

$$A_S(L) = A_S(0) \cdot \cosh\left(\sqrt{\frac{4d_{eff}^2\,\omega_S^2\,\omega_i^2}{k_S k_i c^4}}\, L \cdot |A_P|\right) \approx A_S(0) \cdot \frac{1}{2}\exp\left(\kappa' \cdot |A_P|\right) \qquad (2)$$

with

$$|A_{S,P}|^2 = \frac{1}{2n_{S,P}\varepsilon_0 c} I_{S,P} \qquad (3)$$

The effective nonlinearity is given by d_{eff}, the angular frequencies are denoted by $\omega_{S,i}$ and the wavevectors by $k_{S,i}$. The amplitude is the scaled electric field related to the intensity $I_{S,P}$ through Eq. (3) with the refractive indices $n_{S,P}$. Eq. (2) predicts that the seed amplitude $A_S(0)$ enters linearly into the output and the pump amplitude A_P exponentially with an effective constant κ'. To verify these relations we varied the cw seed power and the pump energy. The result is shown in Fig. 4.

We find a very clean linear dependence of the signal output on the cw seed (Fig. 4a)). However, for zero seed we still find a nonvanishing output that depends on the pump energy just as the output with cw seed. Linear extrapolation of the seed level dependence for each pump level displays a common crossing at zero output. The crossing point nominally corresponds to a negative seed power of -0.27 mW at the signal wavelength. In other words, the seed dependence can be described for all pump levels by Eq. (2) if an additional, additive background field of 0.27 mW power at 532 nm is assumed.

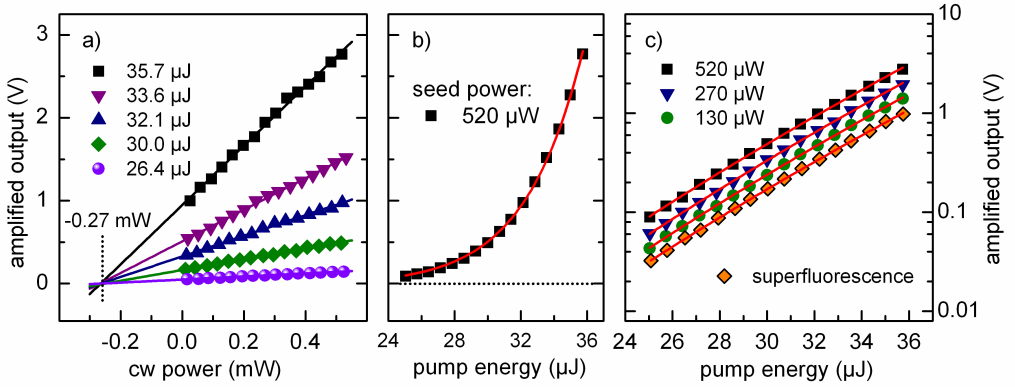

Fig. 4 (a) Amplified output in signal direction as a function of the seed power for pump energies from 26.4 to 35.7 µJ. The colored lines are the best-fit straight lines. (b) Output for varied pump energy and 520 µW seed. (c) Output for seed levels from 130 to 520 µW and varied pump on a logarithmic scale. The orange diamonds correspond to no seed light, just superfluorescence. The red lines are fits to the data.

From Eq. 2 for the amplitudes one can readily derive a relation (4) for the output pulse energy Q_{out} in dependence on the seed energy Q_{seed} and the pump energy Q_{pump}.

$$Q_{out} = \gamma\, Q_{seed} \cdot \exp\left(\alpha\sqrt{Q_{pump}}\right) \tag{4}$$

Since we do not aim to relate the observed amplification to the crystal properties, we contract all relevant material values into the constants γ and α. The exponential dependence of the gain on the pump can be readily seen for 520 µW seed on the linear display in Fig. 4 b). More extended data was recorded for seed levels from 25 to 520 µW (15 values), selected ones are shown logarithmically in Fig. 4 c). The determined α is $3.57 \pm 0.02\sqrt{\mu J}$ for the complete data set. Within experimental precision the pump dependence of the output for no seed can also be fitted with this value. We once again find that the OPF input to the NOPA can be phenomenologically described just like any of the active seed levels. It should be noted that the NOPA is operated in the small signal regime without pump depletion.

The experimental observations lead us to the following **picture of OPF, OPG and OPA**:

- the optical parametric fluorescence OPF results in a contribution to the NOPA output that shows the identical amplification behavior as a purposely applied cw seed beam beam at the signal wavelength.
- both the OPF and the cw seed enter linearly into the output and the pump leads to exponential amplification.
- we associate the effective OPF beam with the zero-point fluctuations of the electromagnetic field. These fluctuations are generally thought to not be observable directly, but become observable through the parametric process [28]. If we think of them as a stream of virtual photons that elude the measurement with a power meter, they still can stimulate the splitting of a pump photon. As a consequence a real signal and a

real idler photon are generated that can be measured and in particular be further amplified in the NOPA crystal.

- zero-point fluctuations at both the signal and the idler wavelength range contribute to the OPF.
- following earlier work [29] we split the crystal length into a first part with critical length l_c where for each relevant mode of the electromagnetic field one pump photon is split into a signal and an idler photon. This splitting is stimulated by the zero-point fluctuations. In this way all the virtual photons lead to one real signal and one real idler photon if l_c is within the crystal length.
- in the remainder of the crystal the usual parametric amplification happens and the zero-point fluctuations only contribute with progressively decreasing importance.
- in this way the OPG is described as the parametric amplification of the OPF. By directly relating the known cw seed power to the effective input noise power describing the OPF we supply an internal standard and can dispose of the specific value of the amplification. The latter has made it impossible in previous measurements to determine the absolute value of the input noise power.

For the parameters of our experiment we find values of l_c ranging from 191 µm for 25 µJ pump to 161 µm for 35 µJ pump. This is less than 10 % of the BBO length. This estimate is based on the focusing of the pump with an f = 500 mm spherical mirror to a 300 µm FWHM diameter in the amplifier crystal. For the modeling of the OPA it is necessary and sufficient to know the effective input noise power as this adds onto the actively supplied seed power and the OPA output can be described by Eq. (4).

Photon flux of parametric fluorescence

To further validate our description of OPF and to supply numbers for the relevant photon flux and the mode density of the vacuum fluctuations we display our measurements in a different fashion in Fig. 5. For selected seed levels we compare the NOPA output with and without seed and derive the contributions from just the seed and just the OPF. The NOPA output due to just the explicitly applied seed is directly obtained by subtracting the output signal without seed from the output with a given seed level at each pump energy (individual pairs of data in Fig. 4 c)). This is justified as we are far from saturation and pump depletion. This calibrates the measured output to the known number of seed photons. With this calibration the output pulse energies without seed are converted into the effective number of noise photons contributing to the NOPA output. The relevant number of seed photons is calculated as average photons for the given seed power per 71 fs pulse length.

Figure 5 shows that indeed the effective number of noise photons is independent of the pump energy and also the cw seed level. We find an effective number of 58 photons in the spectral window of close to 50 nm and the solid angle determined by the aperture in front of the detector of $2 \cdot 10^{-5}$ sr. In this evaluation the contribution of the vacuum modes in the 532

nm range and the ones in the idler range is added. The variation of the signal wavelength by about ± 5% introduces a negligible error. As each virtual idler photon generates a green photon, we can account for the idler contribution by simply assigning half of the effective seed photons, i.e. 29, to the signal and the same number to the idler side.

This model is nicely corroborated by our measurement on the idler side. The observed idler output is much weaker. It converts to a much smaller number of effective noise photons due to the angular dispersion of the idler beam. The used aperture limits the spectrum to about 1/17 and consequently we only detect an idler output equivalent to about 3 noise photons. Again, this is to be split into an average contribution of 1.5 photons from the vacuum modes on the idler side and the same number on the signal side.

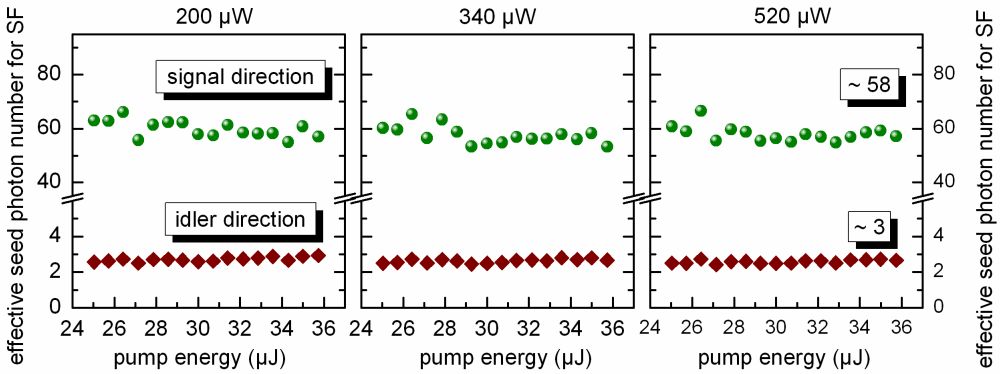

Fig. 5 Effective number of seed photons for the superfluorescence in signal and idler direction in dependence on the pump energy. The superfluorescence is compared to the output for different cw seed levels indicated above each panel.

Variation of amplification area

As a last experimental check we varied the seed and pump spot diameter in the BBO crystal. A factor of 1.94 was used by comparing diameters of 205 and 397 µm. To obtain identical amplification factors given by the same intensity, the pump energy was changed accordingly by a factor of $1.94^2 = 3.8$. Technically, the change in spot size was accomplished by moving the crystal and not by changing the pump beam geometry. Both the pump and the seed beam have their sub-100 µm focus in front of the crystal and the selected size is found some cm behind the focus.

In addition we substituted a strongly attenuated continuum generated in a sapphire plate for the cw seed to closely mimic the situation of an OPCPA. This change also eliminates the need to subtract a slight offset from all measured raw data. This offset due to the cw seed is observed on the photodetector even for the AC coupled circuitry [25]. The temporal overlap between the femtosecond continuum and the pump was adjusted for maximum output. We use about 1 pJ of seed energy (corresponding to 3×10^6 photons) in a spectral window of 3.6. nm FWHM. This width is increased to 7.1 nm for the NOPA output in accord with the broadening of the cw seed upon pulsed amplification.

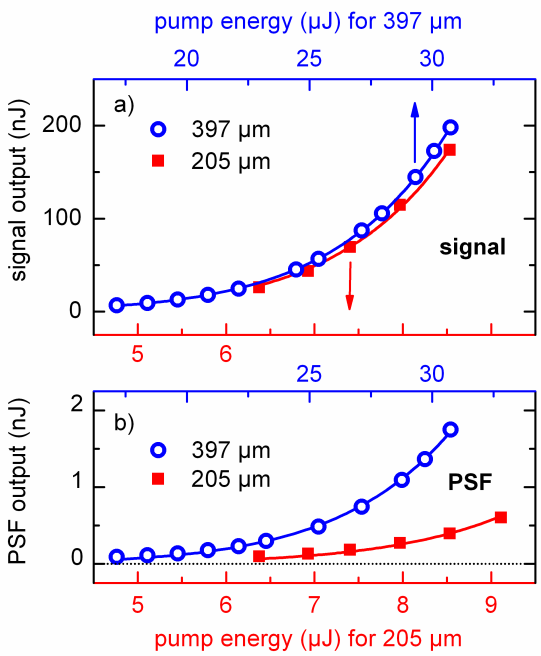

Fig. 6 (a) Signal output in dependence on the pump energy for matching FWHM beam diameters of pump and seed of 205 µm (red) and of 397 µm (blue). The pump energy axis on top (blue) corresponds to the larger beam diameter, the axis on the bottom (red) to the smaller. (b) depicts the superfluorescence output. Measured data is shown as symbols, the fits according to Eq. (4) as lines.

The signal output is found for both cases to increase exponentially with the square root of the pump energy (intensity). In Fig. 6 a) it can be seen that indeed the same amount of seed light is amplified to equal output for matching pump energy in the two interaction geometries. In the figure the pump energy for the two beam sizes is scaled to superimpose the data for the same intensity. The fits according to Eq. (4) shown by the colored lines match within experimental accuracy (see Table 1). The ratio of the α's is 1.88 in excellent agreement with the ratio of the beam diameters of 1.94 and the values for $\gamma\, Q_{seed}$ are equal.

In contrast to the signal output the much weaker parametric superfluorescence output measured with the continuum seed blocked deviates strongly between the two geometries (see Fig. 6 b). To enhance the detection sensitivity all of the visible superfluorescence ring was imaged onto the detector. The fit parameters show that again the amplification scales as expected. However, the effective noise input described by $\gamma\, Q_{seed}$ goes up by a factor of 4.2 upon increase of the parametric interaction area by 3.8.

	signal		superfluorescence	
	$\gamma\, Q_{seed}$ [nJ]	α [1/√µJ]	$\gamma\, Q_{seed}$ [nJ]	α [1/√µJ]
D = 205 µm	$2.44 \cdot 10^{-4}$	4.61	$5.62 \cdot 10^{-7}$	4.61
D = 397 µm	$2.44 \cdot 10^{-4}$	2.45	$2.37 \cdot 10^{-6}$	2.43

Table 1: Fit parameters describing the amplification of fs continuum seed and parametric superfluorescence for 205 µm and of 397 µm diameter of the interaction area.

4. Modeling and Discussion

It is generally accepted that the parametric fluorescence is due to the zero-point fluctuations of the electromagnetic field [20,28,30]. However, the descriptions given in original papers [20,31] and text books [28,30] do not give any formula that allows the practitioner to predict the amount of OPF or the number of downconverted correlated photon pairs [32,33]. Instead scaling relative to measured values in connection with a stochastic variable with Gaussian distribution and zero mean value in the coupled parametric equations has been used [17].

An explicit formula has, however, been derived for the equivalent noise input in stimulated Raman scattering [34,35]. We would like to argue that the amplification in stimulated Raman is analogous to parametric amplification and the parametric fluorescence is analogous to the spontaneous Raman scattering. Consequently we use the description for the equivalent noise input in stimulated Raman I_{noise}^{Raman} to model the present equivalent noise input intensity in the NOPA. From Eqs. (48) and (52) of ref. [34] follows Eq. (13) of ref. [35]

$$I_{noise}^{Raman} = \frac{\hbar\omega^3 n^3}{8\pi^3 c^2}\Delta\Omega\Delta\omega \tag{5}$$

In this equation n is the ordinary refractive index of the crystal, $\Delta\omega$ the detected spectral width and $\Delta\Omega$ the solid angle of the emitted radiation.

The difference between the present case of parametric amplification and Raman scattering is the idler part of the parametric process. The influence of the idler field has been demonstrated in a polarization nondegenerate sub-threshold optical parametric oscillator [36]. A vacuum mode at the associated wavelength around 1440 nm and the correct spatial direction can also stimulate a downconversion process, generating a green photon. Thus we have to multiply the right hand side of Eq. (5) by a factor of 2 for the equivalent noise input intensity I_{noise}^{OPA}.

$$I_{noise}^{OPA} = 2\frac{\hbar\omega^3 n^3}{8\pi^3 c^2}\Delta\Omega\Delta\omega \tag{6}$$

The frequency intervals for the signal and idler are identical due to the energy conservation, only the wavelength intervals differ strongly for nondegenerate OPA. To translate Eq. (6) into readily accessible numbers for the experimentalist, we consider a nonlinear crystal in the focus of a TEM00 Gaussian seed beam with waist w_o and wavelength λ. The aperture in front of the detector is closed far enough to just transmit this fundamental mode. The divergence θ and the solid angle is then given by

$$\theta = \frac{\lambda}{\pi\, w_o} \qquad \text{and} \qquad \Delta\Omega = \pi\,\theta^2 \tag{7}$$

The relevant equivalent noise input power P_{noise} is then given by

$$P_{noise}^{OPA} = I_{noise}^{OPA}\ \pi\ w_o^2 = 2\frac{n^3}{2\pi}\ \hbar\omega\ \Delta\omega \tag{8}$$

This means that the noise power is equal to a small number of about 1.86 times the energy of a photon times the detected bandwidth. It follows that the effective number of noise seed photons is

$$N_{eff} = 2\frac{n^3}{2\pi}\ \Delta\omega\ \tau = 2\ n^3\ 0.441\ \frac{\Delta\nu}{\delta\nu} \approx 2\ n^3\ 0.441\ \frac{\Delta\lambda}{\delta\lambda} \tag{9}$$

The number of signal longitudinal or spectral modes in the visible is roughly equal to the ratio of the visible detection bandwidth $\Delta\nu$ to the smallest resolvable bandwidth $\delta\nu$. This bandwidth is in turn determined by the duration τ of the pump. Since each mode contributes with one photon [28], this number is in turn equal to the number of relevant noise photons from the signal side. The idler range adds the factor 2.

The observation bandwidth of about 50 THz in our measurements (compare Figs. 4 and 5) in signal direction and the measured pulse length for cw seeding, i.e. close to the Fourier limit, of 71 fs yields an estimate of $N_{eff} = 42$ photons. Considering the huge dynamic range between NOPA seed and output, this is extremely close to the observed value of 58. The missing small factor is likely due to the fact that we did not perform the measurements exactly in the Gaussian fundamental mode. For situations where a larger solid angle is observed, one should explicitly consider the number of transversal or spatial modes. Interestingly, the spectral filtering given by the spatial dispersion of the idler from the NOPA gives an estimated idler noise photon number of about 2, and we observe about 3.

In our variation of the parametric interaction volume (compare Fig. 6) we observe an increase of the contributing parametric fluorescence proportional to the pump area. As we collect the full superfluorescence ring, the observation solid angle is now given by the angular dependence of the phase matching [28]. This is not changed by the somewhat varied pump area. Consequently an amount of PSF is observed and contributes to the total OPA output that is proportional to the pump area.

The extreme agreement of the estimated and measured noise photon numbers might be somewhat fortuitous. We are, however, certain that the order of magnitude of just tens of photons is significant. Even for a 10 ps pump pulse we derive as little as 10^4 parametric fluorescence photons as the attainable limit for a proper design of the amplifier. As this is largely different from the 10^9 seed photons typical for OPCPA and even more for the 10^{15} output photons, we hope that the presented determination of the equivalent noise input power is helpful for the future design of OPAs.

5. Conclusion

With the absolute determination of the equivalent noise input to an OPA we can now turn to an interpretation of the various observations mentioned in the introduction. We first use our derived model for the OPF to analyze the level of background reported for various OPCPAs.

Tavella et al. used an 80 ps pump pulse, their output spectral width corresponded to 8 fs and the beam radius was 0.5 mm [17]. We calculate $2.4 \cdot 10^5$ OPF photons compared to 20 pJ seed. The resulting energy contrast would be $2.8 \cdot 10^{-3}$, they deduced a value of $9.4 \cdot 10^{-3}$ from their experimental results. Later the system was augmented by an intermediate multi-pass Ti:sapphire amplifier to increase the seed level to the μJ regime [16]. Indeed a largely improved contrast of $\sim 10^{-8}$ at 5 ps before the main pulse was achieved.

With our results and modeling in mind, we would like to argue that in the design of the first amplifier stage a shortened pump pulse of just a ps duration and care to work in the fundamental Gaussian mode would already have helped considerably. Equally important, the lossy phase management would better be performed after the first stage. At this point the pulse energy is still low enough for the AOPDF and the PSF would be attenuated equally to the signal pulse. The influence of OPF is practically negligible in the later amplifier stages as the pre-amplified seed is quite strong. The latter suggestion agrees with detailed guidelines for optimization of superfluorescence suppression given by Kärtner and coworkers [37]. In deviation to all previous considerations we do not only suggest to properly match the seed and pump duration [18,19], but to absolutely use a short and weakly focused seed and pump. To ensure that both the amplified seed beam and the PSF are in the fundamental Gaussian mode and the lowest possible number of vacuum fluctuations is contributing, the first amplifier should be positioned in the common focus of the beams.

We were wondering earlier how the output of the commercial ultrafast OPG/OPA device TOPAS can be compressed so well even though it is seeded by OPF photons without phase coherence. From Eqs. (8) and (9) it follows together with the operational parameters, that only very few OPF photons on average are most likely responsible for seeding. As a consequence, the output can vanish for single shots when the photon statistics render zero seed photons. For a small number, one of the photons will become effective the earliest and dominate the pulse amplification. In this way the phase matching bandwidth and pump pulse length alone determine the output characteristics and acceptable spectral variations result. A pulse determined by a single seed photon is intrinsically compressible. This picture nicely matches the recent report that each OPG pulse possesses a well defined carrier envelope phase (CEP), with random fluctuations that are not correlated to the pump CEP [38].

Last but not least we would like to consider the spontaneous parametric down-conversion of blue light to generate polarization-entangled photon pairs in the red [32]. For a cw pump beam the critical length l_c is much larger than the crystal length or the Rayleigh length. Consequently only a fraction of the zero-point fluctuations or virtual photons are transferred to real photon pairs. Applying the amplification model according to Eq. (2) together with the noise power given in Eq. (8) we can estimate l_c to 12 m for 10 mW pump and the expected number of photon pairs to $2.8 \cdot 10^6$. This compares reasonably well with the reported value of $1.2 \cdot 10^4$. As the experiment does not correct for the optical losses, particularly in the fiber transmission, and the limited detection efficiency of the avalanche photodiode it can safely be expected that one to two orders of magnitude more photons are generated then detected. As the pump power and intensity is largely increased by an enhancement cavity and the use of a mode locked laser, the number of detected photons is increased to 10^7 [33]. We estimate

$1 \cdot 10^9$ generated photons for a similar detection efficiency as before.

We hope that the developed understanding of the optical parametric fluorescence contribution to various optical parametric amplifier and down-conversion setups will allow the development of improved and still simpler devices. We strongly suggest to use the equivalent noise input intensity, power or energy for simulations as they are directly comparable to the used seed pulses. Use of Eqs. (6) and (8) finally gives an absolute measure for the parametric fluorescence responsible for the background in OPAs.

Acknowledgements

We thank Markus Breuer for early investigations of the cw seeded NOPA and Katrin Peeper for valuable experimental help. Alfred Laubereau, Franz Kärtner, Jeff Kimble and Robert Huber are acknowledged for enlightening discussions. This work was supported by the Deutsche Forschungsgemeinschaft (DFG) through the Cluster of Excellence: Munich-Centre for Advanced Photonics. C.H. gratefully acknowledges the International Max Planck Research School on Advanced Photon Science.

References

[1] S.E. Harris, Proc. IEEE **57**, 2096 - 2113 (1969).

[2] R.L. Byer, in: H. Rabin and C.L. Tang (eds.), Quantum electronics, Volume 1, Nonlinear Optics, Part B (Academic Press, London, 1975), chap. 9.

[3] M.J.T. Milton, T.D. Gardiner, G. Chourdakis, and P.T. Woods, Opt. Lett. **19**, 281 - 283 (1994).

[4] O. Votava, J.R. Fair, D.F. Plusquellic, E. Riedle, and D.J. Nesbitt, J. Chem. Phys. **107**, 8854 - 8865 (1997).

[5] P.E. Britton, N.G.R. Broderick, D.J. Richardson, P.G.R. Smith, G.W. Ross, and D.C. Hanna, Opt. Lett. **23**, 1588 - 1590 (1998).

[[6] B.C. Stuart, M.D. Feit, A.M. Rubenchik, B.W. Shore, and M.D. Perry, Phys. Rev. Lett. **74**, 2248 - 2251 (1995).

[7] V. Krylov, O. Ollikainen, J. Gallus, U. Wild, A. Rebane, and A. Kalintsev, Opt. Lett. **23**, 100 - 102 (1998).

[8] A. Laubereau, L. Greiter, and W. Kaiser, Appl. Phys. Lett. **25**, 87 - 89 (1974).

[9] J.Y. Zhang, J.Y. Huang, Y.R. Shen, and C. Chen, J. Opt. Soc. Am. B **10**, 1758 - 1764 (1993).

[10] V. Petrov, F. Seifert, and F. Noack, Appl. Phys. Lett. **65**, 268 - 270 (1994).

[11] M.K. Reed, M.K. Steiner-Shepard, and D.K. Negus, Opt. Lett. **19**, 1855 - 1857 (1994).

[12] M. Bradler, P. Baum, and E. Riedle, Appl. Phys. B **97**, 561 - 574 (2009).

[13] A. Baltuska, T. Fuji, and T. Kobayashi, Opt. Lett. **27**, 306 - 308 (2002).

[14] P. Baum, M. Breuer, E. Riedle, and G. Steinmeyer, Opt. Lett. **31**, 2220 - 2222 (2006).

[15] G. Cerullo, A. Baltuska, O.D. Mücke, and C. Vozzi, Laser Photonics Rev. **5**, 323 - 351 (2011).

[16] D. Herrmann, L. Veisz, R. Tautz, F. Tavella, K. Schmid, V. Pervak, and F. Krausz, Opt. Lett. **34**, 2459 (2009).

[17] F. Tavella, A. Marcinkevičius, and F. Krausz, New J. Phys. **8**, 219: 1 - 11 (2006).

[18] J. Moses, C. Manzoni, S.-W. Huang, G. Cerullo, and F.X. Kärtner, Opt. Express **17**, 5540 - 5555 (2009).

[19] C. Manzoni, J. Moses, F.X. Kärtner, and G. Cerullo, Opt. Express **19**, 8357 - 8366 (2011).

[20] R. Glauber, and F. Haake, Phys. Lett. **68A**, 29 - 32 (1978).

[21] T. Wilhelm, J. Piel, and E. Riedle, Opt. Lett. **22**, 1494 - 1496 (1997).

[22] E. Riedle, M. Beutter, S. Lochbrunner, J. Piel, S. Schenkl, S. Spörlein, W. Zinth, Appl. Phys. B **71**, 457 - 465 (2000).

[23] C. Homann, N. Krebs, and E. Riedle, Appl. Phys. B **104**, 783 - 791 (2011).

[24] C. Homann, M. Breuer, F. Setzpfandt, T. Pertsch, and E. Riedle, Opt. Express **21**, 730 - 739 (2013).

[25] C. Schriever, S. Lochbrunner, E. Riedle, and D. J. Nesbitt, Rev. Sci. Instr. **79**, 013107-1 - 013107-9 (2008).

[26] J. Piel, E. Riedle, L. Gundlach, R. Ernstorfer, and R. Eichberger, Opt. Lett. **31**, 1289 - 1291 (2006).

[27] R.W. Boyd, Nonlinear Optics, Third Edition (Academic Press, San Diego, 2008), chap. 2.

[28] C.L. Tang, in: H. Rabin and C.L. Tang (eds.), Quantum Electronics, Volume 1, Nonlinear Optics, Part A (Academic Press, London, 1975), chap. 6.

[29] L. Carrion and J.-P. Girardeau-Montaut, J. Opt. Soc. Am. B **17**, 78 - 83 (2000).

[30] A. Yariv, Quantum Electronics, Third Edition (John Wiley & Sons, New York Diego, 1988), chap. 17.7.

[31] D.A. Kleinman, Phys. Rev. **174**, 1027 - 1041 (1968).

[32] P. Trojek, Ch. Schmid, M. Bourennane, H. Weinfurter, and Ch. Kurtsiefer, Opt. Express **12**, 276 - 281 (2004).

[33] R. Krischek, W. Wieczorek, A. Ozawa, N. Kiesel, P. Michelberger, T. Udem, and H. Weinfurter, Nature Photon. **4**, 170 - 173 (2010).

[34] A. Penzkofer, A. Laubereau, and W. Kaiser, Prog. Quant. Electr. **6**, 55 - 140 (1979).

[35] A. Lauberau, in: W. Kiefer and D.A. Long (eds.), Non-Linear Raman Spectroscopy and Its Chemical Applications (D. Reidel Publishing Company, 1982), p. 190.

[36] Z.Y. Ou, S.F. Pereira, and H.J. Kimble, Phys. Rev. Lett. **70**, 3239 - 3242 (1993).

[37] J. Moses, S.-W. Huang, K.-H. Hong, O.D. Mücke, E.L. Falcão-Filho, A. Benedick, F.Ö. Ilday, A. Dergachev, J.A. Bolger, B.J. Eggleton, and F.X. Kärtner, Opt. Lett. **34**, 1639 - 1641 (2009).

[38] C. Manzoni, G. Cirmi, D. Brida, S. De Silvestri, and G. Cerullo, Phys. Rev. A **79**, 033818-1-033818-10 (2009).

Analysis of the output fluctuations of a cw seeded optical parametric amplifier

1. Introduction

In the previous chapters it was shown that seeding a femtosecond optical parametric amplifier (OPA) with a mW level cw laser is not only feasible, but a very useful and valuable means to investigate the amplification process thoroughly.

While in [1] mainly the feasibility of the amplification was demonstrated and the output pulses were characterized in spectrum and pulse length, [2] showed that the amplification can be modeled excellently by

$$Q_{out} = \gamma\, Q_{seed} \cdot \exp\left(\alpha\sqrt{Q_{pump}}\right) \tag{1}$$

with output pulse energy Q_{out}, seed energy Q_{seed}, pump energy Q_{pump}, and two constants γ and α that contain material constants and properties of the involved beams that are kept constant. The cw seed beam was used in this publication as an internal standard that was compared to the parametric fluorescence. In this way, absolute numbers for the number of seed photons acting as source for the parametric superfluorescence could be determined [2]. For this determination, very accurate measurements with weak signals were necessary. However, for the evaluation only average values over typically 5000 shots were used.

Here, we now want to focus on the fluctuations obtained from shot to shot when seeding with low level cw light. When calculating the number of photons of the cw laser that are on average contained in the 71 fs of the amplified output pulses, one finds a number of about 200 photons for 1 mW seed power, and only 20 for 100 µW. This is a regime, where clearly a particle or photon picture is adequate for describing the seed flux. After the amplification with a typical gain of 10^7 to 10^8, and a resulting photon number of up to 10^{10}, the wave picture and describing the flux as a Gaussian beam with a certain pulse length and energy is certainly appropriate.

This means that mediated by the amplification process a transition from the photon to the wave picture takes place. An open question in this respect is how the fluctuations of the input flux are transferred to the output. For the cw seed laser operated far above threshold, one expects a Poissonian distribution [3]. This distribution is characterized by having an equal mean value and variance, which in our case is the photon number N per time.

To analyze the fluctuations, we calculate the root mean square fluctuations (RMS) as the ratio of the standard deviation σ and the root mean square average. For a Poissonian distribution this leads to

$$\mathrm{RMS} = \frac{\sigma}{\langle x \rangle_{rms}} = \frac{\sqrt{N}}{N} = \frac{1}{\sqrt{N}} \tag{2}$$

The question is, if the output will still fluctuate in accordance with the Poissonian statistics of the input, or if this will be washed out, as it is for example the case in photomultiplier tubes, where a constant input already leads to a broad output distribution.

To be able to analyze the output fluctuations of the OPA with respect to the input fluctuations, it is important to get rid of additional technical noise as for example pump pulse fluctuations. How this can be done, and how the output fluctuations then behave will be shown in the following.

2. Experimental setup

Fig. 1 depicts the used setup. As pump laser we use a commercial Ti:sapphire amplifier sys-tem (CPA2001; Clark MXR), which delivers 190 fs pulses around 775 nm with a repetition rate of 1 kHz. Pulses with an energy of 220 µJ are frequency doubled in a 0.7 mm thick BBO crystal, cut at 30° for type I phase matching to generate the pump pulses for the NOPA. A motorized half-wave plate in front of the BBO crystal is used to continuously adjust the energy of the frequency-doubled pulses. A part of the pulses is split off by a dichroic beam splitter and focused towards a large-area photodiode (S1227-66BQ; Hamamatsu Photonics K.K.) integrated in a homebuilt amplifier circuit [4] to measure the pump energy at each single shot. The pulse duration is measured with an autocorrelator based on two-photon absorption [5] in a 100 µm thick gadolinium gallium garnet crystal to 151 fs.

As seed we use a single longitudinal mode cw laser (Torus; LaserQuantum) which delivers up to 100 mW power at 532 nm. A combination of a motorized half-wave plate and a polarizing beam splitter cube is used to adjust the energy sent to the NOPA. Since we were interested in the amplification of low seed powers only, we operated the cw laser at 60 % of its maximal pump current, corresponding to a maximal output power of about 8 mW. The leakage through a highly reflecting dichroic mirror is used to monitor the cw seed power with a photodiode. The seed laser has a sideband suppression of at least -50 dB, which is important as a second longitudinal mode leads to mode beating and consequently a variation in the instantaneous photon number delivered to the amplifier.

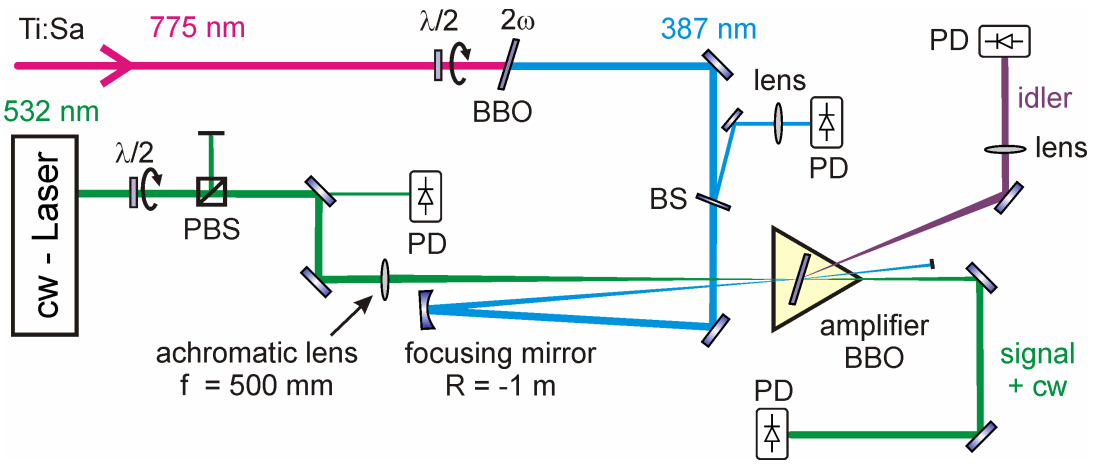

Fig. 1 Setup for noncollinear optical parametric amplification of a cw seed source. λ/2: motorized half-wave plate; PBS: polarizing beam splitter; BS: beam splitter; PD: photodiode.

The pump pulses are focused with a spherical mirror (R = - 1000 mm) towards the amplifier crystal, the cw seed with an achromatic lens (f = 500 mm), whereby both beams have their focus in front of the crystal. The diameter of the pump pulses is 300 µm (FWHM) on the position of the amplifier crystal, the diameter of the seed pulses 150 µm (FWHM). All beam diameters are measured with a CMOS beam profiler (USBeamPro, model 2323, Photon Inc.). As amplifier crystal we use a 2 mm thick BBO crystal, cut at 32.5° for type I phase matching and operated in tangential phase matched geometry.

For the correct settings of the noncollinearity angle between pump and seed and the phase matching angle of the amplifier crystal, seed and amplified signal propagate in the same direction. The amplified output in signal direction is monitored by a photodiode (identical to the photodiode for the pump). The off-axis idler is collected with a lens (f = 50 mm) and focused towards an integrating InGaAs photodiode module with 1 mm^2 active area (PDI-400-1-P, Becker&Hickl GmbH).

A suitable set of neutral density was placed before all photodiodes to optimally use the 14 bit digitizing range of our multi-channel digitizer board (NI PCI-6132; National Instruments), which reads out all photodiodes simultaneously for each laser shot. To suppress straylight each photodiode was placed in a suitable housing, additionally color filters were used for the pump and the idler diode to suppress straylight of other wavelengths.

For a proper spatial stability of the seed and pump at the position of the amplifier crystal a housing of the complete setup to reduce air turbulences was essential. Without housing a position jitter of about ± 3 µm was observed at the crystal position. This reduced to ± 1 µm with housing.

3. Results and data evaluation

The cw seed is amplified in the NOPA by a factor of about 10^7 for 30 µJ pump pulses. This leads to an output pulse energy of about 1 nJ for a seed power of 1 mW. The pulse length of the output pulses was measured with an autocorrelator based on second harmonic generation. The measured autocorrelation curve is almost exactly Gaussian, and the deconvolution delivers a pulse length of 71 fs (see also [1]). This is considerably smaller than the pulse length of the pump pulses of 151 fs, due to the experienced temporal gain narrowing and the almost equal group velocities of all involved beams.

With the measured pulse length $\Delta\tau_{FWHM}$ of 71 fs, we can estimate the number of seed photons n_{seed} that contribute to the amplification process as

$$n_{seed} = \frac{\sqrt{\pi}}{2\sqrt{\ln 2}} \cdot \frac{\lambda}{hc} \cdot P_{cw} \cdot \Delta\tau_{FWHM} \approx \frac{1.064}{hc} \cdot 532\text{nm} \cdot 71\text{ fs} \cdot P_{cw} \approx 202 \cdot P_{cw}[\text{mW}] \quad (3)$$

with the cw seed power P_{cw}, and the seed wavelength λ. The first factor accounts for the Gaussian shape of the output pulses. Note that in our case, only

Fig. 2 shows the measured output in signal and in idler direction for an estimated seed photon number of 620. The fluctuations of the seed photon number according to Eq. (2) are estimated to 4 %. Fig. 2a) shows 5000 consecutive shots, Fig. 2b) a selection of 60 shots out of

this range. In both sets a very high correlation between the outputs is observed. Apart from the applied cw seed, the optical parametric fluorescence (OPF) also contributes as seed for the amplification process. As was shown in [2], this contribution amounts to about 58 photons in signal direction and 3 photons in idler direction for the chosen experimental parameters. This is less than 10 % of the cw seed, contributes therefore only marginally to the overall output fluctuations and should change the fluctuations only by 5 % according to Eq. (2). This explains the high correlation between signal and idler direction.

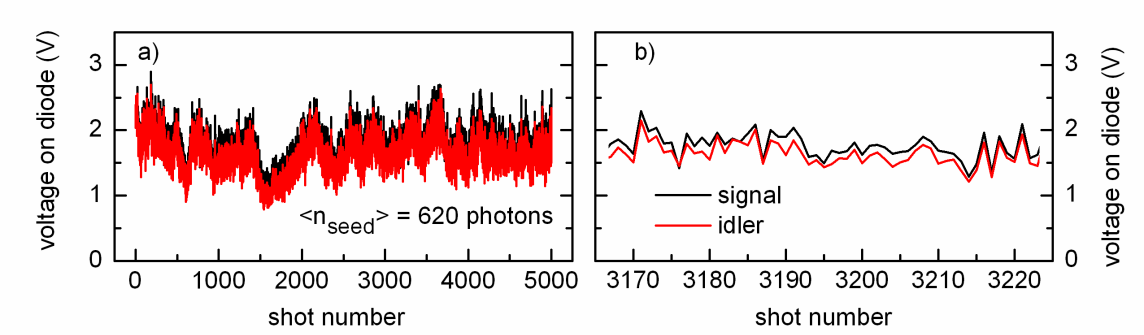

Fig. 2 Correlation between the seeded output in signal and idler direction. Data are shown for 5000 consecutive shots (a) and a selection of 60 (b).

Since the idler is free from the continous cw background and includes much less fluctuations from the OPF due to the lower seed photon number, in the following always the idler output is shown and analyzed. Due to the high correlation to the signal, all statements and conclusions are also valid for the seeded signal output.

To be able to evaluate the output fluctuations in dependence of the seed power, the seed level was scanned from 0.1 mW to 8.3 mW with 100 steps. For each step 5000 consecutive shots were recorded. This includes the pump energy, the instantaneous cw power, the signal and the idler output. The average values of the 5000 shots for the idler output for every seed power step are depicted as black line in Fig. 3a). The deviations from the expected linear behavior are mainly due to the pump pulse fluctuations over the extended measurement time, which enter exponentially in the amplified output. Important for a meaningful evaluation is a proper subtraction of the diode offsets.

The red line in Fig. 3a) results from a surface fit according to Eq. (1) with γ and α as free parameters and the measured pump pulse energy, the seed power and the idler output voltage as dependent parameters.

When the thus determined parameters α and γ are used to calculate the output voltage for every single shot for an average seed power of 6.4 mW, the red curve in Fig. 3b) results. It reproduces the measured values (black curve) very well, which validates the used modeling with Eq. (1).

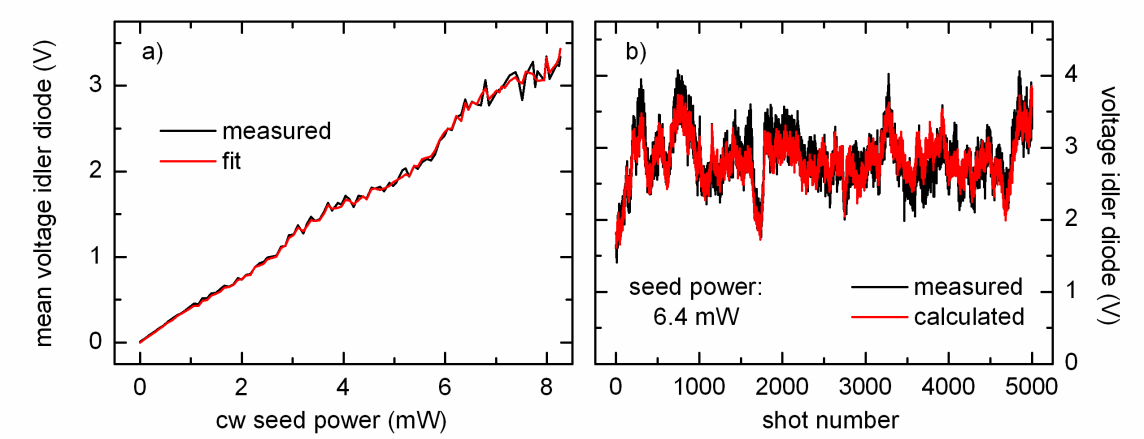

Fig. 3 (a) To the measured average data (black line) a two-dimensional fit (red line) was applied according to Eq. (1) to obtain the constants γ and α. (b) With these constants the expected output for every single shot was calculated (red line). The calculated output matches very well the measured single shot data (black line).

To analyze the output fluctuations, we calculate the RMS according to Eq. (2) for sets of 5000 consecutive shots. Fig. 4a) shows the resulting RMS values in dependence of the seed photon number (orange line). The values clearly rise for small seed photon numbers, but fluctuate strongly.

When a $1/\sqrt{N}$ function is fitted to the determined RMS values for the output fluctuations, only a moderate agreement results. Only the qualitative behavior, a rise for small seed photon numbers, can already be seen. That this rise is due to the seed fluctuations, can be seen impressively, when the RMS values are plotted for data sets, where the output values were calculated according to Eq. (1) for the measured pump energies and average seed powers (black line in Fig. 4a)). Here the fluctuations of the orange line are reproduced, but not the rise for small seed photon numbers.

Te get rid of the strong influence of the pump pulse fluctuations on the output fluctuations, different evaluation procedures were applied. As a first method, only data points where the pump pulse energy deviated less than ± 0.1 % of the average pump energy were selected. This led to a reduction of the sample size from 5000 shots to approximately 400 shots. When the RMS values of such a reduced data set are calculated, the orange line in Fig. 4b) results. It fluctuates much less than the RMS values of the complete data sets, and shows a more pronounced rise for small seed photon numbers. A very similar curve is obtained, when the RMS values are calculated for data sets where the measured output energies are divided by the calculated output energies for every single shot (green line in Fig. 4b)).

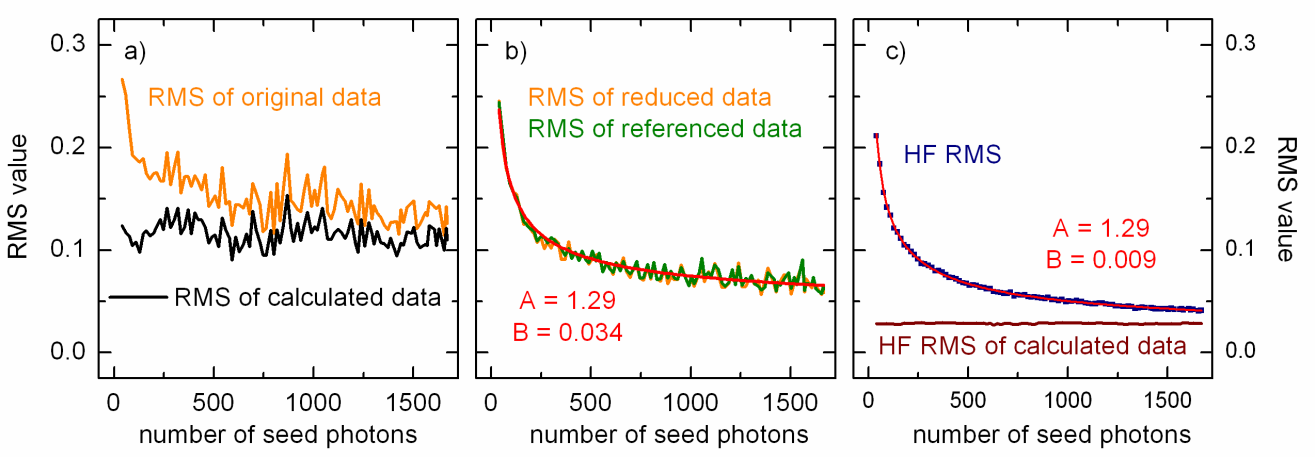

Fig. 4 Comparison of different evaluation methods to obtain RMS values. For details see text.

Both nearly identical curves can be fitted very well with an "extended" Poissonian fit of the form

$$\mathrm{RMS} = \frac{\mathrm{A}}{\sqrt{\mathrm{N}}} + \mathrm{B} \tag{4}$$

with the free parameters A and B. For both curves, the fit (red line in Fig. 4b)) yields a value of A = 1.29 and B = 0.034.

As third evaluation method, the high frequency RMS fluctuations (HF RMS) are calculated. They are obtained by applying a Savitzky-Golay smoothing filter with 5 side points and a polynomial order of 3 to the data. The resulting data set is then subtracted from the original data. Afterwards the mean value is added, and the RMS value is calculated as before. This method removes the fluctuations with low frequencies originating in energy and spatial drifts of the pump laser. The thus obtained HF RMS values are depicted in Fig. 4c) as blue squares. To these data again an extended Poissonian can be fitted very well, with resulting parameters of A = 1.29 and B = 0.009.

The brown line in Fig. 4c) shows the HF RMS fluctuations of the data set with output values calculated according to Eq. (1) for the measured pump energies and average seed powers. This shows impressively that the Poissonian form strictly originates in the seed photon number, but is independent of the pump pulse behavior.

In an additional experiment the cw seed diameter on the amplifier crystal was changed by translating the focusing lens and the same set of measurements were performed as above. Fig. 5 depicts the resulting HF RMS values for three selected beam diameters of 151 µm, 186 µm and 280 µm together with extended Poissonian fits. As can be seen, the fluctuations get lower for smaller seed beam diameter.

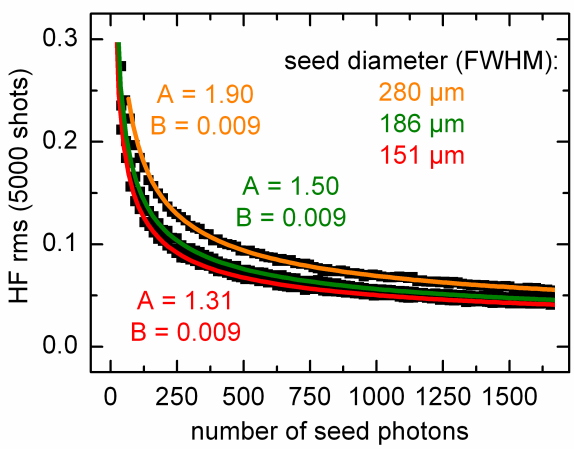

Fig. 5 High-frequency RMS values for data sets with different beam diameters (black points). The color lines are fits to the data.

4. Interpretation of the data and conclusion

As we have seen, the processed data can be fitted very well by the extended Poissonian of Eq. (4). To understand the data fully we now have to give some meaning to the introduced parameters A and B. As can be seen from Fig. 4b) and c), the parameter A stays constant, independent from the used evaluation method. However, it depends on the seed beam diameter as can be seen in Fig. 5. It gets lower with smaller seed beam diameter. On the contrary, the parameter B changes with the evaluation method, but stays constant when the seed diameter is changed.

This points to the conclusion, that A is a measure for the effectively used seed photons, and B is a measure for the residual technical fluctuations. When the seed diameter is large, only part of the seed photons are effectively amplified by the pump, which leads to a large A. When the seed diameter is reduced, more of the seed photons are used for amplification and A gets smaller. The residual technical fluctuations are unchanged by this variation, therefore B stays constant in this case. When using the reduced data set or the referenced data set (compare Fig. 4b)), only the pump energy fluctuations are taken into account. This leads to a B of 0.034. The HF RMS on the contrary removes all slow fluctuations, including fluctuations caused by spatial jitter of the pump versus the seed beam. This explains why B is even smaller for this evaluation method. When the seed photon number gets very large and tends to infinity, the RMS value tends to B. This also supports the interpretation of B as the residual technical noise.

We can therefore conclude that the output fluctuations can be described very well by the expected Poissonian distribution, extended by a correction factor A for the effectively used photon number and an offset B that describes the residual technical noise.

This means the fluctuations of the seed are indeed transferred exactly to the output fluctuations. This indicates that the parametric amplifier is an ideal amplifier in the sense that it shows the same amplification factor for each shot. One can not even see any deviation from the description that each individual seed photon undergoes the same amplification. The parametric amplifier is in this respect much more stable and deterministic as for example the amplification by a photomultiplier tube.

References

[1] C. Homann, M. Breuer, F. Setzpfandt, T. Pertsch, and E. Riedle, "Seeding of picosecond and femtosecond optical parametric amplifiers by weak single mode continuous lasers", Opt. Express **21**, 730 - 739 (2013).

[2] C. Homann and E. Riedle, "Direct measurement of the effective input noise power of an optical parametric amplifier", *submitted to Laser&Photonics Reviews (accepted)*.

[3] M.O. Scully and M.S. Zubairy, *Quantum Optics* (Cambridge University Press, 1997), chapter 1

[4] C. Schriever, S. Lochbrunner, E. Riedle, and D. J. Nesbitt, "Ultrasensitive ultraviolet-visible 20 fs absorption spectroscopy of low vapor pressure molecules in the gas phase", Rev. Sci. Instr. **79**, 013107 (2008).

[5] C. Homann, N. Krebs, and E. Riedle, "Convenient pulse length measurement of sub-20-fs pulses down to the deep UV via two-photon absorption in bulk material", Appl. Phys. B **104**, 783 (2011).

Appendix A1

Octave wide tunable UV-pumped NOPA:
pulses down to 20 fs at 0.5 MHz repetition rate

C. Homann, C. Schriever, P. Baum, and E. Riedle

Opt. Express **16**, 5746 - 5756 (2008)

Octave wide tunable UV-pumped NOPA: pulses down to 20 fs at 0.5 MHz repetition rate

C. Homann*, C. Schriever, P. Baum, and E. Riedle

Lehrstuhl für BioMolekulare Optik, Fakultät für Physik, Ludwig-Maximilians-Universität München, Oettingenstrasse 67, 80538 München, Germany

**Corresponding author: christian.homann@physik.uni-muenchen.de*

Abstract: Femtosecond laser pulses, which are tunable from 440 to 990 nm, are generated at MHz repetition rates by noncollinear parametric amplification (NOPA). The pulses have durations of 20 to 30 fs over the major part of the tuning range and a high energy stability of 1.3% (rms). The NOPA is pumped with ultraviolet pulses from the third harmonic of an ytterbium doped fiber laser system and seeded by a smooth continuum generated in bulk sapphire. The residual second harmonic is used to pump an additional NOPA, which is independently tunable from 620 to 990 nm. Interference experiments show that the two NOPA systems have a precisely locked relative phase, despite of being pumped by different harmonics with a random phase jitter. This demonstrates that the phase of pulses generated by optical parametric amplification does not depend on the pump phase.

OCIS codes: (060.2320) Fiber optics amplifiers and oscillators; (190.2620) Harmonic generation and mixing; (190.4410) Nonlinear optics, parametric processes; (320.7080) Ultrafast devices; (320.7110) Ultrafast nonlinear optics;

References and links

1. C. Schriever, S. Lochbrunner, P. Krok, and E. Riedle, "Tunable pulses from below 300 to 970 nm with durations down to 14 fs based on a 2 MHz ytterbium-doped fiber system," Opt. Lett. **33**, 192-194 (2008).
2. M. Marangoni, R. Osellame, R. Ramponi, G. Cerullo, A. Steinmann, and U. Morgner, "Near-infrared optical parametric amplifier at 1 MHz directly pumped by a femtosecond oscillator," Opt. Lett. **32**, 1489-1491 (2007).
3. J. Rothhardt, S. Hädrich, D. N. Schimpf, J. Limpert, and A. Tünnermann, "High repetition rate fiber amplifier pumped sub-20 fs optical parametric amplifier," Opt. Express **15**, 16729-16736 (2007).
4. J. M. Dudley, G. Genty, and S. Coen, "Supercontinuum generation in photonic crystal fiber," Rev. Mod. Phys. **78**, 1135-1184 (2006).
5. M. Ghotbi, Z. Sun, A. Majchrowski, E. Michalski, I. V. Kityk, and M. Ebrahim-Zadeh, "Efficient third harmonic generation of microjoule picosecond pulses at 355 nm in BiB_3O_6," Appl. Phys. Lett. **89**, 173124 1-3 (2006).
6. A. Dubietis, G. Tamošauskas, and A. Varanavičius, "Femtosecond third-harmonic pulse generation by mixing of pulses with different duration," Opt. Commun. **186**, 211-217 (2000).
7. SNLO nonlinear optics code available from A. V. Smith, Sandia National Laboratories, Albuquerque, NM 87185-1423.
8. H. S. Park, J. S. Baskin, O.-H. Kwon, and A. H. Zewail, "Atomic-Scale Imaging in Real and Energy Space Developed in Ultrafast Electron Microscopy," Nano Lett. **7**, 2545-2551 (2007).
9. G. M. Gale, M. Cavallari, T. J. Driscoll, and F. Hache, "Sub-20-fs tunable pulses in the visible from an 82-MHz optical parametric oscillator," Opt. Lett. **20**, 1562-1564 (1995).
10. T. Wilhelm, J. Piel, and E. Riedle, "Sub-20-fs pulses tunable across the visible from a blue-pumped single-pass noncollinear parametric converter," Opt. Lett. **22**, 1494-1496 (1997).
11. G. Cerullo and S. De Silvestri, "Ultrafast optical parametric amplifiers," Rev. Sci. Instrum. **74**, 1-18 (2003).
12. R. Butkus, R. Danielius, A. Dubietis, A. Piskarskas, and A. Stabinis, "Progress in chirped pulse optical parametric amplifiers," Appl. Phys. B **79**, 693-700 (2004).
13. F. Tavella, A. Marcinkevičius, and F. Krausz, "90 mJ parametric chirped pulse amplification of 10 fs pulses," Opt. Express **14**, 12822-12827 (2006).
14. S. Witte, R. Th. Zinkstok, A. L. Wolf, W. Hogervorst, W. Ubachs, and K. S. E. Eikema, "A source of 2 terawatt, 2.7 cycle laser pulses based on noncollinear optical parametric chirped pulse amplification," Opt. Express **14**, 8168-8177 (2006).

#92904 - $15.00 USD Received 19 Feb 2008; revised 4 Apr 2008; accepted 7 Apr 2008; published 9 Apr 2008

15. I. Z. Kozma, P. Baum, U. Schmidhammer, S. Lochbrunner, and E. Riedle, "Compact autocorrelator for the online measurement of tunable 10 femtosecond pulses," Rev. Sci. Instrum. **75**, 2323-2327 (2004).
16. K. Duncker and W. Widdra, Institut für Physik, Martin-Luther-Universität Halle-Wittenberg, Hoher Weg 8, 06120 Halle, Germany (personal communication, 2008).
17. P. Baum, S. Lochbrunner, J. Piel, and E. Riedle, "Phase-coherent generation of tunable visible femtosecond pulses," Opt. Lett. **28**, 185-187 (2003).
18. P. Baum, E. Riedle, M. Greve, and H. R. Telle, "Phase-locked ultrashort pulse trains at separate and independently tunable wavelengths," Opt. Lett. **30**, 2028-2030 (2005).
19. P. Tzankov, T. Fiebig, and I. Buchvarov, "Tunable femtosecond pulses in the near-ultraviolet from ultrabroadband parametric amplification," Appl. Phys. Lett. **82**, 517-519 (2003).
20. A. Killi, A. Steinmann, G. Palmer, U. Morgner, H. Bartelt, and J. Kobelke, "Megahertz optical parametric amplifier pumped by a femtosecond oscillator," Opt. Lett. **31**, 125-127 (2006).
21. A. Steinmann, A. Killi, G. Palmer, T. Binhammer, and U. Morgner, "Generation of few-cycle pulses directly from a MHz-NOPA," Opt. Express **14**, 10627-10630 (2006).
22. H. Merdji, T. Auguste, W. Boutu, J.-P. Caumes, B. Carré, T. Pfeifer, A. Jullien, D. M. Neumark, and S. R. Leone, "Isolated attosecond pulses using a detuned second-harmonic field," Opt. Lett. **32**, 3134-3136 (2007).

1. Introduction and overview

For the generation of intense femtosecond pulses, laser amplifiers based on fiber technology promise high peak power at high repetition rates, excellent beam quality and good stability. Such characteristics are essential in machining, nonlinear imaging, microscopy, and ultrafast spectroscopy. The combination of high peak intensities with high repetition rates allows for studying or making use of the entire range of nonlinear effects with a high processing or data acquisition rate. To apply fiber lasers in ultrafast spectroscopy, the relevant absorption and emission spectra of the investigated systems must be matched and pulse durations of ~20 fs are required. Typically, molecules and condensed matter absorb in the UV, visible, and near infrared spectral region. A frequency converter for fiber lasers, typically operating around 1035 nm for ytterbium doping, into an as wide as possible tuning range is therefore essential to take advantage of the high repetition rate and stability of fiber lasers in spectroscopy.

Noncollinear optical parametric amplifiers (NOPAs) pumped by Ti:sapphire lasers are well proven devices for the generation of few-cycle tunable pulses. They allow accessing the temporal signatures of ultrafast wavepacket dynamics and structural oscillations in molecules and condensed matter. Now we investigate the use of an ytterbium-doped fiber laser operating at 1035 nm as pump source for NOPAs that allow the full coverage of the near UV, visible and NIR spectral range. In contrast to earlier work performed in our laboratory [1], we focus on a NOPA pumped by the third harmonic of the 1035 nm fiber laser pulses. This should allow extending the tuning range significantly to shorter wavelengths and accessing the UV with simple frequency doubling. To retain the demonstrated NIR coverage, we combine the 345 nm pumped NOPA with a NOPA pumped by the residual frequency doubled pump light.

The manuscript is outlined as follows. In Section 2, we present the experimental arrangement. In Section 3 and 4, we explain the considerations and technical details for seed and pump light generation. Section 5 addresses the NOPA processes and relevant phase matching concepts. The measured spectra, Fourier limits, pulse durations and pulse energies are presented and discussed. The results of a noise analysis and phase investigations are shown and reviewed in Section 6 and 7. We conclude with final remarks in Section 8.

2. Experimental arrangement

The two NOPAs (sketched in Fig. 1) are pumped by an Yb-doped fiber-oscillator/amplifier system (IMPULSE; Clark-MXR, Inc.), which delivers 10 to 12 µJ pulses at 1035 nm (frequency ω_0, red in Fig. 1) with a pulse length of 230 fs at a selectable repetition rate between 200 kHz and 2 MHz. A half-wave plate for 1035 nm in combination with a thin film polarizing beam splitter is used to split off 1.5 µJ pulses for continuum generation (Fig. 1, grey; explained in more detail in Section 3). This scheme is chosen to be able to maintain a constant energy for continuum generation, independent of slight variations of the output energy of the fiber laser. The remaining 8.5 to 10.5 µJ pulses are focused with the lens L_1 towards two BBO crystals for frequency doubling and subsequent tripling. The details of the mixing concept are

#92904 - $15.00 USD Received 19 Feb 2008; revised 4 Apr 2008; accepted 7 Apr 2008; published 9 Apr 2008

discussed in section 4. The resulting light (Fig. 1, blue) is separated by a dichroic mirror (DM), which is highly reflective at 345 nm and highly transmissive at 517 and 1035 nm. After recollimation by the lens L_2, a spherical mirror focuses the 345 nm pulses into a 2 mm thick type-I BBO crystal, cut at 37°, where they act as pump pulses for the NOPA process. A second dichroic mirror (highly reflective for 517 nm and highly transmissive at 1035 nm) extracts the remaining $2\omega_0$ light (Fig. 1, green), which is likewise recollimated by a lens (L_3) and focused by a spherical mirror into a 5 mm thick type-I BBO crystal, cut at 26.5°. As will be shown later in detail, the $3\omega_0$ pumped NOPA works best in the visible part of the spectrum up to 700 nm. In contrast, the $2\omega_0$ pumped NOPA is advantageous in the 700 to 990 nm regime. Therefore a spectral splitting of the seed continuum at approximately 700 nm, for example with a dichroic mirror, is appropriate to obtain the highest seed energy in both NOPAs. If the full tuning range from 440 to 990 nm of the $3\omega_0$ pumped NOPA shall be exploited, a broadband 50% beam splitter can be used instead.

Wavelength tuning is achieved for large parts of the spectral range in both branches by only varying the time delay between the chirped continuum seed and the respective pump pulses. Only towards the short and long wavelength ends of the tuning ranges small changes of the phase matching angles of the BBO crystals and/or the noncollinearity angles are necessary.

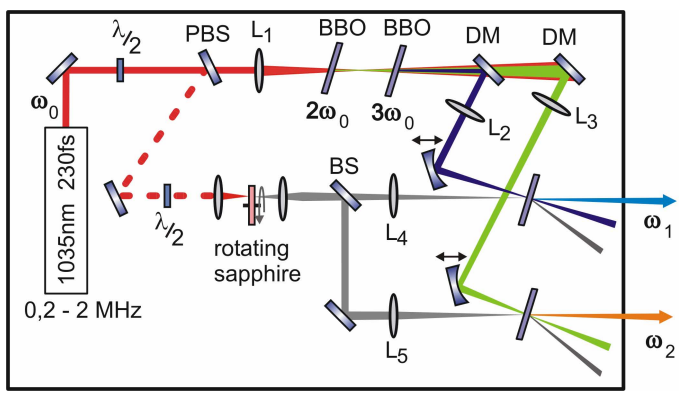

Fig. 1. Experimental arrangement. λ/2, half-wave plate; PBS, polarization beam splitter; L_1-L_5, lenses; DM, dichroic mirror; BS, beam splitter (50%, broadband coating or dichroic mirror)

Most of the experiments described below were performed at 200 kHz repetition rate. Since then the system has been operated continously at 500 kHz without any noticable deterioration of performance and with unchanged output pulse energies. Scaling to the full repetition rate of the fiber laser system (2 MHz) should be straightforward and as before we do not expect any significant changes in the NOPA pulse paramters [1]. The whole setup is placed in a box with dimensions of approximately 80 x 80 x 20 cm^3, is therefore easily portable, compact and protected from the environment.

3. Seed generation

Different approaches for seed light generation with high repetition rate pump systems were reported, such as optical parametric generation in periodically poled lithium niobate [2] or soliton generation in a highly nonlinear photonic crystal fiber [3]. Optical parametric generation often shows high energy fluctuations, and nonlinear fibers typically result in highly structured spectra with phase modulations [4].

Here we use a continuum generated by filamentation in a 4 mm thick sapphire crystal. With a lens of 75 mm focal length we focus pulses at 1035 nm into the sapphire. Collimation of the continuum is achieved by a 30 mm achromatic lens. It smoothly covers a spectral region from 430 to 1000 nm, whereof the region from 500 to 850 nm forms a nearly flat plateau (±30% spectral energy density). In contrast to earlier approaches [1], where a minimum energy of 2.5 µJ per pulse was needed for stable continuum generation, we now find a minimum

#92904 - $15.00 USD Received 19 Feb 2008; revised 4 Apr 2008; accepted 7 Apr 2008; published 9 Apr 2008

gy of 2.5 µJ per pulse was needed for stable continuum generation, we now find a minimum threshold energy of only 1.5 µJ per pulse. This is due to an improved beam profile of the pump light, since we now directly use the output of the fiber laser and avoid prior frequency doubling. In addition, even small improvements in pulse duration seem to have significant effects on the continuum threshold. To avoid damage accumulation due to the high average power, the sapphire disc is rotated at approximately 60 Hz. Instabilities and degradation of the filament are sometimes assumed as drawbacks of continua generated in bulk materials [3]. This was not observed; in contrary we measure energy fluctuations of the continuum as low as 1.1% rms (see Section 6).

4. Ultraviolet pump pulses

In parametric processes, the wavelength of the pump pulses limits the shortest achievable amplification wavelength for a given nonlinear crystal. If the amplified spectrum approaches the pump wavelength, energy conservation results in idler pulses with long wavelengths in the infrared, which are eventually absorbed in the nonlinear crystal. For example, when using the second harmonic of the 1035 nm pulses, amplification of wavelengths below 620 nm ceases in BBO due to idler absorption above 3.1 µm [1]. To be able to amplify a wide spectral range of the seed light on the short wavelength side, a sufficiently short pump wavelength is needed. Therefore we choose the third harmonic at 345 nm as pump pulses.

We apply frequency doubling and subsequent sum-frequency mixing with the remaining fundamental pulses for overall tripling. In the fs-regime, group-velocity mismatch (GVM) between the three pulses plays an important role, because the difference in transit time through the nonlinear crystals becomes comparable to the pulse lengths. Therefore the pulses loose temporal overlap during propagation inside the crystals, which leads to reduced efficiency. The fundamental and second harmonic pulses exit the doubling stage at different times and have to be suitably delayed to restore the temporal overlap in the mixing stage. Conventional schemes for tripling of ultrafast pulses therefore use dichroic beam separation, mechanical delay, and recombination between the doubling and mixing stages [5, 6].

In contrast to these approaches, we use a sequence of two specially selected BBO crystals, which allow for group velocity matching in a simple collinear geometry without the need of additional delay elements. The concept is based on the following considerations. In type-I second harmonic generation in BBO, the fundamental pulses (o-polarized) have a larger group

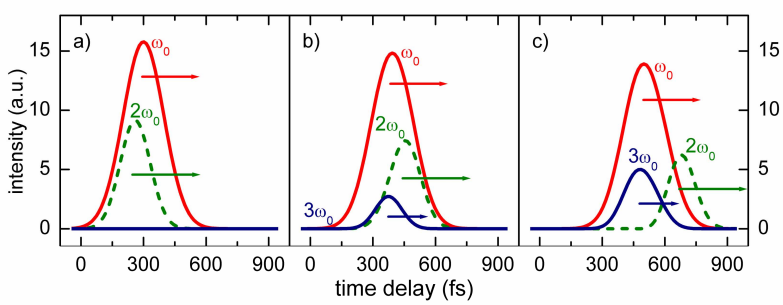

Fig. 2. Simulation of the $3\omega_0$ generation using SNLO [7]. (a) When entering the type-II BBO mixing crystal, the ω_0 pulse leads the $2\omega_0$ pulse by 50 fs due to GVM in the BBO crystal used for second harmonic generation. (b) After 0.5 mm in the mixing crystal, the $2\omega_0$ pulse has overtaken the ω_0 pulse. (c) After 1.0 mm, the $2\omega_0$ pulse starts to separate from the ω_0 pulse, which reduces the efficiency of $3\omega_0$ generation.

velocity than the second harmonic pulses (e-polarized). In our setup, using fundamental pulses with a duration of 230 fs at 1035 nm and a 0.8 mm thick BBO doubling crystal, this group velocity mismatch leads to a separation of the ω_0 and $2\omega_0$ pulses of approximately 50 fs after the doubling crystal (see Fig. 2(a)). For the following sum-frequency mixing process

#92904 - $15.00 USD Received 19 Feb 2008; revised 4 Apr 2008; accepted 7 Apr 2008; published 9 Apr 2008

$\omega_0 + 2\omega_0 \rightarrow 3\omega_0$, there are three phase matching possibilities in BBO (see table 1). They result in different group delays that affect the temporal synchronization between the involved pulses.

A first important consideration is the group delay between the fundamental and the second harmonic pulses (table 1, middle column). In contrast to earlier approaches, which used sum-frequency mixing of type-I (o + o → e) or type-II (e + o → e) [5,6], the third possibility, o + e → e, offers a negative group delay between the ω_0 and $2\omega_0$ pulses. Because the ω_0

Table 1: Group delay of pulses of the quoted frequencies after propagating through 1 mm of BBO for different phase matching configurations (ω_0 corresponding to a wavelength of 1035 nm).

Group delay	ω_0 vs. $2\omega_0$	ω_0 vs. $3\omega_0$
Type-I o + o → e	174 fs	369 fs
Type-II e + o → e	346 fs	468 fs
Type-II o + e → e	-190 fs	85 fs

pulses enter the tripling crystal 50 fs before the $2\omega_0$ pulses, a subsequent negative group velocity mismatch in the tripling crystal, as given by the o + e → e process, allows for the second harmonic pulses to overtake the fundamental pulses during the propagation. This restores a good temporal overlap within the crystal, in order to achieve high conversion efficiency without applying external delay elements (see Figs. 2(b) and 2(c)). The nonlinear conversion coefficient, d_{eff}, is about one fifth of the type-I scheme, but the damage threshold of BBO is high enough to compensate this by slightly reducing the beam sizes for increased intensity. A second advantage of the o + e → e mixing scheme is the small group velocity mismatch between the original ω_0 and $2\omega_0$ pulses with respect to the generated $3\omega_0$ pulses (table 1, right column). Frequency tripled light that is generated in different parts of the crystal therefore adds up without temporal pulse lengthening.

In addition, with the o + e → e scheme no rotation of the polarization between the two crystals is necessary and wave plates or geometrical polarization rotation is avoided. The generated $3\omega_0$ pulses have the same polarization as the $2\omega_0$ pulses and can directly be used for pumping the NOPAs.

Experimentally, an f = 500 mm lens is used to focus the fundamental ω_0 pulses towards the two BBO crystals (type-I, 0.8 mm, 23.5° and type-II, 1.5 mm, 62.8°). The type-I doubling crystal is placed about 70 mm before the focus and the type-II tripling crystal about 50 mm behind. This allows independent fine-tuning of the respective conversion efficiencies by moving the crystals in order to adjust the spot sizes. Total energy conversion efficiencies to the third harmonic of more than 15% are observed. In routine operation, we operated at approximately 11%, to maintain a good energy balance between the $2\omega_0$ and the $3\omega_0$ light, which are both used for NOPA pumping. We did not observe degradation or damage of the BBO crystals in long-term operation.

Our tripling scheme was already successfully used in ultrafast electron microscopy utilizing the same pump laser [8]. The presented concept of group-velocity management in frequency tripling is generally applicable, if conditions can be found where the group velocity difference of ω_0 and $2\omega_0$ changes sign between frequency doubling and sum-frequency-mixing. For BBO, this is the case for type-I frequency doubling and type-II sum-frequency mixing for fundamental wavelengths above 905 nm up to about 1.5 µm.

5. NOPA design and output characteristics

For simultaneous parametric amplification in the UV pumped and green pumped NOPA unit, the collimated seed continuum is split suitably as explained in Section 2. For the UV pumped NOPA, it is then focused with an f = 300 mm fused silica lens towards the corresponding BBO crystal (type-I, 2.0 mm, 37°), which is placed approximately 340 mm behind the lens, and overlapped spatially and temporally with the pump pulses.

#92904 - $15.00 USD Received 19 Feb 2008; revised 4 Apr 2008; accepted 7 Apr 2008; published 9 Apr 2008

To obtain the highest possible amplification bandwidth and thereby the shortest pulses, a noncollinear geometry is chosen. This concept has originally been demonstrated for 400 nm pumping [9-12] and is now widely used for 532 nm pumped optical parametric chirped pulse amplifiers (OPCPAs) [13,14]. The concept can be readily extended to 345 nm pumping. The external noncollinearity angle between the seed and the pump beam is set to ~5.5° for broadband amplification around 590 nm. The crystal is oriented for tangential phase matching to obtain the highest efficiency and the cleaner output beam profile, as compared to the walk-off compensated orientation. The collimated UV pump beam is focused with a spherical mirror (f = 250 mm), placed approximately 260 mm before the BBO crystal, resulting in a beam diameter of about 100 µm in the crystal.

In the green pumped NOPA, we use an f = 350 mm lens for focusing the seed continuum towards the BBO crystal (type-I, 5.0 mm, 26.5°), which is placed about 450 mm behind the lens. The collimated green pump pulses are focused with a spherical mirror (f = 250 mm), which is placed about 270 mm before the BBO crystal, resulting in a beam diameter of about 220 µm on the crystal surface. The external noncollinearity angle is set to ~5° for broadband amplification around 820 nm.

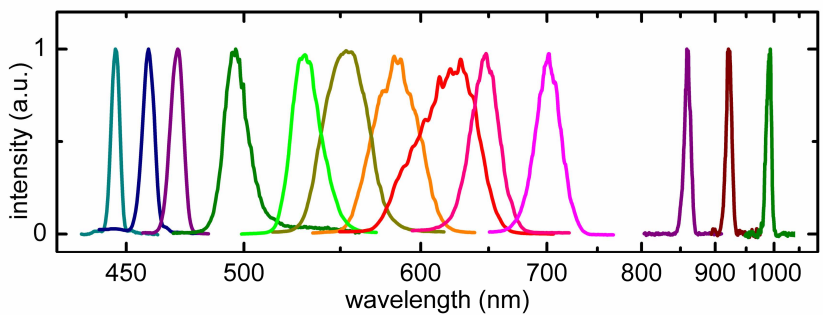

Fig. 3. Typical output spectra of the 345 nm pumped noncollinear optical parametric amplifier, showing the more than octave wide continuous tuning range.

Figure 3 shows typical output spectra from the UV pumped NOPA. Tuning is mainly achieved by delaying the UV pump pulses with respect to the longer (and chirped) continuum pulse (495 – 665 nm), and by slightly adjusting the phase matching angle and noncollinearity for parametric amplification. The resulting output pulses are continuously tunable over more than one optical octave from 440 to 990 nm (303 – 682 THz). Throughout all of the tuning range, the spectra are very smooth and have nearly Gaussian shape. The pulses were compressed using a sequence of fused silica prisms with an apex angle of 68.7°. Typical prism separations (edge to edge) are 500 to 1000 mm. For temporal pulse characterization, autocorrelation traces were obtained with a dispersion-free autocorrelator [15]. Figure 4 shows typical traces, from which the pulse durations are evaluated by assuming a Gaussian pulse shape. The

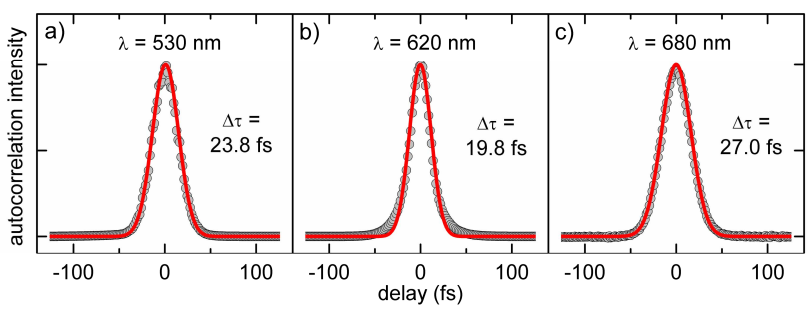

Fig. 4. Typical measured autocorrelation traces (dots) and Gaussian fits to the data (red line) at various wavelengths. The autocorrelation traces are very smooth and pedestal-free, indicating pulses without temporal satellites.

#92904 - $15.00 USD Received 19 Feb 2008; revised 4 Apr 2008; accepted 7 Apr 2008; published 9 Apr 2008

smooth Gaussian shaped spectra in combination with insignificant higher order chirp allow for almost Fourier-limited pulse shapes without temporal satellites, as evident from the pedestal-free autocorrelation traces.

Figure 5 summarizes the calculated Fourier-limits of measured spectra (blue squares) and the measured pulse durations (red diamonds). Between 520 and 680 nm pulse durations of sub-30 fs were measured. The observed increase of the Fourier limits towards shorter and longer wavelengths can be explained by considering phase matching and chirp effects. In the short wavelength region, estimates show that broadband noncollinear phase matching is well possible and that the residual wave vector mismatch between signal and idler allows for Fourier limits of 13 fs from 430 to 690 nm (see blue dashed line in Fig. 5). However, even with perfect phase matching, parametric amplification can only affect such spectral components of the seed light that overlap in time with the pump pulses. The seed continuum is chirped, mainly by dispersion in the achromatic lens used for collimating and the fused silica lens used for relay imaging. Because such material dispersion is particularly severe at short wavelengths, the continuum is chirped strongest in this spectral range and longer Fourier limits are observed. With a proper chirp management, e.g., by compressing the continuum and/or stretching the pump pulses, an amplification bandwidth sufficient for sub-20 fs pulses is expected all the way down to 440 nm.

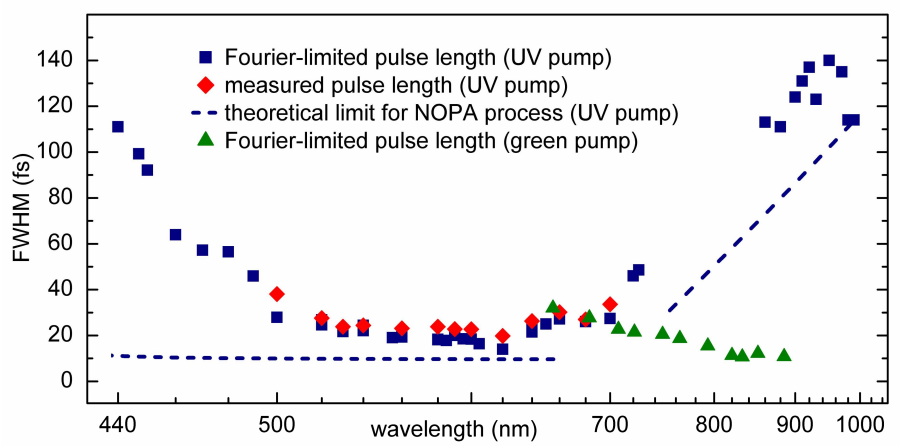

Fig. 5. Summary of calculated Fourier-limited pulse lengths from measured spectra (blue squares for UV pumping, green triangles for green pumping [1]) and calculated pulse lengths from measured autocorrelation traces (red diamonds). The dotted blue lines show theoretical limits for the minimum pulse length, assuming group-velocity matching in the spectral range below 660 nm and based on the group-velocity mismatch between signal and idler above 750 nm.

Above the degeneracy point of 690 nm effective group-velocity matching by a noncollinear geometry is not possible. Therefore a collinear arrangement is advantageous and the amplification bandwidth is mainly given by the first order wave vector mismatch between signal and idler. The dashed blue line shown in Fig. 5 above 750 nm depicts the resulting lower limit for the achievable pulse duration. The somewhat higher measured Fourier limits are explained by a small residual noncollinearity angle that was used in the experiments. The second NOPA, pumped by green pulses at $2\omega_0 \triangleq 517$ nm, therefore exhibits an ideal complement as it delivers sub-30 fs over its complete fundamental tuning range from 620 to 990 nm (see green triangles in Fig. 5). In combination, the two NOPAs provide Fourier-limited pulse lengths of sub-30 fs in a spectral range from 500 to 990 nm.

The output pulse energies are in the range of 140 nJ for the UV pumped NOPA, best at the center of its tuning range. Simultaneously, the second harmonic pumped NOPA delivers pulses with up to 250 nJ energy in a broad range around 800 nm. For both NOPAs the beam profile is visually round and homogeneous. The pulse energies are well sufficient for subsequent frequency conversion processes, for example to extend the tuning range into the ultra-

#92904 - $15.00 USD Received 19 Feb 2008; revised 4 Apr 2008; accepted 7 Apr 2008; published 9 Apr 2008

violet region. The generation of 34 nJ pulses at 290 nm has already been demonstrated [16]. The octave-wide tuning range together with simple frequency doubling leads to a continuous spectral coverage from below 250 nm to nearly 1 µm without any gap.

6. Fluctuation analysis

To elucidate the usability of the MHz NOPA for low-noise spectroscopic applications, we performed a detailed analysis of the pulse-to-pulse intensity fluctuations. The energy in each single pulse was measured by a moderately fast photodiode module, of which the output voltage trace was recorded in time with a fast digital oscilloscope. Such oversampling significantly decreases digitizing effects on low-noise data. To reveal fluctuation correlations between different pulse trains, two identical photodiodes were employed simultaneously. The relative deviations of the individual pulse energies E_k from the average $\bar{E}$ is referred to as laser noise. For the primary fiber laser system, we obtain a total noise of 0.8 % rms when recording 100,000 subsequent pulses at 208 kHz. The frequency-resolved noise density is shown in Fig. 6(a). The relative noise intensity, i.e. the spectral power density normalized to the average power, is below -85 dB/Hz throughout the frequency range of 1 – 100 kHz. We note that the noise spectrum of the fiber laser output is mostly composed of uniform white noise, with a resonance at about 44 kHz.

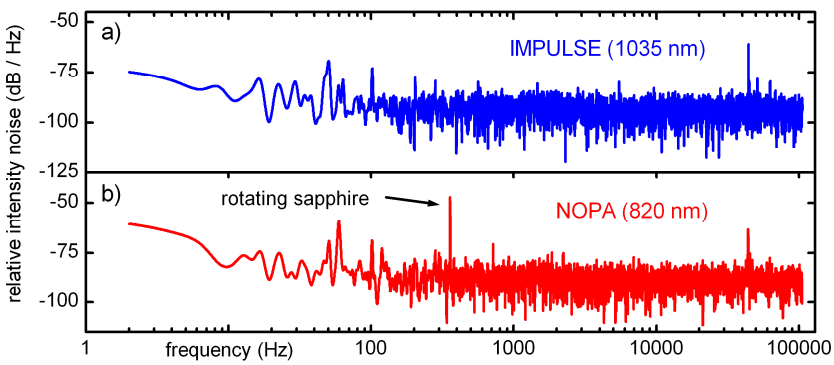

Fig. 6. Relative intensity noise of (a) the fiber laser system and (b) the NOPA.

For the output fluctuations of the green pumped NOPA unit, we obtain a total noise of 1.3 % rms. The spectrum of the NOPA fluctuations (Fig. 6(b)) shows an additional low frequency resonance at 355 Hz, which originates from the rotating sapphire disc and is attributed to slight changes in the overlap between the continuum and the pump pulses in the NOPA crystal, caused by not perfectly parallel surfaces of the disc. However, this rotation is found to contribute only insignificantly to the total noise of the NOPA (1.2 % rms, when excluding the 355 Hz resonance). From the noise spectrum of the NOPA we conclude that a modulation frequency in the range of 5 – 15 kHz is most suitable for low-noise lock-in detection. The fluctuations of the UV-pumped NOPA unit were not analyzed in detail. Since the output is in the visible, the visual impression of no significant instabilities can be taken as indication for comparable fluctuations as in the green pumped NOPA.

The total NOPA output noise is only 1.6 times larger than that of the primary fiber laser, although four nonlinear optical conversion processes are involved (frequency doubling, sum-frequency mixing, continuum generation, and parametric amplification). To investigate the origin of the NOPA noise, we measured energy correlations between the different beams involved within the NOPA. Such an analysis allows for measuring the order of nonlinearity of the involved frequency conversion processes and to investigate the effects of saturation.

Correlation plots of the measured pulse energies as two-dimensional histograms are expected to show tilted ellipsoids with the slope of the main axis given by the order m of the

#92904 - $15.00 USD Received 19 Feb 2008; revised 4 Apr 2008; accepted 7 Apr 2008; published 9 Apr 2008

nonlinearity. Deviations of the measured slope m^* from the expected value m indicate saturation in the conversion process.

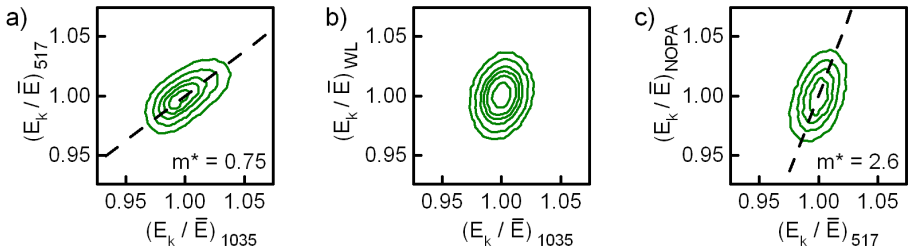

Fig. 7. Scatter density plots of output vs. input noise of various nonlinear processes involved in the generation of the NOPA pulses.

Figure 7(a) shows the noise correlation (binned into a 75 x 75 histogram) between the fundamental fiber laser pulse energy and the energy of the green pump pulses. For frequency doubling $m = 2$ is expected, but experimentally we observe $m^* = 0.75$. This means that the fluctuations in the green pulses are even smaller than those of the fundamental pulses. For high input intensities and doubling efficiencies of more than 30 % depletion of the input pulse becomes significant and the second harmonic pulses are partially back-converted. Exceptionally intense fundamental pulses therefore generate attenuated frequency doubled output pulses, which can result in self-stabilization when a proper intensity regime is chosen. We believe that such a mechanism is the reason for the low fluctuations of the second harmonic and consequently the remarkably high NOPA stability.

Figure 7(b) shows the noise correlation between the fundamental fiber laser pulses and the continuum pulses (800 to 840 nm band pass). For two distinct time scales of 0.5 s and 1 ms (data not shown), we find no correlation and no tilt of the ellipse is measurable. The energy of our continuum pulses has no significant dependence on the pump pulse intensity. This is the result of the threshold behavior of the self-focusing, channeling, and spectral broadening mechanisms involved in the continuum generation. Some noise of about 1.1 % rms is nevertheless observed and contributes to the overall NOPA noise.

The correlation between the output of the green pumped NOPA and the green pump pulses is reasonably high (see Fig. 7(c)). A further improvement of the pump laser stability would therefore lead to an even better NOPA stability. The observed slope of $m^* = 2.6$ is below the expectation for an unsaturated parametric amplification. A similar observation was made for the UV pumped NOPA. This indicates that the two parametric amplification processes are both operated fairly close to saturation, even for the low pump pulse energies used in this setup. Stable NOPA operation is not limited to highly energetic pump pulses, when focus sizes, pulse durations, and beam diameters within the setup are properly designed.

7. Experimental investigation of phase dependencies in optical parametric amplification

The overlapping amplification regions of the two differently pumped NOPA units allow for an instructive interference experiment that renders information about the phase dependencies in the parametric amplification process. The two NOPA units, seeded by the same continuum, are tuned to the same center wavelength of 720 nm and brought to interference with a small angle on a distant screen (see schematic Fig. 8(a)). Such an interferogram yields information about the relative phase jitter between the two NOPAs. In earlier experiments it was demonstrated that stable interference is observed, when two NOPAs are pumped by replicas of the same blue pulse, i.e. pulses with equal phase fluctuations [17,18]. In contrast, the presented experiment involves pump pulses that are derived from different harmonics ($2\omega_0$ and $3\omega_0$) of the primary fiber laser, which is not phase stabilized. The second and third harmonic pulses therefore have carrier-envelope phases with twice or threefold the original phase fluctuations, which makes their relative phase jitter random. Hence, if the phase of the pump pulse has in-

#92904 - $15.00 USD Received 19 Feb 2008; revised 4 Apr 2008; accepted 7 Apr 2008; published 9 Apr 2008

fluence on the phase of the amplified pulse in optical parametric amplification, the phase of the interference pattern, i.e. the position of the minima and maxima, should change statistically from shot to shot.

To test this, we recorded the time dependence of the interference pattern with a linear detector array operated at 1 kHz. A typical measurement is depicted in Fig. 8(c). Over times of several seconds, the position of the interference pattern is extremely stable (see Fig. 8(b)). The associated relative phase between the two NOPAs, shown in Fig. 8(d) and 8(e), has fluctuations of less than 20 mrad rms in the measured frequency range of 0.1 to 1000 Hz. This means that the relative phase of the two parametrically amplified pulses is extremely stable and independent of the phase of the pump pulses.

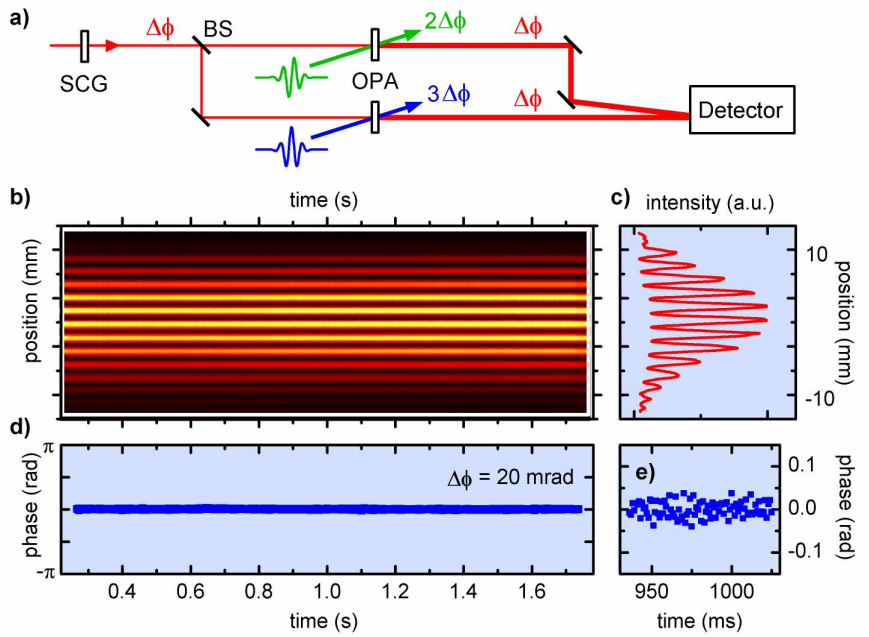

Fig. 8. Interference experiment to investigate phase dependencies in optical parametric amplification (OPA). (a) Experimental setup. SCG: supercontinuum generation, BS: beam splitter. (b) Wrong-color representation of the amplitude of successive interference patterns showing the high phase stability. (c) Single measured spatial interference pattern. (d) and (e) Phase of the interference pattern over time.

8. Concluding remarks

The presented results show that a NOPA based on a MHz fiber laser system is capable of generating sub-20 fs pulses with energies above 100 nJ and is tunable from 440 to 990 nm without a gap. This more than octave wide tuning range is made possible by pumping the parametric amplification with the frequency tripled pump pulses at 345 nm. With simple and straight forward frequency doubling the range from below 250 nm to nearly 1 µm is accessible. Ti:sapphire based systems have so far not been shown to allow this complete spectral coverage. Attempts to pump a NOPA with the third harmonic of the Ti:sapphire system at 267 nm were hampered by the strong two photon absorption in the BBO crystal and the large group velocity mismatch between the three interacting waves [19]. Additionally, the Yb-doped fiber laser system allows at least a tenfold higher repetition rate than Ti:sapphire based amplifier systems. The present rate around 1 MHz is ideal for applications as it provides sufficiently intense pulses for nonlinear interactions, high averaging capability and still ample time for sample exchange or relaxation. The sub-250 fs pulse duration of the used pump system allows direct generation of a high quality continuum in bulk sapphire. This permits a much wider tun-

#92904 - $15.00 USD Received 19 Feb 2008; revised 4 Apr 2008; accepted 7 Apr 2008; published 9 Apr 2008

ing range and smoother spectra than obtained with precompression of longer pump pulses [20,21] or seeding by a spectrally broadened Ti:sapphire laser [3].

The presented NOPA is based on a single stage traveling wave amplifier. Since the parametric amplification depends on the pump intensity and higher pump energies can be accommodated by an increased pump diameter, nearly arbitrary power scaling of the device seems realistic. This opens up the route to UV-pumped OPCPAs at the millijoule or even joule level and OPCPAs with combined green and UV pumping for increased spectral width and pulse durations approaching 5 fs.

The demonstrated phase stability in the optical parametric amplification is an important requirement for many future experiments, such as light wave synthesis. The measured phase stability between the two NOPAs of 20 mrad corresponds to a temporal jitter of only 8 attoseconds. Since our measurement averaged over 200 pulses, we expect a true pulse-to-pulse jitter of not more than 110 attoseconds. The presented amplification concept with its tunability of more than an octave is most promising for generating single attosecond pulses in recently proposed schemes based on a strong pulse with frequency ω and a phase-locked second pulse slightly off the second-harmonic, e.g., 2.2ω [22].

The two NOPAs pumped by the second and the third harmonic have their best performance in different spectral regions and therefore provide powerful sources for two-color ultrafast pump-probe spectroscopy. The high repetition rate is expected to advance for example spectroscopy on surfaces, where extremely weak signals have to be detected and long averaging is needed. As a consequence of the phase stability, the full temporal resolution corresponding to the reported short pulse durations can be utilized even for long averaging times.

Acknowledgments

We thank Clark-MXR, Inc. and HORIBA Jobin Yvon for the generous loan of the IMPULSE system. This work was supported by the Austrian Science Fund within the framework of the Special Research Program F16 (Advanced Light Sources) and by the DFG-Cluster of Excellence: Munich-Centre for Advanced Photonics. The International Max Planck Research School on Advanced Photon Science (C. H.) is gratefully acknowledged.

#92904 - $15.00 USD Received 19 Feb 2008; revised 4 Apr 2008; accepted 7 Apr 2008; published 9 Apr 2008

Appendix A2

Approaching the full octave: Noncollinear optical parametric chirped pulse amplification with two-color pumping

D. Herrmann, C. Homann, R. Tautz, M. Scharrer, P. St.J. Russell, F. Krausz L. Veisz, and E. Riedle

Opt. Express **18**, 18752 - 18762 (2010)

Approaching the full octave: Noncollinear optical parametric chirped pulse amplification with two-color pumping

D. Herrmann,[1,2,*] C. Homann,[2] R. Tautz,[1,3] M. Scharrer,[4] P. St.J. Russell,[4] F. Krausz,[1,5] L. Veisz,[1,6] and E. Riedle[2]

[1] *Max-Planck-Institut für Quantenoptik, Hans-Kopfermann-Str. 1, 85748 Garching, Germany*
[2] *LS für BioMolekulare Optik, LMU München, Oettingenstr. 67, 80538 München, Germany*
[3] *present address: LS für Photonik und Optoelektronik, LMU München, Amalienstr. 54, 80799 München, Germany*
[4] *Max-Planck-Institut für die Physik des Lichts, Günther-Scharowsky-Str. 1/ Bau 24, 91058 Erlangen, Germany*
[5] *LS für Laserphysik, LMU München, Am Coulombwall 1, 85748 Garching, Germany*
[6] *laszlo.veisz@mpq.mpg.de*
[*] *d.herrmann@physik.uni-muenchen.de*

Abstract: We present a new method to broaden the amplification range in optical parametric amplification toward the bandwidth needed for single cycle femtosecond pulses. Two-color pumping of independent stages is used to sequentially amplify the long and short wavelength parts of the ultrabroadband seed pulses. The concept is tested in two related experiments. With multi-mJ pumping pulses with a nearly octave spanning spectrum and an uncompressed energy of 3 mJ are generated at low repetition rate. The spectral phase varies slowly and continuously in the overlap region as shown with 100 kHz repetition rate. This should allow the compression to the Fourier limit of below 5 fs in the high energy system.

OCIS codes: (190.7110) Ultrafast nonlinear optics; (190.4970) Parametric oscillators and amplifiers; (190.2620) Harmonic generation and mixing; (320.5520) Pulse compression; (190.4975) Parametric processes; (260.7120) Ultrafast phenomena

References and links

1. F. Krausz, and M. Ivanov, "Attosecond physics," Rev. Mod. Phys. **81**(1), 163–234 (2009).
2. G. D. Tsakiris, K. Eidmann, J. Meyer-ter-Vehn, and F. Krausz, "Route to intense single attosecond pulses," N. J. Phys. **8**(1), 19 (2006).
3. T. Tajima, "Laser acceleration and its future," Proc. Jpn. Acad. Ser. B **86**(3), 147–157 (2010).
4. M. Nisoli, S. De Silvestri, and O. Svelto, "Generation of high energy 10 fs pulses by a new pulse compression technique," Appl. Phys. Lett. **68**(20), 2793–2795 (1996).
5. C. P. Hauri, W. Kornelis, F. W. Helbing, A. Heinrich, A. Couairon, A. Mysyrowicz, J. Biegert, and U. Keller, "Generation of intense, carrier-envelope phase-locked few-cycle laser pulses through filamentation," Appl. Phys. B **79**(6), 673–677 (2004).
6. G. M. Gale, M. Cavallari, T. J. Driscoll, and F. Hache, "Sub-20-fs tunable pulses in the visible from an 82-MHz optical parametric oscillator," Opt. Lett. **20**(14), 1562–1564 (1995).
7. T. Wilhelm, J. Piel, and E. Riedle, "Sub-20-fs pulses tunable across the visible from a blue-pumped single-pass noncollinear parametric converter," Opt. Lett. **22**(19), 1494–1496 (1997).
8. A. Baltuška, T. Fuji, and T. Kobayashi, "Visible pulse compression to 4 fs by optical parametric amplification and programmable dispersion control," Opt. Lett. **27**(5), 306–308 (2002).
9. S. Adachi, N. Ishii, T. Kanai, A. Kosuge, J. Itatani, Y. Kobayashi, D. Yoshitomi, K. Torizuka, and S. Watanabe, "5-fs, Multi-mJ, CEP-locked parametric chirped-pulse amplifier pumped by a 450-nm source at 1 kHz," Opt. Express **16**(19), 14341–14352 (2008).
10. I. N. Ross, P. Matousek, M. Towrie, A. J. Langley, and J. L. Collier, "The prospects for ultrashort pulse duration and ultrahigh intensity using optical parametric chirped pulse amplification," Opt. Commun. **144**(1-3), 125–133 (1997).
11. S. Witte, R. T. Zinkstok, A. L. Wolf, W. Hogervorst, W. Ubachs, and K. S. E. Eikema, "A source of 2 terawatt, 2.7 cycle laser pulses based on noncollinear optical parametric chirped pulse amplification," Opt. Express **14**(18), 8168–8177 (2006).
12. D. Herrmann, L. Veisz, R. Tautz, F. Tavella, K. Schmid, V. Pervak, and F. Krausz, "Generation of sub-three-cycle, 16 TW light pulses by using noncollinear optical parametric chirped-pulse amplification," Opt. Lett. **34**(16), 2459–2461 (2009).

#129971 - $15.00 USD Received 10 Jun 2010; revised 6 Aug 2010; accepted 7 Aug 2010; published 18 Aug 2010

13. T. S. Sosnowski, P. B. Stephens, and T. B. Norris, "Production of 30-fs pulses tunable throughout the visible spectral region by a new technique in optical parametric amplification," Opt. Lett. **21**(2), 140–142 (1996).
14. E. Zeromskis, A. Dubietis, G. Tamosauskas, and A. Piskarskas, "Gain bandwidth broadening of the continuum-seeded optical parametric amplifier by use of two pump beams," Opt. Commun. **203**(3-6), 435–440 (2002).
15. D. Herrmann, R. Tautz, F. Tavella, F. Krausz, and L. Veisz, "Investigation of two-beam-pumped noncollinear optical parametric chirped-pulse amplification for the generation of few-cycle light pulses," Opt. Express **18**(5), 4170–4183 (2010).
16. G. Tamošauskas, A. Dubietis, G. Valiulis, and A. Piskarskas, "Optical parametric amplifier pumped by two mutually incoherent laser beams," Appl. Phys. B **91**(2), 305–307 (2008).
17. C. Schriever, S. Lochbrunner, P. Krok, and E. Riedle, "Tunable pulses from below 300 to 970 nm with durations down to 14 fs based on a 2 MHz ytterbium-doped fiber system," Opt. Lett. **33**(2), 192–194 (2008).
18. C. Homann, C. Schriever, P. Baum, and E. Riedle, "Octave wide tunable UV-pumped NOPA: pulses down to 20 fs at 0.5 MHz repetition rate," Opt. Express **16**(8), 5746–5756 (2008).
19. M. Bradler, P. Baum, and E. Riedle, "Femtosecond continuum generation in bulk laser host materials with sub-μJ pump pulses," Appl. Phys. B **97**(3), 561–574 (2009).
20. G. Cerullo, M. Nisoli, S. Stagira, and S. De Silvestri, "Sub-8-fs pulses from an ultrabroadband optical parametric amplifier in the visible," Opt. Lett. **23**(16), 1283–1285 (1998).
21. I. Z. Kozma, P. Baum, U. Schmidhammer, S. Lochbrunner, and E. Riedle, "Compact autocorrelator for the online measurement of tunable 10 femtosecond pulses," Rev. Sci. Instrum. **75**(7), 2323–2327 (2004).
22. P. Baum, S. Lochbrunner, and E. Riedle, "Zero-additional-phase SPIDER: full characterization of visible and sub-20-fs ultraviolet pulses," Opt. Lett. **29**(2), 210–212 (2004).
23. S. Witte, R. T. Zinkstok, W. Hogervorst, and K. S. E. Eikema, "Numerical simulations for performance optimization of a few-cycle terawatt NOPCPA system," Appl. Phys. B **87**(4), 677–684 (2007).
24. A. L. Cavalieri, E. Goulielmakis, B. Horvath, W. Helml, M. Schultze, M. Fiess, V. Pervak, L. Veisz, V. S. Yakovlev, M. Uiberacker, A. Apolonski, F. Krausz, and R. Kienberger, "Intense 1.5-cycle near infrared laser waveforms and their use for the generation of ultra-broadband soft-x-ray harmonic continua," N. J. Phys. **9**(7), 242 (2007).
25. J. Park, J. H. Lee, and C. H. Nam, "Generation of 1.5 cycle 0.3 TW laser pulses using a hollow-fiber pulse compressor," Opt. Lett. **34**(15), 2342–2344 (2009).
26. A. Baltuška, and T. Kobayashi, "Adaptive shaping of two-cycle visible pulses using a flexible mirror," Appl. Phys. B **75**(4-5), 427–443 (2002).
27. I. N. Ross, P. Matousek, G. H. C. New, and K. Osvay, "Analysis and optimization of optical parametric chirped pulse amplification," J. Opt. Soc. Am. B **19**(12), 2945–2956 (2002).
28. A. Renault, D. Z. Kandula, S. Witte, A. L. Wolf, R. Th. Zinkstok, W. Hogervorst, and K. S. E. Eikema, "Phase stability of terawatt-class ultrabroadband parametric amplification," Opt. Lett. **32**(16), 2363–2365 (2007).
29. G. Rodriguez, and A. J. Taylor, "Measurement of cross-phase modulation in optical materials through the direct measurement of the optical phase change," Opt. Lett. **23**(11), 858–860 (1998).
30. G. Krauss, S. Lohss, T. Hanke, A. Sell, S. Eggert, R. Huber, and A. Leitensdorfer, "Synthesis of a single cycle of light with compact erbium-doped fibre technology," Nat. Photonics **4**(1), 33–36 (2010).

1. Introduction

High energy ultrafast light pulses are unique tools for applications ranging from the most fundamental science to medical applications. Quasi-single cycle near infrared pulses can generate single attosecond pulses or even single cycle attosecond pulses in the XUV that allow the measurement of the fastest known processes [1,2]. Even with slightly longer pump pulses highly attractive electron acceleration has been shown that offers a tabletop alternative to large scale facilities used in clinical environments [3].

With known laser materials used in multi-stage optically pumped chirped pulse amplifiers the attainable spectral width is limited by either the intrinsic gain bandwidth or even more severely the spectral gain narrowing in going from nJ broadband seed light to the desired Joule output levels. To overcome these limitations, frequency broadening in either gas filled hollow capillary fibers [4] or in filaments [5] is widely used. So far the use is, however, limited to at most a few mJ.

An attractive alternative for the direct generation of high energy extremely broadband pulses is optical parametric amplification. With a noncollinear geometry and pumping by a frequency-doubled femtosecond Ti:sapphire laser, sub-20 fs visible pulses have indeed been generated at 82 MHz repetition rate [6] and multi-μJ pulses at kHz rates [7]. The concept of the noncollinearly phase-matched optical parametric amplifier (NOPA) was optimized to the generation of 4 fs pulses [8].

Pumping by femtosecond Ti:sapphire pulses limits the attainable output energy, even though extremely short pulses with peak powers of 0.5 TW have been demonstrated [9]. Therefore the use of pico- or even nanosecond pump pulses was suggested in combination

#129971 - $15.00 USD Received 10 Jun 2010; revised 6 Aug 2010; accepted 7 Aug 2010; published 18 Aug 2010

with a chirped pulse strategy (OPCPA) [10]. All known and technically available pump lasers with ps pulse duration operate around 1050 nm due to the laser active materials used, e.g. Nd^+ or Yb^+. The use of such pump lasers has already led to 2 TW pulses [11] and lately sub-8 fs pulses centered at 805 nm with more than 130 mJ (16 TW) compressed energy [12]. A further shortening of the pulses in this spectral region becomes increasingly difficult due to the phase-matching bandwidth of the BBO amplifier medium with one-color pumping.

Already 1996 it was shown that multiple amplification stages with slight spectral detuning of the individual amplification range could lead to significant shortening of the output in a 100 kHz OPA [13]. Pumping of a single stage with multiple pump beams allowed the demonstration of pulse shortening from 98 to 61 fs [14] and lately from 8 to 7 fs with an improved temporal structure [15]. The use of different pump wavelengths was even suggested, yet no spectral nor temporal characterization of the output has been provided [16].

For a MHz Yb-based femtosecond pump system it was shown that both the green 2ω light and the UV 3ω light can be used to pump a NOPA [17,18]. Both configurations easily yield sub-20 fs pulse durations even without optimized compression. Interestingly, the 2ω pumping produces these pulses in the red and the 3ω pumping in the green and yellow part of the spectrum. We therefore suggest the simultaneous use of green and UV pumped stages together with a chirped pulse scheme and high energy pumping. This should allow the generation of pulses with unprecedented shortness and pulse energy.

In this communication we report on two pilot experiments that are aimed on testing this hypothesis. With tens of mJ pumping the generation of nearly octave-spanning few-mJ pulses is achieved. For this effort, techniques have been developed to allow efficient frequency conversion of the 78 ps fundamental pump pulses at 1064 nm. In a second experiment at 100 kHz repetition rate the compressibility and spectral phase behavior of the composite pulses is investigated.

2. NOPCPA on the mJ-level approaching the octave

Figure 1 shows the layout of the experimental two-color-pumped NOPCPA setup. We have extended an existing system (denoted as Light-Wave-Synthesizer-20, Ref. [12]), which generates sub-8 fs, 130-mJ pulses at 805 nm central wavelength and 10 Hz repetition rate.

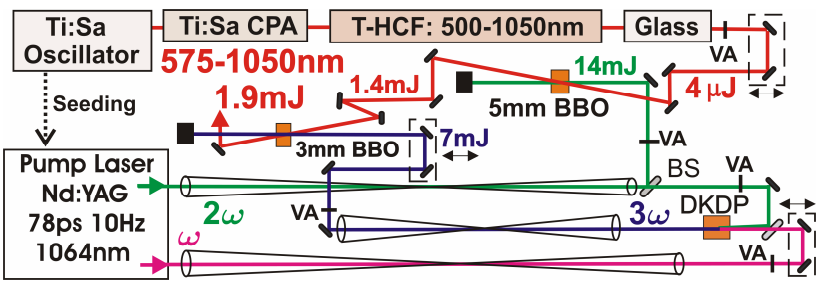

Fig. 1. Layout of the mJ-level two-color-pumped NOPCPA setup, which consists of two cascaded stages employing type-I phase-matching in BBO (T-HCF – tapered hollow-core capillary fiber, VA – variable attenuator, BS – beam splitter). The pump fundamental (1064 nm, ω) and its second- (532 nm, 2ω) and third-harmonic (355 nm, 3ω) are relay-imaged with vacuum telescopes onto the nonlinear optical crystals BBO and DKDP.

The present system consists of a Ti:sapphire master oscillator from which the broadband seed and the pump pulses for the two-stage NOPCPA chain are derived. 60% of the oscillator output is fed into a Ti:sapphire 9-pass chirped-pulse amplifier (Femtopower Compact pro, Femtolasers GmbH), delivering 25-fs, 800-µJ pulses at 1 kHz. After amplification, the pulses are spectrally broadened in a 1 m long tapered hollow-core capillary fiber (T-HCF) filled with neon gas at 2 bar (1500 Torr) absolute pressure, which leads to a seed spectrum ranging from 500 to 1050 nm (30 dB; see Fig. 2). The larger diameter of 500 µm in the first 10 cm together with the small diameter of 200 µm in the main part helps broaden the spectrum by up to

#129971 - $15.00 USD Received 10 Jun 2010; revised 6 Aug 2010; accepted 7 Aug 2010; published 18 Aug 2010

50 nm in the red wing. These pulses are then stretched in time by a variable amount of glass, leading to an adjustable group delay (GD) of the seed spectral boundaries. The seed pulse energy is attenuated to 4 μJ to be comparable with the seed used in Ref. [12].

The remaining 40% of the oscillator output is used to seed the Nd:YAG pump laser (EKSPLA, UAB), providing all-optical synchronization. This pump laser delivers two beams of 78-ps (FWHM), up to 1-J pulses at 1064 nm and 10 Hz repetition rate. Pulses at 532 nm are generated via type-II second-harmonic generation (SHG) of two fundamental 1064 nm beams in a 10 mm long DKDP crystal. The remaining fundamental and a part of the SH are relay-imaged with vacuum telescopes onto a 10 mm long DKDP crystal for type-II sum-frequency generation (SFG). Usually, 6 mJ at 532 nm and 14 mJ at 1064 nm are used to generate 8 mJ pulses of the third-harmonic (TH) at 355 nm. The beam diameters are 5 mm each. A high energy conversion efficiency of 40% and a quantum efficiency of 90% with respect to the SH is observed. The SH and TH pump pulse durations are also approximately 78 ps due to the strong saturation in the conversion.

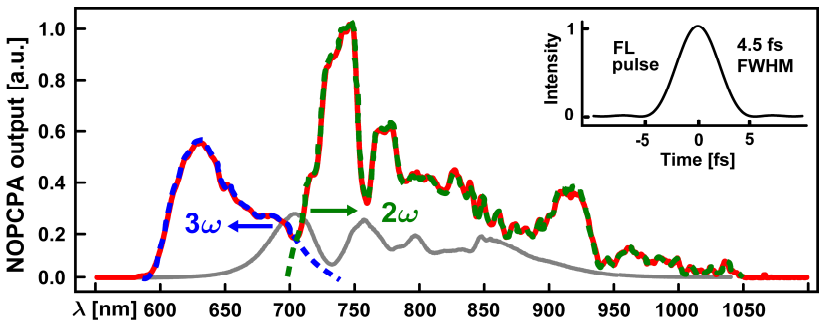

Fig. 2. The spectral energy density of the signal pulse amplified by the second-harmonic and the third-harmonic of the Nd:YAG pump laser (575-1050 nm, red solid curve) allows for a Fourier-limit of 4.5 fs (inset). This spectrum is composed of the spectral region amplified only by the second-harmonic (700-1050 nm, green dotted curve shown as guide to the eye) and the third-harmonic alone (575-740 nm, blue dotted curve). A typical output spectrum of the T-HCF (unamplified seed, not to scale) is shown as gray solid curve.

The first NOPCPA stage (calculated phase-matching angle $\theta = 23.62°$, internal noncollinear angle $\alpha = 2.23°$) consists of a 5 mm long type-I BBO crystal with a slight wedge to avoid adverse effects of internal reflections [9]. It is pumped by 14 mJ of the SH with a 2 mm diameter of the sixth-order super-Gaussian beam and a peak intensity of about 10 GW/cm^2. The second NOPCPA stage ($\theta = 34.58°$, $\alpha = 3.40°$) consists of a 3 mm long type-I BBO crystal and is pumped by 7 mJ of the TH with 1.5 mm diameter and a peak intensity of close to 10 GW/cm^2. Both stages are operated in tangential phase-matching geometry, both pump beams being relay-imaged onto the crystals and being slightly smaller than the seed beam so as to achieve a good spatial signal beam profile. With a group delay of 37 ps for the full seed bandwidth, the seed is amplified from 700 to 1050 nm to an energy of 1.4 mJ in the first stage and further amplified from 575 to 740 nm in the second stage. The particular seed delay was chosen to ensure that the full spectral range of the seed lies within the pump pulse duration. The very high small signal gain of OPCPA allows utilization of the exponentially decreasing seed light at the spectral edges. Overall, an output energy of 1.9 mJ and a spectrum spanning from 575 to 1050 nm is achieved. This nearly octave-wide spectrum supports a Fourier limited pulse of 4.5 fs (see inset in Fig. 2). The results from the seed GD variation are discussed in section 4.1. The positively chirped pulses do not allow the use of the available pulse compressor and hence restrict us to a spectral characterization of the pulses.

3. Proof-of-principle compressibility with high-repetition rate NOPA on the μJ -level

Figure 3 shows the layout for the μJ-level, high-repetition rate NOPA setup. As primary pump laser we use a commercial diode-pumped Yb:KYW disc laser system (JenLas® D2.fs,

#129971 - $15.00 USD Received 10 Jun 2010; revised 6 Aug 2010; accepted 7 Aug 2010; published 18 Aug 2010

Jenoptik AG), delivering 300-fs, 40-μJ pulses at a center wavelength of 1025 nm and a repetition rate of 100 kHz. For generating the seed we split off approximately 1.5 μJ of energy and focus it (all focal lengths are given in Fig. 3) onto a 2 mm thick YAG plate, where a supercontinuum ranging from 470 nm to above 1 μm results [19]. The main part of the pump pulses is focused towards two BBO crystals, where type-I SHG and subsequent type-II SFG are performed in a simple collinear arrangement [18]. In this way we obtain pulses with an energy of 13.5 μJ at the SH and 7.5 μJ at the TH, which are separated by dichroic mirrors and independently collimated with fused silica lenses. The supercontinuum is collimated with a thin fused silica lens and fed into the first NOPA stage ($\theta = 24.0°$, $\alpha = 2.3°$), which consists of a 3 mm long type-I BBO crystal. The first NOPA stage is pumped by the SH, whose energy can be adjusted by a combination of half-wave-plate and polarizer.

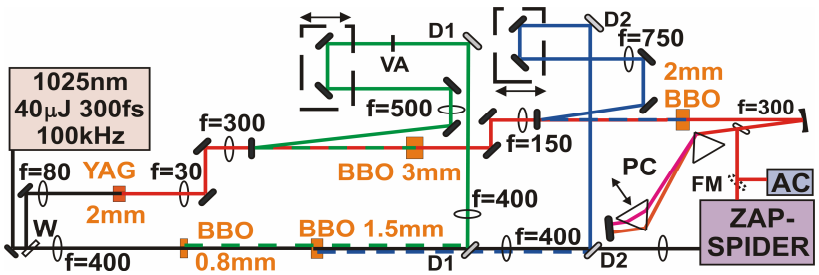

Fig. 3. Layout of the two-color-pumped NOPA setup, which consists of two cascaded stages employing type-I phase-matching in BBO (W - fused silica window, D - dichroic mirror, VA - variable attenuator, PC - prism compressor, FM - flipper mirror, AC - 2nd-order intensity autocorrelator). All focal lengths f are given in mm.

To achieve the necessary pump intensities for a high gain in the NOPA process, focusing of the pump beams and consequently focusing of the seed beams towards the nonlinear crystals is inevitable with this low-energy system, in contrast to the system described above. To achieve a good beam profile with a homogenous spectral distribution after both amplification stages, we find that proper matching of the divergence of pump and seed in both stages is crucial. For this reason we measured the divergence of all relevant beams around the position of the nonlinear crystals with a CCD camera and carefully selected and determined the focal lengths and positions of the respective focusing lenses. The amplified signal of the first stage was then 1:1 relay-imaged onto the BBO crystal (2 mm, type-I) of the second NOPA stage ($\theta = 35.5°$, $\alpha = 2.7°$), which is pumped by the TH.

In each stage special care has to be taken to spatially overlap the amplified signal beam with the respective seed beam, which is not ensured automatically. We have observed, that only in case of the geometry with the pump polarization oriented in the plane defined by seed and pump, spatial overlap of amplified signal and seed can be achieved. Additionally, the BBO crystal had to be set up to Poynting-vector walk-off configuration. We conclude, that the birefringent nature of the BBO crystal and the corresponding pump walk-off can compensate the shift of the amplified signal with respect to the seed direction. In the original design of the NOPA the noncollinear seed pump interaction is arranged in a vertical plane, the polarization of the seed is horizontal and that of the pump vertical [6,7]. Many setups use a horizontal geometry for practical reasons. If the seed is polarized vertical and the pump horizontal in this arrangement, no physical difference originates [8,12,20]. For the horizontal seed polarization and the vertical pump polarization used by us, we explicitly compared the vertical and horizontal pump seed interaction geometry. We found that only for the vertical beam geometry, a proper overlap of seed and signal could be achieved. Slight deviations from the optimum noncollinear and/or phase-matching angle had to be accepted.

We amplify spectral regions from 690 to 830 nm with the second harmonic and from 630 to 715 nm with the third harmonic (Fig. 4(a)). Due to the relatively short pump pulses (estimated to be 220 fs for the SH and 180 fs for the TH) in comparison to the chirped

#129971 - $15.00 USD Received 10 Jun 2010; revised 6 Aug 2010; accepted 7 Aug 2010; published 18 Aug 2010

supercontinuum seed (close to 1 ps), the amplified bandwidth is determined by the temporal overlap of pump and seed. and not the phase-matching bandwidth of the crystals. Variation of only the seed pump delay results in a shift of the spectrum. With a seed energy of 2 nJ, typical output energies are 1 µJ for the first stage when pumped with 9.3 µJ (200 µm diameter, peak intensity of 250 GW/cm^2) and 350 nJ for the second stage when pumped with 6.0 µJ (205 µm diameter, peak intensity of 190 GW/cm^2). The lower efficiency of the second stage is believed to be due to the group velocity mismatch between the UV pump and the visible seed. Both stages operating together typically yield a higher output energy (1.8 µJ) than the sum of the single stages. This is due to the fact that part of the amplified spectrum in the first stage overlaps with the amplification bandwidth of the second stage and therefore acts as a stronger seed than the supercontinuum alone, eventually leading to saturation in the second stage, as is also visible in the signal spectra shown in Fig. 4(a).

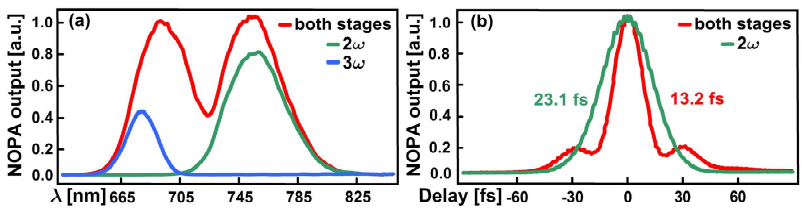

Fig. 4. (a) The spectral energy density of the signal pulse amplified by the SH and the TH of the pump laser (630 – 830 nm, red curve) is composed of the spectral region amplified only by the SH (690 – 830 nm, green curve) and the TH alone (630 – 715 nm, blue curve). These spectra allow for Fourier-limits of 11 fs, 19.7 fs and 28 fs, respectively. The measured spectral energy densities are normalized to the peak of the red curve. The corresponding measured autocorrelation traces with deconvoluted FWHM pulse durations are shown in (b).

After the two amplification stages the output signal is collimated with a spherical mirror and compressed using a sequence of fused silica prisms with an apex angle of 68.7°. Characterization of the pulses is performed online with a dispersion-free autocorrelator that provides direct information in the time domain [21] and alternatively with a ZAP-SPIDER setup that characterizes the pulses in the spectral domain [22]. We use a 30 µm thin BBO crystal for both devices. As auxiliary pulse for the ZAP-SPIDER we use the residual fundamental at 1025 nm after SHG and SFG, which is stretched by transmission through 1270 mm SF57 glass to a FWHM duration of 1.4 ps.

4. Results and discussion

4.1 NOPCPA on the mJ-level approaching the octave

The amplified signal spectrum in case of the mJ-level, cascaded two-color-pumped NOPCPA, which is outlined in section 2, ranges from 575 to 1050 nm with a total confined energy of 1.9 mJ. The pulse has a Fourier-limit of 4.5 fs (FWHM duration, see Fig. 2 inset) and a central wavelength of 782 nm. The spectral boundaries are determined by the effective phase-matching bandwidth shown in Fig. 5(a). The effective phase-mismatch in a BBO crystal of length L is calculated according to Ref. [15] as the sum of crystal-dependent wavevector-mismatch ΔkL and amplification-dependent OPA-phase (Eq. (8) in Ref. [15]). ΔkL leads to a phase-slippage between the pump wave, the seed wave and the idler wave generated in the BBO. The OPA-phase is a phase imprinted on the signal during amplification so as to compensate for the phase-slippage and therefore maintain high gain even in areas of significant ΔkL [15]. A maximum effective phase-mismatch of $\pm\pi$ is acceptable for coherent build-up of the amplified signal in the small-signal gain regime. The compensating effect of the OPA-phase broadens the acceptance bandwidth. In our experiment, the amplified bandwidth in the NOPCPA stage pumped by the SH matches exactly the calculated one shown in Fig. 5(a). In case of the TH-pumped stage, the measured amplified bandwidth is

#129971 - $15.00 USD Received 10 Jun 2010; revised 6 Aug 2010; accepted 7 Aug 2010; published 18 Aug 2010

even slightly broader. This may be because Eq. (8) in Ref. [15] is only valid for low pump depletion.

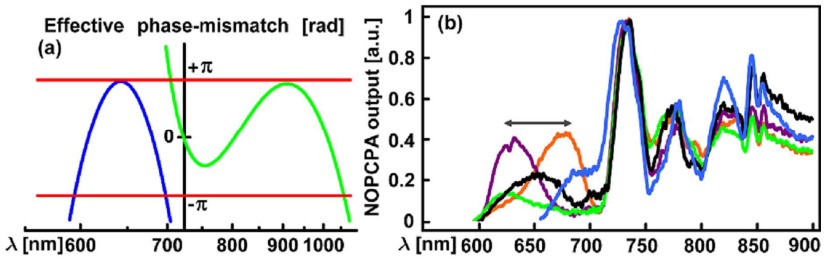

Fig. 5. (a) Effective phase-mismatch as function of seed wavelength including wave-vector-mismatch ΔkL and OPA-phase for the individual NOPCPA stages: $\lambda p = 532$ nm, $\theta = 23.62°$, $\alpha = 2.23°$ (green) and $\lambda p = 354.7$ nm, $\theta = 34.58°$, $\alpha = 3.40°$ (blue). The red horizontal lines label $\pm\pi$. (b) The spectral region below 700 nm is shapeable via adjusting the pump delay and the phase-matching angle (varied colors) in the NOPCPA stage pumped by 3ω.

Figure 5(b) shows a cut-out of signal spectra obtained through amplification by the SH and the TH. A steep spectral edge at around 700 nm leads to satellite pulses in the time domain after almost Fourier-limited compression [12], potentially degrading the temporal pulse contrast on the femtosecond timescale. This can be avoided by spectral shaping of the region below 700 nm via adjusting the pump delay and phase-matching angle in the NOPCPA stage pumped by the TH. Consequently, if one achieves adaptive compression of this octave-spanning pulse close to the Fourier-limit, optimization of the temporal structure of the compressed pulse seems to be possible via spectral shaping in the NOPCPA stages. The spectral structure above 700 nm in the signal spectrum in Fig. 2 is mainly dominated by modulation of the unamplified seed, which is spectrally broadened via self-phase modulation in the tapered hollow-core capillary fiber filled with neon gas.

It has been predicted that the overall pump-to-signal conversion efficiency and the full signal bandwidth of a NOPCPA are functions of group delay of the seed spectral boundaries [23]. Measured results for our cascaded two-color-pumped NOPCPA are summarized in Fig. 6 and represent to our knowledge the first reported measurement. Figure 6 shows that a variation from the seed GD of 37 ps, which is chosen for most of the measurements, can improve the conversion efficiency even further. A GD of (69 ± 2) ps for 575 to 1020 nm leads to the highest overall conversion efficiency of (12.5 ± 1.3)%, while still maintaining the signal bandwidth. The GD for 700 to 1020 nm and for 575 to 740 nm is roughly 33 ps and 43 ps, respectively. In this case, the conversion efficiency is 14.4% and 8.8% in the NOPCPA stages pumped selectively by the SH and the TH, which is the highest conversion efficiency obtained for the SH-pumped stage. In the SH-pumped stage, the pump energy is 16 mJ and the signal energy is 2.3 mJ. For the TH-pumped stage, the corresponding energies are 8 mJ and 0.7 mJ, yielding a total output energy of 3 mJ. Hence, both stages are operated near saturation. At the experimentally verified optimum seed GD, the results show a signal spectrum in the SH-pumped stage similar to that in Ref. [12] but with higher conversion efficiency, although the seed GD for 700 to 1020 nm is similar in both cases. We suspect that this is because we do not use an acousto-optic modulator (Dazzler) in the unamplified seed beam and for this reason observe a spatially and spectrally more homogeneous unamplified seed beam profile in the present experiment.

In general, the temporal overlap between the seed pulse and the 78 ps (FWHM) pump pulse increases with increasing seed GD until the optimum GD is reached. In this range, the conversion efficiency grows and the signal bandwidth stays constant as long as the NOPCPA stage is operated near saturation for most of the seed wavelengths. Otherwise, a decrease in seed intensity because of an enhanced stretching ratio can lead to lower signal bandwidth due to a lack of saturation [23]. Beyond the optimum GD, the seed pulse increasingly experiences the Gaussian temporal shape of the pump pulse, leading to a decrease in signal bandwidth and conversion efficiency.

#129971 - $15.00 USD Received 10 Jun 2010; revised 6 Aug 2010; accepted 7 Aug 2010; published 18 Aug 2010

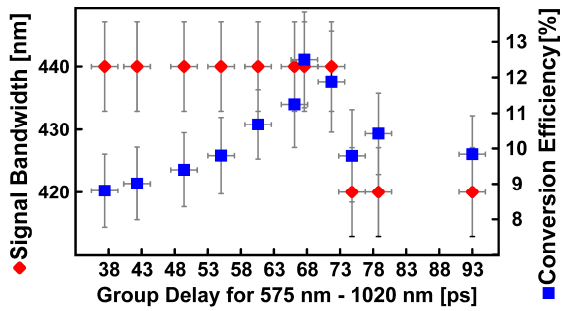

Fig. 6. Measured full signal bandwidth (red diamonds) and the overall pump-to-signal conversion efficiency (blue squares) as function of group delay between the seed spectral boundaries. The optimum group delay is found to be (69 ± 2) ps.

In conclusion, with a proper and precise dispersion management, two-color-pumped NOPCPA with type-I phase-matching in BBO is a promising approach for the generation of sub-two-cycle light pulses on the mJ-level. In this case, the present technique would close the gap between chirped-pulse amplifiers with HCFs (~4 fs, ~1 kHz, ~1 mJ [24,25]) and few-cycle one-color-pumped NOPCPA systems (~8 fs, ~10 Hz, 15-130 mJ [11,12]).

4.2 Proof-of-principle compressibility with high-repetition rate NOPA on the μJ –level

The amplified signal spectrum in case of the μJ-level cascaded two-color-pumped NOPA described in section 3 ranges from 630 to 830 nm with a total confined energy of 1.8 μJ. The spectral overlap is chosen to be similar to that in the mJ-level NOPCPA setup in section 2, with a central wavelength of 740 nm. Figure 4 shows the amplified spectrum and the corresponding measured autocorrelation trace (both in red). With identical prism compressor settings, we measure a FWHM pulse duration of 23.1 fs (Fourier-limit: 19.7 fs) and 95.0 fs (Fourier-limit: 28.0 fs) for the signal pulse amplified only by the SH and only by the TH. The signal pulse amplified in both stages is compressed to 13.2 fs, compared to its Fourier-limit of 11.0 fs. The measurement matches the simulation of our prism compressor and the compressibility is comparable to other experiments employing related prism compressors [20,26].

The prism compressor setting for optimum compression of the signal pulse resulting from amplification in both NOPA stages is also the optimum setting for the signal pulse amplified by the SH alone, in contrast to the signal amplified by the TH alone. To compress the signal amplified in the TH-pumped stage, the second prism of the compressor is further inserted. Consequently, less negative GDD is required if the signal amplified in the TH-pumped stage is to be compressed. During the course of the experiments, a deformable mirror as prism compressor end-mirror was sometimes found to reduce the outer wings of the compressed pulse.

A more detailed understanding can be gained from the determination of the spectral phase of the amplified pulse. Figure 7(a) shows the result of a ZAP-SPIDER [22] measurement for a particular pulse with a total amplified range of 615 to 780 nm. Figure 7(b) shows the amplified and compressed pulses calculated from the measured spectral intensity and phase given in Fig. 7(a). The FWHM pulse durations determined in this way are close to the results obtained with autocorrelation measurements of the same pulses.

The compressibility is determined by three factors. First, the bandwidth, whose phase can be managed throughout the present dispersive bulk materials (YAG and BBO crystals, fused silica lenses) and the fused silica prism-compressor, is limited. In case of the optimum compressor setting for the investigated spectral region a nearly vanishing spectral phase over a wide range results. The GD as a function of the signal wavelength shows a maximum around 710 nm, which limits the bandwidth of the compressed pulse. Furthermore, the third-order dispersion (TOD) due to the dispersive components leads to satellite pulses after compression.

#129971 - $15.00 USD Received 10 Jun 2010; revised 6 Aug 2010; accepted 7 Aug 2010; published 18 Aug 2010

These limitations mean that the spectral components below 660 nm and above 800 nm occur in the wings of the compressed pulse for the case of Fig. 4. This is responsible for the observation of the long pulse durations seen when the signal is amplified only by the TH. Nevertheless, the TH-pumped stage amplifies spectral components not amplified in the SH-pumped stage and whose phase can still be managed in our case using the prism compressor. For this reason, a shorter pulse duration is achieved in case of amplification in both NOPA stages compared to using only the SH-pumped stage, for the same prism compressor settings.

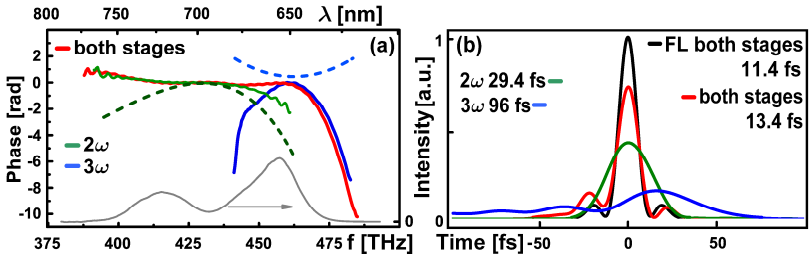

Fig. 7. (a) Spectral phase of the compressed signal pulses retrieved by the ZAP-SPIDER measurement. Solid red curve: amplification by the SH and TH of the pump laser, solid green: amplification only by the SH, solid blue: amplification only by the TH; all for identical settings of the compressor. For comparison the calculated OPA-phase for the two stages is shown with dashed lines. The solid grey curve shows the spectral energy density of the signal. Taking the measured spectral phase, spectral intensity and pulse energy leads to the retrieved pulses shown in (b) with their FWHM pulse duration.

Second, the phase imprinted on the signal to compensate for phase-mismatch and to maintain high gain (OPA-phase) comes into play [27]. As mentioned in subsection 4.1 and outlined in Ref. [15] and Ref. [28], this phase contribution affects ultra-broadband optical parametric amplification. Employing Eq. (8) of Ref. [15] for the case of small depletion, these phase contributions due to amplification in the TH-pumped and the SH-pumped NOPA stages are shown as dashed lines in Fig. 7(a) for the experimentally determined parameters like crystal angles and the pump intensities. One can see that the phase contributions have opposite signs. A positive linear chirp defined in the time domain leads to a parabola with a negative second derivative in the frequency domain via Fourier-transformation. In contrast to the SH-pumped NOPA stage, the phase imprinted on the signal during parametric amplification by the TH shows negative group delay dispersion (GDD). This matches our observation that less negative GDD was required with the prism compressor when the signal pulse was amplified by the TH alone. Moreover, these two phase contributions partially compensate each other and therefore lead to an extended region of reduced residual phase around the spectral overlap.

To experimentally verify this phase effect, we adjusted both NOPA stages to similar amplified spectra centered at 670 nm (different from the pulses previously described) and subsequently compressed the signal pulse amplified by each stage separately with the same prism compressor spacing. These compressed pulses were characterized with the autocorrelator. It was found that for optimum compression of the signal pulse amplified in the TH-pumped NOPA stage, the second prism in the compressor was inserted by about 2 mm more compared to the signal amplified in the SH-pumped stage. This implies that the prism compressor applies less negative GDD to the signal pulse, which matches the signs of the OPA-phase contributions due to parametric amplification shown in Fig. 7(a).

Note that the residual phase of the compressed signal pulse amplified by the SH or the TH alone is different from the residual phases of the corresponding spectral regions in case of amplification in both NOPA stages. Apart from the compensating effect of the phase-contribution due to parametric amplification in the region of spectral overlap, this occurs because Eq. (8) in Ref. [15] is strictly speaking only valid for the case of low pump depletion (i.e. negligible saturation). This observation has the consequence that the two amplification stages and the pulse compression can only be optimized simultaneously.

#129971 - $15.00 USD Received 10 Jun 2010; revised 6 Aug 2010; accepted 7 Aug 2010; published 18 Aug 2010

Third, cross-phase modulation (XPM), which is possible in optical parametric amplification as a result of the high pump intensities, would lead to positive GDD [29]. According to Ref. [29], we calculate the B-integral due to XPM in our NOPA stages to be 1.4 rad in the SH-pumped and 0.8 rad in the TH-pumped stages. This is comparable to the value found in the investigation of XPM [29]. Since the B-integral of the SH-pumped stage is approximately twice as high as that of the TH-pumped stage, a higher additional positive GDD can be present in the SH-pumped stage. This is consistent with our observations.

In conclusion, cascaded two-color-pumped NOPA with type-I phase-matching in BBO is also a promising approach for the generation of sub-two-cycle light pulses on the μJ-level in high-repetition rate NOPA systems.

5. Conclusion and perspectives

In this work results from two novel experimental setups were analyzed to investigate the feasibility of two-color pumping of a NOPCPA for the generation of high energy pulses approaching the single cycle regime. At low repetition rates, 3 mJ pulses with a nearly octave wide spectrum were demonstrated in a first double-stage arrangement. At 100 kHz repetition rate and μJ output energies the spectral phase and compressibility was studied. The two-color scheme exhibits a slowly and continuously varying spectral phase that should be well compensatable with existing compression schemes. The addition of the visible part of the pulse spectrum by the 3ω-pumping indeed shortens the pulse by nearly a factor of two without any change to the prism compressor. We conclude from the combination of results that the concept of two-color pumping can be expanded to multiple stages. Proper care has to be taken in the design and alignment to utilize the full available pump energy. Pulses approaching a J energy and a duration around 5 fs seem on the horizon. While sub-5s pulses were previously reported with 400 nm Ti:sapphire based pumping, this range is now reachable with the 1050 nm pump lasers of much higher energy.

Various challenges have to be resolved to achieve these ambitious goals. Already in the present experiments matching of the wavefront and beam pointing of the two contributions to the composite pulses needed high attention. We suspect that the birefringent nature of the amplifier crystals, possible inhomogeneities in the material, partial depletion of the pump and associated spatially-dependent OPA phase and classically neglected higher-order nonlinear interactions are the main causes of this situation. The OPA phase will depend selectively on the pump color, the degree of saturation and therefore on the OPA's location within an extended amplifier chain, and on the particular phase-matching adjustment of a selected crystal. Therefore an adaptive phase-correction will most likely be desirable for routine operation. An acousto-optic programmable dispersive filter with sufficient bandwidth is already available. Last but not least, the correct stretching ratio of seed and pump for the optimum balance of bandwidth, compressibility and overall efficiency is of high importance. For all these issues the present report provides a first basis.

Two-color pumping potentially allows more efficient usage of the available pump energy. Only for the short wavelength part of the output spectrum are the "expensive" short wavelength pump photons used, while the red part of the spectrum is amplified with the help of the remaining green pump light. Already now the generation of the UV pump utilizes the fundamental pump pulses twice. In future extensions of the concept one could even think of adding another amplifier stage pumped by the residual pump fundamental to widen the spectrum in the near infrared and to add even more energy.

It is interesting to compare the optical principles underlying the present approach for the generation of extremely broadband pulses with other methods of light wave synthesis. Recently it was demonstrated that interferometric spatial addition of phase-locked pulses generated at neighboring wavelength ranges in a fiber-based MHz system leads to single cycle near-infrared pulses [30]. This approach of individual amplification and dedicated compression of the spectral parts allows for more flexibility. On the other hand, the spatially and temporally stable overlap of the contributions, without adverse effects from inhomogeneities in scaling to high pulse energies and consequently large beam sizes, might be

#129971 - $15.00 USD Received 10 Jun 2010; revised 6 Aug 2010; accepted 7 Aug 2010; published 18 Aug 2010

critical. In our approach a common seed and beam path is used and could eventually be more practical.

The motivation for our work was the high energy, low repetition rate regime. In the course of the work we realized that two- or even multiple color pumping for the extension of the output spectrum is also feasible at 100 kHz repetition rates. This might provide interesting sources for spectroscopic investigations of samples in the condensed phase that require only low pulse energies. It is certain that the concept can close existing gaps between Ti:sapphire based systems with hollow-core capillary-fiber compression (~4 fs, ~750 nm, ~1 mJ, ~1 kHz [24,25]) and 8 fs, 800 nm, 10 Hz, 15-130 mJ NOPCPA systems [11,12].

Acknowledgements

This work was supported by Deutsche Forschungsgemeinschaft (contract TR18), the association EURATOM-Max-Planck-Institut für Plasmaphysik, the Cluster of Excellence Munich-Centre for Advanced Photonics (MAP) and by the Austrian Science Fund within the Special Research Program F16 (Advanced Light Sources). We acknowledge support by the cooperation with the King-Saud-University. D. H. is grateful to the Studienstiftung des deutschen Volkes. The International Max Planck Research School on Advanced Photon Science (C. H.) is gratefully acknowledged. The authors thank N. Krebs for valuable support during the SPIDER measurements.

#129971 - $15.00 USD Received 10 Jun 2010; revised 6 Aug 2010; accepted 7 Aug 2010; published 18 Aug 2010

Appendix A3

Approaching the Full Octave: Noncollinear Optical Parametric Chirped Pulse Amplification with Two-Color Pumping

C. Homann, D. Herrmann, R. Tautz, L. Veisz, F. Krausz, and E. Riedle

Ultrafast Phenomena XVII
M. Chergui, D. Jonas, E. Riedle, R.W. Schoenlein, A. Taylor, eds.
(Oxford University Press, Inc., New York 2011), 691 - 693

Approaching the Full Octave: Noncollinear Optical Parametric Chirped Pulse Amplification with Two-Color Pumping

Christian Homann[1], Daniel Herrmann[1,2], Raphael Tautz[2,3], Laszlo Veisz[2], Ferenc Krausz[2,4], and Eberhard Riedle[1]

[1] LS für BioMolekulare Optik, Ludwig-Maximilians-Universität, München, Germany
E-mail: christian.homann@physik.uni-muenchen.de
[2] Max-Planck-Institut für Quantenoptik, Garching, Germany
[3] LS für Photonik und Optoelektronik, Ludwig-Maximilians-Univ., München, Germany
[4] LS für Laserphysik, Ludwig-Maximilians-Universität, Garching, Germany

Two-color pumping as a novel technique for high-power few-cycle light pulses. Multiterawatt few-cycle light pulses are of high interest for numerous applications in high-field science like the generation of surface high-harmonic radiation or laser-based particle acceleration. Noncollinear optical parametric chirped pulse amplification (NOPCPA) provides a powerful method to generate such pulses because of its broad amplification bandwidth and high single pass gain. Current state of the art systems are mainly based on Nd:YAG pump lasers and BBO as amplifying crystal, and are capable of generating pulses down to 7.9 fs duration with energies of up to 130 mJ and spanning a spectral region from 700 – 1000 nm [1]. A further reduction of the pulse duration is not limited by the seed spectrum (500 – 1000 nm), but by the amplification bandwidth of BBO when pumping with the second-harmonic (532 nm) of Nd:YAG lasers. A possible solution for broader amplified spectra is to use other amplification crystals with broader gain spectra (e.g. DKDP), however they typically have much lower effective nonlinearities and lower damage threshold and therefore much lower conversion efficiencies than BBO.

Here we present the use of two different pump wavelengths with neighboring optimal spectral amplification regions for subsequent stages of a NOPCPA chain to achieve a much broader overall amplified bandwidth. By pumping the first stage by the second-harmonic (532 nm), and the second stage by the third-harmonic (355 nm) of a Nd:YAG pump laser, we achieve an overall amplification from 580 – 1000 nm with mJ energy. This allows for a Fourier-limited pulse duration below 5 fs. However, since stretcher and compressor of the used system are not yet capable of dealing with such a broad bandwidth, we have not been able to compress the whole spectrum yet. To test if potential problems like phase discontinuities arise in the spectral overlap region, we performed a proof-of-principle experiment with a low-power laser system of similar fundamental wavelength (1025 nm). We amplified a spectral region from 610 – 670 nm with the third-harmonic and a spectral region from 650 – 760 nm with the second-harmonic of the pump laser. We show that we can compress the composed spectrum to 13 fs by the use of a prism sequence only, close to its Fourier-limit of 11 fs, and considerably shorter than the single signal spectra of either stage permit. This proofs that we have a smooth spectral phase in the overlap region. This work [2] therefore opens up the route to a 5 fs multi-mJ NOPCPA system.

Extremely broadband amplification in the mJ regime. To show the potential of two-color pumping for high-power few-cycle pulse generation, we extended and modified part of the light wave synthesizer LWS-20 [1]. The system consists of a Ti:Sa master oscillator from which the seed and pump pulses for the NOPCPA chain are derived. For the seed, part of the oscillator output is amplified in a 9-pass Ti:Sa multipass amplifier, delivering 25 fs, 800 μJ pulses at 1 kHz. These pulses are broadened in a hollow-core fiber filled with neon at an absolute pressure of 2 bar to a spectrum covering 500 – 1000 nm. The pulses are stretched in 105 mm SF57 glass to roughly match the associated pump pulse durations, leading to a group delay of about 16 ps in the spectral range of 580 – 700 nm. We also attenuate the seed to a pulse energy of 4.5 μJ with neutral density filters, to simulate the expected pulse energy when a more complex stretcher consisting of a combination of grisms and an acousto-optic modulator is used, which will be necessary for a dispersion management allowing full compression of the generated spectra.

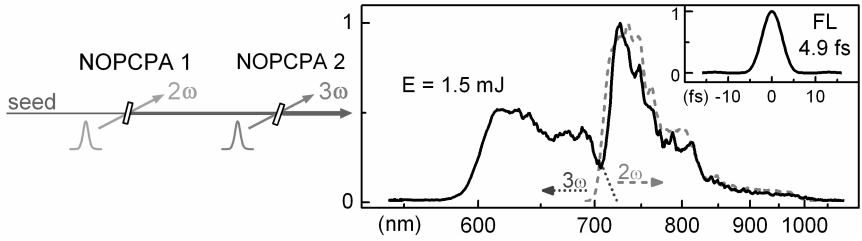

Fig. 1. By pumping the first stage of a NOPCPA chain by the second-harmonic of the Nd:YAG pump laser and the second stage by the third-harmonic, we can amplify a much broader spectral region (580 – 1000 nm, solid curve) than with one pump color alone (532 nm pump, dashed curve), allowing for Fourier-limits below 5 fs (inset).

To generate synchronized pump pulses, the remaining part of the oscillator output is soliton-shifted to 1064 nm in a photonic crystal fiber and seeds a Nd:YAG based regenerative and multipass amplifier chain. It delivers, after frequency doubling in DKDP, up to 1 J, 78 ps pulses at 532 nm with a repetition rate of 10 Hz. To generate the third-harmonic at 355 nm, we split off 4.5 mJ of the 532 nm beam and perform collinear type II sum-frequency mixing with 10 mJ of the remaining 1064 nm light in a 10 mm thick DKDP crystal. In that way we achieve 6.3 mJ at 355 nm implying a very high total energy conversion efficiency above 40%.

For the first NOPCPA stage 14 mJ of the 532 nm beam are split off and relay imaged via telescopes onto a 5 mm long type-I BBO crystal, cut at 24°. With an internal noncollinear angle of 2.2° we achieve broadband amplification of our seed from 700 – 1000 nm (dashed curve in Fig. 1) with an energy of 1.2 mJ. The output signal of this stage is then further amplified in a second NOPCPA stage pumped by the third-harmonic in a 3 mm long BBO crystal, cut at 32.5°. With a noncollinearity angle of 3.4°, we amplify a spectral region from 580 – 720 nm, which neatly connects to the amplified spectrum of the first stage (solid curve in Fig.1). The resulting pulses have a total energy of 1.5 mJ, a spectral range of 580 – 1000 nm, and a Fourier-limit of sub 5 fs.

Compressibility of composite spectra. Pulse compression with the described system has not yet been possible, because the existing stretcher/compressor setup does not support the whole amplified spectrum. Compression of the single spectra of the 2ω pumped stage is already shown [1], and accordingly no difficulties are expected for the 3ω pumped stage alone. Interesting is the spectral overlap region and the question if phase discontinuities arise, e.g., through different OPA phases in the two stages due to the different pump wavelengths.

To test this, we performed a closely related experiment with a commercial Yb-based pump laser system, delivering 300 fs, 40 µJ pulses at a center wavelength of 1025 nm and a repetition rate of 100 kHz. We built two subsequent BBO based noncollinear OPA stages pumped by the second and third-harmonic of the pump laser. As seed light we used a supercontinuum generated in a 2 mm thick YAG plate. We amplified spectral regions from 650 – 760 nm with the second-harmonic and from 610 – 670 nm with the third-harmonic (see Fig.2). Special care had to be taken to spatially overlap the output of the two stages, which was not ensured automatically. The pulses were then compressed in a fused silica prism compressor and the output characterized by a dispersion free autocorrelator and a ZAP-SPIDER setup. With the identical compressor setting we measure a pulse duration of 24 fs for the signal pulse amplified by the 2ω pumped stage alone and a duration of 95 fs for the 3ω pumped stage. Both stages together render a pulse duration of 13 fs, close to the Fourier-limit of the complete spectrum of 11 fs.

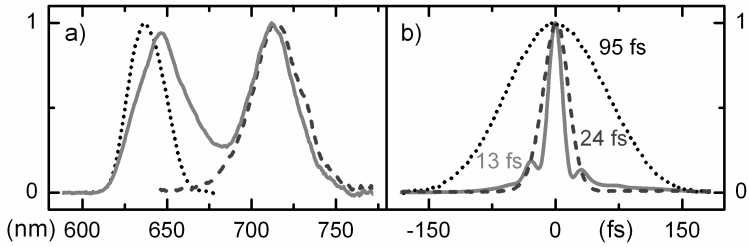

Fig. 2. Normalized amplified signal spectra (a) and autocorrelation traces (b) of the 2ω pumped NOPA stage (dashed), the 3ω pumped stage (dotted) and of both stages operating together (solid).

This demonstrates that no phase discontinuities arise in the spectral overlap region and that our concept is promising for delivering high-energy, few-cycle pulses with previously not reached parameters. Further realizations of our pumping concept can be envisioned, as for example combined ω and 2ω pumping for broadband amplification in the near-infrared spectral region.

1 D. Herrmann, L. Veisz, R. Tautz, F. Tavella, K. Schmid, V. Pervak, and F. Krausz, Opt. Lett. **34**, 2459 - 2461 (2009).

2 D. Herrmann, C. Homann, R. Tautz, M. Scharrer, P. St.J. Russell, F. Krausz, L. Veisz, and E. Riedle, Opt. Express **18**, 18752 - 18762 (2010).

Appendix A4

Mid-IR femtosecond pulse generation on the microjoule level up to 5 µm at high repetition rates

M. Bradler, C. Homann, and E. Riedle

Opt. Lett. **36**, 4212 - 4214 (2011)

Mid-IR femtosecond pulse generation on the microjoule level up to 5 μm at high repetition rates

Maximilian Bradler,* Christian Homann, and Eberhard Riedle

LS für BioMolekulare Optik, Ludwig-Maximilians-Universität München, Oettingenstrasse 67, 80538 Munich, Germany
**Corresponding author: maximilian.bradler@physik.lmu.de*

Received August 11, 2011; accepted September 7, 2011;
posted September 14, 2011 (Doc. ID 152672); published October 25, 2011

We show efficient generation of mid-IR pulses tunable between 1 and 5 μm from 100 kHz class femtosecond systems. The concept can be applied to various sources, particularly based on Ti:sapphire and the newly evolving Yb^+ lasers. The mid-IR pulses are generated as the idler of a collinear optical parametric amplifier pumped by the laser fundamental. The seed for this amplifier is the idler of a previous amplification stage pumped with the second harmonic and seeded with a visible continuum. This enhances the energy and allows us to influence the bandwidth of the final output. Pulses with microjoule energy and Fourier limits of 50 fs are achieved.

OCIS codes: 190.4970, 190.7110, 320.7130.

Femtosecond tunable mid-IR (MIR) pulses are a powerful tool to study ultrafast processes in physics, chemistry, and biology. Time resolved vibrational spectroscopy, carrier dynamics in monolayer graphene, high harmonic generation, and tunneling ionization are interesting research fields that benefit from studies with IR pulses. In most of these experiments weak signals slightly above the detection limit are measured. To achieve a good signal to noise ratio, high repetition rates are needed. Successful approaches generating tunable femtosecond MIR pulses at high repetition rates were already reported in the mid-90s [1–5]. They were based on optical parametric oscillators and amplifiers, as well as difference frequency generation (DFG). Current work extends these concepts by chirped pulse amplification [6,7] and the use of poled lithium niobate crystals [8,9]. A promising approach for higher efficiencies, especially for long wavelengths, is preamplification of the seed by the frequency doubled light [10–14]. However, the generation of ultrashort IR pulses at high repetition rates is still a challenging task. Up to now all approaches either have a complex setup, need synchronized lasers, show limited tunability, or have modest efficiencies or pulse energies.

In this Letter we present a novel concept for efficient and freely tunable MIR femtosecond pulse generation on the microjoule level with a compact setup based on a single laser source. No additional seed or pump lasers are needed, and pulses out to 5 μm are generated without an extra DFG stage. We solely use continuum generation and optical parametric amplification (OPA). Since these processes are not restricted to specific wavelengths, the concept can be applied to a variety of laser systems. Here we show the performance for a Ti:sapphire based system (RegA 9050; Coherent Inc.) that delivers 50 fs pulses at 800 nm with an energy of 5.7 μJ at 93 kHz repetition rate and for a Yb:KYW based system (Jenlas D2.fs; JENOPTIK Laser GmbH) delivering 300 fs pulses at 1025 nm with an energy of 40 μJ at 100 kHz.

Our concept is illustrated in Fig. 1(a). About 5% of the pump light is split off for supercontinuum generation (SCG) in YAG [15]; the main part is used for second harmonic generation (SHG). The SHG light pumps a first collinear OPA (pre-OPA) seeded by the visible part of the YAG continuum. The near-IR (NIR) idler of this pre-OPA is used to seed a second collinear amplifier (IR-OPA) pumped by the remaining fundamental light from the SHG. The collinear geometry in the IR-OPA allows use of the NIR signal and the MIR idler that is predicted to be passively carrier envelope phase stabilized [13,14]. Figure 1(b) shows the wavelength regions for the different stages: visible and NIR light in the pre-OPA (green), as well as NIR and MIR light in the IR-OPA (orange). Figure 1(c) shows spectra from the IR-OPA for the Ti:sapphire laser system and lithium niobate ($LiNbO_3$, orange) as an active medium. Spectra obtained with lithium iodate ($LiIO_3$) at 1 kHz are shown in black. The gray area indicates the absorption of air.

SHG pumped preamplification has two main advantages that are apparent when the desired MIR output is considered. Since there is no continuum seed available in the MIR, the IR-OPA has to be seeded in the NIR. For a wide MIR tunability, continuously tunable NIR light is needed. For the upcoming generation of pump lasers with high repetition rates and high average power, pulse

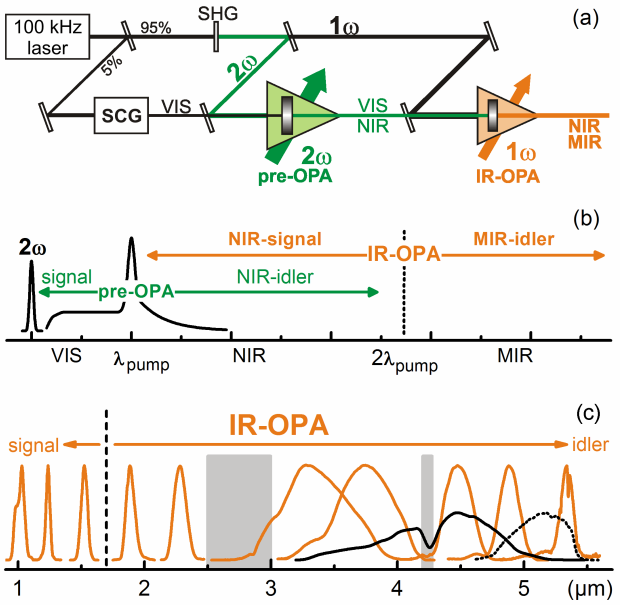

Fig. 1. (a) Scheme of the setup, (b) different wavelength regions involved in the individual amplification stages, (c) typical MIR spectra when applying the concept to a Ti:sapphire system.

durations of 300 fs and longer are typical, and hence octave spanning spectra are only possible by continuum generation in solids [15]. Even these continua show an exponential dropoff on the red side of the pump and therefore only provide a weak NIR seed. However, they show smooth, flat, and gap free spectra in the visible that are well suited to seed an OPA. Therefore we amplify this part of the continuum in the pre-OPA, which is only possible with SHG pumping. The signal of this pre-OPA is in the visible, but the idler is in the desired NIR region and can seed the IR-OPA well.

The second advantage can be seen if the parametric gain G (ratio between signal and seed intensity) is considered as given by the following equation [4]:

$$G = \frac{1}{4}\exp\left(2 \cdot L \cdot \sqrt{\frac{8\pi^2 \cdot d_{\text{eff}}^2 \cdot I_p}{n_p \cdot n_s \cdot n_i \cdot \lambda_s \cdot \lambda_i \cdot \varepsilon_0 \cdot c_0}}\right). \quad (1)$$

I_p is the pump intensity, L the crystal length, d_{eff} the nonlinear coefficient, n_p, n_s, and n_i the refractive indices for pump, signal, and idler, respectively, λ_s and λ_i the signal and idler wavelengths, respectively, ε_0 the vacuum permittivity, and c_0 the speed of light. Bringing the picojoules per nanometer level of an NIR seed [15] over a 100 nm bandwidth to the desired microjoule level affords a gain of 10,000. Using only one amplification stage would necessitate pump intensities of 400 GW/cm^2 or more, even for $LiNbO_3$ with its high $d_{\text{eff}} = 4.04\,\text{pm/V}$ ($\lambda_s = 1.35$ μm, $\lambda_i = 4.2\,\mu$m, $L = 1$ mm effective [see Fig. 2(c)]; the refractive indices are about 2.3). Such high intensities are well in the continuum generation regime and close to the damage threshold. Therefore, multiple amplification stages are necessary (pre-OPA and IR-OPA). Because of the desired MIR output, the final amplifier must be pumped by the fundamental, and to ensure high output energies, it should be pumped with the main part of the available pump energy. In principle, SHG and fundamental pumping are possible in the pre-OPA, because only NIR seed light must be provided for the IR-OPA. Note that SHG pumping causes no loss of pump energy compared to fundamental pumping, because SHG efficiencies of up to 40% are achieved and the remaining fundamental light is used to pump the IR-OPA.

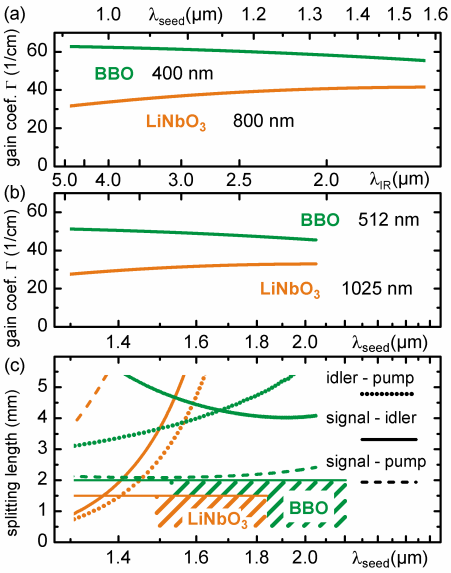

Fig. 2. Wavelength dependence of the gain coefficient in the pre-OPA for (a) BBO pumped by 400 nm, $LiNbO_3$ pumped by 800 nm, and (b) BBO pumped by 512 nm, $LiNbO_3$ pumped by 1025 nm. The scale between (a) and (b) shows the final IR output wavelength. (c) Pulse splitting length of the various wave combinations and crystals for the 1025 nm pump system.

To clarify the advantage of SHG pumping in the pre-OPA, we compare beta barium borate (BBO) pumped by the SHG with $LiNbO_3$ pumped by the fundamental at a pump intensity of 100 GW/cm^2. Fundamental pumping in BBO is not possible due to the idler absorption, and SHG pumping in $LiNbO_3$ causes two photon absorption. The wavelength dependence of the gain coefficient Γ [square root in Eq. (1)] is shown in Fig. 2(a) for a Ti:sapphire system and in 2(b) for a Yb^+ system. Throughout the NIR range (λ_{seed}) needed for MIR pulses out to 5 μm [see scale between Figs. 2(a) and 2(b)], Γ is much larger for the SHG pumped BBO than for the fundamental pumped $LiNbO_3$. The main reason for a higher gain coefficient for SHG pumping is the reduced product of signal and idler wavelength. The higher nonlinear coefficient of $LiNbO_3$ is cancelled by the lower refractive index of BBO. The pulse splitting lengths that limit the useful crystal length are given in Fig. 2(c) for the 1025 nm system. For the BBO crystal all lengths are above the 2 mm length used; for $LiNbO_3$ the range of λ_{seed} needed for MIR pulses in the interesting range of 3.5 to 5 μm results in significantly shorter splitting lengths. This would lead to a reduced amplification, since the gain in the small signal limit depends exponentially on this effective length. These two issues allow gain factors of 1000 in an SHG pumped pre-OPA even with moderate pump intensities, so that only a modest gain of around 10 is necessary for the IR-OPA, again achievable with intensities far below continuum generation or crystal damage. Thus SHG pumped preamplification allows high IR output with pump intensities below 100 GW/cm^2.

As amplifier material for the IR-OPA, we use $LiNbO_3$ because of its high d_{eff} in the MIR, where BBO is not transparent, and the high damage threshold. Since our concept demands only moderate pump intensities, even the use of $LiIO_3$ with its low damage threshold [12,13] was possible [see Fig. 1(c)]. The spectral width of close to 2 μm is due to the favorable acceptance bandwidth of $LiIO_3$ beyond 3 μm. The concept will also work for other typical IR crystals like potassium niobate ($KNbO_3$) or potassium titanyl phosphate (KTP) [16].

A potential challenge is that the seed for the IR-OPA is the idler of the pre-OPA and not a flat continuum. The bandwidth of this idler can easily be larger than the bandwidth supported by the IR-OPA. This means that not all NIR photons contribute to the IR amplification. To use all seed photons, the NIR bandwidth must be matched to the IR-OPA. This is done by chirping the visible seed continuum in the pre-OPA by inserting glass. Now the temporal overlap between seed and pump limits the bandwidth of the pre-OPA, and the bandwidth of the amplified signal (and hence the idler) can be controlled. We find no significant loss of NIR energy due to the seed chirp. Idler spectra of the pre-OPA when using different glasses in the visible seed are shown in Fig. 3(a) for the Yb:KYW pump. The gray area shows the bandwidth

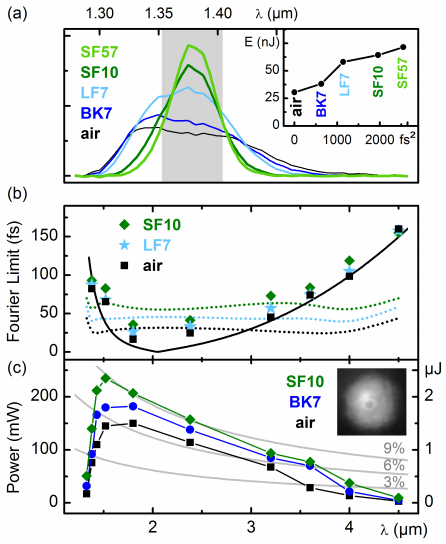

Fig. 3. (a) Idler spectra of 512 nm-pumped pre-OPA with chirped seed continuum. Gray area: bandwidth supported by IR-OPA; inset: energy contained in this area. (b) Fourier limits (symbols) for IR-OPA. Black curve: acceptance bandwidth for $LiNbO_3$; dotted curves: bandwidths of seed pulses. (c) Output power of MIR pulses with overall efficiencies.

supported in the IR-OPA for a 1.5 mm thick $LiNbO_3$ crystal. The inset shows the energy of the pre-OPA contained in this bandwidth. If the idler is narrower than this bandwidth, the MIR output inherits the bandwidth of the NIR seed. Nevertheless, the energy of the MIR output does not suffer, because all seed photons are amplified.

Figure 3(b) shows the Fourier limits and 3(c) the average output power of the MIR pulses for the chirped visible seed. Limits below 50 fs can be achieved over a wide tuning range with a power above 200 mW in the maximum and 50 mW at 4 μm. The maximum output energy with the shortest possible Fourier limit is reached if the bandwidth of the idler of the pre-OPA [dotted curves in Fig. 3(b)] matches the bandwidth supported by amplification in $LiNbO_3$ [black curve in Fig. 3(b)]. In this configuration the output energy increased by a factor of up to 2.6 with a constant Fourier limit.

With the Ti:sapphire system pulses from 1 to 5 μm with energy up to 420 nJ at 1.1 μm and 110 nJ at 3.4 μm with a Fourier limit of 27 fs are demonstrated. At 3.4 μm this corresponds to an overall energy conversion efficiency of 2.0%, i.e., up to 8.2% of the 800 nm photons are converted to IR photons. To show the energy scalability of our concept, we apply it to a 1 kHz Ti:sapphire system (CPA 2001; Clark MXR Inc.) that provides 150 fs pulses at 775 nm. Pulses of 250 μJ are used to operate the OPA. Again pulses tunable from 1 to 5 μm with energies of up to 8 μJ at 3.5 μm with measured pulse durations down to 38 fs are obtained. The low repetition rate allows us to measure the shot to shot stability. Typical values vary from 1% to 2% rms for the entire range. An IR beam profile was recorded [see inset of Fig. 3(c)].

In summary, we have shown ultrafast femtosecond MIR pulse generation at 100 kHz repetition rates based on continuum generation and optical parametric amplification. The compact setup with a footprint of below 1 m^2 operating with a single turn-key pump laser allows stable and reliable day to day operation. The wide tunability from one to 5 μm is only limited by the available amplifier material. Essential is the strong preamplifier pumped by the frequency doubled laser output, which allows use of the flat plateau of the visible continuum, matches the bandwidth to the IR-OPA, and enables high IR output with a modest gain in the IR-OPA pumped by the remaining fundamental. Our method will hopefully help to simplify actual approaches and benefit a new field of spectroscopic experiments due to the wide tuning range and the adjustable bandwidth.

We thank M. Breuer, C. Elsner, M. Betz, and D. J. Nesbitt for pilot investigations, the Deutsche Forschungsgemeinschaft (DFG) through the Cluster of Excellence: Munich-Centre for Advanced Photonics for financial support, and Horiba Jobin Yvon GmbH and JENOPTIK Laser GmbH for technical assistance.

References

1. A. Lohner, P. Kruck, and W. W. Rühle, Appl. Phys. B **59**, 211 (1994).
2. U. Emmerichs, H. J. Bakker, and H. Kurz, Opt. Commun. **111**, 497 (1994).
3. G. R. Holtom, R. A. Crowell, and X. S. Xie, J. Opt. Soc. Am. B **12**, 1723 (1995).
4. M. K. Reed, M. K. Steiner-Shepard, M. S. Armas, and D. K. Negus, J. Opt. Soc. Am. B **12**, 2229 (1995).
5. B. Golubovic and M. K. Reed, Opt. Lett. **23**, 1760 (1998).
6. C. Erny, L. Gallmann, and U. Keller, Appl. Phys. B **96**, 257 (2009).
7. O. Chalus, P. K. Bates, M. Smolarski, and J. Biegert, Opt. Express **17**, 3587 (2009).
8. C. Manzoni, R. Osellame, M. Marangoni, M. Schultze, U. Morgner, and G. Cerullo, Opt. Lett. **34**, 620 (2009).
9. C. Heese, L. Gallmann, U. Keller, C. R. Phillips, and M. M. Fejer, Opt. Lett. **35**, 2340 (2010).
10. G. M. Gale, M. Cavallari, T. J. Driscoll, and F. Hache, Opt. Commun. **119**, 159 (1995).
11. G. M. Gale, G. Gallot, F. Hache, and R. Sander, Opt. Lett. **22**, 1253 (1997).
12. V. Petrov, F. Rotermund, and F. Noack, J. Opt. A **3**, R1 (2001).
13. D. Brida, C. Manzoni, G. Cirmi, M. Marangoni, S. De Silvestri, and G. Cerullo, Opt. Express **15**, 15035 (2007).
14. O. D. Mücke, D. Sidorov, P. Dombi, A. Pugzlys, A. Baltuska, S. Alisauskas, V. Smilgevicius, J. Pocius, L. Giniunas, R. Danielius, and N. Forget, Opt. Lett. **34**, 118 (2009).
15. M. Bradler, P. Baum, and E. Riedle, Appl. Phys. B **97**, 561 (2009).
16. C. J. Fecko, J. J. Loparo, and A. Tokmakoff, Opt. Commun. **241**, 521 (2004).

Appendix A5

Carrier-envelope phase-stable sub-two-cycle pulses tunable around 1.8 µm at 100 kHz

C. Homann, M. Bradler, M. Förster, P. Hommelhoff, and E. Riedle

Opt. Lett. **37**, 1673 - 1675 (2012)

Carrier-envelope phase stable sub-two-cycle pulses tunable around 1.8 μm at 100 kHz

Christian Homann,[1,*] Maximilian Bradler,[1] Michael Förster,[2] Peter Hommelhoff,[2] and Eberhard Riedle[1]

[1]*Lehrstuhl für BioMolekulare Optik, Ludwig-Maximilians-Universität München, Oettingenstrasse 67, 80538 Munich, Germany*

[2]*Ultrafast Quantum Optics Group, MPI für Quantenoptik, Hans-Kopfermann-Strasse 1, 85748 Garching, Germany*

**Corresponding author: christian.homann@physik.lmu.de*

Received November 24, 2011; revised February 13, 2012; accepted February 23, 2012;
posted February 23, 2012 (Doc. ID 158713); published May 10, 2012

We present a simple and efficient concept for the generation of ultrashort infrared pulses with passively stabilized carrier-envelope phase at 100 kHz repetition rate. The central wavelength is tunable between 1.6 and 2.0 μm with pulse durations between 8.2 and 12.8 fs, corresponding to a sub-two-cycle duration over the whole tuning range. Pulse energies of up to 145 nJ are achieved. As a first application we measure the high nonlinearity of multiphoton photoemission from a nanoscale metal tip. © 2012 Optical Society of America

OCIS codes: 190.4970, 320.5520, 320.7110, 120.5050.

The generation of few-cycle light pulses with stable carrier-envelope phase (CEP) at wavelengths around 2 μm is still a challenging task [1–8], recently highlighted by a comprehensive review [9]. High-power pulses at these wavelengths are of great interest to extend the cutoff of high-order harmonic generation toward the water window [8]. Also, in the CEP-sensitive emission of electrons from metal nanostructures, where pulse energies of only 240 pJ at 800 nm sufficed to generate electrons with kinetic energies of up to 13 eV, the use of longer wavelengths is expected to greatly enhance electron energies and to give further insight into the interplay between multiphoton and tunneling ionization [10]. Investigations along these lines, which require high repetition rates, motivated us to develop a tunable few-cycle source.

Because sufficiently broadband laser materials for the generation of few-cycle pulses around 2 μm are still in their early stages of development, all concepts to generate such pulses rely on parametric processes, such as difference-frequency generation (DFG) or optical parametric (chirped pulse) amplification [OP(CP)A]. At repetition rates up to 1 kHz the generation of CEP-stable sub-two-cycle pulses for wavelengths up to 1.8 μm has been successfully demonstrated [5,6]. However, at higher repetition rates only significantly longer pulses with 6 to 7 optical cycles have been shown to date [4,11,12], although spectra with Fourier limits in the 20 fs regime have been achieved [13]. The difficulty in transferring the concepts used at 1 kHz to higher rates originates from the high pulse energies needed. To achieve the required spectral width, various approaches are combined with spectral broadening in hollow-core fibers, either for broadening the seed [2,3] or the final output [5,6], which necessitates pulse energies of several 100 μJ. Implementations without additional spectral broadening, e.g., by DFG of two noncollinear optical parametric amplifier (NOPA) outputs [1] depended on 200 μJ of pump pulse energy at 800 nm, not readily available at 100 kHz. Especially when only moderate pulse energies are needed for the experiment, the generation of hundreds of μJ of pump pulse energy at 100 kHz is unreasonable and might jeopardize future system miniaturization and integration.

In this Letter we present an efficient and simple scheme for the generation of CEP-stable pulses with a duration around 10 fs and energies on the order of 100 nJ at a repetition rate of 100 kHz. The pulses are tunable from 1.6 to 2.0 μm while maintaining a sub-two-cycle duration. To the best of our knowledge this constitutes the shortest pulse durations in this wavelength range for repetition rates above 1 kHz, combined with excellent tunability.

Our concept is based on broadband DFG between the short visible output of a NOPA and the narrow-band pump laser. A schematic of the setup is depicted in Fig. 1. A commercial Yb:KYW based pump laser (Jenlas D2.fs; JENOPTIK Laser GmbH) delivers ~300 fs pulses at 1025 nm with an energy of 40 μJ at 100 kHz repetition rate. For the current setup, 32 μJ of the pulse energy are used. Approximately 5% are split off for SCG in a 4 mm thick YAG crystal producing the seed for the NOPA [14]. The remaining part of the pump pulse is frequency doubled in a 0.8 mm thick BBO crystal cut at 23.5° with an efficiency of about 30%. Due to the small beam size of the pump laser ($1/e^2$ radius of 880 μm), no focusing was needed. The seed and the pump are both focused into a 3 mm thick BBO crystal cut at 20° with an external noncollinearity angle of 3.3°. The amplified spectrum can be tuned in central wavelength between 650 and 700 nm while maintaining a Fourier limit below 10 fs and energies around 2 μJ per pulse. After collimation with a spherical mirror, the output pulses are compressed to sub-20-fs duration using a sequence of fused silica prisms.

The 1025 nm light remaining after frequency doubling is rotated in polarization by 90° with a half-wave plate, and transmitted through a pair of wedges (10°, BK7),

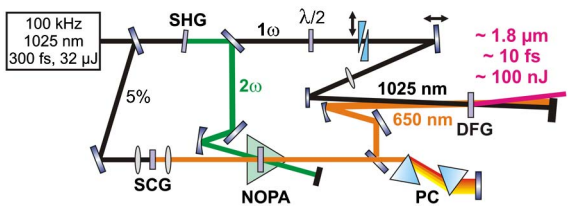

Fig. 1. (Color online) Setup; SHG, second harmonic generation; $\lambda/2$, half wave plate; SCG, supercontinuum generation; NOPA, noncollinear optical parametric amplifier; PC, prism compressor; DFG, difference frequency generation.

0146-9592/12/101673-03$15.00/0

used for controlling the CEP of the 1.8 μm output. It is then focused into a 0.8 mm thick BBO crystal cut at 23.5° together with the compressed NOPA output to perform type-I DFG to the infrared (IR). This crystal thickness is much less than that typically used for an OPA stage and therefore allows a largely increased acceptance bandwidth and minimizes dispersion and group velocity mismatch. The beam radii ($1/e^2$ value) were 120 μm for the 1025 nm beam and 70 μm for the NOPA output for ease of alignment. To avoid the need for dichroic optics, the two beams are combined under a small angle, which is kept as small as possible (~0.9°) to limit the resulting spatial chirp of the IR pulse to below the divergence of 1°.

The spectrum of the IR output can be tuned in a considerable wavelength range by changing the NOPA spectrum and readjusting the phase-matching angle of the DFG and the time delay between the NOPA output and the 1025 nm pulses (Fig. 2, top row). The deconvolved pulse durations, obtained from autocorrelation measurements, lie between 8.2 and 12.7 fs, corresponding to only 1.5 to 1.9 optical cycles (Fig. 2, bottom row). Pulse energies of up to 145 nJ are achieved, however with slightly longer pulses (11.7 fs at 1.6 μm central wavelength). For the shortest pulse durations pulse energies of 40 nJ are achieved, corresponding to 4 mW of average power.

After frequency doubling, the temporal shape and the spectro-spatial phase of the remaining 1025 nm pulses are distorted from the original near-Gaussian, leading to a temporal double peak structure. Varying the delay between the relatively long 1025 nm pulses and the much shorter NOPA output results in two maxima in the IR energy. Interestingly, the shortest pulses are achieved when the NOPA pulses interact with the outer wings of the 1025 nm pulses. This also leads to smooth IR spectra without strong modulations, whereas spectral dips can occur when the NOPA output is overlapped with the distorted part of the 1025 nm pulse.

To substantiate the autocorrelation measurements we performed second-harmonic-generation frequency-resolved optical gating (SHG-FROG). As can be seen in Fig. 3, the measured and retrieved FROG traces show excellent agreement. The spectrum calculated from the frequency doubled spectrum fits the original spectrum

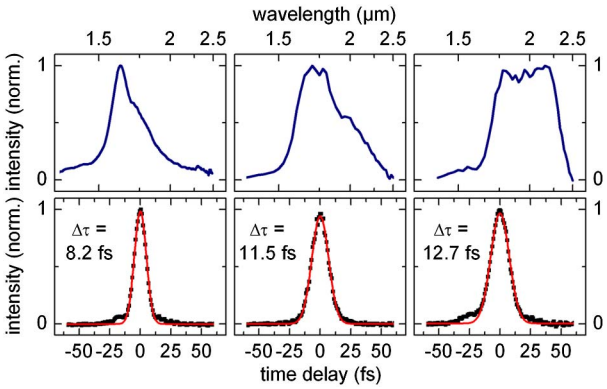

Fig. 2. (Color online) Spectra and corresponding autocorrelation measurements showing the wavelength tunability of our concept while maintaining a sub-two-cycle pulse duration ($\Delta\tau$: deconvolved FWHM Gaussian pulse duration).

measured with the monochromator almost exactly. To be able to compare the spectra, all spectrometers used were intensity calibrated with a black body lamp. The evaluation shows that in this case the IR pulses had some residual chirp resulting in a pulse duration of 13.4 fs.

The compression of the IR pulses is solely adjusted by the chirp of the NOPA output and thus the prism compressor in the visible. The shortest IR pulses are achieved when the NOPA pulses are also nearly optimally compressed. This scheme even allows compensating for material dispersion in the IR, introduced by, e.g., an entrance window to a vacuum chamber. For example, a pulse centered at 1.8 μm with a duration of 14.6 fs is negatively chirped by a 5 mm thick calcium fluoride window to 21.7 fs. By positively chirping the visible pulse through insertion of the second prism of the compressor deeper into the beam and readjusting the temporal overlap with the 1025 nm pulse, the IR pulse is recompressed to 16.1 fs. In principle, a nearly arbitrary pulse shaping of the IR pulse is possible by shaping the visible pulse in its Fourier plane at the end mirror of the compressor by, e.g., a deformable mirror or phase or intensity masks [15].

The NOPA output inherits the CEP fluctuations of the supercontinuum seed and hence of the 1025 nm pump. Since the NOPA output is subsequently difference frequency mixed with the 1025 nm light, the IR output is expected to be CEP stable [1,9]. To verify this, we set up an f-2f interferometer [12,16]. In our scheme, the phase-matching angle chosen for broadband DFG is close to that for frequency doubling of the 1.8 μm pulses, which leads to some weak 0.9 μm output. This light was separated from the main IR output by a dichroic mirror and rotated in polarization by 90°. The IR pulses were transmitted through a silicium filter and focused with a reflective microscope objective into a highly nonlinear fiber to broaden their spectrum. The broadened pulses and the frequency doubled light were then collinearly recombined by a metallic beam splitter and focused into a spectrometer with a time delay of ~400 fs. For proper

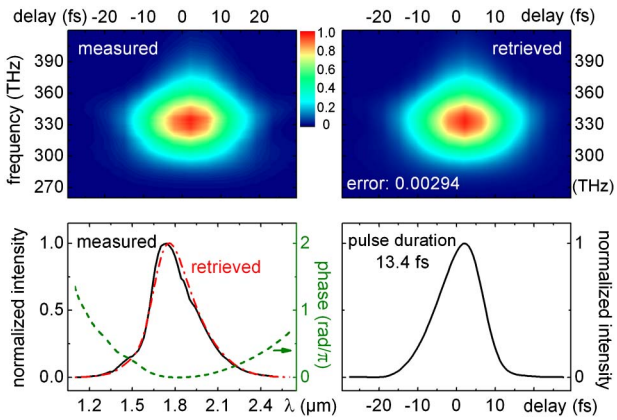

Fig. 3. (Color online) SHG-FROG measurement of the IR output pulse. The measured and retrieved FROG trace show excellent agreement, as do the directly measured spectrum around 1.8 μm and the calculated spectrum from the SH spectrum (dashed–dotted curve). The spectral phase (dashed curve) indicates some residual chirp. Bottom right: Retrieved intensity in the time domain.

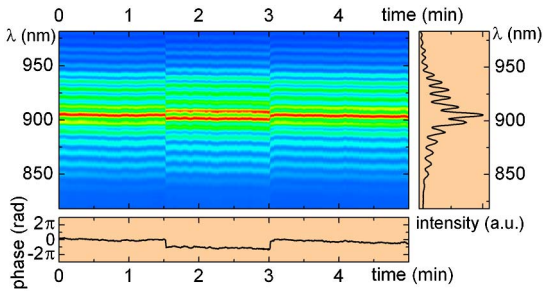

Fig. 4. (Color online) f-2f interference measurement. The right panel shows the spectrum of a single scan, the lower panel the evaluated phase. After 1.5 min. a CEP shift of π is induced by moving a wedge, which is reversed after 3 min.

alignment of the NOPA continuum generation, we observe a high contrast interference pattern that directly shows the CEP stability of the IR pulses. When integrating over 1 ms and acquiring 500 consecutive spectra (i.e., 0.5 s acquisition time), we measure phase fluctuations of only 78.5 mrad rms. Fig. 4 shows a measurement over 5 min (averaged over 100 ms). After 1.5 min we induce a CEP change of π by translating one of the wedges in the 1025 nm beam in front of the DFG stage (see Fig. 1) by approximately 6 μm. After 3 min the wedge is moved back. This clearly shows that we have full control of the CEP and can compensate for the observed slow drift. For the slower fluctuations (0.1 to 5 Hz) we find a value of 135 mrad rms.

As a first experimental application of our new source, we tightly focused pulses centered at ~2.0 μm and with durations of ~20 fs onto a nanoscale tungsten tip, with the laser polarization parallel to the tip-pointing direction. This leads to photoemission of electrons from the tip, which we accelerate by an electric dc field toward a microchannel plate (MCP) detector. Fig. 5 shows the count rate on the MCP screen as function of the incident pulse energy in a double-logarithmic plot. The fitted slope of 3.8 is close to the expected value for multiphoton photoemission, when the reduction of the work function due to the applied dc field (1.9 GV/m at the tip) is taken into account [10].

In summary, we have demonstrated the generation of CEP-stable sub-two-cycle pulses with tunable central wavelength from 1.6 to 2.0 μm and energies in the range of 100 nJ at 100 kHz repetition rate. The necessary spectral bandwidth is efficiently achieved by DFG in a mixing crystal much thinner than used in typical OPAs. The compression is achieved by just a simple prism compressor in the intermediate NOPA output. The principle is not limited to the sub-2-μm range, but can be readily extended far into the IR. The new setup is a highly attractive source for numerous applications, such as the study of electron emission from nanoscale metal tips, as demonstrated with the first experimental data. The photoemission from the metal tip shows that already extremely weak pulses are sufficient for this interesting regime of nonlinear optics.

Our concept is also an interesting seed source for high power applications. It allows omitting the Ti:Sa oscillator/amplifier with subsequent intra-pulse DFG [3], which has to be synchronized to the pump laser. Additionally, it

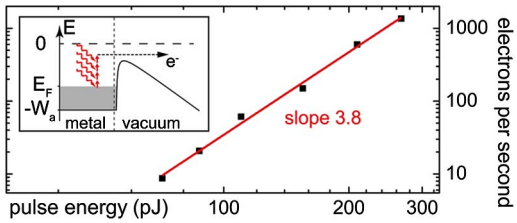

Fig. 5. (Color online) Current as function of the pulse energy focused onto a tungsten tip. Inset: schematic of the multiphoton photoemission process: E_F, Fermi energy; W_a, work function.

would provide much more seed energy than the reported few picojoules [7] to nanojoules, which will lead to a drastic improvement in pulse contrast. The remaining challenge will be to either generate a stable supercontinuum from the typical picosecond pump pulses or to boost the Jenlas D2.fs output pulses to the millijoule regime.

We thank M. Schenk and M. Krüger for experimental support with the electron measurement, and the DFG-Cluster of Excellence: Munich-Centre for Advanced Photonics for financial support.

References

1. C. Manzoni, G. Cerullo, and S. De Silvestri, Opt. Lett. **29**, 2668 (2004).
2. C. Vozzi, G. Cirmi, C. Manzoni, E. Benedetti, F. Calegari, G. Sansone, S. Stagira, O. Svelto, S. De Silvestri, M. Nisoli, and G. Cerullo, Opt. Express **14**, 10109 (2006).
3. X. Gu, G. Marcus, Y. Deng, T. Metzger, C. Teisset, N. Ishii, T. Fuji, A. Baltuska, R. Butkus, V. Pervak, H. Ishizuki, T. Taira, T. Kobayashi, R. Kienberger, and F. Krausz, Opt. Express **17**, 62 (2009).
4. O. D. Mücke, D. Sidorov, P. Dombi, A. Pugžlys, A. Baltuška, S. Ališauskas, V. Smilgevicius, J. Pocius, L. Giniunas, R. Danielius, and N. Forget, Opt. Lett. **34**, 118 (2009).
5. C. Li, D. Wang, L. Song, J. Liu, P. Liu, C. Xu, Y. Leng, R. Li, and Z. Xu, Opt. Express **19**, 6783 (2011).
6. B. E. Schmidt, A. D. Shiner, P. Lassonde, J.-C. Kieffer, P. B. Corkum, D. M. Villeneuve, and F. Légaré, Opt. Express **19**, 6858 (2011).
7. K.-H. Hong, S.-W. Huang, J. Moses, X. Fu, C.-J. Lai, G. Cirmi, A. Sell, E. Granados, P. Keathley, and F. X. Kärtner, Opt. Express **19**, 15538 (2011).
8. M.-C. Chen, P. Arpin, T. Popmintchev, M. Gerrity, B. Zhang, M. Seaberg, D. Popmintchev, M. M. Murnane, and H. C. Kapteyn, Phys. Rev. Lett. **105**, 173901 (2010).
9. G. Cerullo, A. Baltuska, O. D. Mücke, and C. Vozzi, Laser Photon. Rev. **5**, 323 (2011).
10. M. Krüger, M. Schenk, and P. Hommelhoff, Nature **78**, 475 (2011).
11. C. Heese, L. Gallmann, U. Keller, C. R. Phillips, and M. M. Fejer, Opt. Lett. **35**, 2340 (2010).
12. A. Thai, M. Hemmer, P. K. Bates, O. Chalus, and J. Biegert, Opt. Lett. **36**, 3918 (2011).
13. M. Bradler, C. Homann, and E. Riedle, Opt. Lett. **36**, 4212 (2011).
14. M. Bradler, P. Baum, and E. Riedle, Appl. Phys. B **97**, 561 (2009).
15. T. Witte, D. Zeidler, D. Proch, K. L. Kompa, and M. Motzkus, Opt. Lett. **27**, 131 (2002).
16. M. Kakehata, H. Takada, Y. Kobayashi, K. Torizuka, Y. Fujihara, T. Homma, and H. Takahashi, Opt. Lett. **26**, 1436 (2001).

Danksagung

Diese Dissertation wäre nicht entstanden ohne die tatkräftige Mithilfe vieler Personen, denen ich zu großem Dank verpflichtet bin.

An erster Stelle ist dies mein Doktorvater **Herr Prof. Dr. Eberhard Riedle**, der mir diese Arbeit erst ermöglicht und sie wissenschaftlich bestens betreut hat. Sein herausragendes Engagement und seine Begeisterungsfähigkeit haben mich dabei immer zu neuen Leistungen und Experimenten angespornt. Seine Hilfe reichte dabei von so kleinen Dingen wie sinnvollen Formatierungseinstellungen in Word, über praktische experimentelle Tipps im Labor, zu höchst ergiebigen Diskussionen über meine Resultate, und den großen Fragen was wie und warum zu verstehen ist, und welche Experimente ich als nächstes machen könnte.

Ich danke außerdem **Herrn Prof. Dr. Wolfgang Zinth**, der meine Arbeit im Rahmen des Institusseminars immer interessiert und aufmerksam verfolgt hat, und mir bei Fragen mit Rat und Tat zur Seite stand.

Viele meiner Projekte entstanden in Zusammenarbeit mit externen Kooperationspartnern oder sind erst aus deren Wünschen nach neuartigen Laserimpulsquellen hervorgegangen.

Vielen Dank dafür an Herrn Prof. **Dr. Wolf Widdra** und seinem Team aus Halle, deren Nachfrage nach einem NOPA mit MHz-Wiederholrate mir schon früh zur ersten Veröffentlichung verhalf. Herrn **Dr. Enrico da Como** und seinem Team, die nach Impulsen im Mittelinfraroten dürsteten, woraus ein spannendes Projekt erwuchs. **Prof. Dr. Ferenc Krausz** und **Dr. Laszlo Veisz** mit Ihrem Team, speziell **Dr. Daniel Herrmann** und **Dr. Rafael Tautz**, durch die ich Zugang zum Lasersystem LWS-20 am Max-Planck Institut für Quantenoptik erhielt und zu dessen Weiterentwicklung beitragen durfte. Außerdem herzlichen Dank an **Prof. Dr. Peter Hommelhoff** und sein Team, speziell **Michael Förster**, die mir ebenfalls ein interessantes Projekt ermöglichten und mich an ihren Elektronenspitzen mitmessen ließen, was zu schönen Daten führte.

Wichtig für das Gelingen dieser Arbeit waren auch die Nutzung und das zuverlässige Funktionieren diverser Lasersysteme. Einen entscheidenden Anteil daran dass dies fast immer der Fall war, und eventuelle Fehler schnellstmöglich beseitigt wurden, haben vor allem **Gerald Jung** und **Dr. Hans-Erik Swoboda** von Horiba Jobin Yvon, sowie **Bert Kremser** und **Rene Beilschmidt** von Jenoptik. Vielen Dank dafür!

Was wäre diese Zeit ohne meinen langjährigen Bürokollegen **Maximilian Bradler** gewesen? Mit ihm zusammen entstanden unzählige spannende wissenschaftliche Ergebnisse, sowie einige schöne Veröffentlichungen. Mindestens genauso wichtig war aber die lustige und gute Büroatmosphäre, die erst gar keine schlechte Stimmung aufkommen ließ, auch wenn im Labor einmal etwas nicht funktionierte.

Herzlichen Dank auch an alle anderen Kollegen am BMO, die zu der guten, freundlichen und hilfsbereiten Atmosphäre am Institut beigetragen haben und für mich immer ein offenes Ohr hatten. Stellvertretend für alle anderen seien genannt **Christian Sailer**, **Nils Krebs**, **Dr. Igor Pugliesi**, **Peter Lang**, **Florian Lederer**, **Karin Haiser** und **Franziska Graupner**, sowie die „Ehemaligen“ **Dr. Uwe Megerle, Dr. Patrizia Krok**, **Dr. Peter Baum**, **Andreas C. Böck** und **Markus Breuer**.

Bedanken möchte ich mich auch bei „meiner“ ehemaligen Diplomandin **Katrin Peeper** und meinen Bacheloranden **Alexandra Waritschlager** und **Peter Sterflinger**, deren wertvolle Ergebnisse auch Eingang in diese Arbeit gefunden haben.

Herzlichen Dank auch an das großartige Werkstattteam, bestehend aus **Rudi Schwarz**, **Alfons Stork** und **Christian Hausmann**, die alle Arbeiten zuverlässig, präzise und in dringenden Fällen auch sofort für mich erledigten. Speziell Rudi hatte dabei immer jede Menge hervorragender Ideen, wie meine ursprünglichen Pläne umgesetzt werden könnten. Außerdem gebührt mein Dank **Harald Hoppe** für die ausgezeichneten Optikarbeiten.

Danke auch an Frau **Monika Wild** stellvertretend für die ganze IMPRS-APS, durch die ich viele nette und interessante Leute kennen gelernt habe, und vielen anregenden Seminaren in toller Umgebung beiwohnen durfte.

Zu guter letzt möchte ich mich auch bei meiner Familie bedanken, die immer für mich da war und mir Kraft und Ruhe gegeben hat, auch und vor allem wenn einmal etwas nicht nach Wunsch lief.